Electronic and photoelectron spectroscopy of substituted benzene molecules

William Duncan Tuttle

Thesis submitted to the University of Nottingham for the degree of Doctor of Philosophy

July 2018

Abstract

Intramolecular vibrational redistribution (IVR) has long been investigated in *para*-fluorotoluene (*p*FT), with many comparisons made to *para*-difluorobenzene (*p*DFB). These comparisons have shown an increased IVR rate for *p*FT compared to *p*DFB at similar internal energies, and there are two factors which could influence this – the addition of the methyl group and the lowering of the symmetry of the molecule. This thesis looks to separate these two effects by introducing a comparison of *p*FT to *para*-chlorofluorobenzene, as well as an additional comparison of *para*-xylene (*p*Xyl) to *p*DFB.

Resonance-enhanced multiphoton ionisation (REMPI) spectra of these four molecules are presented, with zero-electron-kinetic-energy (ZEKE) photoelectron spectra recorded *via* many intermediate levels up to $\sim 0^0+1200\ cm^{-1}$ for both *p*FT and *p*Xyl. These ZEKE spectra allow the assignment of many torsional, vibrational and vibration-torsion levels in these two molecules, with *p*Xyl treated with the appropriate G_{72} molecular symmetry group for the first time. Several reassignments, as well as many new assignments, are presented for *p*FT and *p*Xyl.

Use of the REMPI and ZEKE techniques allows for the probing of any couplings between levels in the S_1 state, as well as providing ground state cation information, and this is supplemented by comparison of REMPI activity between the four *para*-disubstituted benzene molecules. Proposed couplings, which appear to become more widespread at higher internal energies, are supported by density of states calculations, and a discussion of the influence of both the methyl group and the molecular symmetry on the couplings is presented.

Publications covered in this thesis

"Torsion and vibration-torsion levels of the S_1 and ground cation electronic states of *para*-fluorotoluene" – A. M. Gardner, W. D. Tuttle, L. Whalley, A. Claydon, J. H. Carter and T. G. Wright, *J. Chem. Phys.*, **145**, 124307 (2016).

"Molecular symmetry group analysis of the low-wavenumber torsions and vibration-torsions in the S_1 state and ground cationic state of *p*-xylene: an investigation using resonance-enhanced multiphoton ionization (REMPI) and zero-kinetic-energy (ZEKE) spectroscopy" – A. M. Gardner, W. D. Tuttle, P. Groner and T. G. Wright, *J. Chem. Phys.*, **146**, 124308 (2017).

"Vibrational and vibrational-torsional interactions in the 0-600 cm^{-1} region of the $S_1 \leftarrow S_0$ spectrum of *p*-xylene investigated with resonance-enhanced multiphoton ionization (REMPI) and zero-kinetic-energy (ZEKE) spectroscopy" – W. D. Tuttle, A. M. Gardner, K. B. O'Regan, W. Malewicz and T. G. Wright, *J. Chem. Phys.*, **146**, 244309 (2017).

"Vibration and vibration-torsion levels of the S_1 state of *para*-fluorotoluene in the 580-830 cm^{-1} range: Interactions and coincidences" – W. D. Tuttle, A. M. Gardner, L. E. Whalley and T. G. Wright, *J. Chem. Phys.*, **146**, 244310 (2017).

"Effects of symmetry, methyl groups and serendipity on intramolecular vibrational energy dispersal" – W. D. Tuttle, A. M. Gardner, L. E. Whalley, D. J. Kemp and T. G. Wright, *Phys. Chem. Chem. Phys.*, (in press).

Publications not covered in this thesis

Theoretical studies of group 14 cation-rare gas complexes

"Interaction Potentials, Spectroscopy and Transport Properties of $C^+(^2P_J)$ and $C^+(^4P_J)$ with Helium" – W. D. Tuttle, R. L. Thorington, L. A. Viehland and T. G. Wright, *Mol. Phys.*, **113**, 3767 (2015).

"Theoretical study of $Si^+(^2P_J)$-RG complexes and transport of $Si^+(^2P_J)$ in RG (RG = He-Ar)" – W. D. Tuttle, R. L. Thorington, L. A. Viehland and T. G. Wright, *Mol. Phys.*, **115**, 437 (2017).

"Interactions of C^+ with rare gas atoms: Incipient chemical interactions, potentials and transport coefficients" – W. D. Tuttle, R. L. Thorington, L. A. Viehland, W. H. Breckenridge and T. G. Wright, *Phil. Trans. Roy. Soc. A.*, **376**, 20170156 (2018).

Substituted benzene vibrational labelling schemes

"Consistent assignment of the vibrations of symmetric and asymmetric *para*-disubstituted benzene molecules" – A. Andrejeva, A. M. Gardner, W. D. Tuttle and T. G. Wright, *J. Mol. Spectrosc.*, **321**, 28 (2016).

"Consistent assignment of the vibrations of symmetric and asymmetric *ortho*-disubstituted benzenes" – W. D. Tuttle, A. M. Gardner, A. Andrejeva, D. Kemp, J. C. A. Wakefield and T. G. Wright, *J. Mol. Spectrosc.*, **344**, 46 (2018).

"Consistent assignment of the vibrations of symmetric and asymmetric *meta*-disubstituted benzenes" – D. J. Kemp, W. D. Tuttle, F. M. S. Jones, A. M. Gardner, A. Andrejeva, J. C. A. Wakefield and T. G. Wright, *J. Mol. Spectrosc.*, **346**, 46 (2018).

Experimental studies

"Resonance-enhanced multiphoton ionization (REMPI) spectroscopy of *p*-chlorofluorobenzene" – W. D. Tuttle, A. M. Gardner and T. G. Wright, *Chem. Phys. Lett.*, **684**, 339 (2017).

"Direct observation of vibrational energy dispersal via methyl torsions" – A. M. Gardner, W. D. Tuttle, L. E. Whalley and T. G. Wright, *Chem. Sci.*, **9**, 2270 (2018).

Publications from research conducted during my employment at the University of Nottingham (September 2017 – May 2018)

"Vibrations of the *p*-chlorofluorobenzene cation" – D. J. Kemp, L. E. Whalley, W. D. Tuttle, A. M. Gardner, B. T. Speake and T. G. Wright, *Phys. Chem. Chem. Phys.*, **20**, 12503 (2018).

"Zero-electron-kinetic-energy (ZEKE) spectroscopy of *p*-difluorobenzene: identifying complex Fermi resonances" – D. J. Kemp, A. M. Gardner, W. D. Tuttle, J. Midgley, K. L. Reid and T. G. Wright, *J. Chem. Phys.*, (submitted).

Publications from studies conducted during my MSci research project

"Vibrations of the S_1 State of Fluorobenzene-h_5 and Fluorobenzene-d_5 *via* Resonance-enhanced Multiphoton Ionization (REMPI) Spectroscopy" – J. P. Harris, A. Andrejeva, W. D. Tuttle, I. Pugliesei, C. Schriever, T. G. Wright, *J. Chem. Phys.*, **141**, 244315 (2014).

"Assignment of the Vibrations of the S_0, S_1, and D_0^+ States of Perhydrogenated and Perdeuterated Isotopologues of Chlorobenzene" – A. Andrejeva, W. D. Tuttle, J. P. Harris and T. G. Wright, *J. Chem. Phys.*, **143**, 104312 (2015).

"Resonance-enhanced multiphoton ionization (REMPI) spectroscopy of bromobenzene and its perdeuterated isotopologue: assignment of the vibrations

of the S_0, S_1 and D_0^+ states of bromobenzene and the S_0 and D_0^+ states of iodobenzene" – A. Andrejeva, W. D. Tuttle, J. P. Harris and T. G. Wright, *J. Chem. Phys.*, **143**, 244320 (2015).

Acknowledgements

I am indebted to my supervisor, Professor Timothy Wright, who gave me the opportunity to study for a PhD, and with whom I have been working since I undertook an undergraduate summer research project in 2012. His support and guidance over the years has been invaluable. Particular thanks must also go to Dr Adrian Gardner, with whom I have had the privilege of working for the past three years. He has been great fun to work with, as well as a very patient mentor, and together we spent many a late night gathering experimental data.

I have worked with a number of international collaborators during my PhD: Professor Peter Groner's work establishing the G_{72} molecular symmetry group for *para*-xylene was indispensable, and communication with Professor Warren Lawrance and Dr Jason Gascooke regarding the *para*-fluorotoluene work was extremely helpful. I am also grateful for the support of the PhD students that I have worked with over the years – my thanks go to Dr Anja Andrejeva and Dr Joe Harris, as well as more recently to Laura Whalley, with whom I worked to collect some of the data included in this thesis.

I have been fortunate enough to work with many talented undergraduate students, undertaking summer and MSci research projects. My thanks go to all of these students for their hard work and for being so entertaining to work with – Rebecca Thorington, Johnny Wakefield, Angus Taylor, Joe Carter, Andrew Claydon, Will Malewicz, Kieran O'Regan and Florence Jones. Most recently, I worked with David Kemp, who is now a PhD student in the group, and I wish him all the best with his PhD.

Finally, it would be remiss of me not to thank the technical staff in the School of Chemistry, in particular Neil Barnes, Paul Gaetto and David Litchfield, who were always on hand to assist with any issues and aid with construction of new apparatus and setting up of electronics.

Table of Contents

List of Figures ..... **xv**

List of Tables ..... **xix**

1. Introduction and theoretical background **1**

1.A. Introduction 1

1.B. The Born-Oppenheimer approximation 4

1.C. Molecular vibrations 5

1.C.1. Diatomic harmonic oscillator 5

1.C.2. Diatomic anharmonicity 6

1.C.3. Polyatomic vibrations 7

1.D. Vibrational coupling 9

1.D.1. Fermi resonance 9

1.D.2. Coriolis coupling 11

1.E. Transition intensities in electronic excitation and photoelectron spectra 11

1.E.1. Electronic transitions 12

1.E.2. Photoionisation transitions 13

1.E.3. Vibrational and torsional structure 14

1.E.3.1. Within the Born-Oppenheimer approximation 15

1.E.3.2. Outside the Born-Oppenheimer approximation 17

1.E.3.2.1. Vibration-electronic transitions 17

1.E.3.2.2. Torsion-electronic transitions 20

1.F. Intramolecular vibrational redistribution (IVR) 21

1.F.1. Restricted IVR 21

1.F.2. Doorway states and statistical IVR 24

1.G. Vibrational labelling 26

1.H. References 28

2. Methodology **31**

2.A. Experimental techniques 31

2.A.1. Resonance-enhanced multiphoton ionisation (REMPI) spectroscopy 31

2.A.2. Zero-electron-kinetic-energy (ZEKE) photoelectron spectroscopy (PES) 33
2.A.3. Supersonic jet expansions 35
2.B. Experimental apparatus 36
2.C. Computational methodology 38
2.D. References 41

3. A single rotor case: the low wavenumber torsion and vibration-torsion region of *para*-fluorotoluene 43
3.A. *para*-fluorotoluene and the single rotor 43
3.A.1. Previous work 43
3.A.2. The single rotor 46
3.A.2.1. The free rotor 46
3.A.2.2. The hindered rotor 48
3.A.2.3. Molecular symmetry group treatment 51
3.A.2.4. Allowed and forbidden torsional excitations accompanying electronic excitation 56
3.A.2.5. Vibration-torsion levels 66
3.A.2.6. $D_0^+ \leftarrow S_1$ transitions 67
3.A.2.7. Vibration-torsion interactions 70
3.B. The low wavenumber region of the S_1 state of *para*-fluorotoluene 70
3.B.1. Below 100 cm^{-1}: the pure torsional region 71
3.B.1.1. Spectra and assignments 74
3.B.1.2. Discussion 79
3.B.2. 100 – 400 cm^{-1}: vibration-torsion levels 84
3.B.2.1. The D_{20} vibration-torsion levels: 110 – 220 cm^{-1} 84
3.B.2.2. D_{14} and the m = 6 levels 91
3.B.2.3. The D_{19} vibration-torsion levels: 250 – 325 cm^{-1} 95
3.B.2.4. Rationalising the intensities of transitions to vibration-torsion levels 99
3.B.2.5. The “ripples” and the region below 400 cm^{-1} 102
3.B.2.6. Discussion 106
3.B.2.6.1. Comparison to previous work 106
3.B.2.6.2. Transition energetics and couplings 108
3.C. Origin ZEKE spectrum 111
3.C.1. Overview of vibrational activity 111

3.C.2. Low wavenumber torsion and vibration-torsion activity 112
3.D. References 114

4. A double rotor case: the low wavenumber torsion and vibration-torsion region of *para*-xylene 119
4.A. *para*-xylene and the double rotor 119
4.A.1. Previous work 119
4.A.2. The double rotor 121
4.A.2.1. Molecular symmetry group treatment 122
4.A.2.1.1. G_{72} molecular symmetry group – key points 123
4.A.2.1.2. "Cold" torsional levels 128
4.A.2.2. Allowed and forbidden torsional excitations accompanying electronic excitation 131
4.A.2.3. Vibrations and torsions accompanying the $D_0^+ \leftarrow S_1$ transition 137
4.A.2.4. Vibration-torsion bands 138
4.B. The low wavenumber region of the S_1 state of *para*-xylene 140
4.B.1. Below 100 cm^{-1}: the pure torsional region 141
4.B.1.1. Spectra and assignments 141
4.B.1.2. Discussion 149
4.B.2. Vibration-torsion levels 150
4.B.2.1. The D_{20} vibration-torsion levels and the "m = 5" levels 150
4.B.2.2. The "double excitation" torsional levels and the "D_{20} m = 4" levels 159
4.B.2.3. The D_{19} vibration-torsion levels 162
4.B.3. Other possible transitions 166
4.B.4. Comparison to previous work 167
4.B.5. Discussion 169
4.C. Origin ZEKE spectrum 173
4.C.1. Overview 173
4.C.2. Discussion 175
4.D. References 178

5. Low wavenumber region of *para*-fluorotoluene and *para*-xylene (350 – 600 cm^{-1}) 181
5.A. Overview of vibrational wavenumbers trends 183
5.B. Selected ZEKE spectra and S_1 assignments 185

5.B.1. The D_{28} vibration in *para*-fluorotoluene and *para*-xylene 185
5.B.2. The D_{29} vibration in *para*-xylene.....187
5.B.3. The $2D_{19}$ vibration in *para*-fluorotoluene.....189
5.C. *para*-fluorotoluene: 400 cm^{-1} features.....189
5.C.1. Overview.....190
5.C.2. Discussion.....192
5.D. *para*-xylene: 400 – 450 cm^{-1} features.....194
5.D.1. Overview 194
5.D.2. Discussion.....198
5.E. Summary.....203
5.F. References.....207

6. Intermediate wavenumber region of *para*-fluorotoluene and *para*-xylene (600 – 900 cm^{-1}) 209
6.A. Expected vibrations in this wavenumber range.....209
6.B. Region A: *para*-fluorotoluene 580 – 800 cm^{-1} features.....212
6.B.1. Overview of ZEKE spectra.....212
6.B.1.1. The uncoupled levels.....213
6.B.1.2. The coupled levels.....219
6.B.2. Discussion.....223
6.C. Region B: *para*-fluorotoluene 800 – 850 cm^{-1} features.....225
6.C.1. Overview of ZEKE spectra.....225
6.C.1.1. The 0^0+797 cm^{-1} and 0^0+804 cm^{-1} bands 225
6.C.1.1.1. Dominant transitions 225
6.C.1.1.2. Comparison to time-resolved studies 231
6.C.1.1.3. Other $\Delta(v,m) = 0$ transitions 233
6.C.1.2. The 0^0+818 cm^{-1} band 236
6.C.1.3. The 0^0+846 cm^{-1} band 238
6.C.2. Discussion.....240
6.D. Region C: *para*-xylene 770 – 810 cm^{-1} features 242
6.D.1. Overview of ZEKE spectra.....242
6.D.2. Discussion.....245
6.E. Comparison to *para*-difluorobenzene and *para*-chlorofluorobenzene 249
6.F. References.....252

7. High wavenumber region of *para*-fluorotoluene and *para*-xylene (900 – 1400 cm^{-1}) **255**
7.A. Expected vibrations in this wavenumber range 255
7.B. *para*-fluorotoluene: 1180 – 1270 cm^{-1} 258
7.B.1. Overview of ZEKE spectra 258
7.B.2. Discussion 267
7.B.3. Comparison to time-resolved studies 270
7.C. *para*-xylene: 1120 – 1260 cm^{-1} 273
7.C.1. Overview of ZEKE spectra 274
7.C.2. Discussion 277
7.D. Comparison to *para*-difluorobenzene and *para*-chlorofluorobenzene 279
7.E. Density of states calculations 282
7.E.1. Total density of states up to 1400 cm^{-1} 283
7.E.2. The density of states at low wavenumber (0 – 600 cm^{-1}) 289
7.E.3. The density of states at intermediate wavenumber (600 – 900 cm^{-1}) 291
7.E.4. The density of states at high wavenumber (900 – 1400 cm^{-1}) 295
7.F. References 298

8. Concluding remarks and further work **301**
8.A. Concluding remarks 301
8.B. Further work 305
8.C. References 308

A. Vibrational mode diagrams **311**

B. Calculated and experimental vibrational wavenumbers **313**

C. *para*-xylene torsion and vibration-torsion symmetries **317**

List of Figures

1.1 Schematic depictions of *para*-fluorotoluene and *para*-xylene 1

2.1 Schematic depictions of 1+1 and 1+1′ REMPI 32
2.2 Schematic depiction of the ZEKE-PFI technique employed 34
2.3 Schematic depiction of the experimental apparatus 37

3.1 Schematic illustration of the lowest free rotor and hindered rotor energy levels 50
3.2 Diagram of toluene showing atomic numbering 53
3.3 Newman projections illustrating the G_{12} molecular symmetry operations 54
3.4 Overview of the low wavenumber *para*-fluorotoluene REMPI spectrum 71
3.5 Comparison of low wavenumber toluene and *para*-fluorotoluene REMPI spectra 72
3.6 ZEKE spectra recorded *via para*-fluorotoluene torsional levels 76
3.7 Comparison of ZEKE spectra recorded *via* the *para*-fluorotoluene S_1 origin and $m = 3(+)$ levels 78
3.8 ZEKE spectra recorded *via para*-fluorotoluene bands within the range 100 – 150 cm^{-1} 86
3.9 ZEKE spectra recorded *via para*-fluorotoluene D_{20} vibration-torsion levels 90
3.10 ZEKE spectra recorded *via para*-fluorotoluene D_{14} and $m = 6(+)$ levels 92
3.11 ZEKE spectra recorded *via para*-fluorotoluene D_{19} vibration-torsion levels 96
3.12 ZEKE spectra recorded *via para*-fluorotoluene bands within the range 300 – 370 cm^{-1} 104
3.13 Origin ZEKE spectrum of *para*-fluorotoluene up to 1900 cm^{-1} 111
3.14 Origin ZEKE spectrum of *para*-fluorotoluene up to 600 cm^{-1}, recorded with increased laser power 113

4.1 Diagram of *para*-xylene 121
4.2 Correlation of G_{12} and G_{72} molecular symmetry groups 126

4.3 Comparison of low wavenumber *para*-fluorotoluene and *para*-xylene REMPI spectra 141

4.4 ZEKE spectra recorded *via para*-xylene torsional levels 144

4.5 ZEKE spectra recorded *via* the *para*-xylene {0,4}, $\{1,4\}^-$ and $\{1,-4\}^-$ levels 148

4.6 Comparison of the *para*-fluorotoluene and *para*-xylene REMPI spectra up to 240 cm^{-1} 150

4.7 ZEKE spectra recorded *via para*-xylene excitation positions within the range 100 – 120 cm^{-1} 152

4.8 ZEKE spectra recorded *via para*-xylene D_{20} vibration-torsion levels 156

4.9 Comparison of the *para*-fluorotoluene and *para*-xylene REMPI spectra up to 350 cm^{-1} 162

4.10 ZEKE spectra recorded *via para*-xylene D_{19} vibration-torsion levels 163

4.11 REMPI spectrum of *para*-xylene up to 350 cm^{-1}, illustrating particular couplings 174

4.12 Origin ZEKE spectrum of *para*-xylene up to 600 cm^{-1} 176

5.1 Comparison of REMPI spectra of *para*-difluorobenzene, *para*-fluorotoluene and *para*-xylene up to 600 cm^{-1} 181

5.2 ZEKE spectrum recorded *via* the band at 0^0+554 cm^{-1} in *para*-xylene 185

5.3 ZEKE spectrum recorded *via* the band at 0^0+372 cm^{-1} in *para*-xylene 187

5.4 ZEKE spectrum recorded *via* the band at 0^0+484 cm^{-1} in *para*-fluorotoluene 188

5.5 A "2D-ZEKE" spectrum of *para*-fluorotoluene exciting over the range 395 – 415 cm^{-1} 191

5.6 A "2D-ZEKE" spectrum of *para*-xylene exciting over the range 420 – 445 cm^{-1} 195

5.7 Schematic representation of the contributions to the profile of band C 199

5.8 Expanded view of the 400 – 500 cm^{-1} region of ZEKE spectra C_2 and D_2 for *para*-xylene 201

5.9 Expanded view of the 390 – 460 cm^{-1} region of the *para*-xylene REMPI spectrum 202

5.10 Comparison of the REMPI spectra of *para*-chlorofluorobenzene, *para*-difluorobenzene, *para*-fluorotoluene and *para*-xylene up to 600 cm^{-1}, including the assignments of this chapter 204

6.1 Comparison of the REMPI spectra of *para*-chlorofluorobenzene, *para*-difluorobenzene, *para*-fluorotoluene and *para*-xylene up to 900 cm^{-1} . 211

6.2 ZEKE spectra recorded *via para*-fluorotoluene bands within the range 580 – 780 cm^{-1} 214

6.3 ZEKE spectra recorded *via para*-fluorotoluene bands within the range 580 – 780 cm^{-1}, part two 220

6.4 ZEKE spectrum recorded *via* the band at 0^0+710.5 cm^{-1} for *para*-fluorotoluene 222

6.5 A "2D-ZEKE" spectrum of *para*-fluorotoluene exciting over the range 792 – 800 cm^{-1} 226

6.6 A "2D-ZEKE" spectrum of *para*-fluorotoluene exciting over the range 800 – 812 cm^{-1} 227

6.7 Comparison of unnormalized *para*-fluorotoluene ZEKE spectra recorded *via* the 0^0+797 cm^{-1} and 0^0+804 cm^{-1} bands 228

6.8 Sections of the unnormalized *para*-fluorotoluene ZEKE spectra recorded *via* the 0^0+797 cm^{-1} and 0^0+804 cm^{-1} bands compared to the origin ZEKE spectrum 230

6.9 A "2D-ZEKE" spectrum of *para*-fluorotoluene exciting over the range 814 – 822 cm^{-1} 237

6.10 ZEKE spectrum recorded *via* the band at 0^0+846 cm^{-1} in *para*-fluorotoluene 239

6.11 REMPI spectrum of *para*-fluorotoluene from 790 – 860 cm^{-1} illustrating the assignments 241

6.12 ZEKE spectra recorded *via para*-xylene bands within the range 760 – 820 cm^{-1} 243

6.13 REMPI spectrum of *para*-xylene from 730 – 860 cm^{-1} illustrating the assignments 248

6.14 Comparison of the REMPI spectra of *para*-chlorofluorobenzene, *para*-difluorobenzene, *para*-fluorotoluene and *para*-xylene up to 900 cm^{-1}, including the assignments of this chapter 250

7.1 Comparison of the REMPI spectra of *para*-chlorofluorobenzene, *para*-difluorobenzene, *para*-fluorotoluene and *para*-xylene up to 1400 cm^{-1} 256

7.2 ZEKE spectra recorded *via para*-fluorotoluene bands within the range 1180 – 1270 cm^{-1} 259

7.3 REMPI spectrum of *para*-fluorotoluene from 1180 – 1270 cm^{-1} illustrating expected contributions 262

7.4 ZEKE spectra recorded *via para*-xylene bands with the range 1120 – 1230 cm^{-1} 275

7.5 Comparison of the REMPI spectra of *para*-chlorofluorobenzene, *para*-difluorobenzene, *para*-fluorotoluene and *para*-xylene up to 1400 cm^{-1}, including the assignments of this chapter 280

7.6 The calculated density of states for *para*-chlorofluorobenzene, *para*-fluorotoluene, *para*-difluorobenzene and *para*-xylene from 0 – 1400 cm^{-1} 286

7.7 ZEKE spectra recorded *via* the D_9 level for *para*-chlorofluorobenzene, *para*-difluorobenzene, *para*-fluorotoluene and *para*-xylene 293

7.8 ZEKE spectra recorded *via* the D_5 level for *para*-chlorofluorobenzene, *para*-difluorobenzene, *para*-fluorotoluene and *para*-xylene 296

A.1 D_i vibrational mode diagrams 311

List of Tables

3.1 G_{12} molecular symmetry group character table 52

3.2 G_{12} torsional (m) level symmetries 55

3.3 Component wavefunctions, ϕ, which together give an overall allowed symmetry, Γ_{tot}, for Φ_{tot} 60

3.4 Predicted free rotor transitions and experimental band positions 73

4.1 Transformation properties of nuclear spin, free internal rotor, asymmetric rotor and electronic dipole moment terms 123

4.2 Component wavefunctions, ϕ, which together give an overall allowed symmetry, Γ_{tot}, for Φ_{tot} 129

4.3 Experimental band positions for torsion and vibtor bands 170

7.1 Total density of states information (0 – 1400 cm^{-1}) 287

7.2 Density of states for D_{11}, $2D_{14}$ and $2D_{19}$ ± 5 cm^{-1} 290

7.3 Density of states for D_9, $2D_{29}$, $2D_{11}$ and $2D_{18}$ ± 5 cm^{-1} 292

7.4 Density of states for D_5 and D_6 ± 5 cm^{-1} 295

B.1 TD-B3LYP/aug-cc-pVTZ scaled calculated and experimental S_1 vibrational wavenumbers 314

B.2 UB3LYP/aug-cc-pVTZ scaled calculated and experimental D_0^+ vibrational wavenumbers 315

C.1 G_{72} symmetries of *para*-xylene torsion and vibration-torsion levels 318

1. Introduction and theoretical background

1.A. Introduction

This thesis covers work on the electronic spectroscopy of *para*-disubstituted benzene molecules, with a focus on two methyl group-containing molecules: the single rotor *para*-fluorotoluene (*p*FT) and the double rotor *para*-xylene (*p*Xyl), shown in Figure 1.1. Reference will also be made throughout to work on *para*-difluorobenzene (*p*DFB) and *para*-chlorofluorobenzene (*p*ClFB), as well as previous studies on the single rotor molecule toluene. These molecules are investigated in their S_1 and D_0^+ states using a combination of resonance-enhanced multiphoton ionisation (REMPI) and zero-electron-kinetic-energy (ZEKE) photoelectron spectroscopy (PES). These techniques will be discussed in Chapter 2, while this chapter will introduce some of the themes of the work, the motivations and some general theoretical background.

Understanding energy dispersal in a range of molecules is key to understanding photophysical phenomena such as photostability. This is important in many different systems, with energy needing to be rapidly dispersed to prevent bond breakage/dissociation, such as after a chemical reaction or in a biological molecule after absorbing radiation[1,2], the latter of which can lead to radical products that can be involved in cancer initiation.[3] Alternatively, one might want to attempt to reduce the energy dispersal, keeping energy localised in a single

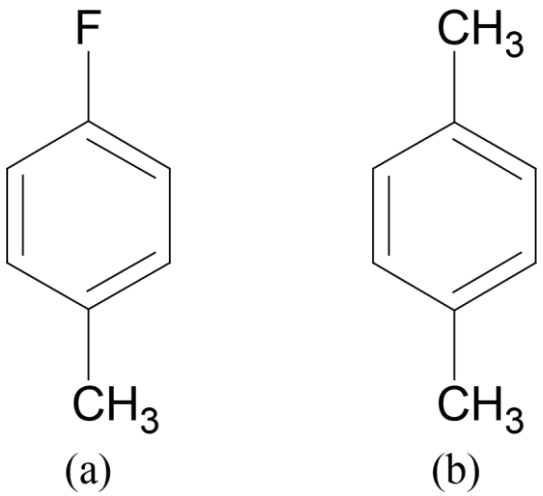


Figure 1.1 – Schematic depictions of (a) para-fluorotoluene and (b) para-xylene.

coordinate in order to control a chemical reaction.[4] As such, understanding of energy dispersal pathways is important in designing new molecules with a variety of uses, such as more efficient sunscreens.[5,6]

There are many pathways by which a molecule can relax in order to disperse energy internally, with routes to the ground electronic state for electronically excited molecules being one example.[7–9]. Alternatively (or alongside electronic relaxation), and the focus of the present work, this could be pathways within a particular electronic state, where energy dispersal is mediated by the coupling of internal energy levels, with the most obvious case being vibrational levels coupling in what is commonly known as intramolecular vibrational redistribution (IVR)[4,10–16]. Such energy dispersal occurs for a range of molecules, but the focus in the present work is on substituted benzene molecules, and specifically *para*-disubstituted benzene molecules.

There are several reasons for the choice behind this group of molecules for the current work, including:

(i) They tend to be spectroscopically bright, making it (relatively) easy to study these molecules with electronic and resonant photoelectron spectroscopies.
(ii) The electronic spectra are similar between different molecules, suggesting tractable, consistent, geometry changes.
(iii) Their ring-localised vibrations remain very similar between molecules.
(iv) The range of different substituents that such molecules can have allows a thorough investigation into the effect of the symmetry of the molecule, and the addition of methyl groups and the influence of their internal rotor levels.
(v) Significant previous work on IVR in *p*FT and *p*DFB, such as that by Parmenter and co-workers[13,14,17–27] and the Reid group[28–35].
(vi) Some understanding of more complex molecules, such as the amino acids phenylalanine and tyrosine, can be gained by studying the simpler toluene or *para*-cresol molecules respectively.

As mentioned, the focus of this thesis is on the *p*FT and *p*Xyl molecules, which can be considered in the C_{2v} and D_{2h} point groups respectively if the methyl groups are treated as point masses, or in the G_{12} and G_{72} molecular symmetry groups if explicitly including the methyl groups. The interest is in how the methyl groups affect the observed spectra and the couplings within the electronic states, with significant previous work by Parmenter and co-workers[13,14,17–27] showing enhanced IVR for *p*FT compared to *p*DFB. While that work commented on the symmetry lowering from *p*DFB to *p*FT accompanying the addition of the methyl group, it did not explicitly separate these two effects, something which will be explored in this thesis with the addition of other molecules to the comparison.

The first few chapters will deal with the relevant theoretical background for the methyl groups, and then the low wavenumber parts of the REMPI spectra, where transitions to torsion and vibration-torsion (termed vibtor in this thesis) levels are observed. These levels will be assigned and discussed in the S_1 state based on ZEKE spectra recorded *via* them, and the obtained vibrational fundamentals in the S_1 and D_0^+ states will prove useful in assigning the higher internal energy structure. As well as drawing comparisons between the molecules, on moving to higher internal energies (with ZEKE spectra recorded and presented *via* levels up to ~1200 cm^{-1} internal energy), comparison will be made between key spectra recorded for *p*FT and *p*Xyl, and analogous transitions in the C_{2v} *p*ClFB and D_{2h} *p*DFB molecules. This allows for a separation of the effect of symmetry from the influence of the methyl group on the observed IVR at different internal energies, and the thesis will conclude with a brief discussion of the couplings observed in the spectra, with reference to calculated densities of states for these molecules.

The focus of this thesis is on the methyl-containing *p*FT and *p*Xyl molecules, and so significant emphasis will be given to understanding the single and double rotor formalisms; however, the remainder of this chapter provides an overview of the general theoretical background underpinning the electronic and photoelectron spectroscopy experiments undertaken in this work. This primarily

relates to molecular vibrations, mechanisms by which electronic/photoelectron transitions can gain intensity, and couplings between vibrational levels.

1.B. The Born-Oppenheimer approximation

In much of the discussion in this thesis, use is made of the Born-Oppenheimer (BO) approximation. This well-known assumption is what allows one to even entertain the idea of a potential energy surface, and it is the recognition that electrons generally move significantly faster than atomic nuclei, such that the electronic and nuclear wavefunctions, and thus their associated energies, are separable, to a very good approximation. Although not so good an approximation, one can go a step further and separate the nuclear wavefunction into the component internal degrees of freedom. One might separate the nuclear wavefunction into its component vibrational and rotational parts[a], as well as a torsional component[b] in molecules which have these. Finally, one can include a separable nuclear spin term to make up the total wavefunction. In this case:

$$\Psi_{tot} = \psi_{elec}\psi_{vib}\psi_{rot}\psi_{tor}\psi_{ns} \qquad \text{Eq. 1.1}$$

$$E_{tot} = E_{elec} + E_{vib} + E_{rot} + E_{tor} + E_{ns} \qquad \text{Eq. 1.2}$$

This separation of the internal degrees of freedom proves useful for understanding the theory of, primarily in this thesis, vibrations and methyl torsions, but it can break down when vibration-electronic (vibronic) or torsion-electronic (toronic) coupling mechanisms are involved. Such mechanisms couple the nuclear and electronic degrees of freedom to some degree, and thus represent a breakdown of the Born-Oppenheimer approximation.

[a] Applying the rigid rotor approximation.
[b] Separable from, for example, vibration, owing to the different timescales of the motions.

1.C. Molecular vibrations

1.C.1. Diatomic Harmonic Oscillator

As a consequence of the BO approximation, one can treat molecular vibration independently of rotational and torsional motion. In the simple case of a diatomic molecule, one can initially assume the two atoms are connected by an unbreakable spring, and then use Hooke's law as if it were a classical spring. In such a scenario, the potential energy is given by:

$$V(x) = \frac{1}{2}kx^2 \qquad \text{Eq. 1.3}$$

Where *k* is the force constant of the bond, also known as the stiffness, and *x* is the displacement from the equilibrium geometry. Noting the x^2 dependence, one can see that this is a parabolic potential, and chemical intuition indicates that this is unrealistic, something that will be returned to in the next section.

With the potential energy in hand, one can then solve the Schrödinger equation with the one-dimensional harmonic oscillator Hamiltonian:

$$H = -\frac{\hbar^2}{2\mu}\frac{d^2}{dx^2} + \frac{1}{2}kx^2 \qquad \text{Eq. 1.4}$$

Where the reduced mass, μ, has been used for the diatomic molecule, and $\hbar$ is $h/2\pi$. One can solve the above equation with an appropriate wavefunction, and this results in the following expression for the energy:

$$E_{vib} = h\left(v + \tfrac{1}{2}\right)\omega \quad \text{where } v = 0, 1, 2, \ldots \qquad \text{Eq. 1.5}$$

Where v is the vibrational quantum number and ω is the vibrational frequency, given by:

$$\omega = \frac{1}{2\pi}\sqrt{\frac{k}{\mu}} \qquad \text{Eq. 1.6}$$

One can immediately see that the vibrational frequency is proportional to the square root of the force constant, such that a stronger bond will have a higher vibrational frequency. Similarly, there is a mass dependence, with an increase in the reduced mass of the molecule reducing the vibrational frequency.

Finally, it is common practice to report vibrational wavenumbers rather than frequencies. One then writes the vibrational term value, with dimensions of cm^{-1}, as:

$$G(v) = \omega\left(v + \frac{1}{2}\right) \qquad \text{Eq. 1.7}$$

1.C.2. Diatomic Anharmonicity

The harmonic oscillator is an unrealistic depiction of diatomic vibration and is only satisfactory when the displacement from the equilibrium geometry is small. Under the harmonic oscillator approximation, it is impossible for the molecule to dissociate at large internuclear separations, recalling the treatment of the molecule as an unbreakable spring, and this is obviously untrue. At higher vibrational quanta, the displacements also reach increasingly shorter internuclear separations, which fails to account for the increased repulsion as the two nuclei approach closer to one another. These deviations from the harmonic oscillator can be termed mechanical anharmonicity, and they also modify the vibrational wavefunctions and therefore the term values. Indeed, a better representation of the potential energy would be a Morse function rather than a parabola, and the term value becomes[36]:

$$G(v) = \omega_e\left(v + \frac{1}{2}\right) - \omega_e x_e\left(v + \frac{1}{2}\right)^2 + \omega_e y_e\left(v + \frac{1}{2}\right)^3 - \omega_e z_e\left(v + \frac{1}{2}\right)^4 + \cdots \qquad \text{Eq. 1.8}$$

Which is a converging power series in $\left(v+\frac{1}{2}\right)$. Owing to its converging nature, one can consider primarily just ω_e and $\omega_e x_e$, and the subtraction of (a positive) $\omega_e x_e$ is the reason that, in reality, the vibrational levels converge with increasing vibrational quantum number, up to the dissociation limit. At this point, with a large internuclear separation, the molecule falls apart and the force constant becomes zero; the atoms should now be treated separately as they are no longer bound.

1.C.3. Polyatomic vibrations

Having treated the harmonic and (mechanically) anharmonic components of diatomic vibrational motion, it is appropriate to move on to polyatomic molecules. For a non-linear polyatomic molecule such as those in this thesis, there are $3N-6$ vibrational normal modes, where N is the number of atoms. This is derived from the $3N$ degrees of freedom of the N atoms, subtracting the three translational and three rotational degrees of freedom, leaving the remainder as vibrational.

For the initial, harmonic, approach to the problem, one can envisage a polyatomic molecule having springs linking all of the atoms. This is the approach used by Hollas[36], who uses the water molecule as a simple example of this. It is important to clarify that all of the atoms, not just those which are formally bonded, are linked by springs in this model. Those which are not formally bonded are joined by weaker springs, representing the weaker interactions. In such a model, one obtains $3N-6$ harmonic normal modes, where for a particular normal mode, all of the nuclei are moving with the same frequency and in-phase with one another, but with potentially differing amplitudes. One can imagine this molecule, with all atoms connected by springs, being perturbed in some way by a force applied to even a single atom, and the whole molecule vibrating through the springs. Such a motion can be described by a combination of these normal modes of vibration – it could be a vibrational fundamental, an overtone, or a combination involving different vibrations.

One can imagine carrying out a treatment analogous to the one-dimensional harmonic oscillator in the diatomic case, but now for the polyatomic normal modes. This yields the following vibrational term values:

$$\sum_i G(v_i) = \sum_i \omega_i \left(v_i + \frac{1}{2}\right) \qquad \text{Eq. 1.9}$$

Where there is now a vibrational wavenumber, ω_i, and vibrational quantum numbers, v_i, for each of the i vibrations. Pertinent to the current work is the simple *para*-disubstituted benzene molecule *p*DFB, which has twelve atoms. It thus has thirty vibrational normal modes, and in the treatment so far these would be harmonic, each with their own vibrational wavenumber.

One now needs to account for anharmonicity. Again, this can be thought of by analogy to the diatomic case, yielding:

$$\sum_i G(v_i) = \sum_i \omega_i \left(v_i + \frac{1}{2}\right) + \sum_{i \le j} x_{ij} \left(v_i + \frac{1}{2}\right)\left(v_j + \frac{1}{2}\right) + \sum_{i \le j \le k} x_{ijk} \left(v_i + \frac{1}{2}\right)\left(v_j + \frac{1}{2}\right)\left(v_k + \frac{1}{2}\right) + \cdots \qquad \text{Eq. 1.10}$$

Where x_{ij}, x_{ijk} and higher terms are analogous to the $\omega_e x_e$, $\omega_e y_e$ and higher terms in the diatomic case in that they represent anharmonicity, although now there are two types of anharmonicity to distinguish. Only x_{ij} will be treated here, but the same principles apply to the higher order terms such as x_{ijk}.

If $i \neq j$, then x_{ij} represents an anharmonic mixing between two of the harmonic normal modes, i and j. This was not possible in the diatomic case as there was only a single harmonic vibration. However, if $i = j$, then $x_{ij} = x_{ii}$ and this represents the same anharmonic effect as in a diatomic molecule, with the vibrational level spacings (generally) closing up with increasing vibrational quantum number. One might envisage, hypothetically, a matrix containing all of these anharmonic terms, with dimensions of 3*N*-6 vibrational normal modes by

3*N*-6 vibrational normal modes, and in that case x_{ij} is often called off-diagonal anharmonicity, while x_{ii} is called diagonal anharmonicity.

1.D. Vibrational coupling

One can imagine that, in general, vibrational fundamentals, overtones, and combination levels which are of the same symmetry and close energetically can perturb one another, although for larger energetic separations these perturbations will be small. These perturbations are described by the off-diagonal anharmonic elements discussed above. However, if the levels start particularly energetically close to one another the perturbation can be substantial, and this is commonly referred to as a Fermi resonance. In the below, such a perturbation between two vibrational levels will be discussed.

1.D.1. Fermi resonance

The precise formalism depends on the nature of the two coupled levels. If one is a vibrational fundamental and the other an overtone or combination level, then it is referred to as a Fermi resonance[37]. If both levels are overtones or combination levels, then it is referred to as a Darling-Dennison resonance[38]. In either case, the two levels, which start close energetically and are of the same symmetry, mix with one another and push each other apart energetically, in a similar way to two atomic orbitals forming two molecular orbitals. The resulting wavefunctions of the perturbed levels, which are the ones observed in the spectra, are linear combinations of the unperturbed levels. For example, if two levels *a* and *b*, with unperturbed wavefunctions ψ_a^0 and ψ_b^0, are in Fermi resonance, the resulting wavefunctions take the form:

$$\psi_1 = c_1\psi_a^0 - c_2\psi_b^0$$

$$\psi_2 = c_2\psi_a^0 + c_1\psi_b^0 \qquad \text{Eq. 1.11}$$

Where c_1 and c_2 are coefficients which represent the weightings of the two levels in the resulting wavefunctions (eigenstates). Note that the superscript zero on the unperturbed wavefunctions signifies that these are the zero-order states, a term that will be returned to later.

The coupling between the two levels (and thus the values of the coefficients) is determined by two factors. The first is the energetic separation of the unperturbed levels. If the unperturbed levels are precisely energetically degenerate, then the coefficients will both be 0.5, and there will be an equal mixture of the two unperturbed levels. This will completely mix the two vibrational motions. However, if the separation of the unperturbed levels is greater than zero, the mixing will be unequal, and for large separations between the unperturbed levels it will become negligible such that $c_1 >> c_2$ or *vice versa*. In this final case, the perturbation is negligible, it is no longer a Fermi resonance, and the vibrations remain very much like their diagonally anharmonic vibrational modes.

The second factor is the interaction strength; to couple, it is expected that the two vibrations share some similarity in motion. This is a natural evolution of the idea that levels of different symmetries cannot couple, with the degree of similarity in the two vibrations (loosely) determining the interaction strength. One can also think of this in terms of quanta changes between the two coupled levels; larger changes in quanta between two levels is suggestive of a lower interaction strength[4]. This interaction strength would be reflected in the x_{ij} (or higher) terms, if they are known for the system, and these could be derived from a deperturbation treatment of the coupled levels.

It is important to recognise that the levels themselves will either be coupled or not, irrespective of whether transitions to them are observed in the spectra; those coupled levels that are observed are simply those which have one (or more) "bright states"[c] involved in the coupling. In different experiments, such as

[c] This term is somewhat ambiguous as it is transitions, rather than levels/states, that are "bright", and so it depends on other factors like the population of the initial levels and the spectroscopic technique used. However, owing to the ubiquity of the term, it will still be used in this thesis.

IR+UV double resonance for example, different bright states and thus different couplings could be observed.

Before moving on, it is important to note that in this thesis, a Fermi resonance or a Darling-Dennison resonance between two vibrational levels is often simply referred to as Fermi resonance, and any interaction between more than two vibrational levels will often be referred to under the general umbrella term of "coupling". Similarly, upon involvement of the torsional levels, the term "coupling" will also be used, to avoid overly cumbersome terminology.

1.D.2. Coriolis coupling

Coriolis coupling of rotational and vibrational degrees of freedom is also possible. A simple example of this is a linear molecule vibrating along its internuclear axis, for example undergoing an asymmetric stretch, while simultaneously rotating about a perpendicular axis. This combination of motions serves to impart some vibrational bending character to the molecule, owing to the coupling of the rotational and vibrational degrees of freedom.

In the present work, all spectra are recorded with jet cooled samples, which will have population in only the lowest rotational levels in the S_0 state, which in turn implies only a small range of rotational levels excited in the S_1 state for each vibrational level (yielding narrow bands). As such, since only the lowest rotational levels will be populated during the experiment, Coriolis coupling is thought to be minimal in the present work and is neglected from the spectral analyses of this thesis. This is supported by previous work[39], which found Coriolis coupling to be significantly weaker than anharmonic coupling under jet cooled conditions.

1.E. Transition intensities in electronic excitation and photoelectron spectra

This section contains a discussion of the mechanisms by which transitions in electronic excitation spectra gain intensity. This is general, and one can refer to

texts such as Hollas' "High Resolution Spectroscopy"[36] for this type of discussion.

First, one may consider the case of a general spectroscopic transition, in which a molecule absorbs a photon and undergoes a transition from state *a* to state *b*. If such a transition involves the electric component of the absorbed light, such as will be considered in this thesis, then one can define the following transition moment:

$$\boldsymbol{M} = \langle \psi' | \boldsymbol{\mu} | \psi'' \rangle \qquad \text{Eq. 1.12}$$

Where $\boldsymbol{M}$ is the transition moment, ψ'' is the lower state wavefunction and ψ' the upper state wavefunction, and $\boldsymbol{\mu}$ is the electric dipole moment operator. The square of the transition moment gives the transition probability, and so the above obviously relates to transition intensity. As such, if $\boldsymbol{M} = 0$, the transition is electric dipole forbidden, and if $\boldsymbol{M} \neq 0$, the transition is electric dipole allowed.

1.E.1. Electronic transitions

Bearing this general case in mind, one might consider explicitly an electronic transition:

$$\boldsymbol{M}_e = \langle \psi'_e(\boldsymbol{q}) | \boldsymbol{\mu} | \psi''_e(\boldsymbol{q}) \rangle \qquad \text{Eq. 1.13}$$

Here, $\boldsymbol{M}_e$ is the electronic transition moment, and the upper and lower wavefunctions correspond to the two electronic states involved in the transition; these depend on the electronic coordinates, $\boldsymbol{q}$. $\boldsymbol{\mu}$ is the electric dipole moment operator, as above, which has components along the three Cartesian axes, such that one can define:

$$\boldsymbol{\mu} = \mu_x + \mu_y + \mu_z \qquad \text{Eq. 1.14}$$

An electronic transition will be polarised along one of these axes. Since it is only necessary to determine if the integral in Eq. 1.13 will be zero or non-zero, one can carry out a simple symmetry-based analysis.

Taking the example of the $S_1 \leftarrow S_0$ transition of *p*DFB, D_{2h} is the appropriate point group based upon the symmetry of the molecule, and the S_0 and S_1 states are known to have A_g and B_{2u} symmetries respectively[40]. This assumes that the *z*-axis is along the C-F bonds, the *x*-axis is perpendicular to the plane of the molecule, and the molecule lies in the *yz* plane. Using the D_{2h} character table, one can establish that the components of $\boldsymbol{\mu}$ along the *x*, *y* and *z* axes transform as the symmetries B_{3u}, B_{2u} and B_{1u} respectively. With this knowledge, and the understanding that for $\boldsymbol{M}_e$ to be non-zero, the integral must resolve as totally symmetric (A_g symmetry), one can write:

$$\psi'_e(\boldsymbol{q}) \otimes \psi''_e(\boldsymbol{q}) \supset B_{3u}, B_{2u}\ or\ B_{1u}$$

Here, the product of the two electronic wavefunction symmetries is B_{2u}, which shows that the electronic transition is allowed and polarised along the *y*-axis. To avoid the possible switches in symmetries when using Cartesian axes, one might instead opt to use the principal axes of the molecule of interest, *a*, *b* and *c*, which are defined based upon the moments of inertia about the three axes[d], and are thus unique (at least for the molecules in this thesis). As such, this transition discussed for *p*DFB could also be said to be *b*-polarised, and this is the general case for the $S_1 \leftarrow S_0$ electronic transition in substituted benzene molecules.

1.E.2. Photoionisation transitions

The work in this thesis will use the REMPI technique to probe the $S_1 \leftarrow S_0$ transition of substituted benzene molecules, and the ZEKE spectroscopy technique to probe the $D_0^+ \leftarrow S_1$ transition. Having considered the electronic excitation in the previous section, the photoionisation process shall now be discussed briefly.

[d] The moment of inertia (I) about the *a*-axis, I_a, is the smallest one, the one about the *c*-axis, I_c, is the largest, and the one about the *b*-axis, I_b, takes an intermediate value, with all three axes perpendicular.

This is similar to the electronic transition, but now there is the ejection of an electron:

$$\boldsymbol{M}_e = \langle \psi_e^+(\boldsymbol{q})\chi_e|\boldsymbol{\mu}|\psi_e''(\boldsymbol{q})\rangle \qquad \text{Eq. 1.15}$$

Where ψ_e'' and ψ_e^+ are the wavefunctions for the intermediate (here S_1) and cationic (here D_0^+) electronic states, and χ_e represents the wavefunction of the ejected electron. This electron takes symmetries which derive from the molecular orbital which it was ejected from.

In the ZEKE technique used in this thesis, however, the situation is subtly different, owing to exciting the electron to a high-lying Rydberg orbital prior to ionisation, as discussed in Chapter 2. In this case, χ_e represents the symmetry of this Rydberg orbital, and one can write the symmetry of the Rydberg state as $\psi_e^+ \otimes \chi_e$. Thus, in theory, for $\boldsymbol{M}_e$ to be non-zero, one simply needs to excite the electron to a Rydberg orbital of the correct symmetry. Since the symmetries of the Rydberg orbitals which are occupied before the ionisation in the ZEKE experiments of this thesis are not known, it makes it slightly trickier to discuss the "allowed" photoionisation transitions. It is noted that, if one assumes that the Rydberg orbital (and thus the Rydberg state) can take any symmetry, then effectively any photoionisation transition would be allowed. However, from the spectra presented later, it appears that specific non-totally symmetric vibrations appear in the spectra, rather than all vibrations as the above approach would suggest; this will be addressed in Chapter 3, where a brief discussion of potential mechanisms for the appearance of non-totally symmetric vibrations is provided.

1.E.3. Vibrational and torsional structure

In general, one could write the expression for the intensity of a transition from a vibrational level in one electronic state (a vibronic state) to another vibronic state as:

$$\boldsymbol{M}_{ev} = \langle \psi_{ev}'(\boldsymbol{q})|\boldsymbol{\mu}|\psi_{ev}''(\boldsymbol{q})\rangle \qquad \text{Eq. 1.16}$$

Here, $\boldsymbol{M}_{ev}$ is the vibronic transition moment. Depending on whether the BO approximation holds, one can factorise the vibronic wavefunctions given here into electronic and vibrational wavefunctions. This BO approximation case will be dealt with first, and subsequently the case where the BO approximation does not hold, and they cannot be factorised, will be discussed.

1.E.3.1. Within the Born-Oppenheimer approximation

Considering first the situation that arises under the BO approximation, separating the electronic and vibrational degrees of freedom, one finds:

$$\boldsymbol{M}_{ev} = \langle \psi'_e(\boldsymbol{q}) | \boldsymbol{\mu} | \psi''_e(\boldsymbol{q}) \rangle \langle \psi'_v | \psi''_v \rangle \qquad \text{Eq. 1.17}$$

Where the first integral is for the standard electronic transition discussed above, and so for the *p*DFB $S_1 \leftarrow S_0$ transition this would be *b*-polarised, and the second integral is a vibrational overlap integral, the square of which is the Franck-Condon Factor (FCF). This describes the intensity of a transition from a vibrational level in the lower electronic state to a vibrational level in the upper electronic state. When the overlap between these wavefunctions is significant, the transition will have significant intensity.

It is an important fact that the Franck-Condon principle assumes that an electronic transition takes place much faster than any motion of the nuclei, i.e. the nuclei are essentially stationary during the electronic transition, and one thus observes a vertical transition, which is easiest to visualise in the case of a diatomic molecule, with potential energy curves for the two electronic states.

One can think of two regimes for Franck-Condon activity. If there is a significant change in the geometry of the molecule, between the initial and final electronic states, or a significant change in the vibrational character from the initial to the final vibrational level, then one would expect to observe a vibrational progression. This can be most easily visualised for a diatomic molecule, by shifting the excited state potential to longer (or shorter) equilibrium internuclear separations, where one will get wavefunction overlap with several levels in the

excited state potential. Alternatively, if the geometries are very similar (and the vibrational character is very similar), one would expect a single intense transition from the initial vibrational level to the same vibrational level in the final electronic state. This can again be visualised for the diatomic case, but this time with the two potentials having the same equilibrium internuclear separation, and thus significant wavefunction overlap with only a single level in the excited potential. The Franck-Condon principle applies in both electronic and photoelectron spectroscopy and forms the basis of vibrational assignments in such spectra.

It is notable that for the transition in Eq. 1.17 to have intensity, both the electronic integral and the vibrational overlap integral must be non-zero. For the latter, this means that the initial and final vibrational wavefunctions must be of the same symmetry, and so if the molecule starts in the zero-point level for its vibrations, i.e. a totally symmetric level, then the FCF will only be non-zero for totally symmetric final vibrational levels.

As this thesis is focused on the molecules *p*FT and *p*Xyl, it is sensible to ask how transitions to torsional and vibtor levels could occur. One can answer this by looking at a generalised form of the FCF:

$$\mathrm{FCF} = \left\langle \psi_i' \middle| \psi_j'' \right\rangle^2 \qquad \text{Eq. 1.18}$$

Here the two wavefunctions are general, and can be vibrational, torsional or vibtor levels. As such, if the two levels are of the same symmetry, the transition can have intensity, regardless of whether the two levels are torsional, vibrational or vibtor in character. This does not mean that there will be significant intensity, merely that the transition could have intensity; a point which will be returned to in the next section. In this thesis, transitions like these involving vibrations, torsions or vibtor levels will be referred to as “symmetry-allowed”.

1.E.3.2. Outside the Born-Oppenheimer approximation

1.E.3.2.1. Vibration-electronic transitions

This above case assumes the separability of the electronic and vibrational degrees of freedom, i.e. the BO approximation. If these are non-separable, then the BO approximation breaks down and one should consider vibronic coupling. This differs from the above as the electronic and vibrational wavefunctions can no longer be separated:

$$\boldsymbol{M}_{ev} = \langle \psi'_{ev}(\boldsymbol{q}) | \boldsymbol{\mu} | \psi''_{ev}(\boldsymbol{q}) \rangle \qquad \text{Eq. 1.19}$$

Now there is only one integral, with the lower and upper vibronic state wavefunctions ψ''_{ev} and ψ'_{ev} illustrating the coupling of the vibrational and electronic degrees of freedom. Thus, for this integral to be non-zero, one can see that:

$$\psi'_{ev}(\boldsymbol{q}) \otimes \psi''_{ev}(\boldsymbol{q}) = \ \psi'_{e}(\boldsymbol{q}) \otimes \psi'_{v} \otimes \psi''_{e}(\boldsymbol{q}) \otimes \psi''_{v} \supset \mu_a, \mu_b \ or \ \mu_c$$

Unlike in the BO case, one is not limited to the electronic transition being *b*-type for a substituted benzene molecule, as the vibrational wavefunctions now also contribute to this integral. This allows one to deduce a larger selection of allowed transitions, by virtue of vibronic coupling. For example, if one continues the *p*DFB example above, and assumes ψ''_{v} is the zero-point level, i.e. of A_g symmetry¸ and the initial electronic state is S_0 (A_g), then:

$$\psi'_{e}(\boldsymbol{q}) \otimes \psi'_{v} \supset B_{3u}, B_{2u} \ or \ B_{1u}$$

If ψ'_{e} is the S_1 (B_{2u}) state:

$$B_{2u} \otimes \psi'_{v} \supset B_{3u}, B_{2u} \ or \ B_{1u}$$

Which can be satisfied for:

a-type transitions to ψ_v' of b_{3g} symmetry,

b-type transitions to ψ_v' of a_g symmetry, and

c-type transitions to ψ_v' of b_{1g} symmetry

The *b*-type transition is effectively the same answer as one would get within the BO approximation on Franck-Condon grounds, although here these transitions would be allowed on vibronic coupling grounds. The *a*-type and *c*-type transitions were forbidden within the BO approximation above. The fact that, when one includes vibronic coupling, the *b*-type transitions to vibrations of A_g symmetry can have intensity on Franck-Condon grounds and/or from vibronic coupling is another reason why transitions between vibrational levels of the same symmetry are referred to as "symmetry-allowed" rather than "Franck-Condon allowed" in this thesis; the spectra do not imply whether the intensity is Franck-Condon or arises from vibronic coupling.

One way of interpreting intensity owing to vibronic coupling is Herzberg-Teller intensity stealing[41], which arises due to a dependence of the electronic transition moment, $\boldsymbol{M}_e$, on the nuclear (vibrational) motions. As a starting point, one can return to this familiar, BO separated, equation:

$$\boldsymbol{M}_{ev} = \langle \psi_e'(\boldsymbol{q})|\boldsymbol{\mu}|\psi_e''(\boldsymbol{q})\rangle \langle \psi_v'|\psi_v''\rangle = \boldsymbol{M_e} \langle \psi_v'|\psi_v''\rangle \qquad \text{Eq. 1.20}$$

Where $\boldsymbol{M_e}$ represents the electronic transition moment, as above. Herzberg and Teller recognised that $\boldsymbol{M_e}$ can change during a vibration (i.e. the electronic wavefunctions are dependent on the vibrational coordinates) when the vibrational overlap integral is non-totally symmetric, implying a breakdown of the Franck-Condon approximation, as one will recall that the Franck-Condon principle assumes stationary nuclei during the electronic transition, and this is no longer the case.

The way that they accounted for this dependence was to employ a Taylor expansion[36,42] of $\boldsymbol{M}_e$ in terms of the vibrational coordinates, Q_i. This can be written as:

$$\boldsymbol{M_e} = (\boldsymbol{M_e})_{\boldsymbol{eq}} + \sum_i \left(\frac{\partial \boldsymbol{M_e}}{\partial Q_i}\right)_{eq} Q_i + \frac{1}{2!}\sum_{i,j}\left(\frac{\partial^2 \boldsymbol{M_e}}{\partial Q_i Q_j}\right)_{eq} Q_i Q_j + \cdots \quad \text{Eq. 1.21}$$

Where this expansion is carried out about the equilibrium structure, and so is implicitly assuming only small changes to the geometry.

One can then combine this expression for $\boldsymbol{M}_e$ with that for $\boldsymbol{M}_{ev}$:

$$\boldsymbol{M}_{ev} = (\boldsymbol{M}_e)_{eq}\langle\psi_v'|\psi_v''\rangle + \sum_i \left(\frac{\partial \boldsymbol{M}_e}{\partial Q_i}\right)_{eq} Q_i \langle\psi_v'|\psi_v''\rangle + \frac{1}{2!}\sum_{i,j}\left(\frac{\partial^2 \boldsymbol{M_e}}{\partial Q_i Q_j}\right)_{eq} Q_i Q_j \langle\psi_v'|\psi_v''\rangle \quad \text{Eq. 1.22}$$

Or, expanding out the bra-ket notation:

$$\boldsymbol{M}_{ev} = (\boldsymbol{M}_e)_{eq}\int \psi_v'\psi_v''\, d\tau + \sum_i \left(\frac{\partial \boldsymbol{M}_e}{\partial Q_i}\right)_{eq}\int \psi_v'\, Q_i\, \psi_v''\, d\tau + \frac{1}{2!}\sum_{i,j}\left(\frac{\partial^2 \boldsymbol{M_e}}{\partial Q_i Q_j}\right)_{eq}\int \psi_v'\, Q_i Q_j \psi_v''\, d\tau \quad \text{Eq. 1.23}$$

One can consider the first (zero-order) term to be equivalent to the starting point, i.e. effectively an electronic transition and a Franck-Condon factor. For an initial vibrational level which is totally symmetric, this term will be zero for non-totally symmetric final vibrational levels, as expected. The second term (first order) is the first one that can account for vibronic coupling, as it is possible for this term to be non-zero. It represents a dependence of the transition moment on a vibrational coordinate, Q_i. This can be thought of as the final vibronic level

having a character similar to a nearby electronic state, allowing intensity to be stolen from an (allowed) transition to that nearby state.

The higher order terms are expected to be smaller (as the Taylor series is expected to converge), and these represent vibrational combinations. For example, the third (second order) term represents the possible vibronic coupling involving the vibrational combination of coordinates Q_iQ_j.

One can now see how transitions to non-totally symmetric vibrational levels might be observed in the spectrum of a substituted benzene molecule, such as the b_{3g} vibrations observed in the $S_1 \leftarrow S_0$ excitation spectrum of *p*DFB[40]. Here, Q_i is a b_{3g} symmetry vibrational coordinate, and for this non-totally symmetric vibration, the first order term in the Taylor expansion can be non-zero. Physically, this represents mixing of the S_1 electronic state (B_{2u}) with b_{3g} vibrational character, yielding a B_{1u} vibronic state, which takes the same symmetry as the S_2 state in *p*DFB, to which a transition is symmetry-allowed from the S_0 state. Thus, the transition to the vibronic B_{1u} level can "steal" intensity from the allowed electronic transition to the S_2 (B_{1u}) state, giving rise to a transition to a non-totally symmetric b_{3g} vibrational level in the $S_1 \leftarrow S_0$ excitation spectrum, which is not expected on Franck-Condon grounds.

1.E.3.2.2. Torsion-electronic transitions

One might also consider the equivalent of vibronic coupling for torsional levels; a torsion-electronic (toronic) coupling. As the theoretical framework of the methyl rotor has yet to be presented, this will be discussed in more detail in Chapter 3 in relation to the single rotor system. Here, it is sufficient to note that one carries out a very similar analysis to that for the vibronic coupling above, but instead of expanding the electronic transition moment as a Taylor series in terms of the vibrational coordinates, one expands the electronic transition moment as a Fourier series (this is chosen rather than a Taylor expansion owing to the large amplitude motion of the methyl group) in terms of the torsional angle, α:

$$\boldsymbol{M}_{et} = \langle \psi'_e(\boldsymbol{q};\alpha)|\boldsymbol{\mu}|\psi''_e(\boldsymbol{q};\alpha)\rangle \langle m'|m''\rangle = \boldsymbol{M}_e(\alpha) \langle m'|m''\rangle \qquad \text{Eq. 1.24}$$

Where m' and m'' are the upper and lower electronic state torsional levels, and $\boldsymbol{M}_{et}$ is the toronic transition moment, which is dependent on the torsional angle. This dependence on the torsional angle introduces toronic coupling in the same way that dependence on the vibrational coordinates, Q_i, introduced vibronic coupling. As such, one imagines an intensity stealing mechanism akin to that described in the vibronic coupling case. For brevity, in this thesis, these couplings involving an electronic state will all be referred to as vibronic coupling, such that this umbrella term refers to vibration-electronic, torsion-electronic, or in the case of a vibration-torsion level, vibration-torsion-electronic coupling. In the latter case, one might imagine a dependence of the transition moment on both Q_i and α.

1.F. Intramolecular vibrational redistribution (IVR)

Having discussed the nature of vibrational levels and how electronic and photoelectron transitions, and their accompanying torsional and vibrational structure, can gain intensity, a return will be made to the simple coupling ideas discussed earlier. Here, these ideas will be generalised in the commonly used framework of IVR, with an overview of the standard terminology relevant to this thesis given. Useful papers for understanding the different IVR regimes and general terminology are the landmark review by Nesbitt and Field[4], as well as work by Reid and co-workers[16,31–33].

1.F.1. Restricted IVR

In discussing IVR, one must consider some standard terminology. In the frequency domain experiments of this thesis, it is always an eigenstate (or multiple overlapping eigenstates) which is (are) excited, and these are inherently time-independent. These may be vibrational, torsional, or vibtor in nature. However, in time domain experiments, where the pulse width is sufficient to coherently excite multiple eigenstates, a wavepacket is formed, which is a superposition of these eigenstates. If one can probe this wavepacket at different

delays after initial excitation, on the same timescale as the phasing and dephasing of the eigenstates in the wavepacket (i.e. a picosecond or femtosecond timescale), one will observe time-dependent behaviour. This arises as, unlike the individual eigenstates, the wavepacket will evolve with time.

Initially, it will be assumed that two eigenstates are excited in the wavepacket and that these correspond to two coupled levels, in a traditional Fermi resonance. It will also be assumed that one of the "uncoupled" levels, known as zero-order states[e] (also referred to as zero-order levels in this thesis), will have a transition to it which is intrinsically bright, while the other is intrinsically dark. The former is referred to as the zero-order bright state, and the latter as the zero-order dark state, in the usual IVR terminology. It is possible for multiple of the excited zero-order states to be bright, rather than just one, and this would further complicate the picture.

Probing immediately after forming the wavepacket (i.e. no delay), one will observe the zero-order bright state from the superposition of eigenstates, and at some later time one will observe the zero-order dark state. If this interaction is truly localised to only these two levels, phasing and dephasing will continue periodically, and probing at many time delays over, for example, hundreds of picoseconds, will lead to the observation of "quantum beating", where the transitions associated with the zero-order bright and dark states oscillate out-of-phase with one another owing to the phasing and dephasing. This is typically referred to as the population "flowing" back and forth between the bright and dark zero-order states. One example of quantum beating relevant to this thesis is found in the study of Davies and Reid[43], who observed a beating pattern over relatively long times when exciting a vibration in *p*FT. This study will be discussed at the relevant point later in this thesis.

This Fermi resonance picture, of two coupled zero-order levels forming two eigenstates, is known as restricted IVR, since the interaction is localised between

[e] These zero-order states can be most sensibly thought of as the (diagonally anharmonic) vibrational normal modes, with the exclusion of the off-diagonal anharmonic coupling between modes. This anharmonic coupling is then what generates the eigenstates from the zero-order states.

the two levels. The Fourier transform of the beating pattern for a particular spectral band over long time then gives the separation of the initially excited eigenstates, which relates to the oscillation period of the beating pattern. This differs from the frequency domain experiments of this thesis, in which the eigenstates are excited, and the projection of these onto the D_0^+ state is used to infer whether the eigenstates arise from interacting zero-order levels or not.

One can imagine a situation where more than two eigenstates are excited in the wavepacket in a time domain experiment. In order to consider this, it is easiest to bear in mind a specific experiment, such as the picosecond time-resolved photoelectron spectroscopy (tr-PES) technique employed by Reid and co-workers[28,29,31–34,43,44]. There, photoelectron spectra are recorded at different time delays after the initial wavepacket formation, and the transitions observed will change in intensity as the eigenstates in the wavepacket phase and dephase. If all of the zero-order levels which the eigenstates are composed of yield transitions to the same level in the D_0^+ state (such as all having a transition to the D_0^+ zero-point level), the beating pattern observed at this cationic internal energy over time will be complicated, owing to the superposition of multiple beating patterns from the multiple eigenstates phasing and dephasing. The Fourier transform will then yield multiple eigenstate separations.

Continuing the photoelectron spectroscopy example used above, a frequency-resolved photoelectron spectrum, such as the ZEKE spectra of this thesis, would project the S_1 eigenstate(s) excited onto the D_0^+ state. The projection of the S_1 eigenstates onto the D_0^+ eigenstates allows the zero-order contributions to be determined, at least qualitatively. There are some assumptions in this, such as the levels being coupled in the S_1 state but not in the D_0^+ state, and the vibrations taking the same form in both states, but these are both commonly true, as will be seen throughout this thesis. This allows qualitative conclusions on eigenstate makeup to be drawn from the frequency domain experiments of this thesis, and the results compared to previous time domain studies.

1.F.2. Doorway states and statistical IVR

The restricted IVR discussed above occurs between a small number of levels, with time domain experiments showing no population loss over long timescales. In contrast to this, statistical IVR is the coupling of the bright state (or states) to the "bath" of nearby (dark) states (i.e. many nearby states which can be coupled to). In time domain spectra, such as those from tr-PES, if one looks at the time-dependence of a particular band, statistical IVR is manifested as an exponential decay of the intensity. This is rationalised as population loss from the zero-order bright state, which gives rise to that transition at zero time delay, with the population transferred to the bath of states. An example of this is given in the recent work of Davies *et al*. on *p*FT[33]. In a frequency domain spectrum, one can imagine that there are many eigenstates resulting from the coupling of many zero-order levels. As such, a photoelectron spectrum recorded *via* an eigenstate may have its intensity spread among many levels in the cation[f], leading to broad, structureless, spectra. This is a typical sign of statistical IVR.

There is also an intermediate regime. The exponential decay observed in the time domain experiments discussed above suggests that the bright state is directly coupled to the bath of states. However, it could be coupled to the bath of states *via* another level, often called a "doorway state", and in this case, the time-dependence would show a quantum beating superimposed on an exponential decay. This represents the phasing and dephasing of the eigenstates (or the population "moving" between the zero-order bright state and the doorway state), with a gradual loss of population to the bath of states as it "leaks" out of the doorway state. In frequency domain experiments, it may be harder to elucidate the influence of a doorway state. Here, one must record spectra *via* multiple S_1 eigenstates, and look to see if there is evidence of restricted IVR between certain levels alongside evidence of widespread coupling, something that will be discussed later in this thesis.

[f] Assuming that the S_1 eigenstate is composed of many coupled zero-order levels which are not coupled in the cation, i.e. the zero-order levels and eigenstates in the cation are effectively the same. This is a reasonable approximation, since many vibrations change their wavenumber significantly between the S_1 and D_0^+ states.

An alternative interpretation of the quantum beating superimposed on an exponential decay would be that the bright state is coupled to many states, but coupled more strongly to one particular state, which yields the beating pattern. Here, the doorway state would not be needed. It is difficult to distinguish between these two possibilities, and if there are multiple bright states it becomes even more complex, with the possibility of one of the bright states acting as a doorway state for the other, while itself being directly coupled to the bath of states.

These different IVR regimes - restricted, doorway state-dominated and statistical - depend on the number of nearby levels and whether the bright state being excited is coupled to them or not. As such, the prevalence of IVR increases at higher internal energies, since the density of states is increasing. This is illustrated by Fermi's Golden Rule[4], which suggests that the exponential decay of the bright state population observed in the time domain experiments correlates with the density of dark states, but is also related to the strength of coupling to these. Doorway states could mediate access to the bath of states, and this could potentially occur at lower internal energies than direct access in statistical IVR, as would be predicted by Fermi's Golden Rule. A discussion of the density of states of *p*ClFB, *p*DFB, *p*FT and *p*Xyl is provided in Chapter 7 of this thesis, to support the observations made from the REMPI and ZEKE spectra presented.

As a guide to the reader on where statistical IVR becomes prevalent in different molecules, the dispersed fluorescence spectra of Parmenter and Stone[25] show well-resolved vibrational structure when exciting at ~0^0+1600 cm^{-1} for *p*DFB, while for *p*FT, structure is completely lost at this internal energy. These spectra were recorded at 300 K, and so show more congestion than ZEKE spectra presented in this thesis at similar internal energies, but still give the reader an idea of the statistical IVR onset in *p*DFB and *p*FT. The lower internal energy statistical IVR onset for *p*FT compared to *p*DFB was proposed to be due to the influence of the methyl group, and the frequency domain spectra presented in reference 25 were supported by IVR lifetimes from chemical timing experiments; IVR lifetimes of ~10 ps for *p*FT and 290 ps for *p*DFB were given for exciting a level ~0^0+1600 cm^{-1} in each molecule. The influence of the methyl

group on the onset of statistical IVR, and the prevalence of restricted couplings at low internal energies, are explored in this thesis, which also attempts to account for the changing molecular symmetry between *p*DFB and *p*FT by introducing comparisons to *p*Xyl and *p*ClFB.

Finally, one should consider the strength of coupling between levels. This can be loosely correlated with the quanta changes between the coupled levels, with a smaller change indicating a stronger coupling, as discussed by Nesbitt and Field[4]. This is known as the tier model of IVR. Assuming a single zero-order bright state (which does not have to be the case), this is most strongly coupled to a few nearby levels (with small quanta changes), known as Tier 1. Tier 2 represents larger quanta changes from the bright state, and thus weaker couplings, with the same again for Tier 3. One can easily understand the concept of a doorway state within the tier model; for example, if a level in Tier 1 couples strongly to the bright level, and to many levels in Tier 2 or 3 more strongly than the bright level couples to them directly, it will be acting as a doorway state.

1.G. Vibrational labelling

This thesis uses the D_i, *para*-disubstituted benzene, labelling scheme proposed by our group[45], which was a natural extension of previous work on a monosubstituted benzene molecule labelling scheme[46]. Briefly, the D_i notation takes the vibrational modes of *p*DFB, and places them in a C_{2v} Mulliken[47] ordering (i.e. a_1, a_2, b_1 then b_2 symmetry, with vibrations ordered from high to low wavenumber within each). The forms of these vibrations were shown in reference 45 to be effectively the same for a range of substituents, both monatomic and polyatomic, of different masses, and with different force constants for the bond connecting them to the benzene ring. This allows the same label to be used for the same vibration in different molecules, and this is applicable to the *p*DFB, *p*ClFB, *p*FT and *p*Xyl molecules discussed in this thesis. Schemes used previously by others, such as the Mulliken[47], Wilson[48] and Varsányi[49] labelling schemes, do not lend themselves to comparisons between molecules, since different labels end up being applied to effectively the same

vibration in different molecules. As such, the use of a consistent labelling scheme throughout this thesis aids in the comparison between molecules.

Note that, as this labelling scheme is based on *p*DFB, it includes only ring-localised vibrations. While for *p*FT and *p*Xyl, there are additional methyl-localised vibrations, these are not considered in this thesis, primarily because there is no evidence of their involvement in the excitation spectra of halotoluene or xylene molecules. This makes sense, as the electronic transition is ring-localised, and so the methyl-localised vibrations are not going to have significant FCFs. Additionally, they tend to be at higher wavenumbers; for example, for *p*Xyl, there are only a handful of methyl-localised vibrations in the 0 – 1400 cm^{-1} range considered in this thesis, with none below 800 cm^{-1}, and so they can be safely neglected.

Additionally, while the vast majority of ring-localised vibrations remain the same when the molecule is asymmetrically substituted (such as in the *p*ClFB or *p*FT cases), some of the vibrational modes become more localised. This is most apparent with D_5 and D_6, where in the symmetrically-substituted *p*DFB and *p*Xyl molecules these are symmetric and asymmetric carbon-substituent stretches. For *p*ClFB and *p*FT these become local modes, with D_5 a carbon-fluorine stretch, and D_6 a carbon-chlorine or carbon-methyl stretch in *p*ClFB and *p*FT respectively. This is a point worth bearing in mind when comparing the spectra of the molecules, and one which will be returned to in Chapter 7.

Finally, the vibrational mode diagrams for the thirty D_i modes given in reference 45 are reproduced here in Appendix A, so that the reader can see the motions of the vibrations under discussion throughout this thesis.

1.H. References

[1] Y. He, C. Wu, and W. Kong, *J. Phys. Chem. A*, **107**, 5145 (2003).

[2] C.S. Byskov, F. Jensen, T.J.D. Jørgensen, and S.B. Nielsen, *Phys. Chem. Chem. Phys.*, **16**, 15831 (2014).

[3] E.R. Gonzaga, *Am. J. Clin. Dermatol.*, **10** (suppl. 1), 19 (2009).

[4] D.J. Nesbitt and R.W. Field, *J. Phys. Chem.*, **100**, 12735 (1996).

[5] N.D.N. Rodrigues, M. Staniforth, and V.G. Stavros, *Proc. R. Soc. A*, **472**, (2016).

[6] L.A. Baker, B. Marchetti, T.N. V. Karsili, V.G. Stavros, and M.N.R. Ashfold, *Chem. Soc. Rev.*, **46**, 3770 (2017).

[7] H. Kang, B. Jung, and S.K. Kim, *J. Chem. Phys.*, **118**, 6717 (2003).

[8] S. Matsika, *J. Phys. Chem. A*, **108**, 7584 (2004).

[9] D.S.N. Parker, R.S. Minns, T.J. Penfold, G.A. Worth, and H.H. Fielding, *Chem. Phys. Lett.*, **469**, 43 (2009).

[10] P.M. Felker and A.H. Zewail, *J. Chem. Phys.*, **82**, 2961 (1985).

[11] P.M. Felker and A.H. Zewail, *J. Chem. Phys.*, **82**, 2975 (1985).

[12] P.M. Felker and A.H. Zewail, *J. Chem. Phys.*, **82**, 2994 (1985).

[13] R.A. Coveleskie, D.A. Dolson, and C.S. Parmenter, *J. Phys. Chem.*, **89**, 645 (1985).

[14] R.A. Coveleskie, D.A. Dolson, and C.S. Parmenter, *J. Phys. Chem.*, **89**, 655 (1985).

[15] D. Boyall and K.L. Reid, *Chem. Soc. Rev.*, **26**, 223 (1997).

[16] K.L. Reid, *Int. Rev. Phys. Chem.*, **27**, 607 (2008).

[17] D.B. Moss and C.S. Parmenter, *J. Chem. Phys.*, **98**, 6897 (1993).

[18] H.J. Elston, E.R. Davidson, F.G. Todd, and C.S. Parmenter, *J. Phys. Chem.*, **97**, 5506 (1993).

[19] Z.-Q. Zhao and C.S. Parmenter, *Ber. Bunsenges. Phys. Chem.*, **99**, 536 (1995).

[20] D.A. Dolson, C.S. Parmenter, and B.M. Stone, *Chem. Phys. Lett.*, **81**, 360 (1981).

[21] C.S. Parmenter, *J. Phys. Chem.*, **86**, 1735 (1982).

[22] K.W. Holtzclaw and C.S. Parmenter, *J. Phys. Chem.*, **88**, 3182 (1984).

[23] K.W. Holtzclaw and C.S. Parmenter, *J. Chem. Phys.*, **84**, 1099 (1986).

[24] D.A. Dolson, K.W. Holtzclaw, D.B. Moss, and C.S. Parmenter, *J. Chem. Phys.*, **84**, 1119 (1986).

[25] C.S. Parmenter and B.M. Stone, *J. Chem. Phys.*, **84**, 4710 (1986).

[26] D.B. Moss, C.S. Parmenter, and G.E. Ewing, *J. Chem. Phys.*, **86**, 51 (1987).

[27] Z.-Q. Zhao, C.S. Parmenter, D.B. Moss, A.J. Bradley, A.E.W. Knight, and K.G. Owens, *J. Chem. Phys.*, **96**, 6362 (1992).

[28] S.M. Bellm, P.T. Whiteside, and K.L. Reid, *J. Phys. Chem. A*, **107**, 7373 (2003).

[29] A.K. King, S.M. Bellm, C.J. Hammond, K.L. Reid, M. Towrie, and P. Matousek, *Mol. Phys.*, **103**, 1821 (2005).

[30] C.J. Hammond, V.L. Ayles, D.E. Bergeron, K.L. Reid, and T.G. Wright, *J. Chem. Phys.*, **125**, 124308 (2006).

[31] J.A. Davies and K.L. Reid, *J. Chem. Phys.*, **135**, 124305 (2011).

[32] J.A. Davies, A.M. Green, A.M. Gardner, C.D. Withers, T.G. Wright, and K.L. Reid, *Phys. Chem. Chem. Phys.*, **16**, 430 (2014).

[33] J.A. Davies, L.E. Whalley, and K.L. Reid, *Phys. Chem. Chem. Phys.*, **19**, 5051 (2017).

[34] J. Midgley, J.A. Davies, and K.L. Reid, *J. Phys. Chem. Lett.*, **5**, 2484 (2014).

[35] K.L. Reid, T.A. Field, M. Towrie, and P. Matousek, *J. Chem. Phys.*, **111**, 1438 (1999).

[36] J.M. Hollas, *High Resolution Spectroscopy*, Second Ed. (Wiley, Chichester,

1998).

[37] E. Fermi, *Z. Phys.*, **71**, 250 (1931).

[38] B.T. Darling and D.M. Denison, *Phys. Rev.*, **57**, 128 (1940).

[39] E. Hudspeth, D.A. McWhorter, and B.H. Pate, *J. Chem. Phys.*, **109**, 4316 (1998).

[40] A.E.W. Knight and S.H. Kable, *J. Chem. Phys.*, **89**, 7139 (1988).

[41] G. Herzberg and E. Teller, *Z. Phys. Chem.*, **B21**, 410 (1933).

[42] A. Ellis, M. Feher, and T. Wright, *Electronic and Photoelecton Spectroscopy: Fundamentals and Case Studies* (Cambridge University Press, Cambridge, 2005).

[43] J.A. Davies and K.L. Reid, *Phys. Rev. Lett.*, **109**, 193004 (2012).

[44] J.A. Davies, K.L. Reid, M. Towrie, and P. Matousek, *J. Chem. Phys.*, **117**, 9099 (2002).

[45] A. Andrejeva, A.M. Gardner, W.D. Tuttle, and T.G. Wright, *J. Mol. Spectrosc.*, **321**, 28 (2016).

[46] A.M. Gardner and T.G. Wright, *J. Chem. Phys.*, **135**, 114305 (2011).

[47] R.S. Mulliken, *J. Chem. Phys.*, **23**, 1997 (1955).

[48] E.B. Wilson Jr., *Phys. Rev.*, **45**, 706 (1934).

[49] G. Varsányi, *Assignments of the Vibrational Spectra of Seven Hundred Benzene Derivatives* (Wiley, New York, 1974).

2. Methodology

2.A. Experimental techniques

For the resonance-enhanced multiphoton ionisation (REMPI) and zero-electron-kinetic-energy (ZEKE) photoelectron spectroscopy (PES) experiments performed for this thesis, a single experimental apparatus was used. The two techniques will be discussed first, followed by a discussion of the principles of supersonic jet expansions.

2.A.1. Resonance-enhanced multiphoton ionisation (REMPI) spectroscopy

There are several techniques which are commonly utilised to record electronic excitation spectra of gaseous molecules, with REMPI and laser-induced fluorescence (LIF) being the most common laser-based ones. To some extent, REMPI is more flexible than LIF, as the latter requires the molecule to fluoresce while the former has no such requirement. Additionally, REMPI spectroscopy can be readily used alongside ZEKE spectroscopy to study both an intermediate electronic state and the cationic ground state, as in this thesis.

In the first step of a REMPI process, the molecule is excited to a particular level in an excited electronic state, known as the intermediate level. In this work, this is a level in the first excited singlet state, S_1. In this thesis, this step is a single photon absorption, but it can also be a multiphoton absorption. The second step is the ionisation of the intermediate level, and again in this thesis this step utilises a single photon. The generated ions are then detected by time-of-flight (TOF) mass spectrometry, which allows ions of different masses to be separated and thus only the molecule of interest to be detected, and, where applicable, a particular isotopologue of the molecule. A significant number of ions are only generated when the excitation photon is resonant with a transition to an S_1 state level, and so one can scan the excitation photon energy and monitor the ion current to generate an excitation spectrum. Although non-resonant ions can also

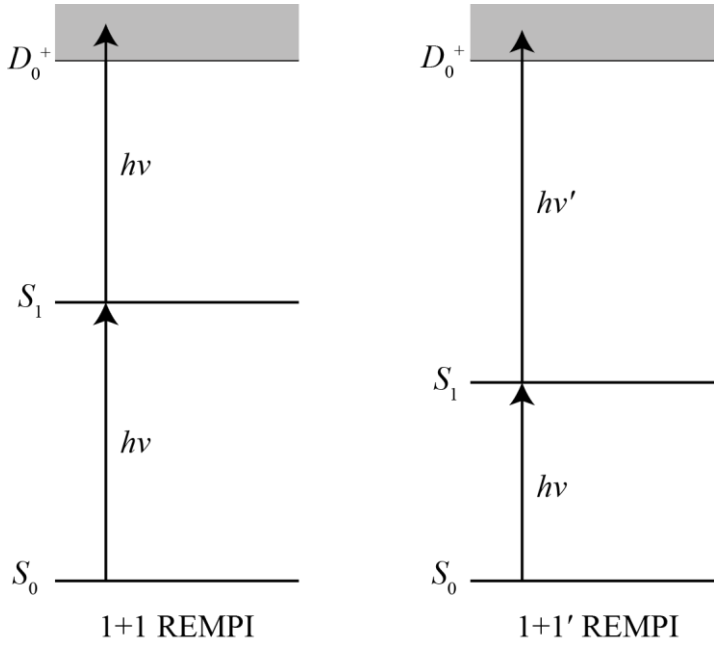


Figure 2.1 – Schematic depictions of 1+1 (left) and 1+1′ (right) REMPI processes.

be generated, the powers of the excitation and ionisation lasers can be adjusted to minimise their generation.

When one photon is used to excite, and another photon of the same energy is used to ionise the molecule, this is referred to as a 1+1 REMPI process, as illustrated on the left side of Figure 2.1. However, an alternative is to use a single photon of a different energy to the excitation photon to ionise the molecule, in what is called a 1+1′ REMPI process, where the 1′ indicates a different photon energy for the ionisation photon compared to the excitation one. This is illustrated on the right side of Figure 2.1. A REMPI process involving photons of the same energy (such as 1+1 REMPI) is referred to as a one-colour process, while if it involves photons of different energy (such as 1+1′ REMPI) it is referred to as a two-colour process.

In this thesis, both 1+1 and 1+1′ REMPI spectra will be shown. For the molecules *para*-xylene (*p*Xyl) and *para*-fluorotoluene (*p*FT), which are the focus of this thesis, 1+1 REMPI spectra were recorded. However, for *para*-difluorobenzene (*p*DFB) and *para*-chlorofluorobenzene (*p*ClFB), 1+1′ REMPI spectra are presented. This is because for *p*DFB and *p*ClFB, the S_1 state lies slightly below the midpoint of the S_0 and D_0^+ states, which means a 1-colour

REMPI spectrum would require a 1+2 photon process to ionise the low-lying S_1 levels. As such, a 2-colour, 1+1′, approach was taken, where this single photon ionisation can occur across the whole of the spectral range of interest.

It is noted that the resolution in REMPI spectroscopy is limited by the laser bandwidth (here, ~0.3 cm^{-1} for the doubled, UV, output of the dye lasers used), and the bands in the REMPI spectra presented in this thesis have full-width at half-maximum (FWHM) values of ~4 cm^{-1}, depending on the levels involved.

2.A.2. Zero-electron-kinetic-energy (ZEKE) photoelectron spectroscopy (PES)

To investigate the nature and possible couplings of different S_1 levels, photoelectron spectra have been recorded *via* different intermediate levels, using the technique of ZEKE spectroscopy in the form of ZEKE pulsed-field ionisation (PFI).

In a "true" ZEKE experiment, an intermediate level is excited with a fixed photon energy, and then the molecule is ionised to a particular cationic level with a photon that is resonant with that transition, such that electrons are generated that have zero kinetic energy. This process can generate both zero kinetic energy and kinetic energy electrons (with the latter from excitation to lower cationic levels, with the excess photon energy converted to electron kinetic energy). To separate these, one waits a short time (usually a few microseconds) for the kinetic energy electrons to leave the detection region, before applying an electric field to attract or repel the remaining (ZEKE) electrons to the detector. One can scan the ionisation laser through the levels of the cation, detecting only ZEKE electrons, to give a high-resolution photoelectron spectrum, with the resolution of such a "true" ZEKE experiment determined by the laser bandwidth.

In practice, this "true" ZEKE experiment is hard to achieve. Although some "true" ZEKE electrons will be formed, there is an alternative process which also occurs involving the high lying Rydberg levels of a molecule. In this process,

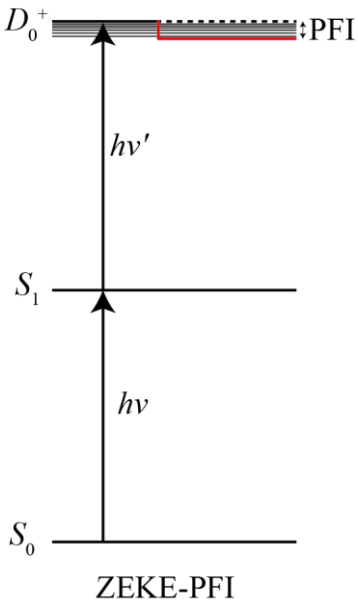


Figure 2.2 – Schematic depiction of the ZEKE-PFI technique employed. The red line indicates the effective lowering of the ionisation energy by the pulsed electric field, allowing ionisation of a range of Rydberg levels, shown just below the D_0^+ state.

the second photon in the ZEKE experiment excites an electron to one of these Rydberg levels, lying just below the ionisation energy of the molecule. Such Rydberg levels are atomic-like orbitals spatially distant from the ionic core, and these (high lying) Rydberg levels have long lifetimes, on the order of tens of microseconds[1,2]. They can be ionised by stray electric fields in the apparatus, and the ZEKE-PFI technique, illustrated in Figure 2.2, involves applying an electric field with the intention of ionising them, rather than trying to obtain "true" ZEKE electrons. The difficulty of shielding against ionising stray fields is the key reason why ZEKE-PFI is commonly employed instead of "true" ZEKE spectroscopy.

One might note that the ionisation energy obtained from pulsed-field ionisation will be slightly lower than that of a "true" ZEKE experiment[3], with field ionised electrons having been confused with "true" ZEKE electrons in early work[4]. No attempt is made to account for this lowering in the present work.

In the experiments carried out for this thesis, after exciting to the Rydberg levels, a pulsed (positive) field is applied after a delay of 2 μs to ionise the Rydberg levels and attract the PFI electrons towards the detector. These field-ionised "ZEKE electrons" (or "PFI electrons"), while not "true" ZEKE electrons, will still be referred to as ZEKE electrons in the remainder of this thesis for simplicity.

The resolution of the ZEKE-PFI technique (simply referred to as ZEKE spectroscopy throughout this thesis) is poorer than "true" ZEKE, as the resolution is now determined by the width of the slice of Rydberg levels ionised by the pulsed electric field. In the work presented here, a field of ~10 V cm^{-1} is applied, and ZEKE bands are observed with a FWHM of as low as ~7 cm^{-1}. This is a much lower FWHM than would be expected for this applied field, owing to the well-known rapid decay of low-lying Rydberg states[2,5], which allows one to obtain relatively narrow ZEKE bands even with higher pulsed fields. As such, although the resolution is poorer than for "true" ZEKE, ZEKE-PFI is still of significantly higher resolution than other, traditional, photoelectron spectroscopy techniques.

2.A.3 Supersonic jet expansions

When carrying out spectroscopic measurements of a room temperature sample, owing to the population of many rotational (and some excited vibrational) levels, the spectra can become very congested. In this thesis, a supersonic jet expansion is employed to cool these internal degrees of freedom and reduce the spectral congestion, making the interpretation of the spectra more tractable.

The key element of a supersonic jet expansion apparatus is that there is a gas reservoir containing a (relatively) high pressure of a monatomic gas on one side of a very small orifice, and on the other side a very low pressure (vacuum). For context, the experiments in this thesis used ~1.5 bar of argon on the "high pressure" side, with the base vacuum pressure ~10^{-10} bar, achieved using three turbomolecular pumps across two chambers and a time-of-flight tube, backed by rotary pumps. If the mean free path of the gas, λ, is much lower than the diameter of the orifice, D, then collisions will occur between the gas atoms upon passing through the orifice[1]. This slows down atoms which are moving faster, and speeds up atoms which are moving slower, narrowing the velocity distribution. The effect of this is that, on average, the atoms are moving slightly faster than they were in the gas reservoir, but, importantly, there is a much narrower distribution of velocities, and thus, by this measure, the translational temperature of the

sample is very low, and an effectively collision free environment has been created.

The name supersonic arises owing to the speed of the gas exceeding the local speed of sound, i.e. a Mach number of >1. This itself arises owing to the temperature dependence of the local speed of sound, which is proportional to $T^{0.5}$, and so very high Mach numbers (of 50 – 100) can be obtained.[1,6]

If one seeds a sample molecule into this monatomic gas (known as a "carrier gas"), as well as the aforementioned translational cooling, the internal degrees of freedom of the molecule can be cooled. In the region of the orifice, where many collisions are occurring, the monatomic argon carrier gas will collide with the sample molecule and take away excess rotational (and vibrational) energy as translational energy. The propensity for removal of rotational energy is higher than for vibrational energy, as the amount of energy involved is smaller. This is usually not a problem, since most vibrations are effectively in their zero-point level at room temperature, and low frequency vibrations can be cooled in the manner described.

2.B. Experimental apparatus

A schematic of the experimental apparatus used for both the REMPI and ZEKE experiments is given in Figure 2.3, and what follows is a description of the experimental setup.

The vapour above a room temperature sample of *p*FT (99% purity, Alfa Aesar), *p*Xyl (99.5% purity, Sigma-Aldrich), *p*DFB (99% purity, Sigma-Aldrich) or *p*ClFB (98% purity, Aldrich) was seeded into ~1.5 bar of Ar, and the gaseous mixture passed through a General Value puled nozzle (750 μm orifice diameter, operating at 10 Hz with an opening time of 180 – 210 μs) to create the free jet expansion.

The dye laser (Sirah Cobra-Stretch) used to generate the excitation photon was pumped with the third harmonic (355 nm) of either a Surelite I or Surelite III

Nd:YAG laser. This dye laser operated with either the Coumarin 503 or Coumarin 540A laser dye, depending on the region of the excitation spectrum and the molecule, with the output frequency doubled with a BBO crystal.

The dye laser (Sirah Cobra-Stretch) used to generate the ionisation photon was pumped with the third harmonic (355 nm) of a Surelite I or Surelite III Nd:YAG laser for *p*DFB and *p*ClFB or the second harmonic (532 nm) of the same lasers for *p*FT and *p*Xyl. The dye laser operated on either Coumarin 503 or 540A for the *p*DFB and *p*ClFB experiments, and on DCM or Pyromethene 597 for the *p*Xyl and *p*FT experiments, with the output frequency doubled by a BBO or KDP crystal, as appropriate.

The focused, frequency-doubled outputs of the dye lasers were overlapped both spatially and temporally and passed through the vacuum chamber coaxially and counterpropagating. They intersected the jet expansion between two electrical grids (labelled “Ion extraction plates” in Figure 2.3) in the extraction region of

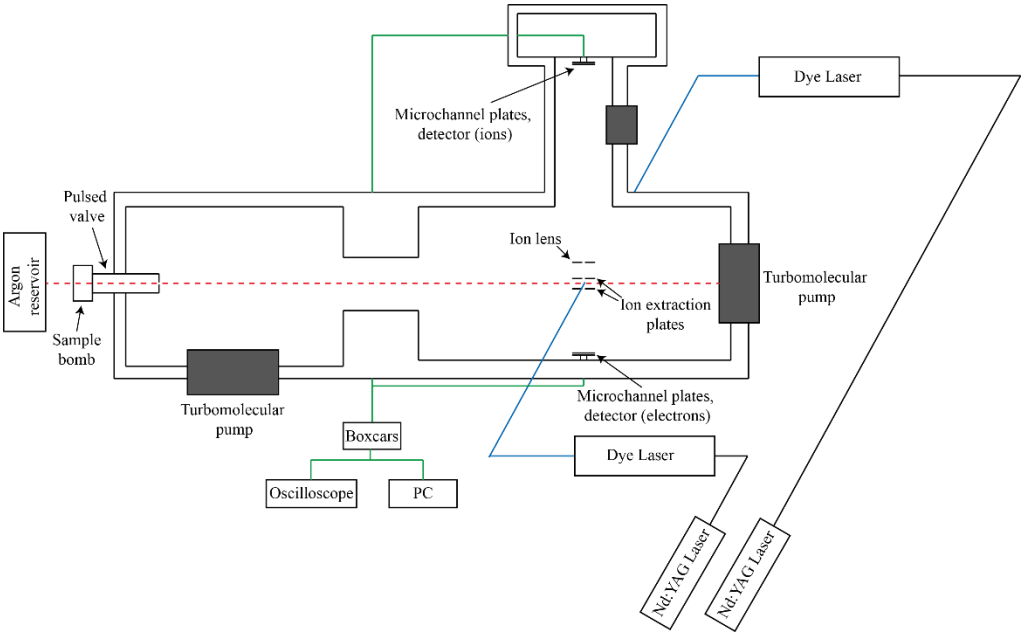


Figure 2.3 – Schematic depiction of the experimental apparatus used for the REMPI and ZEKE spectroscopy experiments discussed in this thesis. The blue lines illustrate the spatially and temporally overlapped, frequency doubled, outputs of the two dye lasers. The red dashed line indicates the path of the jet expansion through the vacuum system, and the green lines indicate the signal being taken from one of the two detectors.

a Wiley-McLaren time-of-flight mass spectrometer. In the REMPI experiments, these extraction plates were used to accelerate the ions up the time-of-flight tube to the top dual microchannel plate (MCP) detector. In the ZEKE experiments, the upper ion extraction plate was grounded and after a delay of up to 2 μs, a small positive voltage was applied to the lower ion extraction plate (the ionisation/extraction pulse), which gave a typical field of ~10 V cm^{-1}. This extracted the ZEKE electrons and accelerated them towards a dual MCP detector, located at the bottom of the chamber in Figure 2.3. The signal in each experiment was monitored on an oscilloscope, integrated and averaged by a boxcar and then sent to a PC.

2.C. Computational methodology

To aid in assigning the observed vibrational structure in the REMPI and ZEKE spectra, calculations were undertaken to obtain the vibrational wavenumbers of *p*ClFB, *p*DFB, *p*FT and *p*Xyl in both the S_1 and D_0^+ states, using the Gaussian09 software package[7]. Based on previous work[8–15], the density functional theory (DFT) was employed, with the functional B3LYP being used throughout; additionally, the aug-cc-pVTZ Dunning style basis sets were used. This combination seems to give good agreement with experimental vibrational wavenumbers for the ground electronic state[12], and UB3LYP/aug-cc-pVTZ good agreement for the cationic ground state[13,14]. Similarly, one gets reasonable agreement[9–11,13–15] with experimental wavenumbers for the S_1 state, using time-dependent B3LYP/aug-cc-pVTZ[a], with the caveat that the D_{14} vibration (analogous to M_{14} in previous work on monosubstituted benzene molecules) appears to be particularly poorly described by this method[9–11] in the S_1 state. Since the current work uses a combination of REMPI and ZEKE spectroscopy, the calculated D_0^+ wavenumbers, alongside comparison to other molecules, means less reliance needs to be placed on the S_1 values.

[a] In general, the agreement is lower than for the S_0 or D_0^+ wavenumbers, with the out-of-plane modes giving poorest experimental agreement out of all the vibrations of interest in this thesis (i.e. those below ~1200 cm^{-1}).

The calculated vibrational wavenumbers obtained are scaled by 0.97, as suggested by the National Institute of Standards and Technology (NIST) Computational Chemistry Comparison and Benchmark DataBase (CCCBDB)[16], with the scaling factor based on the average deviation of B3LYP/aug-cc-pVTZ calculated vibrational wavenumbers from experiment for 1447 vibrations in 137 molecules. This scaling factor thus accounts for deficiencies in the calculations and anharmonicity of the vibrations in an averaged fashion.

For *p*FT and *p*Xyl, various geometries corresponding to the different conformations of the methyl group(s) were trialled in each electronic state. For *p*FT, there are two possible conformers: staggered (one C-H bond of the methyl group perpendicular to the benzene ring) and eclipsed (one C-H bond of the methyl group in the plane of the benzene ring). For *p*Xyl, there are five conformers:

- Both methyl groups staggered with respect to the ring and staggered with respect to one another, referred to here as *trans*-staggered-staggered.
- Both methyl groups staggered with respect to the ring and eclipsed with respect to one another, referred to here as *cis*-staggered-staggered.
- Both methyl groups eclipsed with respect to the ring and eclipsed with respect to one another, referred to here as *cis*-eclipsed-eclipsed.
- Both methyl groups eclipsed with respect to the ring and staggered with respect to one another, referred to here as *trans*-eclipsed-eclipsed.
- One methyl group staggered with respect to the ring and the other eclipsed with respect to the ring, referred to here as staggered-eclipsed.

For *p*FT, the lowest energy geometry was the staggered conformer in both the S_1 and D_0^+ states. For *p*Xyl, the lowest energy S_1 state geometry was *cis*-staggered-staggered, while for the D_0^+ state it was *trans*-staggered-staggered. The calculated, scaled, vibrational wavenumbers for the S_1 and D_0^+ states, for the lowest energy conformers, are given in Tables B.1 and B.2 in Appendix B.

Note that these are not necessarily the lowest energy conformers in reality, as the torsional potential has been proposed to be determined, at least in part, by van der Waals interactions between methyl and ring hydrogen atoms[17], something unlikely to be well-described by B3LYP. Additionally, if the torsional barrier is low, which it is expected to be based on previous work on toluene[18,19], it will be even trickier (and perhaps not meaningful) to obtain the lowest energy conformer. No attempt is made to calculate the torsional potentials here; the calculations are used only for the vibrational wavenumbers, which did not change significantly between the conformers at the B3LYP/aug-cc-pVTZ level used in this thesis.

2.D. References

[1] A. Ellis, M. Feher, and T. Wright, *Electronic and Photoelecton Spectroscopy: Fundamentals and Case Studies* (Cambridge University Press, Cambridge, 2005).

[2] K. Müller-Dethlefs and E.W. Schlag, *Angew. Chemie Int. Ed.*, **37**, 1346 (1998).

[3] M.C.R. Cockett, *Chem. Soc. Rev.*, **34**, 935 (2005).

[4] G. Reiser, W. Habenicht, K. Müller-Dethlefs, and E.W. Schlag, *Chem. Phys. Lett.*, **152**, 119 (1988).

[5] X. Zhang, J.M. Smith, and J.L. Knee, *J. Chem. Phys.*, **97**, 2843 (1992).

[6] J.M. Hollas, *High Resolution Spectroscopy*, Second Ed. (Wiley, Chichester, 1998).

[7] M.J. Frisch, G.W. Trucks, H.B. Schlegel *et al.*, Gaussian 09, Revision E.01 (2016).

[8] A.M. Gardner and T.G. Wright, *J. Chem. Phys.*, **135**, 114305 (2011).

[9] J.P. Harris, A. Andrejeva, W.D. Tuttle, I. Pugliesi, C. Schriever, and T.G. Wright, *J. Chem. Phys.*, **141**, 244315 (2015).

[10] A. Andrejeva, W.D. Tuttle, J.P. Harris, and T.G. Wright, *J. Chem. Phys.*, **143**, 104312 (2015).

[11] A. Andrejeva, W.D. Tuttle, J.P. Harris, and T.G. Wright, *J. Chem. Phys.*, **143**, 244320 (2016).

[12] A. Andrejeva, A.M. Gardner, W.D. Tuttle, and T.G. Wright, *J. Mol. Spectrosc.*, **321**, 28 (2016).

[13] A.M. Gardner, A.M. Green, V.M. Tamé-Reyes, V.H.K. Wilton, and T.G. Wright, *J. Chem. Phys.*, **138**, 134303 (2013).

[14] A.M. Gardner, A.M. Green, V.M. Tamé-Reyes, K.L. Reid, J.A. Davies, V.H.K. Parkes, and T.G. Wright, *J. Chem. Phys.*, **140**, 114308 (2014).

[15] W.D. Tuttle, A.M. Gardner, and T.G. Wright, *Chem. Phys. Lett.*, **684**, 339

(2017).

[16]"*https://Cccbdb.Nist.Gov/Vibscale2x.Asp?Method=8&basis=18*" Accessed (2018).

[17] D.B. Moss, C.S. Parmenter, and G.E. Ewing, *J. Chem. Phys.*, **86**, 51 (1987).

[18] J.R. Gascooke, E.A. Virgo, and W.D. Lawrance, *J. Chem. Phys.*, **142**, 024315 (2015).

[19] J.R. Gascooke, E.A. Virgo, and W.D. Lawrance, *J. Chem. Phys.*, **143**, 044313 (2015).

3. A single rotor case: the low wavenumber torsion and vibration-torsion region of *para*-fluorotoluene

In this chapter, resonance-enhanced multiphoton ionisation (REMPI) spectra of the $S_1 \leftarrow S_0$ transition of *para*-fluorotoluene (*p*FT) are presented, and these are accompanied by zero-electron-kinetic-energy (ZEKE) photoelectron spectroscopy (PES) spectra recorded at many different intermediate S_1 internal energies. Initially, an overview of the relevant previous literature on *p*FT is provided, followed by theoretical background for the single rotor, and subsequent discussion of the spectra and possible couplings.

3.A. *para*-fluorotoluene and the single rotor

3.A.1. Previous work

There is a wealth of previous work on *p*FT investigating the $S_1 \leftarrow S_0$ transition examined here, owing to the spectral accessibility of the molecule and the hypothesised influence of the methyl group on IVR rates. One need look no further than the influential early work of Parmenter *et al*., who pioneered the technique of chemical timing[1], whereby O_2 is added to a fluorescence cell containing the molecule of interest to quench the S_1 electronic state, and so the only fluorescence observed is that which occurs on a timescale between absorption to the selected S_1 level and the collisionally-induced quenching. This effectively allows for a monitoring of picosecond timescale dynamics, and Parmenter and co-workers combined this with traditionsal single vibronic level fluorescence (SVLF; this technique will be referred to as dispersed fluorescence (DF) throughout this thesis) experiments for both dynamical and spectroscopic information, allowing thorough comparisons of the internal energy onset of IVR processes and the IVR lifetimes in *para*-difluorobenzene (*p*DFB)[1–7] and *p*FT[2,8-12], determining a significantly accelerated IVR for *p*FT when compared to *p*DFB.[10] It should be noted that many of the traditional DF experiments were carried out under collision-free, supersonic jet expansion, conditions, whereas when DF was combined with chemical timing, the experiments could not be

carried out in a jet expansion owing to the need to add O_2 as a quenching agent, and so those fluorescence experiments were carried out in sample bulbs at room temperature.

With this in mind, work by Zewail and co-workers[13] in 1988 obtained *p*DFB and *p*FT IVR lifetimes by picosecond time-resolved fluorescence measurements in a molecular beam, and found that IVR was not as prevalent under these conditions as under the room temperature conditions of the chemical timing measurements. One should take some care in interpreting both the chemical timing experiments of Parmenter and co-workers and the picosecond time-resolved fluorescence measurements of Zewail and co-workers. The former, as mentioned above, were carried out at room temperature, and so couplings may be observed which, owing to a lack of population, would not be observed under jet expansion conditions. The latter used a laser pulse with an estimated laser bandwidth of 5 cm^{-1}, with a 300 ps detector response time. As such, the reduced prevalence of IVR suggested by Zewail and co-workers[13], even at relatively high internal energies, is not particularly surprising, as the laser pulse is not likely to encompass all of the coupled levels and thus the wavepacket will not represent a complete picture of the coupling.

Significant later work was undertaken by the Reid group[14–19], who recorded picosecond time-resolved photoelectron spectra (tr-PES) *via* a range of intermediate S_1 vibrational levels, elucidating IVR lifetimes and identifying doorway states populated by the IVR process after the initial excitation. Interestingly, when exciting at ~0^0+1200 cm^{-1} in the S_1 state[14], the Reid group observed an IVR timescale consistent with the room temperature chemical timing measurements of Parmenter at this internal energy[10], in contrast with the findings of Zewail and co-workers[13], even though the work in reference 14 was carried out under jet-cooled conditions. The study of the Reid group used shorter pulses of 1 picosecond, with an estimated bandwidth of 13 cm^{-1}, and this larger bandwidth is likely to encompass a more complete set of the coupled levels when exciting the wavepacket, with this being one explanation for the difference in IVR timescale observed in the various studies.

Much of the previous frequency domain spectroscopy of *p*FT has been focussed on the low internal energy, "pure" torsional region of the $S_1 \leftarrow S_0$ excitation spectrum. In 1985, Okuyama *et al.*[20], using the techniques of laser-induced fluorescence (LIF) and DF, investigated the torsional levels of *p*FT, as well as the *ortho*- and *meta*- analogues, and from these experiments drew conclusions regarding the torsional potentials in the S_0 and S_1 states. Later work by Zhao and Parmenter[21,22] used REMPI and LIF (referred to as fluorescence excitation therein) spectroscopies to again probe the $S_1 \leftarrow S_0$ transition, supplementing this with further DF results, all from a jet-cooled sample. In much of the work in reference 21 the focus is on the torsional levels, with a larger breadth of work on *p*FT, *p*FT.Ar, and some reassignments given in Zhao's thesis[22]. Hu *et al.*[23] reported REMPI spectra over the torsional regions of *ortho*-, *meta*- and *para*-fluorotoluene in a study on the fluorotoluene.Ar complexes, while REMPI and mass-analysed threshold ionisation (MATI) spectra of *p*FT and *p*FT.Ar were reported by Georgiev *et al.*[24], with the MATI spectra recorded *via* the S_1 origin and a vibration at 0^0+398 cm^{-1}, labelled therein as $9b^1$, in the Wilson[25]/Varsányi[26] notation of that work.

There is also earlier work investigating the torsional levels of the *ortho*-, *meta*- and *para*-fluorotoluene cations by Takazawa *et al.*[27], utilising ZEKE spectroscopy, which inferred information about the height of the torsional potential and the lowest energy (eclipsed or staggered) conformer in the ground cationic, D_0^+, state. Additionally, the Wright group has previously studied both the S_1 and D_0^+ states of *p*FT with REMPI and ZEKE spectroscopies[28,29], the latter of these in collaboration with the Reid group, with the focus of these investigations primarily being ZEKE spectra recorded *via* higher wavenumber S_1 vibrational levels rather than torsional levels.

Considering this previous work, one can see many studies on the IVR processes of *p*FT *via* a range of S_1 intermediate levels, but with the focus of frequency domain studies primarily on the low wavenumber "pure" torsional region. The current work aims to provide a more thorough frequency domain study of *p*FT (and a comparison to *para*-xylene (*p*Xyl)), and as such in later chapters, a significant number of ZEKE spectra will be presented across not just the pure

torsional region, but spanning a range of intermediate levels up to ~0^0+1200 cm^{-1}. The interpretation of these spectra will then be compared to previous results from tr-PES where available, and it will be possible to see whether one can extract similar information about the coupled levels in the frequency rather than the time domain, taking advantage of the higher spectral resolution afforded to this work by the use of nanosecond laser systems and ZEKE spectroscopy, giving a clearer picture of what levels/transitions are present at particular internal energies.

This chapter will focus on the low wavenumber torsion and vibration-torsion (vibtor) region, with ZEKE spectra recorded *via* many (weak) REMPI bands, providing a good understanding of which transitions to torsion and vibtor levels are observed in the REMPI spectrum, which will be of use in discussing higher wavenumber regions in the later chapters.

3.A.2. The single rotor

The theoretical considerations associated with dealing with a single internal rotor, in this case a single methyl group, have been discussed by many authors, and of particular note are papers by Zhao *et al*.[21] and Okuyama *et al*.[20], a review by Spangler[30], as well as the significant body of work by Weisshaar and co-workers on toluene[31,32], a range of substituted toluenes[32–36] and phenylsilane[37] and more recently publications by Gascooke and Lawrance on toluene[38–42] and the toluene.Ar complex[43]. This section gives an overview of the theory of single rotor systems, with reference to those previous studies. It is notable that the treatment of the single rotor is identical for toluene and for *p*FT, and some use will be made of this comparison throughout this thesis.

3.A.2.1. The free rotor

In considering, for simplicity, a molecule in its ground electronic state, one can start, as in the review by Spangler[30], by imagining a system where the methyl group is internally rigid and rotating about the bond which connects it to some parent molecule of effectively infinite mass relative to the methyl group. If one

then assumes that this is a free internal rotation, with no barrier to hinder it, then this can be treated analogously to a particle on a ring[44], where the Hamiltonian can be expressed as:

$$H = F\frac{\delta^2}{\delta\varphi^2} \qquad \text{Eq. 3.1}$$

Where *F*, the effective internal rotation constant, is:

$$F = \hbar^2/2I \qquad \text{Eq. 3.2}$$

And the moment of inertia, *I*, is given by:

$$I = \frac{I_{Methyl}I_{Parent}}{I_{Methyl} + I_{Parent}} \qquad \text{Eq. 3.3}$$

Where I_{Parent} represents the parent molecule to which the methyl group is attached (such as the phenyl ring in the toluene case).

Since it has already been assumed that the parent molecule is of effectively infinite mass, which is a reasonable assumption for a substituted (or unsubstituted) phenyl ring relative to a methyl group, *I* is essentially equal to I_{Methyl}, which is effectively equal to the moment of inertia of methane (a spherical top). This yields an effective[a] internal rotation constant, *F*, of ~5.4 cm^{-1},[30] which is assumed in much of the work on these systems and is a good approximation, at least in the first instance.

If one follows through with the solution to this particle on a ring treatment, one arrives at the following expression for the allowed energies[30,44]:

$$E = \underline{\mathrm{m}}^2 F \qquad \text{Eq. 3.4}$$

[a] This is an effective internal rotation constant as, unlike in methane, the rotation has to be counteracted by the rotation of the rest of the molecule in the opposite direction, which has a small effect on the rotational constant.

Where m is the torsional quantum number for the free rotor, using the notation of Gascooke *et al.*[40], and takes values: m = 0, ±1, ±2,… etc. Some important, conclusions from this are: there is no zero-point energy for these pure torsional levels, the separation of the energy levels increases with higher m owing to the quadratic dependence, and all of the levels above m = 0 are doubly degenerate (the positive and negative signs correspond to the methyl group rotating clockwise and anticlockwise[38]). These "free rotor" levels are illustrated schematically in Figure 3.1.

3.A.2.2. The hindered rotor

In reality, the methyl group is not undergoing completely "free" internal rotation as described above, but rather there is some barrier hindering this rotation. If one imagines rotating the methyl group about a bond linking it directly to an infinite mass, it is evident that any potential barrier which hinders this rotation will be (at least) threefold periodic owing to the symmetry of the methyl group. In toluene or *p*FT, if one looks down the bond linking the methyl group to the phenyl ring, in a manner analogous to a Newman projection, it becomes apparent that the barrier is sixfold periodic because of the twofold symmetry of the rest of the molecule. This torsional potential can be expressed in a general form[30]:

$$V = \frac{V_3}{2}[1 - \cos(3\alpha)] + \frac{V_6}{2}[1 - \cos(6\alpha)] + \frac{V_9}{2}[1 - \cos(9\alpha)] + \cdots \quad \text{Eq. 3.5}$$

Where V is the torsional potential and V_n, where n is an integer multiple of three, are the various potential terms of the expansion. α is the angle of internal rotation, which is defined to be 0^o for an eclipsed conformation, i.e. one in which a methyl C-H bond is in the same plane as the phenyl ring. In the case of *p*FT (and toluene) discussed here, V_6 is the leading term, as V_3 is zero owing to the

symmetry of these species[b], and as such the relevant potential for these molecules is sixfold periodic:

$$V = \frac{V_6}{2}[1 - \cos(6\alpha)] \qquad \text{Eq. 3.6}$$

Although the inclusion of higher order terms can alter the shape of the potential, as noted by Spangler[30], in many cases the leading term, shown in Eq. 3.6, is in sufficient agreement with experimental results to be used alone. One might also note that the barrier is particularly sensitive to the electronic state of the molecule, since the potential is a fine balance of significant steric, resonance and hyperconjugation or donor-acceptor interactions[9,30,33], which makes qualitative predictions regarding the barrier difficult.

Inspection of the form of the torsional potential for *p*FT shows that V_6 represents the height of the barrier to internal rotation. One might reasonably ask, if the barrier is significant, how the torsional energy levels are perturbed from the free rotor case.

It has been shown in previous literature[30,40] that, in the case of the sixfold potential, a $-V_6/4$ term couples free rotor $\underline{m}$ levels which differ by $\Delta\underline{m} = \pm 6$. However, because most of the levels that are separated by $\Delta\underline{m} = \pm 6$ are also significantly energetically separated from one another (such as $\underline{m} = \pm 1$ and $\underline{m} = \pm 7$, or $\underline{m} = \mp 2$ and $\underline{m} = \pm 4$ for example), the coupling is negligible in most cases, and the $\underline{m} = 0, \pm 1, \pm 2, \pm 4, \pm 5, \pm 7, \ldots$ etc free rotor levels remain essentially unperturbed in the hindered rotor case, with the non-zero levels retaining their degeneracies, and these are now denoted $m = 0, 1, 2, 4, 5, 7, \ldots$ etc in the hindered rotor case, following the notation of Gascooke *et al.*[40] The $\underline{m} = \pm 3$ levels, however, are more strongly coupled by the V_6 potential, since these are energetically degenerate in the free rotor, and separated by $\Delta\underline{m} = \pm 6$. This yields

[b] Briefly, as discussed by Spangler[30], for toluene or a *para*-substituted toluene, there is a twofold symmetry of the phenyl ring about the C-CH_3 bond, leading to two, equal and opposing, threefold contributions to the potential, the cancellation of which leaves a negligible V_3 term. However, for an *ortho*- (or *meta*-) substituted toluene, there is no twofold symmetry of the phenyl ring about the C-CH_3 bond, and so there will be a contribution from a V_3 (leading) term.

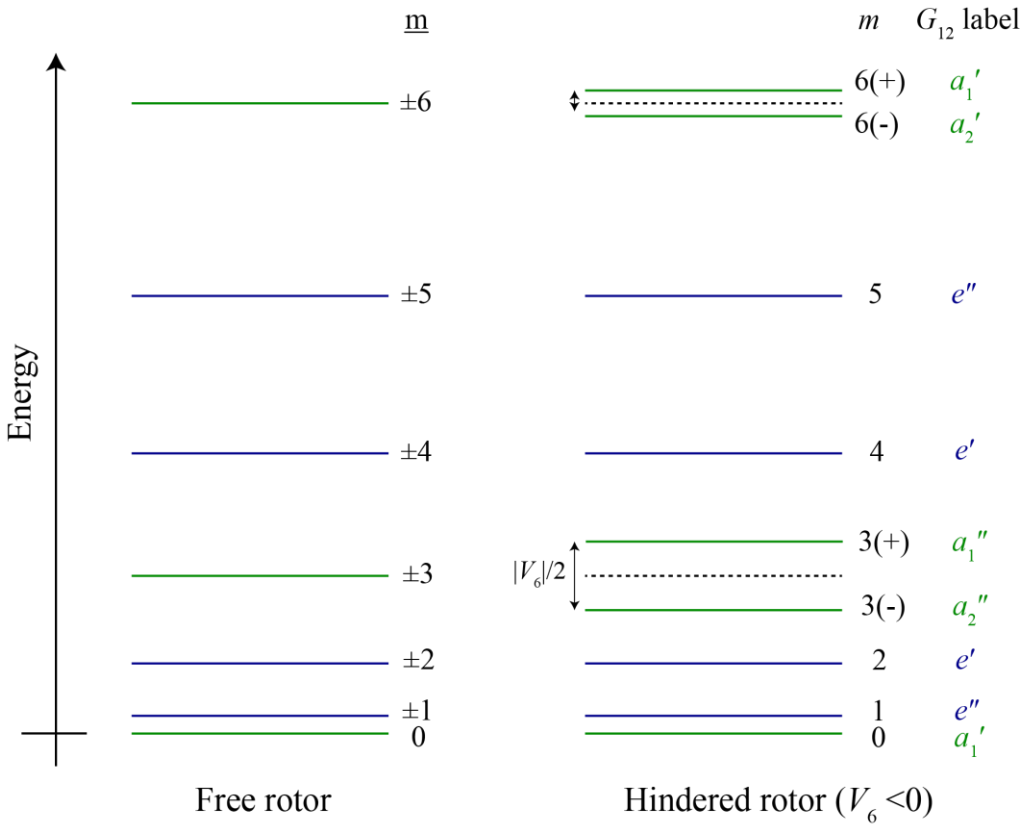


Figure 3.1 – A schematic illustration of the lowest energy free rotor levels (left) and hindered rotor levels (right) for toluene or para-fluorotoluene. The ordering of the hindered rotor 3(+)/3(-) and 6(+)/6(-) levels shown is for a negative V_6 barrier. On the far right the appropriate G_{12} molecular symmetry group label for each level is given, with "e" levels shown in blue while "a" levels are given in green. Note that this represents the case for a hindered rotor with a relatively low V_6 barrier, such as was found for toluene[41].

two hindered rotor levels that are linear combinations of the free rotor levels, denoted as m = 3(+) and m = 3(-) for the symmetric and antisymmetric combinations respectively, again employing the notation of Gascooke *et al.*[40] Owing to the $-V_6/4$ coupling term which mixes these free rotor levels, the hindered rotor levels are separated by $|V_6|/2$, with one increasing in energy by $|V_6|/4$ and the other decreasing in energy by $|V_6|/4$ relative to the free rotor. An analogous mixing of the $\underline{m}$ = ±6 levels yields the m = 6(+) and m = 6(-) levels, but in this case the levels are coupled indirectly *via* $\underline{m}$ = 0,[39] and so the separation of the mixed levels is reduced compared to the $\underline{m}$ = ±3 case, with the separation decreasing further if these levels are above the height of the torsional barrier.

The hindered rotor levels are illustrated schematically in Figure 3.1, where the deviations in the m = 3 and m = 6 levels from the free rotor are apparent.

It is notable that V_6 is a signed parameter. If it takes a positive value, then the minima in the potential will be at geometries where the methyl group has one C-H bond eclipsing the phenyl ring. If it takes a negative value, the potential will be inverted, and the minima will now be at geometries where the methyl group is staggered with respect to the phenyl ring. Additionally, the sign of V_6 determines the ordering of the m = 3(+)/3(-) and 6(+)/6(-) hindered rotor levels[32]: for a negative V_6 (staggered lowest energy conformer), 3(-) < 3(+) while for a positive V_6 (eclipsed lowest energy conformer), 3(+) < 3(-), assuming no other perturbations. As such, if one can observe, and identify, transitions involving both the m = 3(-) and 3(+) levels experimentally, it is possible, in theory, to deduce the lowest energy conformation of the molecule, and to extract the torsional barrier height. However, as will be discussed later, one must be wary of other interactions which perturb the observed transitions, as discussed by Gascooke and Lawrance in the case of toluene[40,41].

3.A.2.3. Molecular symmetry group treatment

These hindered rotor levels belong to a particular symmetry within the appropriate molecular symmetry group, which is of spectroscopic use in determining which torsional levels will be populated under jet-cooled conditions and subsequently identifying allowed and forbidden transitions involving torsions accompanying electronic excitation, both discussed in the next section.

If one considers toluene or *p*FT and treats the methyl group as a point mass, as has been done in the past to study the vibrational activity in these molecules[28,45,46], then the molecule can be treated as having C_{2v} point group symmetry, with vibrations and electronic states classified as a_1, a_2, b_1 or b_2 symmetries. When one explicitly includes the methyl group however, a point group symmetry is no longer sufficient to describe the system[30,47,48] as the nuclei of the methyl group are moving within the molecule with respect to the phenyl ring, and so one must use a permutation-inversion group, also known as a

molecular symmetry group (MSG), instead, which for the cases of toluene and *p*FT is G_{12}. Particular note should be made of the work of Longuet-Higgins[47] regarding this approach, and also the book by Bunker and Jensen[48]; indeed in reference 47 the CH_3BF_2 molecule – also of the G_{12} MSG and analogous to the current work – was treated thoroughly.

The character table for the G_{12} MSG is shown in Table 3.1, and has been adapted from reference 48. Figure 3.2 illustrates the hydrogen numbering system that has been chosen for this G_{12} MSG analysis, illustrated for the case of toluene, but *p*FT is analogous. Note that the *para*-position hydrogen in toluene (or the fluorine in *p*FT) does not have a label as it is unchanged by any of the permutation-inversion operations. Also shown in Figure 3.2 are the principal axes of the molecule, and the chosen Cartesian axis system for this work. The choice of the latter derives from striving to attain a consistency between symmetric and asymmetric *para*-disubstituted benzene molecules, and monosubstituted benzene molecules, but where possible the discussion will be framed in terms of the principal axes as these are unambiguous.

In passing, it is notable that the irreducible representations are the same as those in the point group D_{3h}, this is because the G_{12} MSG is isomorphic with the D_{3h} point group, and so the same labels are used for the irreducible representations.[47] It can be conceptually helpful to correlate permutation-inversion operations with

Table 3.1 – G_{12} molecular symmetry group character table[a]

G_{12}	E	(123)	(23)*	(ab)(cd)	(123)(ab)(cd)	(23)(ab)(cd)*	
[b]	1	2	3	1	2	3	
A_1'	1	1	1	1	1	1	T_a/T_Z, *ee*
A_1''	1	1	1	-1	-1	-1	T_b/T_y, J_c, *oe*
A_2'	1	1	-1	1	1	-1	J_a, *eo*, Γ^*
A_2''	1	1	-1	-1	-1	1	T_c/T_x, J_b, *oo*
E'	2	-1	0	2	-1	0	
E''	2	-1	0	-2	1	0	

[a] Note that the numbers and letters of the operators correspond to hydrogen nuclei, as shown in Figure 3.2.
[b] Number of operators in class; can be easily obtained from the isomorphic D_{3h} character table.

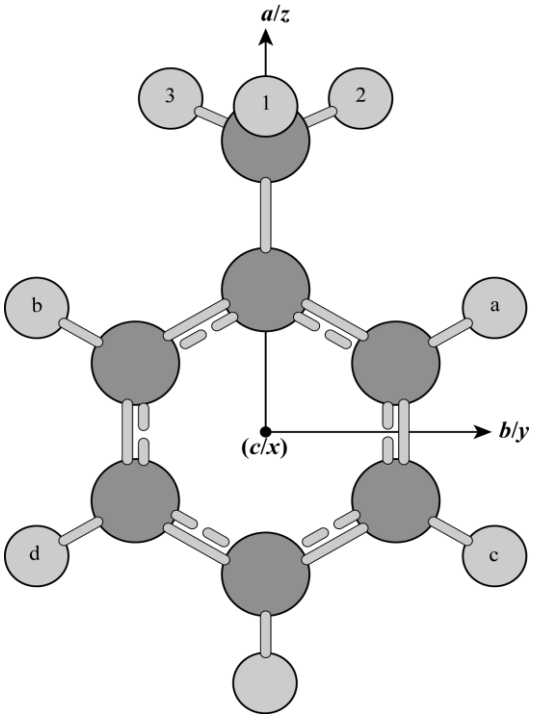


Figure 3.2 – A schematic of toluene showing the atomic numbering, consistent with the permutation-inversion operations of Table 3.1. Note that the principal axes are indicated, as well as the Cartesian axes used in this work. The unlabelled hydrogen in the position para- to the methyl group is unchanged by these operations, and the same would be true if it were a fluorine atom in para-fluorotoluene.

the respective D_{3h} operations, such as (123) with C_3, but one must be very cautious in doing this as, for non-rigid molecules such as toluene and *p*FT, these point group symmetry operations are not appropriate.

So, what are the operations in the G_{12} MSG? The operation E is analogous to that in a point group and represents doing nothing. The hypothetical operation (12) would represent exchanging hydrogen atoms 1 and 2, while the operation (123) is equivalent to exchanging hydrogen 3 for 2 and then 2 for 1. The asterisk indicates an inversion operation, which changes the sign of the coordinates of all of the nuclei. For example, (23)* indicates exchange of hydrogen atoms 2 and 3 and an inversion. The outcomes of these operations are illustrated schematically in Figure 3.3.

One can, as stated above and shown by Longuet-Higgins[47], assign G_{12} symmetry labels to the torsional levels. To do this, use is made of the fact that the eigenfunctions which correspond to the solution of the particle on a ring for a free rotor are of the form[30,44,47]:

$$\phi = e^{\pm im\alpha} \qquad \text{Eq. 3.7}$$

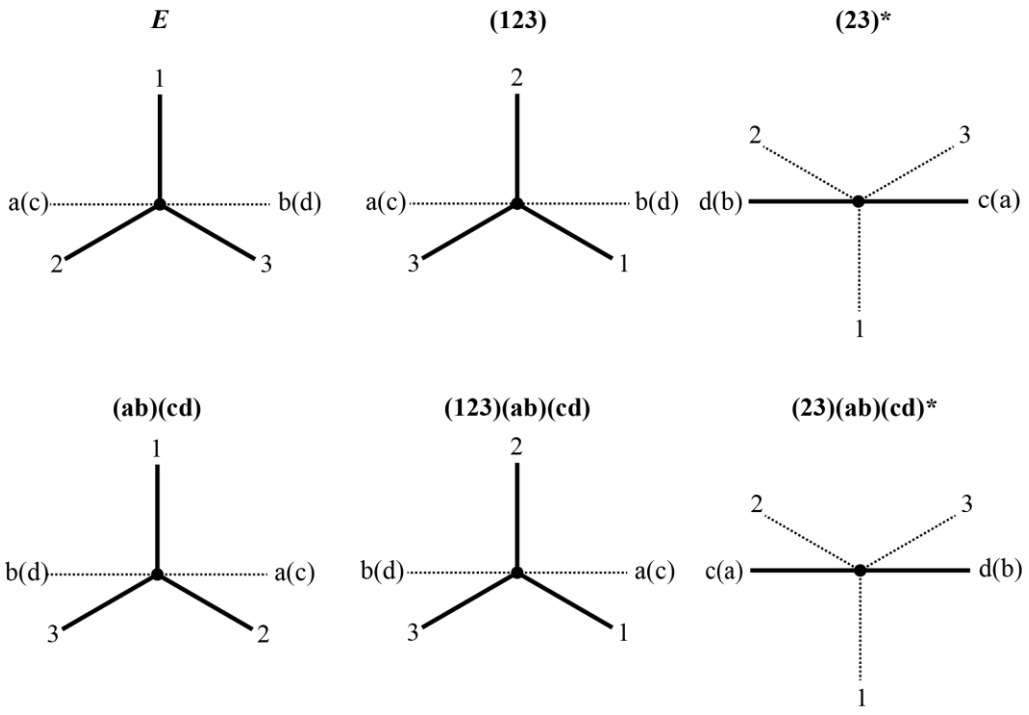


Figure 3.3 – Newman projections illustrating the outcomes of each of the G_{12} symmetry operations on the toluene/pFT molecule described by Figure 3.2. Note that the initial Newman projection (E) is oriented down the methyl carbon-ring carbon bond from Figure 3.2, and for any operation containing an inversion, the methyl group ends up on the other side of the ring. Solid and dashed lines are used to indicate the foreground and background respectively. Note that for the ring hydrogens, the ones given in parentheses are behind the ones outside of parentheses.

Recalling that m is the torsional quantum number and α is the torsional angle. In this instance, one can define the torsional angle as the angle of rotation between a ring hydrogen and a methyl hydrogen. One can then see how this varies for each of the G_{12} symmetry classes, and this information can be used (alongside the solution of the particle on a ring given above) to generate Table 3.2, which illustrates how the m levels are distinguished by symmetry. This table is adapted from Longuet-Higgins.[47] It is these G_{12} MSG labels that one applies to the torsional levels in toluene and *p*FT, with the appropriate labels shown adjacent to the hindered rotor levels in Figure 3.1.

While on the topic of molecular symmetry groups, it will be beneficial to discuss both other internal degrees of freedom and electronic states in the same framework. One can assign a G_{12} symmetry label to a vibration, and this will be

Table 3.2 – G_{12} torsional (m) level symmetries

m	E	(123)	(23)*	(ab)(cd)	(123)(ab)(cd)	(23)(ab)(cd)*	G_{12} symmetry
0	1	1	1	1	1	1	a_1'
1	2	-1	0	-2	1	0	e''
2	2	-1	0	2	-1	0	e'
3	2	2	0	-2	-2	0	$a_1'' + a_2''$
4	2	-1	0	2	-1	0	e'
5	2	-1	0	-2	1	0	e''
6	2	2	0	2	2	0	$a_1' + a_2'$

important later when discussing possible interactions between vibrational and torsional levels. This is a relatively straightforward process, and one need only look at the vibrational character (which in this case can be done by looking at the mode diagrams for the ${}^{p}D_{\mathrm{i}}$ vibrations from reference 49, given here in Appendix A), and use the (23)* and (ab)(cd) operations to determine the G_{12} symmetries. The (ab)(cd) operation provides a distinction between primed a_1'/a_2' and double primed a_1''/a_2'' vibrations, i.e. between C_{2v} a (a_1/a_2) and b (b_1/b_2) vibrations by distinguishing symmetry about the carbon-substituent bond (C_2) axis. The (23)* operation then provides a distinction between the a_1 (a_1'/a_1'') and a_2 (a_2'/a_2'') vibrations, i.e. between C_{2v} in- and out-of-plane vibrations respectively. This allows the following correlations to be drawn:

C_{2v} vibrational symmetry	G_{12} vibrational symmetry
a_1	a_1'
a_2	a_2'
b_1	a_2''
b_2	a_1''

There are no C_{2v} irreducible representations equivalent to the G_{12} e ones, and so no vibrations are of these symmetries.

While one can assign G_{12} symmetry labels to the rotational levels, as the current work does not obtain rotational resolution, and is focussed on vibration-vibration and vibration-torsion couplings between levels, the methodology for doing this will not be discussed within this thesis.

Finally, one can assign a G_{12} symmetry label to the electronic state. Since the correlation between C_{2v} and G_{12} symmetries has already been shown for vibrations, one can use these correlations for the relevant electronic state symmetries. For example, the ground electronic state of toluene or *p*FT is A_1 symmetry in a C_{2v} framework (where the methyl group is treated as a point mass) and is thus of A_1' symmetry in the G_{12} framework. Additionally, the first excited singlet, S_1, state of these molecules is of B_2 C_{2v} symmetry, and thus of A_1'' symmetry in a G_{12} context, while the cationic ground state, D_0^+, is of B_1 C_{2v} symmetry, and thus here is A_2''. These C_{2v} labels are assigned based on the chosen Cartesian axis system shown in Figure 3.2, but the G_{12} labels are unique as these are based on the molecular principal axes. It can be appreciated that this MSG approach is extremely useful in allowing the treatment of electronic states, vibrations, rotations, and torsions of a non-rigid molecule within the same symmetry framework.

3.A.2.4. Allowed and forbidden torsional excitations accompanying electronic excitation

Having discussed both the free and hindered rotor cases, gaining an understanding of the torsional energy level structure within an electronic state, two questions can now be tackled:

1) What torsional levels are populated under the "cold" experimental conditions of a supersonic jet expansion?

And subsequently:

2) What transitions involving torsional levels should one expect to see in an electronic excitation (or photoelectron) spectrum?

It is often stated that only the lowest two levels, m = 0 and m = 1, will be populated under jet expansion conditions, as discussed by Walker *et al*.[32] To deduce this, one must look at the symmetries of all of the component wavefunctions, ϕ, of the total wavefunction, Φ_{tot}, such that the overall symmetry of the total wavefunction, Γ_{tot}, is allowed. One can then examine all of the possible makeups of the allowed Φ_{tot} and draw conclusions regarding which torsional levels are allowed to interconvert in the jet expansion.

To establish the "allowed" symmetries of Φ_{tot}, use must be made of the MSG character table for the G_{12} group being dealt with, shown in Table 3.1. From the Pauli principle, it is known that Φ_{tot} must be antisymmetric with respect to interchanging odd numbers of pairs of fermionic hydrogen nuclei, and symmetric with respect to interchanging even numbers. By inspection of the character table, in particular the operations (123) and (ab)(cd) which represent permutations of even numbers of pairs of hydrogen nuclei[c], one can see that the only allowed symmetries of Φ_{tot} will be A_1' and A_2'.

Φ_{tot} can be broken down into its component electronic, vibrational, rotational, torsional and nuclear spin wavefunctions (assuming the separability of electronic and nuclear motions, as per the Born-Oppenheimer approximation, as well as the separability of torsional, vibrational and rotational degrees of freedom). As the ground electronic state is being treated, the electronic wavefunction, ϕ_{elec}, will be totally symmetric (A_1'). Owing to the jet-cooled conditions of the experiments, the vibrational wavefunction, ϕ_{vib}, will also be of A_1' symmetry as the molecule will be in the zero-point level for all vibrations. These two totally symmetric wavefunctions can thus be combined with the rotational wavefunction, ϕ_{rot}, and the resulting wavefunction, ϕ_{evr}, will have the same symmetry as ϕ_{rot}. With regard to the rotational wavefunction, *p*FT (and toluene) is an asymmetric rotor, and so has rotational levels with symmetries depending on the parity of the K_a and K_c levels that can be classified as even (e) or odd (o) for the pairs K_aK_c as: *ee*, *eo*, *oe* and *oo*. These were indicated in Table

[c] In passing, it is noted that (123) = (12)(23) (where the rightmost operator acts first), a permutation of an even number of pairs of hydrogen nuclei.

3.1 above to have G_{12} symmetries of A_1', A_2', A_1'' and A_2'' respectively. As such, all ϕ_{evr} wavefunctions have one of the symmetries A_1', A_2', A_1'' or A_2''.

With the symmetries of ϕ_{evr}, and the torsional wavefunction, ϕ_{tor} - discussed in the previous section and given in Figure 3.1 - obtained, all that remains is to obtain the nuclear spin wavefunction, ϕ_{ns}, symmetries. These can be derived, as was done by Longuet-Higgins[47] for CH_3BF_2, by assigning variations of either an α or a β spin to each of the hydrogen nuclei (the three methyl hydrogens, 1 – 3, and the four ring hydrogens, a – d) and observing how the resulting functions transform under the G_{12} MSG operations. Note that a fifth ring hydrogen (in toluene, and the fluorine atom in *p*FT), in the position *para*- to the methyl group, can be excluded for now as it will remain unchanged under any symmetry operation. Rather than looking at the rather complex picture of all possible α and β combinations of the seven hydrogen nuclei together, one can separate these into the various combinations of the α and β for the three methyl hydrogen nuclei and similarly the combinations for the ring hydrogen nuclei. One can then subsequently multiply each of the reducible representations obtained for the methyl hydrogen nuclei by all of those obtained for the ring hydrogens. Remembering then that the *para*-position hydrogen (or fluorine) can have either α or β spin, one has to multiply the computed reducible representations by two, and finally one can sum the reducible representations for each operation, and use the standard reduction formula to obtain the nuclear spin symmetries, which are:

$$80\,A_1' + 0\,A_2' + 48\,A_1'' + 0\,A_2'' + 40\,E' + 24\,E''$$

Following the above discussion, Table 3.3 summarises the various combinations of ϕ_{evr}, ϕ_{tor} and ϕ_{ns} that would give an overall allowed symmetry for Φ_{tot}. Note that ϕ_{ns} symmetries which are given in square brackets do not exist, and so that combination does not exist; these are included for completeness. Also of note is that there are no ϕ_{evr} functions which have an overall *e* symmetry, and so for any torsional level which has an *e* symmetry, the allowed nuclear spin symmetry must also be of *e* symmetry. This leads to the immediate conclusion that it is not possible to interconvert *e* and *a* symmetry torsional levels in the jet expansion, as it is not possible to interconvert between levels with different nuclear spin

symmetry, and as such there will always be population in at least $m = 0$ and $m = 1$ under jet-cooled conditions.

One can now deduce the symmetries of the torsional levels which can be interconverted in the jet expansion, by considering that, as just noted, the nuclear spin must remain unchanged, but that ϕ_{evr} can change during such a process.

Starting with the *e* symmetry levels, any torsional level of *e*″ symmetry, the same symmetry as the lowest *e* level, $m = 1$, can be collisionally cooled into that $m = 1$ level; this applies to the $m = 5$ and $m = 7$ levels, for example. If one instead takes the *e*′ symmetry levels, such as $m = 2$ or $m = 4$, these can also be collisionally cooled into the $m = 1$ level, in the following manner. In a situation with an *e*′ symmetry torsional level (for example $m = 4$), with a nuclear spin also of *e*′ symmetry, this can be cooled into the $m = 1$ level (*e*″ torsional symmetry) with an accompanying ϕ_{evr} change from A_1'/A_2' to A_1''/A_2''. One can see that an analogous situation would also apply if the nuclear spin symmetry was *e*″ rather than *e*′, and one can conclude that any *e* symmetry torsional level (*e*′ or *e*″) can be cooled into the $m = 1$ (*e*″) level in the jet expansion, but not into the $m = 0$ (a_1') level.

Looking now at the *a* symmetry torsional levels, any level with the same symmetry as the lowest ($m = 0$) level, a_1', can be collisionally cooled into that level; for example, the $m = 6(+)$ level. For an a_1'' level, such as $m = 3(+)$, if the nuclear spin is also a_1'', then this can be cooled into the a_1' $m = 0$ level by an accompanying change in ϕ_{evr} from A_1'/A_2' to A_1''/A_2''. Similarly, if the nuclear spin was a_1', it could be cooled into $m = 0$ with an accompanying change in ϕ_{evr} from A_1''/A_2'' to A_1'/A_2'. One can use Table 3.3, and the same logic, to conclude that a_2' ($m = 6(-)$) and a_2'' ($m = 3(-)$) levels can also be collisionally cooled into $m = 0$ by an accompanying change in ϕ_{evr}. This leads to the conclusion often stated in the literature: all *a* symmetry torsional levels (a_1', a_1'', a_2' and a_2'') can be cooled into the $m = 0$ (a_1') level and all *e* symmetry torsional levels (*e*′ and *e*″) can be cooled into the $m = 1$ (*e*″) level, placing population in just the $m = 0$ and $m = 1$ levels in the coldest jet expansions.

Table 3.3 - Component wavefunctions, ϕ, which together give an overall allowed symmetry, Γ_{tot}, for Φ_{tot}.

Γ_{tot}	ϕ_{evr}	ϕ_{tor}	ϕ_{ns}[a]
A_1'	A_1'	a_1'	a_1'
		a_1''	a_1''
		a_2'	$[a_2']$
		a_2''	$[a_2'']$
		e'	e'
		e''	e''
	A_2'	a_1'	$[a_2']$
		a_1''	$[a_2'']$
		a_2'	a_1'
		a_2''	a_1''
		e'	e'
		e''	e''
	A_1''	a_1'	a_1''
		a_1''	a_1'
		a_2'	$[a_2'']$
		a_2''	$[a_2']$
		e'	e''
		e''	e'
	A_2''	a_1'	$[a_2'']$
		a_1''	$[a_2']$
		a_2'	a_1''
		a_2''	a_1'
		e'	e''
		e''	e'
A_2'	A_1'	a_1'	$[a_2']$
		a_1''	$[a_2'']$
		a_2'	a_1'
		a_2''	a_1''
		e'	e'
		e''	e''
	A_2'	a_1'	a_1'
		a_1''	a_1''
		a_2'	$[a_2']$
		a_2''	$[a_2'']$
		e'	e'
		e''	e''
	A_1''	a_1'	$[a_2'']$
		a_1''	$[a_2']$
		a_2'	a_1''
		a_2''	a_1'
		e'	e''
		e''	e'
	A_2''	a_1'	a_1''
		a_1''	a_1'
		a_2'	$[a_2'']$
		a_2''	$[a_2']$
		e'	e''
		e''	e'

[a] The square brackets indicate that these nuclear spin symmetries do not exist and so the combination corresponding to these is not an allowed combination.

It is now possible to answer the second question: what transitions involving torsional levels should one expect to see in an electronic excitation spectrum? This has been tackled by Weisshaar and co-workers[32], who proposed using a Fourier expansion of the change in the electronic transition moment with respect to the torsional angle to explain band intensities, as opposed to a Taylor expansion as would be used for vibrations. This was also more recently addressed by Virgo, Gascooke and Lawrance[39], who focused on understanding the intensities of transitions to the m = 3(+) and 3(-) levels.

Following the ideas of reference 32, one must look at the dependence of the electronic transition moment on the torsional angle:

$$\boldsymbol{M} = \langle m'|\langle \psi'(\boldsymbol{q};\alpha)|\boldsymbol{\mu}|\psi''(\boldsymbol{q};\alpha)\rangle|m''\rangle \qquad \text{Eq. 3.8}$$

Where $\boldsymbol{\mu}$ is the electric dipole moment operator, m' and m'' are the torsional quantum numbers in the upper and lower electronic states respectively, and one can see the dependence of the electronic wavefunctions, ψ, on both the electronic coordinates, $\boldsymbol{q}$, and the torsional angle, α. One can look at the components of $\boldsymbol{\mu}$ along the principal axes a, b and c, which one can see from Table 3.1 transform as the G_{12} symmetries A_1', A_1'' and A_2'' respectively, and by analogy to vibronic selection rules,[50] the criterion for allowed transitions here is that:

$$m' \times \psi' \times \boldsymbol{\mu} \times \psi'' \times m'' \supseteq A_1'.$$

Tackling the problem first for the $S_1 \leftarrow S_0$ transition, and having indicated in section 3.A.2.3. that the symmetries of the S_0 and S_1 electronic states are A_1' and A_1'' respectively, it may be seen that $\psi' \times \boldsymbol{\mu} \times \psi''$ will transform as A_1'', A_1' and A_2' for the a, b and c components of the electric dipole moment operator respectively. In passing, it is noted that the purely electronic transition will be polarized along the b-axis, as $\psi' \times \psi''$ corresponds to T_b, as shown in Table 3.1. Carrying out the Fourier expansion in terms of the torsional angle:

$$\boldsymbol{M}(\alpha) = M_0 + M_3\cos(3\alpha) + M_6\cos(6\alpha) + M_6'\sin(6\alpha) + \ldots \quad \text{Eq. 3.9}$$

Where M_i are the expansion coefficients. The leading terms can then be separated by their symmetries:

$$M^a(\alpha) = M_3\cos(3\alpha) \quad A_1''$$
$$M^b(\alpha) = M_0 + M_6\cos(6\alpha) \quad A_1'$$
$$M^c(\alpha) = M_6'\sin(6\alpha) \quad A_2'$$

With the symmetries based on understanding that, with α = 0 defined as the eclipsed conformer, sin(3α) transforms as a_2'', cos(3α) transforms as a_1'', sin(6α) transforms as a_2' and cos(6α) transforms as a_1' in the G_{12} MSG. All that is left is to combine the m' and m'' symmetries with the above, such that the resulting products are totally symmetric, to obtain all of the allowed transitions.

Since m'' must be either m = 0 (a_1') or m = 1 (e''), one can simply work out all *a*, *b* and *c*-type transitions which can arise from those levels. Here, only transitions up to a Δm = 6 are considered, as higher order terms are expected be negligible, owing to convergence of the series.

For m'' = 0, an a_1' level, the m' which will combine to give an overall totally symmetric electronic transition moment are:

a-type: m' = 3(+) (a_1'')
b-type: m' = 0, 6(+) (a_1')
c-type: m' = 6(-) (a_2')

For m'' = 1, an e'' level, the m' which will combine to give an overall totally symmetric electronic transition moment are:

a-type: m' = 2, 4 (e')
b-type: m' = 1, 5, 7 (e'')

c-type: $m' = 1, 5, 7 \quad (e'')$

Now that all of the possible allowed transitions have been derived, there are a few aspects to consider regarding any intensity that these may have. First, it should be noted that the M_0 term will drive $\Delta m = 0$ transitions, the M_3 term will drive $\Delta m = \pm 3$ transitions and the M_6 terms will drive $\Delta m = \pm 6$ transitions, and that larger changes in Δm give rise to weaker transitions, since the higher M_n terms will be smaller, and perhaps negligible, as the series is expected to converge[32,39].

The *b*-type transitions are transitions to torsional levels of the same symmetry as $m = 0$ and $m = 1$, and so the intensities of these transitions can be described in an analogous way to Franck-Condon factors for vibrations[32]; this covers transitions such as m_0^0, m_1^1, m_1^5, m_1^7 and $m_0^{6(+)}$, where this is a standard spectroscopic notation, m_i^j, where i is the m level in the lower electronic state (here S_0) and j is the m level in the upper electronic state (here S_1). The M_0 term drives $\Delta m = 0$ transitions, while the $M_6 \cos(6\alpha)$ term drives $\Delta m = \pm 6$ transitions, recalling that the *e* levels are signed and degenerate such that an $m = \pm 1 \rightarrow \mp 5$ transition is a $\Delta m = \pm 6$ change. As discussed above, the non-zero *a*-symmetry levels (3,6… etc) are signed but not degenerate, but the same Δm arguments apply, for example $m = 0 \rightarrow 6(+)$ or $m = 0 \rightarrow 6(-)$ are $\Delta m = 6$ transitions.

The *a*-type transitions are driven by the M_3 term and are $\Delta m = \pm 3$ transitions. These are not Franck-Condon allowed, but rather are allowed by a vibronic[d] coupling mechanism involving a higher electronic state such as the S_2 electronic state (of A_1' symmetry). This is analogous to the Herzberg-Teller intensity stealing mechanism invoked for the appearance of non-totally symmetric vibrations in electronic excitation spectra.

[d] As a reminder, in this thesis the term "vibronic coupling" will be used as an umbrella term to include vibration-electronic, torsion-electronic and vibration-torsion-electronic coupling. Here it is really a torsion-electronic coupling mechanism.

Weisshaar and co-workers[32] have rationalised the observation that the $m_0^{3(+)}$ transition is observed with up to twice the intensity of the m_1^2 and m_1^4 transitions. As was discussed by them, there are twice as many nuclear spin functions of *a* symmetry compared to *e* symmetry (shown above, for example, 80 A_1' vs 40 E'' functions), while there are effectively twice the number of torsional levels of *e* symmetry compared to *a* symmetry (from *m* = 1 to *m* = 6 there are 8 *e* symmetry and 4 *a* symmetry levels). Weisshaar and co-workers state that at 300K, these two factors cancel almost exactly, and so under the jet expansion conditions used in the current work, there is a ~1:1 ratio of the *m* = 0 to *m* = 1 initial populations. Thus, for *N* molecules, there are *N*/2 in the *m* = 0 level, and so *N*/2 can undergo the $m_0^{3(+)}$ transition. For the *m* = 1 levels, there are *N*/4 in *m* = +1 and *N*/4 in *m* = -1, and so the transitions m_{+1}^{-2}, m_{-1}^{+2}, m_{+1}^{+4} and m_{-1}^{-4} each have *N*/4 molecules contributing. Thus, populations do not explain the intensity difference, which appears to be determined by an additional factor: the transition moment for $m_0^{3(+)}$ is larger than for m_1^2 and m_1^4 by a factor of √2, with the intensities dependant on the square of the transition moment.[32]

Reference 32 also notes that the sum of the intensities of the m_1^2 and m_1^4 transitions is equal to that of the $m_0^{3(+)}$ transition, and that the V_6 barrier can couple the m = ±2 to the ∓4 levels, albeit only weakly for a small barrier. It was proposed that this coupling shifts intensity from m_1^2 to m_1^4 for a negative V_6 barrier, and from m_1^4 to m_1^2 for a positive V_6 barrier; complete mixing would occur in the case of an infinite barrier, and lead to the observation of only m_1^4 for a negative V_6 barrier and m_1^2 for a positive V_6 barrier.

The *c*-type transitions could again derive intensity from vibronic coupling; for example, in theory one could observe a transition to the *m* = 6(-) level if the transition to such an a_2' torsion in an A_1'' electronic state, A_2'' overall, stole intensity from an allowed electronic transition to a nearby A_2'' state, although no such state is thought to be energetically close to the S_1 state. However, in the case of *m* = 6(-), the transition would correspond to a $\Delta m = \pm 6$ change, and so would be expected to be weak at best, and as discussed below, there are other mechanisms which can explain the intensity of *m* = 6(-), such as torsion-rotation

coupling. Note that all of the *c*-type transitions are Δm = 6 changes, and so expected to be weak, whereas the *a*-type transitions were all Δm = 3 changes. As such, the *a*-type and *b*-type transitions will be seen to dominate the spectra, rather than the *c*-type transitions.

Although the terms Franck-Condon allowed/forbidden have been used above, it is important to clarify that: (a) it is not formally "Franck-Condon" in the sense that these are not vibrations and: (b) although a transition may be "Franck-Condon" allowed in the sense that the initial and final torsion/vibtor levels are of the same symmetry, this does not mean that any intensity is "Franck-Condon" intensity. Intensity could also come from a vibronic coupling mechanism, and so later in the chapter, the term "symmetry-allowed" will be used to describe such transitions.

Finally, for the $S_1 \leftarrow S_0$ transition, one should note that none of the leading terms of the Fourier expansion can give rise to a transition to the m = 3(-) level but such transitions have been observed weakly in $S_1 \leftarrow S_0$ electronic excitation spectra[21,38]. Such a transition would require an a_2'' term, i.e. a $\sin(3\alpha)$ term in the Fourier expansion. This has been explained by Weisshaar and co-workers[32], and more recently shown by Virgo, Gascooke and Lawrance[39], as owing to an incomplete mixing of the $\underline{m}$ = +3 and $\underline{m}$ = -3 free rotor levels, mediated by a torsion-rotation coupling mechanism. Summarising that work, one can see that if the two free rotor levels are perfectly degenerate, in the absence of torsion-rotation coupling, the m = 3(+) (symmetric) combination will have equal and complementary contributions from $\underline{m}$ = +3 and -3, while the m = 3(-) (asymmetric) combination will have equal and opposing contributions from these levels, leading to zero intensity for the m = 3(-) transition. However, upon invoking torsion-rotation coupling, which is sensitive to the sign of K and $\underline{m}$, the degeneracies of the $\pm K$ and $\underline{m}$ = ±3 levels are each broken. This means that the free rotor contributions to the m = 3(-) level do not completely cancel, and the extent of mixing between the free rotor levels becomes sensitive to the barrier height (lower barriers will lead to less complete mixing) and the rotational temperature (as the torsion-rotation coupling term is K-dependent). In the same

way, it was also predicted that this mechanism will give some intensity to the $m_0^{6(-)}$ transition at the expense of the $m_0^{6(+)}$ one.

3.A.2.5. Vibration-torsion levels

Having discussed the intensities of pure torsional transitions, transitions to so-called vibtor (vibration-torsion) levels will now be considered briefly. Technically, a vibtor level is a vibration in combination with any torsional level other than $m = 0$, but often in this thesis, $m = 1$ is implicitly included in the designation of a vibration rather than a vibtor level. For example, in a REMPI spectrum of *p*FT, one observes totally symmetric vibrations such as D_{11}, and one is observing transitions to both the D_{11} $m = 0$ and D_{11} $m = 1$ levels as both $m = 0$ and $m = 1$ torsional levels have population in the jet expansion. As such, it makes sense to treat a pure vibration as including both $m = 0$ and $m = 1$ levels, and in those cases the vibration is simply written with the D_i label, implying both torsional components. A vibtor level is then any other torsional level in combination with a vibration. For non-totally symmetric vibrations, it is possible that only one of the $m = 0$ or $m = 1$ levels (or neither) is observed, and in those cases the observed component is written explicitly, for example as D_{20} $m = 1$, which will be seen later.

One can think of the intensities of transitions to vibtor levels analogously to the discussion for torsional levels above. There are symmetry-allowed transitions to terminating vibtor levels which take the same symmetry as $m = 0$ (a_1') or $m = 1$ (e''), analogous to the *b*-type torsional transitions discussed above. For vibtor levels of a_1'' or e' symmetry, these can gain intensity through an electronic state coupling mechanism, referred to in this thesis as vibronic coupling, by analogy to vibronic coupling for the *a*-type torsional transitions discussed above. *c*-type transitions are also analogous to those discussed for torsions above, with vibronic coupling an option for intensity, but no state of the correct symmetry is thought to be close to the S_1 state.

3.A.2.6. $D_0^+ \leftarrow S_1$ transitions

The above discussion of the expected torsional and vibtor transitions, and a guide as to their intensities, has been framed with respect to the $S_1 \leftarrow S_0$ electronic transition, but what about transitions from $D_0^+ \leftarrow S_1$, such as will be observed in the ZEKE spectra? Simply, one expects ZEKE spectra recorded *via* different intermediate torsion, vibration and vibtor levels to be dominated by symmetry-allowed structure, which can have significant Franck-Condon intensity. The dominant transition in a ZEKE spectrum is expected to be the $\Delta m = 0$, $\Delta v = 0$ or $\Delta(v,m) = 0$ transition, with other accompanying symmetry-allowed structure. These propensity rules are based on the expected similarity of the S_1 and D_0^+ electronic states, and the expected similarity of the torsional and vibrational coordinates in those two states, such that the most significant Franck-Condon overlap is expected with the level in the cation analogous to the one initially excited in the S_1 state.

One can also observe weak structure in ZEKE spectra that is not symmetry-allowed. For example, recent work by our group has investigated the C_{2v} symmetry *para*-chlorofluorobenzene (*p*ClFB) molecule[51,52], and a ZEKE spectrum recorded *via* the S_1 origin showed weak bands attributable to D_{20} (b_1), D_{19} (b_1) and D_{14} (a_2), and these three vibrations are also observed in origin ZEKE spectra recorded previously for *p*DFB[53,54]. These non-totally symmetric bands are thought to arise owing to vibronic coupling, but interestingly, the same vibrations were observed in the one-photon MATI spectrum recorded by Kwon *et al*.[55] for *p*DFB. Since ionisation is occurring from the S_0, A_g, electronic state in that case, and from the S_1, B_{2u}, electronic state in the ZEKE case, if the mechanism were an intensity stealing, Herzberg-Teller, one, different symmetry vibrations would be expected to be observed in the two cases. Additionally, only one electronic state is expected close (within 1 eV) to the D_0^+ state in the cation[56] (with the others expected over 2.5 eV away), placing further doubt that a Herzberg-Teller mechanism could explain the intensity in these Franck-Condon forbidden transitions.

Reiser *et al*.[53] noted that, for *p*DFB, emission of an electron of the correct symmetry (i.e. a Rydberg orbital of the correct symmetry) would allow effectively any transition to be vibronically allowed. Since one does not observe all transitions, this does not seem likely, and additionally, this assumes Rydberg orbitals of *s*, *p*, *d* and *f* types are populated. However, one might make the (sensible) assumption that if the Rydberg state symmetry is important, then there is some interaction between the ionic core and the Rydberg electron, and so one would only expect the most penetrating Rydberg orbitals (*s* and *p*) to be important.

An alternative mechanism was discussed in our recent work on *p*DFB[54], and will not be discussed in detail here. This was based upon earlier work by Poliakoff, Lucchese and co-workers[57,58], who discussed the idea of "intrachannel coupling" as an explanation for the activity of Franck-Condon forbidden vibrations in the photoelectron spectra of CO_2. This mechanism does not depend on the proximity of a nearby electronic state like the Herzberg-Teller mechanism does (that mechanism would be termed "interchannel coupling"), and instead arises from the inseparability of the electronic and nuclear motions. If this mechanism is important, it would also explain why the same non-totally symmetric activity is observed in the one-photon MATI and the two-photon ZEKE experiments.

Thus, it seems that a number of different (vibronic coupling) mechanisms may contribute to the observation of non-totally symmetric vibrations in the ZEKE spectra. However, the key observation is that in both *p*ClFB and *p*DFB (and as will be seen later *p*FT and *p*Xyl), the same non-totally symmetric vibrations are observed, suggesting the same mechanism(s) is/are at work for these molecules. For *p*FT, one can make the natural extension of including the torsional levels, with the origin ZEKE spectra recorded *via* both $m = 0$ and $m = 1$ levels, allowing transitions from both to be observed. Although the coupling mechanisms are analogous for both levels, different transitions could be observed from the $m = 1$ initial level, owing to its different symmetry.

For ZEKE spectra recorded *via* non-totally symmetric initial levels, the same arguments apply, but different symmetry terminating levels may be observed in the ZEKE spectra.

From previous work on different substituted benzene molecules[34,37], it is possible to observe both the m = 3(-) and m = 3(+) terminating levels in the origin ZEKE spectra, as opposed to only expecting significant intensity for transition to m = 3(+) in the REMPI spectrum. This is thought to be owing to the proximity of low-lying electronic states, with intensity for transitions to these levels from a Herzberg-Teller type mechanism[e]. The m = 3(-) level is of a_2'' symmetry, and the D_0^+ state is of A_2'' symmetry, yielding a vibronic symmetry of A_1', and so a transition to this level from the m = 0 level of the S_1 state could steal intensity from a transition to a low-lying $^2A_1'$ state in the cation (or more likely be observed owing to the intrachannel mechanism mentioned above). The m = 3(+) level is of a_1'' symmetry, and so has a vibronic symmetry in the D_0^+ state of A_2', and thus its intensity is thought to be dependent on the proximity of a low-lying $^2A_2'$ electronic state in the cation – this is the state found to be within 1 eV in reference 56.

Based on a comparison of different molecules, discussed briefly later in this chapter, it appears that the m = 3(-) terminating level is always observed in these methyl-substituted benzene molecules, while in some molecules m = 3(+) is observed[34,37], and in others it is not[31,45,f], with the appearance of transitions to m = 3(+) correlating with the observation of vibrations of the same symmetry in the origin ZEKE spectra. This supports the involvement of a low-lying $^2A_2'$ state in molecules where the transition to m = 3(+) is observed.

[e] While an intrachannel mechanism could be important, especially for the transition to m = 3(-) which takes the same symmetry as the observed D_{20} and D_{19} vibrations, the fact that one does not always observe the transition to m = 3(+) in the origin ZEKE spectra of a range of molecules is suggestive of the involvement of another electronic state which changes in energy between species.

[f] It is notable that Lu *et al.*[31] assigned a band and a shoulder to the terminating levels m = 3(+) and m = 3(-) in their ZEKE spectrum recorded *via* the toluene S_1 origin. As discussed later in this chapter, this entire band is now thought to arise from a transition to m = 3(-), with the shoulder owing to rotational effects.

In summary, although it is not entirely clear what mechanism(s) give rise to non-totally symmetric structure in the origin ZEKE spectra of these molecules, since the most significant structure in the ZEKE spectra is expected to be symmetry-allowed, it is sufficient in the current work to assign the weaker structure by analogy to the vibronic structure in other molecules, such as *p*ClFB and *p*DFB.

3.A.2.7. Vibration-torsion interactions

Vibration-torsion interactions will be observed throughout the low wavenumber region of *p*FT discussed in this chapter. These will be discussed at the appropriate points, but a few general remarks can be made.

Vibration-torsion coupling can be visualised as the torsional potential changing as the molecule vibrates along a particular coordinate[9], thus coupling the vibrational and torsional motions together. This then leads to myriad couplings between levels observed in the excitation spectra, as shown by Gascooke and Lawrance for toluene.[41]

As with coupling between vibrations, such as Fermi resonance, the levels involved must be of the same symmetry and close energetically (in the zero-order picture) for a strong interaction to occur. In Chapter 1, it was noted that stronger couplings tend to occur between levels that have smaller quanta changes between them[59]. Here, it will be seen that $\Delta v = 1$, $\Delta m = 3$ changes appear to give strong couplings, and a number of these will be discussed.

3.B. The low wavenumber region of the S_1 state of *para*-fluorotoluene

Having discussed the most important theoretical background for the single rotor *p*FT molecule, attention will now be given to the spectra, starting with an overview of the REMPI spectrum shown in Figure 3.4. The intense S_1 origin transition is offset to 0 cm^{-1}, such that the spectrum is presented on an internal energy scale for the S_1 state. A similar approach will be undertaken with the

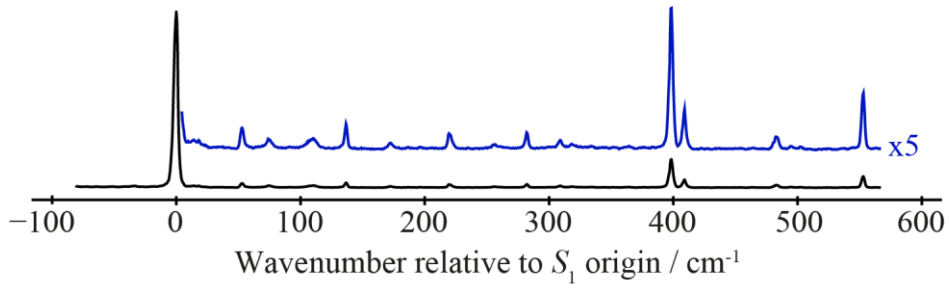


Figure 3.4 – An overview of the low wavenumber region of the $S_1 \leftarrow S_0$ REMPI spectrum of pFT.

ZEKE spectra, where the adiabatic ionisation energy (AIE) has been calibrated to 70946 cm^{-1}, in line with earlier work[28], and in the spectra presented here is offset to 0 cm^{-1} to yield an internal energy scale for the cationic ground state. The S_1 origin transition has been calibrated to be 36859.9 cm^{-1} based on the work of Okuyama *et al.*[20], although the value of this has no effect on the relative energy scales presented here as a simple offset is used. The plethora of features in the REMPI spectrum is immediately apparent, and a cursory glance at the B3LYP/aug-cc-pVTZ calculated S_1 vibrational wavenumbers given in Table B.1 in Appendix B, indicates that the lowest wavenumber S_1 state vibration, D_{20}, is expected around 110 cm^{-1}, and as this vibration is non-totally symmetric one might expect the lowest vibrational band to be its first overtone at around 220 cm^{-1}. This suggests that much of the low wavenumber structure must be assignable to transitions to the torsional levels, and attention will initially be given to this low wavenumber region.

For the REMPI and ZEKE spectra, the spectroscopic notation $v_a^b\, m_i^j$ will be used to denote the transitions. Often the lower levels will be omitted, and will be obvious from context, but these are sometimes retained to emphasise the different torsional ladders arising from $m = 0$ and $m = 1$.

3.B.1. Below 100 cm^{-1}: the pure torsional region

Figure 3.5, trace (b), shows the region of the *p*FT REMPI spectrum up to around 125 cm^{-1}. Before looking at the ZEKE spectra recorded *via* the various features in this region, a few general remarks can be made. First, the previous study of this region by Okuyama *et al.*[20] (with the later study of Zhao *et al.*[21] being

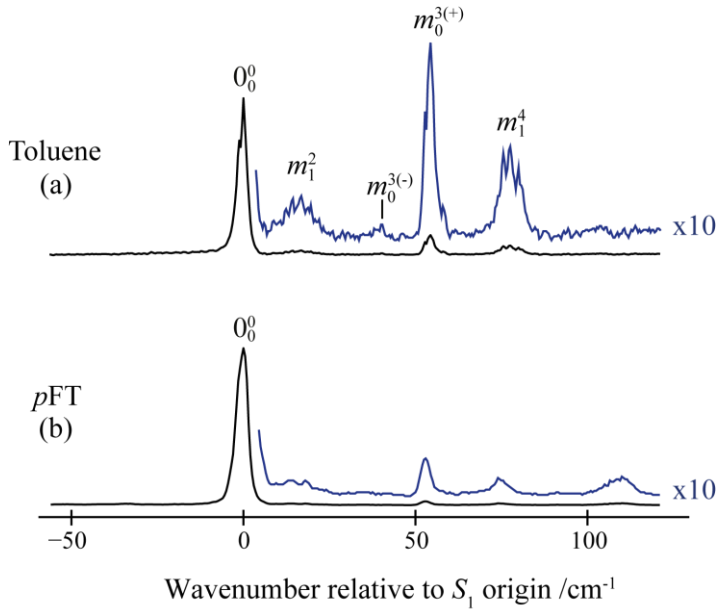


Figure 3.5 – The toluene (a) and pFT (b) $S_1 \leftarrow S_0$ REMPI spectra up to 125 cm^{-1} are shown. The toluene spectrum is reproduced from data published in reference 45.

consistent with that work) assigned the structure below 100 cm^{-1} to transitions to the pure torsional levels m = 2, m = 3(+) and m = 4, with assignments deduced with the aid of DF spectroscopy, and from these and higher wavenumber assignments, they obtained an S_1 state internal rotation constant value of F = 4.879 cm^{-1} and a barrier to internal rotation of V_6 = -33.7 cm^{-1}. These values will be returned to shortly.

As discussed in section 3.A.2.2., all of the free rotor levels except $\underline{m}$ = ±3 and $\underline{m}$ = ±6 will be effectively unperturbed by the V_6 barrier, and as such it should be straightforward to predict the internal energies of the m = 2 and m = 4 levels from Eq. 3.4. Assuming that the fluorine in *p*FT has no influence on the internal rotation constant (since it is along the same axis as the methyl group) then its value can be taken to be the same as for toluene. By comparing the REMPI spectra of *p*FT and toluene, as has been done in Figure 3.5, one can see that the structure appears at almost identical wavenumbers in the two cases, suggesting strongly that it can be assigned as torsional activity, and that using the same F value for *p*FT as was derived for toluene is a valid approach. This does neglect any other couplings, which will be returned to later, but regardless is a good first approximation.

Table 3.4– Predicted free rotor transitions and experimental band positions

m level	Predicted free rotor transitions using F for pFT from Okuyama *et al.*[20] /cm^{-1}	Predicted free rotor transitions using F for toluene[40,41] /cm^{-1}	Experimental band positions /cm^{-1}
0	0.0	0.0	0.0
1	-0.6[a]	0.0[b]	0.0
2	14.1	16.4	16.5
3[c]	43.9	49.1	-[d]
4	72.6	81.8	76.0
5	116.5	130.9	142.0
6[c]	175.6	196.4	-[d]

[a] This is because of the difference in the S_0 and S_1 F values of reference 20.
[b] The values of F in the S_0 and S_1 states of toluene are very close, with the transition to m = 1 effectively degenerate with the transition to m = 0, and certainly degenerate within the resolution of this experiment.
[c] As this is for the free rotor, the mixing of these levels by the V_6 barrier has not be accounted for. These, as with all non-zero free rotor m levels, are signed and degenerate.
[d] There will be two different transition energies (if both are observed), one for each of the linear combinations, and neither will be at the free rotor positions, even if unperturbed by coupling with other levels – see text.

Gascooke, Virgo and Lawrance[41] have shown F to be 5.455 cm^{-1} for the S_1 state of toluene, and using this value, the m = 2 level is expected at 21.8 cm^{-1}, while the m = 4 level is expected at 87.2 cm^{-1}. In order to compare these to the spectrum shown, these need to be converted to transition energies, since transitions to m = 2 and m = 4 (i.e. e symmetry levels) must start in m = 1 rather than m = 0, so one must subtract the m = 0 – 1 spacing in the ground electronic state (with F = 5.45 cm^{-1}, as for the S_0 state of toluene[40,g]). Thus, the predicted m_1^2 transition is at 16.4 cm^{-1}, while the predicted m_1^4 transition is at 81.8 cm^{-1}. These predicted free rotor transition energies and the experimental band positions from this work are given in Table 3.4 for the "pure" torsional excitations.

One can see that the observed m_1^2 transition wavenumber agrees well with the predicted transition wavenumber but the observed m_1^4 is discrepant by around 6 cm^{-1}. This could be down to the choice of F, although this seems unlikely based on the similarity of the m_1^2 torsional band in the REMPI spectra of pFT

[g] This is very similar to the value of 5.46 cm^{-1} proposed by Okuyama *et al.*[20] and Zhao *et al.*[21] for pFT.

and toluene. One could instead use the F values proposed by Okuyama *et al*.[20], and the free rotor levels predicted in this way are also shown in Table 3.4, but these are in overall poorer agreement, and as will be shown later, misassigned levels were used in the fit to generate their value of F = 4.879 cm^{-1} in the S_1 state. Additionally, one might expect to be able to observe the separation of the m_0^0 and m_1^1 transitions if the values of Okuyama *et al*. are correct, and this was not possible. Since it seems that using F values from toluene is a sensible approach, either the previous assignments are incorrect, or one or more of these S_1 torsional levels are perturbed by interaction with higher vibrations or vibtor levels, as discussed in the work of Gascooke and Lawrance on toluene, for example that of reference 41.

With regard to the m = 3 levels, if the V_6 value of -33.7 cm^{-1} from the work of Okuyama *et al*.[20] is correct, then the m = 3(+) level is expected to be the higher of the two levels, at $|V_6|/4$ above the free rotor energy, and the m = 3(-) level to be the lower of the two, at $|V_6|/4$ below the free rotor energy. This would place the m = 3(+) level at 57.5 cm^{-1} and the m = 3(-) level at 40.7 cm^{-1}, using the free rotor energy predicted by the toluene constants.

This predicted m = 3(+) energy is close to the observed band position of 53.5 cm^{-1}, which is the band assigned to this level in the work of Okuyama *et al*. and Zhao *et al*.[21], but one must be careful about interpreting the difference between observed $m_0^{3(+)}$ / $m_0^{3(-)}$ transitions and the predicted free rotor position as being directly related to the V_6 barrier, owing to the possibility of other perturbations, as discussed by Gascooke and Lawrance in reference 41 for the S_1 state of toluene. This point will be returned to shortly.

3.B.1.1. Spectra and assignments

The discussion now turns to the ZEKE spectra shown in Figure 3.6, which are recorded at positions within the three bands under discussion at 16.5 cm^{-1}, 53.5 cm^{-1} and 76.0 cm^{-1}. A ZEKE spectrum has also been recorded *via* the S_1 origin, part of which is shown in trace (b) of Figure 3.6, where the S_1 origin band itself is composed of the overlapping m_0^0 and m_1^1 transitions, which are

degenerate within the resolution of this experiment owing to the similarity of the internal rotation constant in both the S_0 and S_1 electronic states. This ZEKE spectrum will be discussed in more detail at the end of this chapter. For now, it is sufficient to note that ZEKE spectra were recorded on either side of the S_1 origin band profile, but it was not possible to distinguish the m = 1 and m = 0 levels in the ZEKE spectra, suggesting that the m_0^0 and m_1^1 transitions from $D_0^+ \leftarrow S_1$ remain energetically degenerate within the resolution of the ZEKE spectra. As such, the origin ZEKE spectrum presented in this thesis is one that was recorded at the centre of the band profile.

Trace (c) of Figure 3.6 shows the ZEKE spectrum recorded *via* the 0^0+16.5 cm^{-1} band and yields an intense band at 17 cm^{-1} in the cation and a weaker feature at 0 cm^{-1} in the cation, i.e. at the ionisation energy (IE). The intense band is assigned as a Δm = 0 transition to the m = 2 level, since there is nothing else expected at such a low internal energy, and this leads to the conclusion that the initial level is m = 2 in the S_1 state, as expected from the previous work and the free rotor predictions. The transition at the IE is a m_2^1 transition and represents the first of many Δm = 3 transitions (+2 to -1 and -2 to +1, recalling that all *e* symmetry *m* levels are signed and degenerate) that will be observed in the ZEKE spectra recorded *via* torsional and vibtor levels.

Trace (e) of Figure 3.6 shows the ZEKE spectrum recorded at 0^0+76.0 cm^{-1}, and the spectrum is dominated by a transition with a maximum at 79 cm^{-1}. Once again, based on the free rotor calculations and the lack of any vibrations calculated at such low internal energies, this can be assigned as a Δm = 0 transition, m_4^4, yielding an S_1 assignment of m = 4 in agreement with Okuyama *et al.*[20] and Zhao *et al.*[21]. Again, a Δm = 3 transition is observed to the IE, this time a m_4^1 transition, but additionally a band is observed at 114 cm^{-1} the assignment of which ($20_0^1 m_4^1$) will be returned to in section 3.B.2.1. In passing, it is noted that these ZEKE spectra recorded *via* the m = 2 and m = 4 levels are in good agreement with those of Takazawa *et al.*[27]

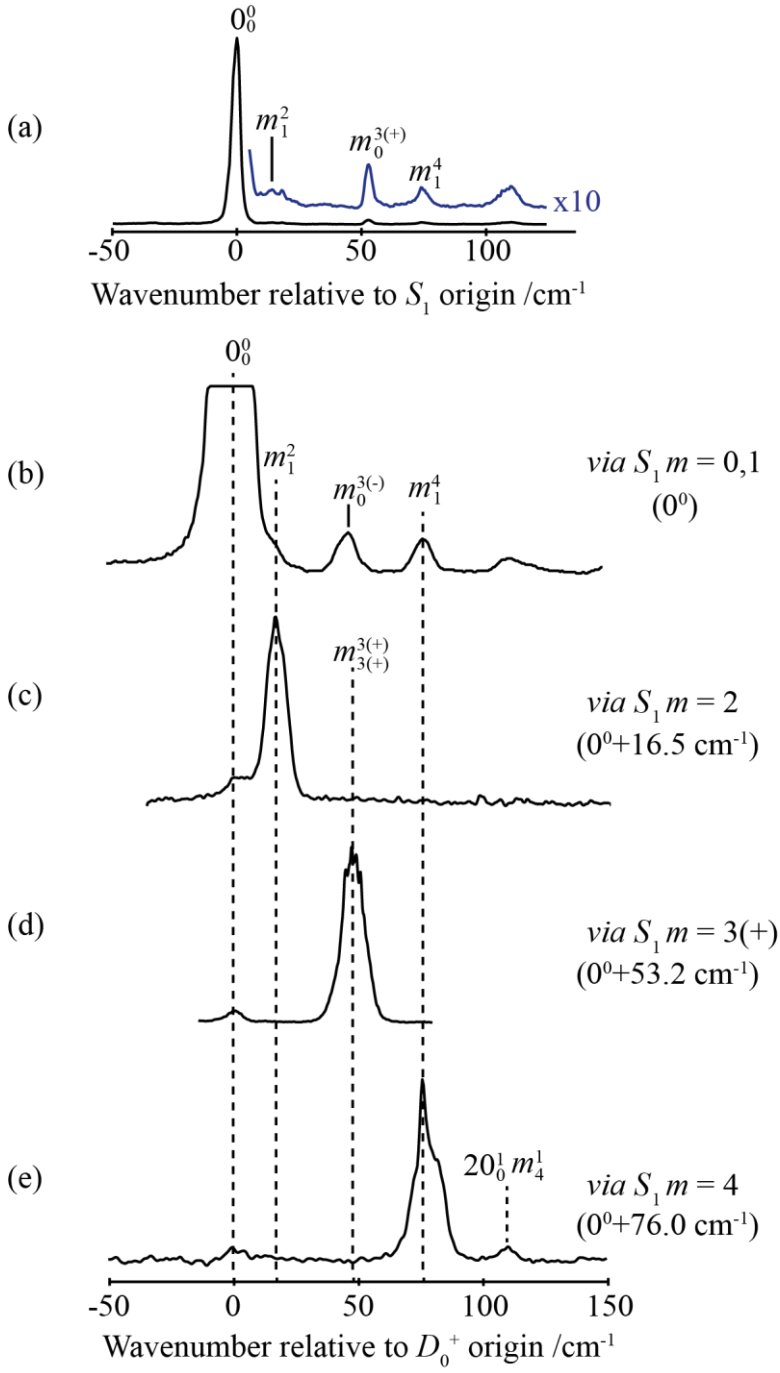


Figure 3.6 – The pFT $S_1 \leftarrow S_0$ REMPI spectrum up to 125 cm^{-1} is shown in (a). Traces (b) – (e) show ZEKE spectra recorded via the S_1: origin (m = 0,1 levels), m = 2 level, the m = 3(+) level and the m = 4 level respectively.

Trace (d) of Figure 3.6 shows a ZEKE spectrum recorded at 0^0+53.2 cm^{-1}, a position within the feature centred around 53.5 cm^{-1}, showing a single intense band with a maximum at 48 cm^{-1}. A transition to the m = 3(+) level is observed in the S_1 state of toluene, but a transition to the m = 3(-) level is not allowed by the same mechanism, as discussed in section 3.A.2.4., and so a transition to the

m = 3(-) level is either not present or significantly weaker. Based on this analogy with toluene, since only an *m* = 3 level would be expected at this excitation position, the S_1 level can be straightforwardly assigned as *m* = 3(+), with the analogous level in the cation at 48 cm^{-1}. Although this $m_{3(+)}^{3(+)}$ transition dominates this ZEKE spectrum, once again another Δm = 3 transition is observed, this time the $m_{3(+)}^{0}$ transition.

Looking at Figure 3.6, one can see that the assigned *m* = 2 and *m* = 4 terminating levels in the cation also appear in the ZEKE spectrum recorded *via* the origin, and at first glance it appears that the *m* = 3(+) terminating level is also present in the origin ZEKE spectrum. It will be seen in section 3.C. that D_{19} and D_{20} are observed in the origin ZEKE spectrum, as they are for other molecules, and since *m* = 3(-) takes the same symmetry as these it would also be expected in the origin ZEKE spectrum. It was discussed in section 3.A.2.6. that in some molecules a transition to *m* = 3(+) is also observed in the origin ZEKE spectrum, and this was thought to be due to the proximity of a nearby electronic state of A_2' symmetry, in order for it to gain intensity in a Herzberg-Teller fashion.

As such, it is not immediately apparent which of these assignments is correct for the band in the origin ZEKE spectrum. The band in the *m* = 3(+) ZEKE spectrum is at 48 cm^{-1}, while the band in the origin ZEKE spectrum is at 45 cm^{-1}, suggesting that they are different transitions, although transitions to the same level in the cation are observed to shift by a couple of reciprocal centimetres in spectra recorded *via* different S_1 intermediate levels, so one has to be cautious. This is likely due to excitation of different rotational levels depending on the part of the band profile excited, as illustrated below when exciting different parts of the $m_0^{3(+)}$ band profile.

In order to investigate this, multiple ZEKE spectra were recorded at various excitation positions over the S_1 origin band profile and the $m_0^{3(+)}$ band profile, to observe the position of the maximum of this "*m* = 3" ZEKE band. A selection of these spectra are shown in Figure 3.7, with the blue traces representing spectra recorded on the high wavenumber side of the bands, the red traces spectra on the

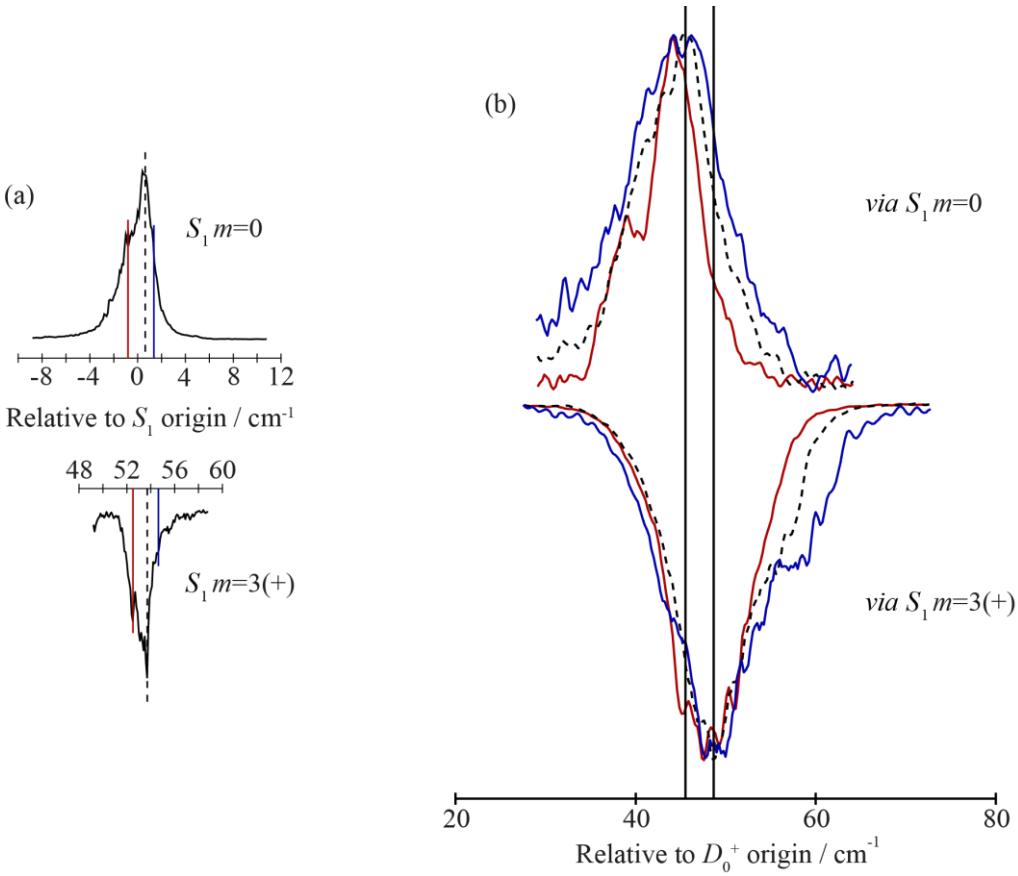


Figure 3.7 – (a) The top (upright) REMPI trace shows the S_1 origin of pFT and the bottom (inverted) REMPI trace shows the $m_0^{3(+)}$ of pFT, with the coloured and black lines indicating excitation positions for the ZEKE spectra. (b) Shows the ZEKE spectra recorded via these excitation positions over the region in which transitions to the m = 3(+) and m = 3(-) levels are expected in the cation. Once again, the top (upright) traces show ZEKE spectra recorded via the S_1 origin, while the bottom (inverted) traces show those recorded via the m = 3(+) level.

low wavenumber side of the bands, and the black traces recorded in the centre of the bands. One can see from the inverted traces in Figure 3.7(b) that the maximum of the $m_{3(+)}^{3(+)}$ transition is in the same position, 48 cm^{-1}, regardless of excitation position, and from the upright traces the transition in the origin ZEKE spectra is also consistently in the same position, 45 cm^{-1}. This, combined with the differences in the profiles of these ZEKE bands, leads to the conclusion that the band observed in the S_1 origin ZEKE spectrum is assignable to a transition to the m = 3(-) level and not the m = 3(+) level.

Before continuing, one may observe that the ZEKE spectrum recorded on the high wavenumber side of the m = 3(+) band contains a significant shoulder, but that this shoulder is absent when exciting at the centre of the band or on the low wavenumber side. Since there is no obvious assignment for this shoulder to a separate torsion, vibration or vibtor level, this suggests that it arises from exciting a different part of the rotational envelope of the band. A similar example was shown by Reiser *et al*.[53] for *p*DFB, who showed five ZEKE spectra exciting different parts of the band profile of the S_1 origin, and who also observed significant broadening to higher wavenumber in the ZEKE spectrum when exciting on the high wavenumber side of the feature.

If one compares the ZEKE spectra shown here to the one recorded by Takazawa *et al*.[27], in that work there is no obvious shoulder, and so that spectrum looks very similar to the one recorded at the centre of the band in this work. One can also look to other, similar, molecules such as toluene, where Lu *et al*.[31] observed a shoulder in their ZEKE spectrum recorded *via* the toluene S_1 m = 3(+) level, which they assigned to a transition to m = 3(-) in the cation, something which is obviously not the case here, and it is hypothesised that it was also not the case there. Consequently, one must be very cautious in disentangling overlapping features using ZEKE spectroscopy, as what may appear to be overlapping S_1 features manifesting as shoulders in the ZEKE spectra may in fact be excitation of different parts of the rotational envelope.

3.B.1.2. Discussion

Table 3.4 shows the predicted band positions from the toluene internal rotation constants. It was suggested in the previous section that the disagreement between the observed band positions and the predicted free rotor band positions could arise from an incorrect value of F, incorrect assignments, or perturbation to the torsional levels because of couplings. The ZEKE spectra shown in the previous section confirm the assignments of the m_1^2, $m_0^{3(+)}$ and m_1^4 bands in the REMPI spectrum, and so incorrect assignments can be ruled out. The remaining issues of choosing the correct value of F and perturbations to the levels must be

tackled together as these issues are coupled; to get a "true" value of F, one must look only at unperturbed levels.

One might look at the comparison of the *p*FT and toluene spectra shown in Figure 3.5 to aid in this, since it is assumed that *p*FT takes a similar F value to that of toluene, and the interactions between the levels in toluene are well understood thanks to the work of Gascooke and Lawrance[38,40–42]. They showed that many of the "pure" torsional levels interact with the lowest wavenumber vibration, and its associated torsional levels, a vibration referred to as M_{20} in the monosubstituted benzene labelling scheme[60] used for toluene. It will be seen in the following section that a similar picture holds true here, but for now it is worth noting that the low wavenumber m levels were perturbed significantly less than the higher (m = 5 – 7) levels in the case of toluene, owing to their energetic separation from the vibration/vibtor levels with which they were coupled. In this regard, one may expect the same to hold true for *p*FT if the lowest wavenumber vibration/vibtor level is similarly energetically separated from these low wavenumber torsions.

Of note is that the m = 3(+) level (of a_1'' symmetry) was essentially unperturbed in toluene, as there were no other levels of a_1'' symmetry nearby with which it could interact. A glance at Table B.1 in Appendix B shows that the same will be true here, as the lowest wavenumber a_1'' vibration (D_{30}) is calculated to be at 307 cm^{-1} in the S_1 state[h], and the lowest wavenumber vibtor levels which can have this symmetry would be D_{14} m = 3(-) (predicted at 221 cm^{-1}) and D_{20} m = 6(-) (predicted at 306 cm^{-1}), with these predicted positions from the toluene free rotor torsional positions and the calculated *p*FT vibrational wavenumbers. One can immediately see a significant energetic separation between the m = 3(+) and any of these levels, and as such, one can conclude that the m = 3(+) level is effectively unperturbed by any interaction with vibration or vibtor levels.

[h] Note that a_1'' symmetry vibrations are of b_2 symmetry in the C_{2v} point group and are well known to be observed in $S_1 \leftarrow S_0$ electronic excitation spectra of substituted benzene molecules by a Herzberg-Teller vibronic coupling mechanism.

If one assumes that the m = 2 level is perturbed little from the free rotor, as excluding m = 0 and m = 1, it is the torsional level most energetically removed from any vibtor levels, then the excellent agreement between the predicted m_1^2 transition from the internal rotation constants of toluene and the observed m_1^2 transition energy suggests that the F value for toluene is close to that of *p*FT.

One might be tempted to estimate a V_6 barrier by taking the difference between the (effectively unperturbed) m = 3(+) level and the predicted $\underline{m}$ = 3 position as $|V_6|/4$, yielding $|V_6|$ = 17.6 cm^{-1}. Subsequently, one could assume a staggered conformation based on: the previous work on S_1 state toluene[41], and the m = 3(+) being observed above, rather than below, the predicted $\underline{m}$ = 3 position. This approach gives V_6 = -17.6 cm^{-1}. This can be termed this $V_6^{observed}$.

This approach fails to account for the fact that the free rotor $\underline{m}$ = 3 position is on a different relative energy scale to the observed m = 3(+) position, as even if the m = 3(+) is not perturbed, the m = 0 level can be involved in interactions and perturbed lower in wavenumber in the observed case than $\underline{m}$ = 0 in the free rotor case. This means this $V_6^{observed}$ will be an overestimate compared to $V_6^{unperturbed}$; doing the same analysis for toluene gives $V_6^{observed}$ = -19.2 cm^{-1}, and it has been shown that $V_6^{unperturbed}$ = -5.59 cm^{-1} for that molecule.[41] It will be seen later that the vibtor levels with which m = 0 can interact are lower in wavenumber in *p*FT than in toluene, which would imply a larger perturbation of the m = 0 level and thus a larger overestimate of $V_6^{observed}$ relative to $V_6^{unperturbed}$ above, suggesting a very low barrier, perhaps lower than toluene.

It may not be immediately obvious why $V_6^{unperturbed}$ is important. The most obvious use of this is to correctly predict the lowest energy conformer, for which the unperturbed V_6 barrier is required, rather than the observed (perturbed) one which is distorted by the couplings. However, when the unperturbed barrier is low, the lowest energy conformer is not particularly important, as most of the torsional levels lie above the barrier and, as discussed by Gascooke, Virgo and Lawrance[40], the probabilities (from the torsional wavefunction) become almost independent of the torsional angle, i.e. the molecule does not really favour one conformer or the other. In the present study, little can be said other than what

was mentioned above – that the unperturbed V_6 is expected to be very small, and as such, the molecule is likely sampling both conformations significantly.

It is apparent $m_0^{3(-)}$ is not observed in the REMPI spectrum of *p*FT presented in Figure 3.5, whereas it is present in the toluene spectrum presented there. Additionally, it is notable that $m_0^{3(-)}$ was observed for toluene by Gascooke and Lawrance[41], albeit very weakly, although it does not appear to be present in the spectrum presented by Lu *et al*.[31]. In previous work on *p*FT, there is a feature to lower wavenumber than $m_0^{3(+)}$ which could be assigned to $m_0^{3(-)}$ in the LIF spectrum of Okuyama *et al*.[20], and it also appears (and is assigned) in the spectrum of Zhao *et al*.[21], who record a DF spectrum *via* it. This being the case, in the present work the conditions were varied to try to induce the $m_0^{3(-)}$ band (as it has a rotational temperature dependence), and a helium backing gas was also trialled, but no spectra were recorded which showed the $m_0^{3(-)}$ transition. As such, it is not possible to comment on its position in the S_1 state, perturbed or unperturbed, although the band position of the $m_0^{3(+)}$ reported by Zhao *et al*.[21] is 53 cm^{-1}, in good agreement with the value obtained here, and so one expects that their reported value of 37 cm^{-1} for $m_0^{3(-)}$ is correct. The observation of the $m_0^{3(-)}$ under certain conditions and not others is highly supportive of a low V_6 barrier, and thus incomplete mixing of the free rotor levels.

Finally, a few comments can be made regarding the torsional potential and the internal rotation constant in the cationic ground state. It is notable that the $m = 2$ level is at effectively the same internal energy in the cation as in the S_1 state, while the $m = 4$ level is around 3 cm^{-1} higher in the cation. That the $m = 2$ level is in the same position is suggestive of the value of F being similar in the cation and the S_1 state, and $m = 4$ is closer to the predicted value than in the S_1 state, consistent with weaker interaction in the cation owing to larger energetic separation with the relevant vibtor levels. Making refinements of the F value from the ZEKE spectra is difficult, owing to a full-width at half-maximum (FWHM) of the ZEKE transitions of around 7 cm^{-1}, but the indications are that the F value is not particularly sensitive to the electronic state, something noted by Gascooke and Lawrance for toluene with their refined values of F for the S_0

and S_1 states.[40,41] This being the case, it appears that here, the F value is very similar in the S_1 and D_0^+ states (and S_0 based on previous work[21]), and that it takes a value similar to the 5.45 cm^{-1} value of toluene.

The observed positions of m = 3(+) and m = 3(-) in the cation are 48 cm^{-1} and 45 cm^{-1} respectively. As in the S_1 state, there are no other levels of a_1'' symmetry nearby which can interact with the m = 3(+), which is effectively unperturbed, as in the S_1 state. This being the case, it would perhaps be surprising that the m = 3(+) level is below the free rotor prediction of 49.1 cm^{-1}, assuming the same value of F in the D_0^+ state as in the S_1 state. This suggests that the cation is an eclipsed minimum energy geometry, i.e. a positive V_6 value, and thus m = 3(+) should be lower than m = 3(-), but that m = 3(-) has been perturbed down energetically such that this ordering is reversed. If the V_6 barrier is low, as expected, it need only be perturbed a small amount to switch ordering with the m = 3(+) level. One can use the observed m = 3(+) position in the cation of 48 cm^{-1} (versus an expected free rotor position of 49.1 cm^{-1}) to place an upper estimate on the barrier of V_6 < +4.4 cm^{-1}.

One could look to the intensity of the m_1^2 and m_1^4 to help with elucidating the sign of V_6 in the cation, as proposed by Weisshaar and co-workers,[32] but the m_1^2 band is overlapped with the origin band in the ZEKE spectrum, making it difficult to draw any definitive conclusions. One can say, however, that the bands seem of similar intensity, suggesting a low barrier regardless of sign.

Previous work by Lu *et al.*[31] suggests a minimum energy eclipsed conformation in the cation for toluene, based on calculations, consistent with the above proposal, but Takazawa *et al.*[27] suggest a V_6 barrier in the cation of -27 cm^{-1} for *p*FT. Such a large barrier seems unlikely based on the observed m = 3(-) and 3(+) positions and the expected couplings.

As with the F and V_6 values proposed by Okuyama *et al.*[20] for the S_1 state, it appears that incorrect assignments were used in the fit of Takazawa *et al.*[27] in determining F for the cation, as will be discussed in the next section, and this led to an incorrect determination of V_6. Finally, Weisshaar and co-workers[32] note

in a footnote that they have recorded higher resolution ZEKE spectra than those of reference 27, which suggest $|V_6| \leq 5$ cm^{-1}, but that they were unable to comment on the sign of V_6. This work does not appear to have been published but would be consistent with the current work and the barrier proposed above.

3.B.2. 100-400 cm^{-1}: vibration-torsion levels

3.B.2.1. The D_{20} vibration-torsion levels: 100 – 220 cm^{-1}

Moving up in internal energy, Figure 3.8(a) shows an expanded portion of the REMPI spectrum focusing on the region 100 – 150 cm^{-1}. The feature centred around 110 cm^{-1} was assigned in the previous work of Okuyama *et al.*[20] and Zhao *et al.*[21] to the m_1^5 transition, reported at 108 cm^{-1} in those papers, and one might assume this to be the case following the observation of the m_1^2, $m_0^{3(+)}$ and m_1^4 bands in the lower region. However, the free rotor level would be expected at around 130.9 cm^{-1}, based on the internal rotation constants of toluene, suggesting that the $m = 5$ level is either strongly perturbed or that this is not a transition to that level. Additionally, the transitions to lower wavenumber discussed in the previous section were $\Delta m = \pm 3$ transitions, whereas this would be a $\Delta m = \pm 6$ transition and so expected to be significantly weaker, and it can be seen from Figure 3.4 that this band is as intense as the m_1^4 transition. Takazawa *et al.*[27] reported a ZEKE spectrum *via* what they call $m = 5$, however the excitation position is not reported, and this will be commented upon further in the below.

Because of the breadth of the 110 cm^{-1} band, three ZEKE spectra were recorded at different parts of the band profile, A_1 – A_3, as shown in traces (b) – (d) of Figure 3.8. One can see an intense band (at 117 – 121 cm^{-1}, depending on the spectrum) dominating the ZEKE spectra at all three positions. In trace (c) there is a shoulder on the low wavenumber side of this transition, at 112 cm^{-1}, which appears to be much weaker in the other traces, suggesting that it arises from a transition from an overlapped S_1 level at this excitation position.

The intense band could be assigned as a transition to the $m = 5$ level, as a $\Delta m = 0$ transition, however it would have to undergo significant perturbation pushing it lower in wavenumber than the free rotor prediction. Recalling that in toluene the lowest wavenumber vibration was observed with various torsional levels, one can look at the lowest wavenumber vibration here, D_{20}, which is of the same symmetry as the lowest wavenumber vibration in toluene, and look for possible vibtor levels as alternative assignments. The D_{20} vibration is calculated to be 110 cm^{-1} in the S_1 state and 109 cm^{-1} in the D_0^+ state, but vibtor levels involving this would potentially undergo perturbations owing to coupling with the nearby torsion, and other vibtor, levels of the same MSG symmetry. Strong interactions were observed for toluene between levels differing in m by three and vibrational quanta by one, with the coupling diagram in Figure 6 of reference 41 an illustration of this. Such a $\Delta m = 3$, $\Delta v = 1$ change tends to occur for two levels of the same symmetry, and since such levels also tend to be relatively close energetically, this can lead to significant perturbations from the zero-order picture.

Looking at the ZEKE spectrum in trace (c), there is a weak feature at approximately 77 cm^{-1}, suggestive of a transition to $m = 4$ in the cation, and the intensity of this feature seems to die off in the adjacent traces, seemingly following the intensity of the 112 cm^{-1} shoulder. Looking back at the ZEKE spectrum *via* $m = 4$ in Figure 3.6(e), a weak feature was observed at 114 cm^{-1}, which could correspond to the same terminating level as the shoulder here. The presence of both m^4 and this 112 – 114 cm^{-1} band in both spectra suggest that this is a level which is coupled to $m = 4$, and invoking a $\Delta m = 3$, $\Delta v = 1$ change would yield an assignment of the 112 – 114 cm^{-1} feature as 20^1m^1. It appears that this is a $\Delta(v,m) = 0$ transition, $20_1^1m_1^1$, and that it is coincidentally overlapped with whatever is giving rise to the most intense band in these spectra. Note that although the S_1 levels at 0^0+76 cm^{-1} and 0^0+112 cm^{-1} are being referred to as $m = 4$ and D_{20} $m = 1$ respectively, the observed eigenstates are in reality admixtures of these two zero-order levels and would be better referred to as $m = 4 \ldots D_{20}$ $m = 1$ and D_{20} $m = 1 \ldots m = 4$, with the first contribution being dominant in each case. However, because the ZEKE spectra suggest that the

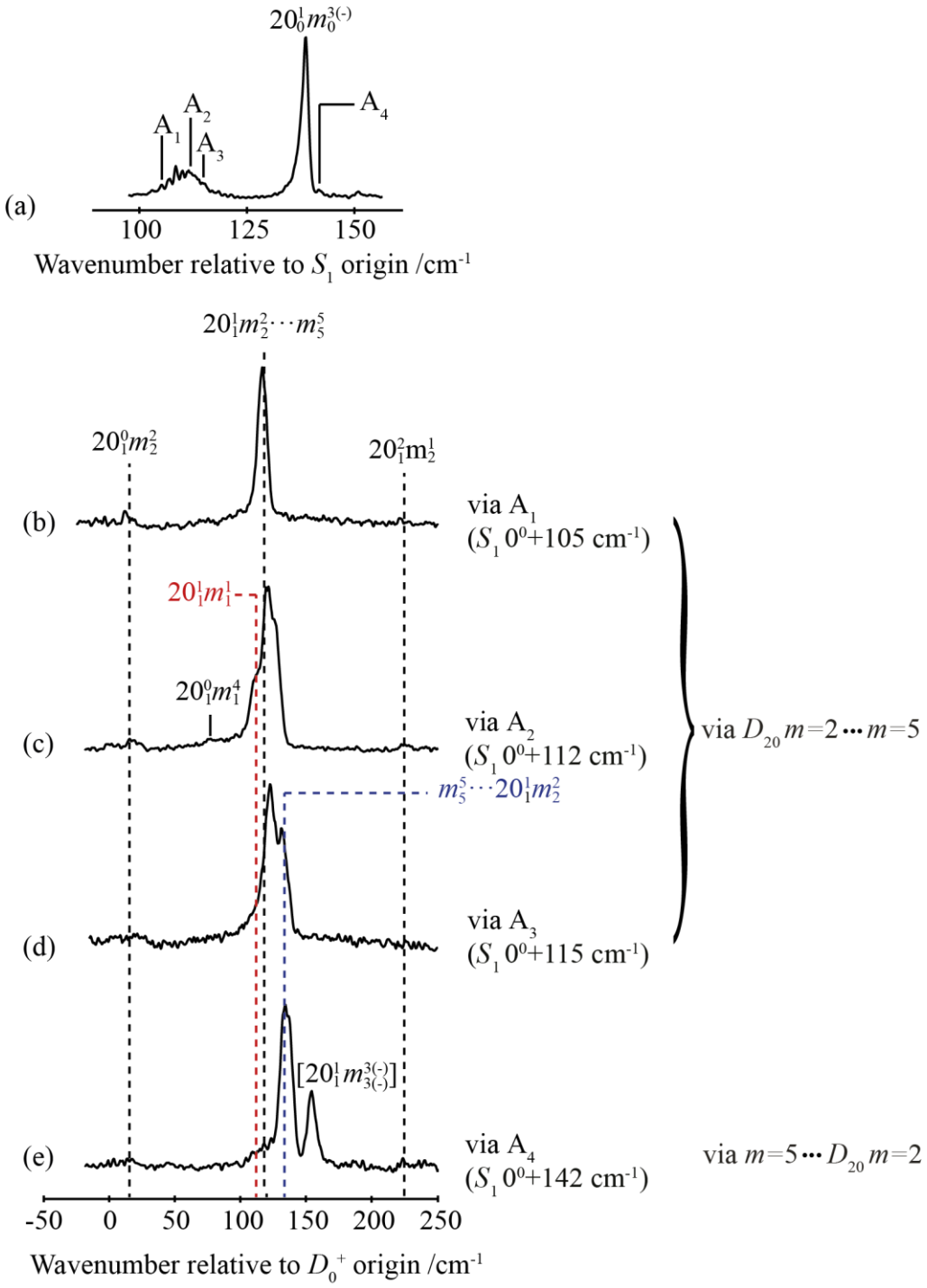


Figure 3.8 – An expanded portion of the pFT $S_1 \leftarrow S_0$ REMPI spectrum from 100 – 150 cm^{-1} is shown in (a), with ZEKE spectra recorded at positions A_1 – A_4 shown in traces (b) – (e) respectively.

mixing is small, the levels are labelled by only the dominant contribution for simplicity.

With regard to the largest contribution to the ZEKE spectra in Figure 3.8(b) – (d), the most obvious assignment is a transition to either D_{20} m = 2 or m = 5, with either of these being perturbed to be in this position in both the S_1 and D_0^+ states. A weak feature at around 16 cm^{-1} is present in all three spectra, suggestive of the m = 2 level in the cation, but this could be attributable to either a Δv = -1 transition from D_{20} m = 2, or a Δm = 3 transition from m = 5. If one looks at trace (d), there is a transition at 132 cm^{-1} with significant intensity, and this appears to be the same transition which is dominating the spectrum in trace (e), recorded at the higher wavenumber position A_4, where here the ZEKE band is at 134 cm^{-1}. This is again suggestive of two coupled levels, located at positions A_3 and A_4 in the S_1 state, with the ZEKE spectrum recorded at A_3 dominated by the 121 cm^{-1} transition and at A_4 by the 134 cm^{-1} transition, and based on these ZEKE spectra it seems that the S_1 eigenstates are significant mixtures of the two zero-order levels. It is proposed that the zero-order levels in the S_1 state are D_{20} m = 2 and m = 5, which can couple in a Δm = 3, Δv = 1 manner.

Based on the calculated values of D_{20} in the S_1 and D_0^+ states being in reasonable agreement with the observed D_{20} m = 1 level (consistent with only weak interaction with m = 4), one can use the calculated D_{20} value and the free rotor torsional calculations to predict the transition to the unperturbed D_{20} m = 2 at 126.4 cm^{-1} and the unperturbed m = 5 at 130.9 cm^{-1}, suggesting that D_{20} m = 2 will be the largest contributor to the lower eigenstate centred at 110 cm^{-1} in the S_1 state, while m = 5 will be the largest contributor to the higher eigenstate at 142 cm^{-1} in the S_1 state. The proximity of the predicted positions of the zero-order levels explains why such a strong mixture of the two is observed.

Although the obvious evidence of interaction is only in trace A_3, traces A_1 and A_2 also correspond to the D_{20} m = 2…m = 5 eigenstate, with the appearance of m = 5 being dependent on excitation position within the band profile perhaps attributable to some rotational dependence affecting the coupling. Finally, there is another intense transition in trace (e) of Figure 3.8; this is because of a slight overlap with the rotational profile of the adjacent S_1 band, as can be seen in trace (a), and the assignment of the adjacent band will be dealt with in the below.

Having assigned transitions to the D_{20} m = 1 and D_{20} m = 2 torsional levels in the REMPI spectrum, on moving to investigate the higher wavenumber bands shown in Figure 3.9, one might expect to see more D_{20} vibtor levels, analogous to the M_{20} vibtor levels observed for toluene.[41] Starting with the ZEKE spectrum recorded by the band at 0^0+137 cm^{-1} (this is the most intense REMPI transition in Figure 3.8(a)), presented in Figure 3.9(b), one can immediately see the dominance of a single intense transition in the ZEKE spectrum, at 155 cm^{1}. This is suggestive of a Δm = 0, Δv = 0, i.e. a $\Delta(v,m)$ = 0, transition, following the usual propensity rule arguments. A pure torsional transition can be ruled out on energetic grounds (having assigned m^5 in the S_1 and D_0^+ states, and being significantly below the expected position for the m = 6(+)/6(-) levels), and a transition involving a pure vibration can also be ruled out based on the calculated S_1 and D_0^+ vibrational wavenumbers in Tables B.1 and B.2 in Appendix B. This leaves only a vibtor level assignment, and the $\Delta(v,m)$ = 0 transition can be readily assigned as the $20_1^1 m_{3(-)}^{3(-)}$, yielding an S_1 assignment of $20^1 m^{3(-)}$, in agreement with Zhao's[22] assignment of this S_1 band. One can confirm this by the presence of the $20_1^0 m_{3(-)}^{3(-)}$ band in the ZEKE spectrum at 45 cm^{-1}, a Δv = -1 transition, and consistent with the $m_0^{3(-)}$ band observed in the origin ZEKE spectrum, and also the presence of the $20_1^1 m_{3(-)}^0$ band, a Δm = 3 transition, at 114 cm^{-1}. The assignment of every feature will not be discussed in detail, but attention is drawn to the bands assigned to the terminating levels D_{19} D_{20} m = 3(-), D_{14} D_{20} m = 3(-) and D_{11} D_{20} m = 3(-), which are the $\Delta(v,m)$ = 0 transition in combination with the D_{19}, D_{14} and D_{11} vibrations. These vibrational fundamentals are all observed in the origin ZEKE spectrum, discussed in section 3.C, and the combination of these with the $\Delta(v,m)$ = 0 band is something which is common in these spectra, as will be seen later. One may also note that a transition to the D_{20} overtone, 2D_{20}, is observed, which must be to the 2D_{20} m = 0 level, as the m = 1 level is inaccessible from the starting D_{20} m = 3(-) level. Not labelled in the figure owing to it being extremely weak, is the hint of a feature at 189 cm^{-1}, consistent with the m = 6(+) position in the cation determined below; this would be of the correct symmetry to interact with the D_{20} m = 3(-) level, and may suggest a very weak interaction, as it is difficult to see why it would be observed as a symmetry-allowed transition in this spectrum. It is notable that in toluene, the

M_{20} m = 3(-) and the m = 6(+) levels were strongly coupled[41], owing to their energetic proximity, but since D_{20} here is significantly lower in wavenumber than M_{20} was in toluene, there appears to be only a very weak coupling in the current case. Finally, it is noted that a transition to the m = 5 level is attributable to the overlap of the S_1 state band profiles of $20^1m^{3(-)}$ and m^5; there is no interaction between these as they are of different symmetry, with m = 5 of e'' symmetry and D_{20} m = 3(-) of a_1' symmetry.

In trace (c) of Figure 3.9 is the ZEKE spectrum recorded *via* a weaker feature at 0^0+172 cm^{-1}, with a strong $\Delta(v,m) = 0$ transition at 188 cm^{-1}. This can be readily assigned as the $20_1^1m_4^4$ transition, following on from the other vibtor levels of the D_{20} vibration. A Δv = -1 transition to the m = 4 level is observed, as is a Δm = 3 transition to the D_{20} m = 1 level. As in the ZEKE spectrum recorded *via* the D_{20} m = 3(-) level, a transition to $2D_{20}$ is observed, but this time to the m = 1 level only, rather than the m = 0 level.

Also as for the D_{20} m = 3(-), the D_{19}, D_{14} and D_{11} vibrations are observed in combination with the $\Delta(v,m) = 0$ transition. Finally, one may note the assignment of a transition to the D_{14} m = 1 terminating level at 351 cm^{-1}, which is an unexpected transition to be observed on symmetry-allowed (Franck-Condon) grounds. This could be attributable to a coupling between D_{20} m = 4 and D_{14} m = 1 (a Δm = 3, Δv = 2 coupling, and so weaker than those discussed above) in either electronic state, although these levels will be much closer energetically in the S_1 state, and so that is where any interaction would be strongest. This point will be returned to later, and importantly, the intensity of the transition to the D_{14} m = 1 level in this ZEKE spectrum is very low relative to the $\Delta(v,m) = 0$ transition, and so any interaction between the levels is suggested to be weak.

The final trace, trace (d), of Figure 3.9 was recorded *via* the reasonably intense feature at 0^0+220 cm^{-1}, and has an intense $\Delta(v,m) = 0$ transition at 222 cm^{-1}. These wavenumbers are close to twice those calculated for the D_{20} vibration. Thus the $\Delta(v,m) = 0$ transition is assigned as the overlapping $20_2^2m_0^0$ and $20_2^2m_1^1$ transitions, noting in particular the presence of both m = 0 and m = 1 levels. One can confirm the presence of both m = 0 and m = 1 levels from assigning the

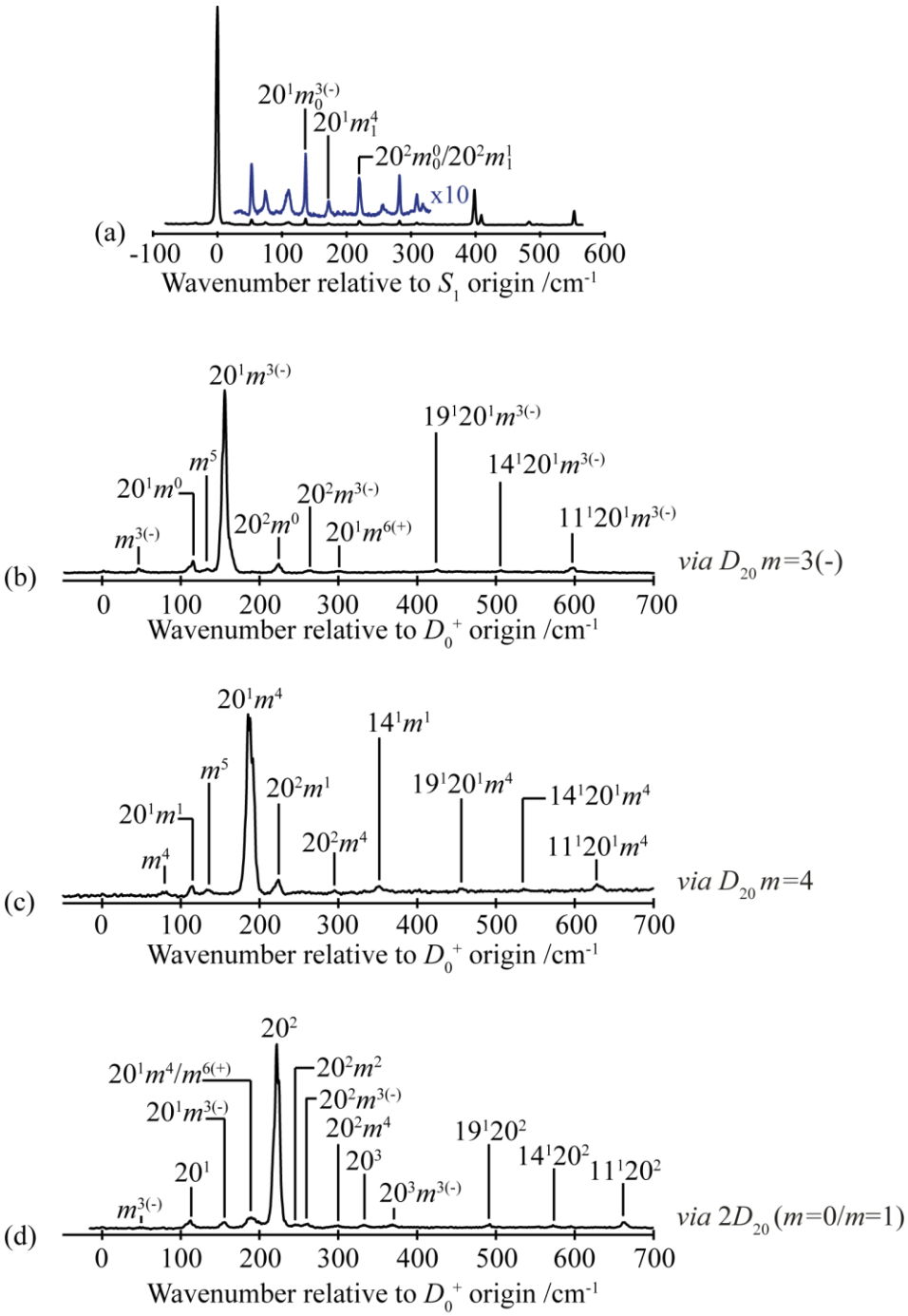


Figure 3.9 – The pFT $S_1 \leftarrow S_0$ REMPI spectrum up to ~570 cm^{-1} is shown in (a) with bands where ZEKE spectra were recorded indicated, and these ZEKE spectra shown in traces (b) – (d).

weaker structure in the ZEKE spectrum, where one can assign the transitions $20_2^1m_0^{3(-)}$ and $20_2^1m_1^4$, among others (although the latter may alternatively/also be a transition to m = 6(+) in the cation). These could arise simply through being symmetry-allowed, and so having Franck-Condon activity, but both are also separated from the $2D_{20}$ level by $\Delta m = 3$, $\Delta v = 1$

changes, and can potentially interact in both the S_1 and D_0^+ states. Once again, the D_{19}, D_{14} and D_{11} vibrations are observed in combination with the $\Delta(v,m) = 0$ band.

Although one may be tempted to say that any interactions between $2D_{20}$ and D_{20} m = 3(-) and/or D_{20} m = 4 will be stronger in the cation, since the levels are closer in the cation, the positions of the unperturbed vibtor levels are not known, and indeed the observed separation could be greater in the S_1 state because of increased interaction. If one assumes that the unperturbed value of D_{20} is similar in both electronic states, and that the value of F for the D_{20} vibtor levels is similar in both states to that of the "pure" torsions, then one would conclude that the unperturbed positions are very similar in both electronic states, suggesting that the D_{20} m = 3(-) and D_{20} m = 4 vibtor levels have undergone a more significant perturbation in the S_1 state.

3.B.2.2. D_{14} and the m = 6 levels

From the REMPI spectrum in Figure 3.9(a), a few very weak features between the $20_0^1 m_1^4$ and $20_0^2 m_0^0$/ $20_0^2 m_1^1$ bands can be seen, and attention will now be given to these, with an expanded REMPI spectrum over this range presented in Figure 3.10(a). The first of the weak features is at 0^0+188 cm^{-1}, with the second at 0^0+198 cm^{-1}; the first of these is thought to be attributable to the *p*FT.Ar complex, as discussed in our publication[61]. It is noted that the m = 6 free rotor levels are expected at 196.4 cm^{-1}, and so one (or both) of the transitions to the m = 6(+) or m = 6(-) levels could contribute here. Additionally, previous work by Ayles *et al*.[28] has shown the $2D_{14}$ overtone to be involved in the band at 400 cm^{-1}, placing the D_{14} fundamental around the position of the second band at 0^0+198 cm^{-1}.

It is notable that the experimental D_{14} value is in poor agreement with the calculated D_{14} value, and this vibrational coordinate, identical to M_{14} in monosubstituted benzene molecules, has been observed to be problematic to calculate in the S_1 state with B3LYP for other substituted benzene molecules,[62–64] and so one has to treat the calculated value with caution. On the other hand,

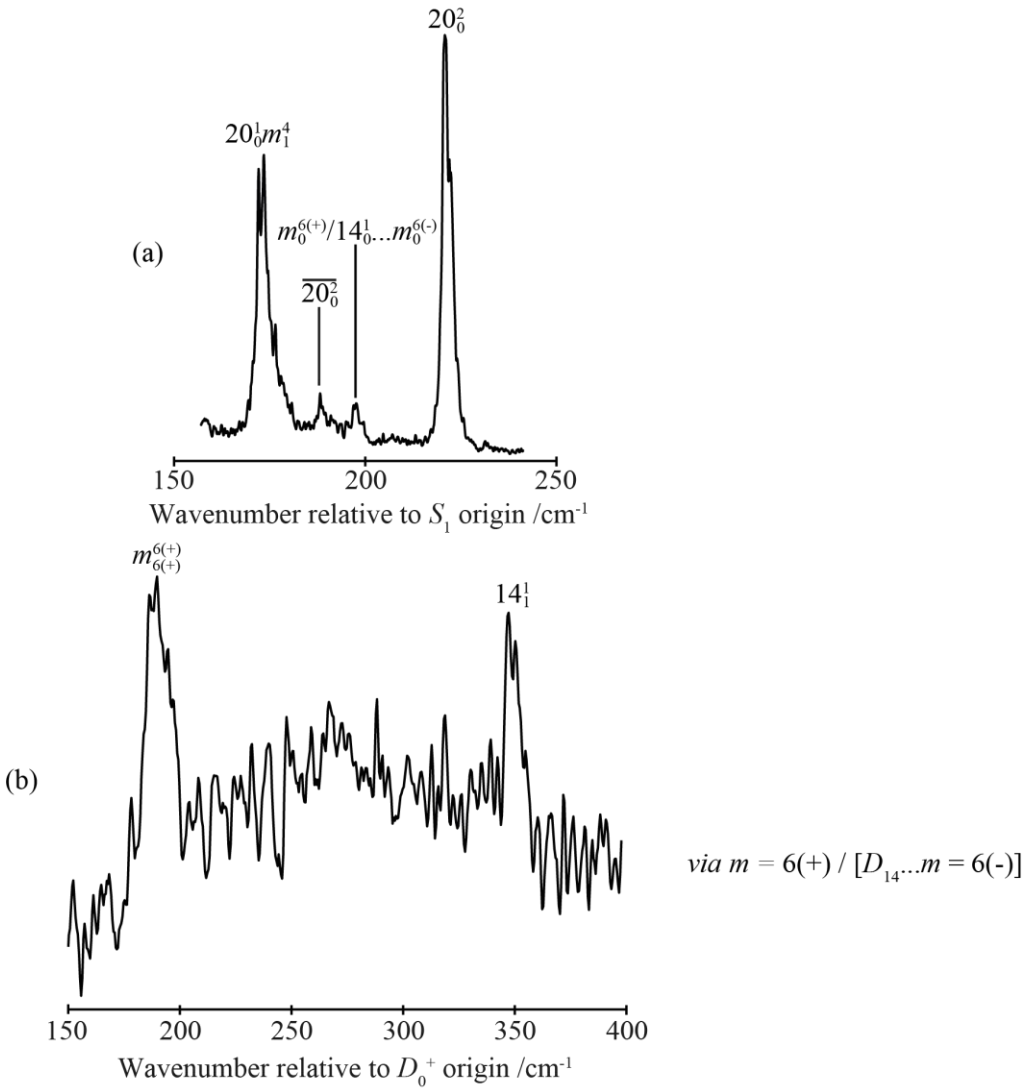


Figure 3.10 – A portion of the pFT $S_1 \leftarrow S_0$ REMPI spectrum covering the range 160 – 240 cm^{-1} is shown in (a) with the ZEKE spectrum recorded via the band labelled $m^{6(+)}/14^1$ shown in (b). Note that only one of the suggested assignments is given on the figure, see text for details of the alternative.

in the cation the calculation is in excellent agreement with the observed D_{14} wavenumber, and as a general rule of thumb the calculations for the ground cationic state are in better agreement with experiment, especially for this mode.

Because of the large shift the D_{14} vibration undergoes between the S_1 state and the cation (from 199 to 350 cm^{-1}), to elucidate whether this level is present in the S_1 state, a ZEKE spectrum was recorded *via* the 0^0+198 cm^{-1} feature and is presented in Figure 3.10(b). Although the signal-to-noise ratio is poor owing to the weakness of the intermediate level, there are two transitions of similar intensity in the ZEKE spectrum, one at 189 cm^{-1} and the other at 349 cm^{-1}, with

the latter readily assigned as 14_1^1 as a $\Delta(v,m) = 0$ transition. The similarity in the intensities of the two ZEKE bands indicates two $\Delta(v,m) = 0$ transitions, arising either from exciting an eigenstate with significant contributions from two zero-order levels, or two overlapping levels in the S_1 state.

The ZEKE band at 189 cm^{-1} could be a $\Delta m = 0$ transition from the $m = 6(+)$ level, which is of a_1' symmetry and so is symmetry-allowed in the S_1 state; the $S_1 \leftarrow S_0$ transition would be $\Delta m = \pm 6$ and so expected to be weak, as the intermediate feature is. However, this would suggest that the S_1 band is composed of two overlapping features, and while not impossible, the S_1 feature is not particularly broad. Alternatively, the ZEKE band could be a transition to the $m = 6(-)$ level, which is of a_2' symmetry. The $m = 6(-)$ level is of the same symmetry as the D_{14} $m = 0$ level, and so these could be coupled in the S_1 state (a $\Delta m = 6$, $\Delta v = 1$ coupling), giving $m = 6(-)$ character to the intermediate eigenstate and explaining its presence in the ZEKE spectrum.

It is difficult based upon the current work to determine which of these possibilities is correct. However, if one looks at the FWHM of the two ZEKE bands, the one corresponding to the 14_1^1 transition is ~7 cm^{-1}, while the 189 cm^{-1} band is ~13 cm^{-1}. This is suggestive of two transitions comprising the 189 cm^{-1} ZEKE band, and so it is concluded that it is attributable to transitions to both $m = 6(+)$ and $m = 6(-)$. This being the case, the intermediate level may be assigned as both $m = 6(+)$ and D_{14} $m = 0 \ldots m = 6(-)$. Note that no band has been assigned in the REMPI spectrum presented in Figure 3.10(a) to the corresponding $m = 6(-) \ldots D_{14}$ $m = 0$ partner eigenstate, although this could be the weak structure above the assigned band, or perhaps underneath the other weak band to lower wavenumber; it is not possible to establish this from the current work.

One may look at the origin ZEKE spectrum, discussed in section 3.C, where a band at 186 cm^{-1} could again be either $m = 6(+)$ (symmetry-allowed from the initial $m = 0$ level in the S_1 state) or potentially $m = 6(-)$ (with intensity from

vibronic coupling[i]). Since that band is also broad, it seems that both transitions could contribute to it, consistent with the 189 cm^{-1} band under discussion here, and it is illustrative that the separation of the m = 6(+)/6(-) levels in the cation is very small. Note that this is not unexpected, as if the barrier is low then these levels will be significantly above the barrier and split by only a small (perhaps negligible) amount, with further separation potentially introduced by interaction with nearby vibration/vibtor levels.

Transitions to the D_{14} m = 0 and the m = 6(-) levels in the S_1 state, if observed by a vibronic coupling mechanism, would require an A_2'' electronic state nearby, of which none is thought to be nearby. As such, any intensity in these transitions to such a_2' levels are likely owing to another mechanism such as torsion-rotation coupling, and this is supported by the weakness of these levels compared to those previously discussed where intensity was gained by vibronic coupling.

One may note that the ZEKE band position of 189 cm^{-1} is remarkably close to the previously assigned D_{20} m = 4 level in the cation at 188 cm^{-1}, and that in the ZEKE spectrum recorded *via* the D_{20} m = 4 level a band associated with D_{14} m = 1 was assigned. It is possible, as was suggested in the discussion of that spectrum, that the two levels are coupled in the S_1 state, and this would be a Δm = 3, Δv = 2 coupling. If this is the case, the coupling appears extremely weak based on the intensity of the D_{14} m = 1 band in the D_{20} m = 4 ZEKE spectrum, and so one may not expect to observe D_{20} m = 4 in the ZEKE spectrum *via* the D_{14} m = 1 level being discussed. Nevertheless, it is possible that the D_{20} m = 4 level is also a contributor to the 189 cm^{-1} ZEKE band here. The D_{14} m = 1 is of e'' symmetry, and so is symmetry-allowed in the REMPI spectrum from the m = 1 level of the S_0 state. This being the case, it may be that the D_{14} m = 0 and m = 6(-) levels, of a_2' symmetry, are not observed at all (or are weaker contributors) in the S_1 state.

[i] Note that D_{14} is of the same symmetry as m = 6(-) and is also observed in the origin ZEKE spectrum.

In summary, the two proposed assignments for the 0^0+198 cm^{-1} REMPI band are:

(i) $14_0^1 m_0^0$ and $m_0^{6(+)}$, with the 349 cm^{-1} ZEKE band being the $\Delta(v,m) = 0$ $14_1^1 m_0^0$ transition, and the 189 cm^{-1} ZEKE band being the $\Delta m = 0$ transition $m_{6(+)}^{6(+)}$ as well as the $14_1^0 m_0^{6(-)}$, suggesting a coupling of the D_{14} $m = 0$ and $m = 6(-)$ levels in the S_1 state. There is some evidence for this option from unpublished work shared by Gascooke and Lawrance, who assigned a band to $m^{6(-)}$ in their 2D-LIF spectrum.

(ii) $14_0^1 m_1^1$ and $m_0^{6(+)}$, with the 349 cm^{-1} ZEKE band being the $\Delta(v,m) = 0$ $14_1^1 m_1^1$ transition, and the 189 cm^{-1} ZEKE band being the $\Delta m = 0$ transition $m_{6(+)}^{6(+)}$ as well as the $14_1^0 20_0^1 m_1^4$, suggesting a couple of the D_{14} $m = 1$ and D_{20} $m = 4$ levels in the S_1 state.

3.B.2.3. The D_{19} vibration-torsion levels: 250 – 325 cm^{-1}

Having dealt with the structure below 220 cm^{-1} – assignable to a range of torsional transitions involving m levels up to $m = 6(+)/6(-)$, vibtor levels involving D_{20}, as well as the D_{14} and the $2D_{20}$ levels – the focus will now be shifted up in wavenumber, covering the weaker features before the intense structure at 400 cm^{-1} which will be dealt with in Chapter 5.

Figure 3.11 illustrates ZEKE spectra recorded *via* a selection of bands in the region below 325 cm^{-1}, and from the indicated bands in trace (a), one can see a striking resemblance in structure to the set of bands assigned as $20_0^1 m_1^2$, $20_0^1 m_0^{3(-)}$ and $20_0^1 m_1^4$ in the region 100 – 200 cm^{-1}. This is suggestive of another set of vibtor levels involving a vibration of the same symmetry as D_{20}, with the next lowest being D_{19}, expected at 243 cm^{-1} in the S_1 state and 266 cm^{-1} in the D_0^+ state based on the calculated wavenumbers, which appear to be in good agreement with experiment for D_{20}.

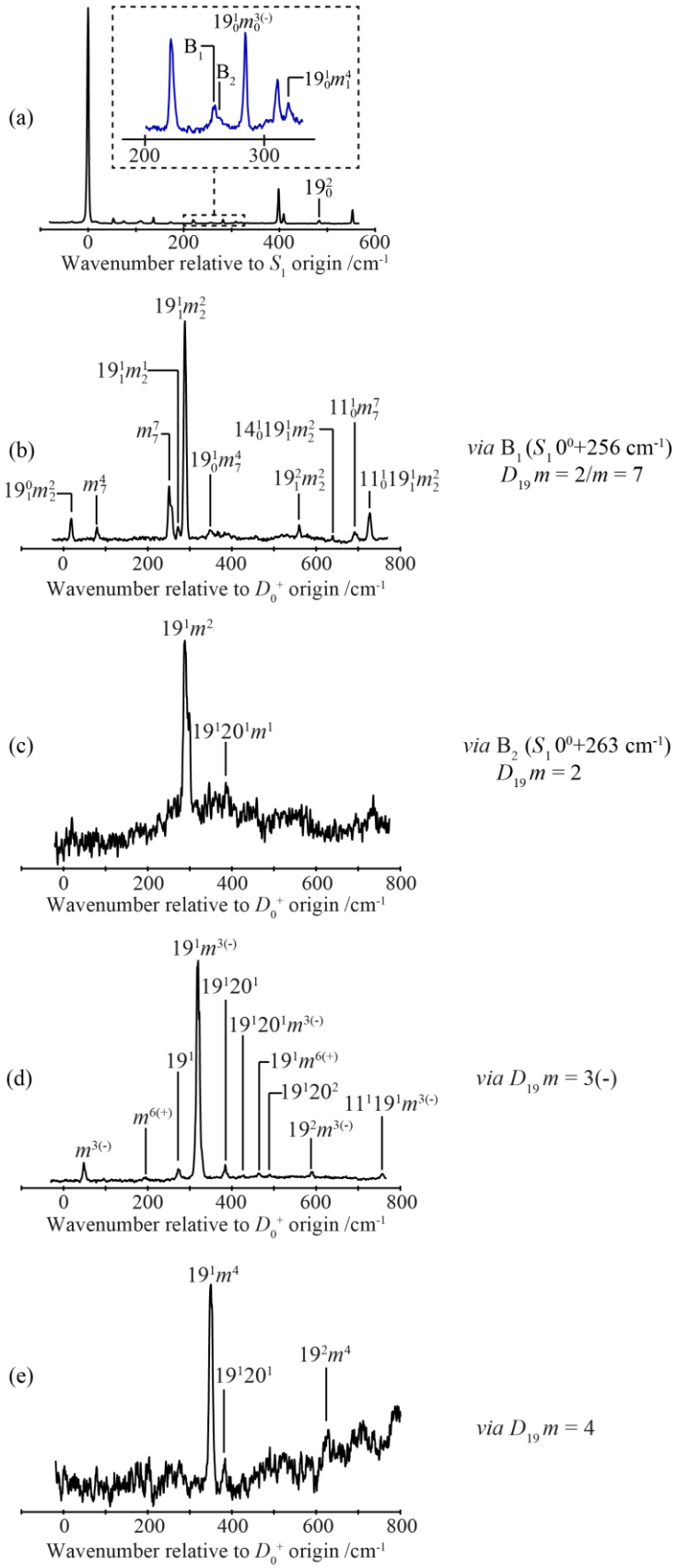


Figure 3.11 – An enhanced portion of the pFT $S_1 \leftarrow S_0$ REMPI spectrum covering the range 200 – 325 cm^{-1} is shown in (a) with the ZEKE spectra recorded via the labelled bands shown in traces (b) – (e).

The ZEKE spectrum recorded *via* the most intense of these features at 0^0+283 cm^{-1} is shown in Figure 3.11(d), and shows an intense $\Delta(v,m) = 0$ transition at 319 cm^{-1}. A simple sum of the 266 cm^{-1} calculated D_{19} value and the observed $m = 3(-)$ level in the cation of 45 cm^{-1} gives an approximate position of 311 cm^{-1} in the cation for D_{19} $m = 3(-)$, ignoring any discrepancy between the calculation and experiment, and any perturbation of the level. As such, this ZEKE band can be assigned as $19_1^1 m_{3(-)}^{3(-)}$, yielding an S_1 level of D_{19} $m = 3(-)$ in analogy to the most intense of the D_{20} vibtor transitions being $20_0^1 m_0^{3(-)}$. As in other ZEKE spectra recorded *via* vibtor levels, a $\Delta v = -1$ transition is observed, $19_1^0 m_{3(-)}^{3(-)}$, as well as a $\Delta m = 3$ transition, $19_1^1 m_{3(-)}^0$. The $\Delta(v,m) = 0$ transition is also observed in combination with the D_{19} and D_{11} vibrations, and there is possibly an inkling of a band at 671 cm^{-1} which would correspond to the $\Delta(v,m) = 0$ transition in combination with D_{14}. Finally, there is a weak band at 192 cm^{-1}, for which the most obvious assignment is $m = 6(+)$, as this is of the same symmetry as D_{19} $m = 3(-)$, perhaps indicating a weak coupling between the two levels in the S_1 (and potentially also in the D_0^+) state; it seems that the $m = 6(+)$ interacts weakly with both D_{20} $m = 3(-)$ to lower wavenumber and D_{19} $m = 3(-)$ to higher wavenumber.

As an aside, one might note that the $19_0^1 m_0^{3(-)}$ and $20_0^1 m_0^{3(-)}$ bands in the REMPI spectrum are more intense than the other vibtor levels involving these vibrations – this is analogous to $m_0^{3(+)}$ being more intense than the m_1^2 and m_1^4 transitions.

Traces (b) and (c) of Figure 3.11 show ZEKE spectra recorded at two different excitation positions within the band at ~260 cm^{-1}, with position B_1 being the peak of the feature and B_2 being the shoulder to higher wavenumber. The most intense band in these two spectra is in the same position, 287 cm^{-1}, and is suggestive of the same $\Delta(v,m) = 0$ transition in both cases. This can be assigned as the $19_1^1 m_2^2$ based on the assignment of $19_1^1 m_{3(-)}^{3(-)}$ in trace (d) and the calculated D_{19} vibrational wavenumber in both states in combination with the

m = 2 observed position. This suggests that the S_1 band is attributable to a transition to the D_{19} m = 2 level.

In trace (b) one can see the D_{19}, D_{14} and D_{11} vibrations in combination with the $\Delta(v,m)$ = 0 transition, which is now expected, the also predictable Δv = -1 transition, $19_1^0 m_2^2$, and the Δm = 3 transition, $19_1^1 m_2^1$. These are absent from trace (c) because of the signal-to-noise ratio of that ZEKE spectrum. Also in trace (b) is a reasonably intense transition with a maximum at 250 cm^{-1}, which does not fit any D_{20} or D_{19} vibtor level that might be expected to be present in the S_1 or D_0^+ states, ruling those out as $\Delta(v,m)$ = 0 transitions and on symmetry-allowed grounds. Indeed, the only sensible assignment which would be near this position would involve the m = 7 level (expected at 261.8 cm^{-1} in the S_1 state based on the free rotor F values for toluene, and effectively the same position in the cation). A transition from the D_{19} m = 2 level in the S_1 state to m = 7 in the cation would be symmetry-allowed, but corresponds to a Δv = 1, Δm = 9 change, and so would be expected to be extraordinarily weak. As such, the 250 cm^{-1} ZEKE band is assigned as a Δm = 0, m_7^7, transition, giving the m = 7 level in the S_1 state at position B_1, under the low wavenumber side of the band profile, supported by its absence in trace (c) recorded *via* the higher wavenumber side.

It is notable that the 250 cm^{-1} ZEKE band is reasonably broad, with a FWHM of 11 cm^{-1} compared to only 7 cm^{-1} for the $19_1^1 m_2^2$ band, but there is no immediately obvious assignment for another component of the band. This makes the position of the m = 7 slightly less certain in the cation, as it could be either side (or the whole) of that ZEKE band profile, and so the centre of the band is determined from the FWHM to be 253 cm^{-1}, and this is taken to be the cationic m = 7 position. This is very close to the position in the S_1 state, which is again masked slightly, this time by the $19_0^1 m_1^2$ band profile, and is suggestive of similar interactions in the two states. These observed positions are slightly lower in wavenumber than the expected 261.8 cm^{-1} position noted above, suggesting a dominating interaction with a higher level or levels; it is possible that this is D_{19} m = 4, as evidenced by the $19_0^1 m_7^4$ ZEKE band, or indeed D_{19} m = 2 itself; although the S_1 $19_0^1 m_1^2$ band profile and that of the m_1^7 are overlapping, which

would imply little interaction between them, other interactions with lower levels could serve to counteract any separation of these.

Regarding trace (c), the signal-to-noise ratio is much poorer, but one can make out what appears to be a transition to the D_{11} D_{19} m = 2 level at around 730 cm^{-1}. It is notable that both that band and the $\Delta(v,m)$ = 0 band are much broader in this spectrum, and although this could be attributable to another transition, it is thought to be due to the part of the rotational profile being excited, as discussed earlier for ZEKE spectra recorded *via* the S_1 origin and $m_0^{3(+)}$ bands.

Finally, trace (e) shows the ZEKE spectrum recorded at 0^0+320 cm^{-1}; the REMPI band at 0^0+310 cm^{-1} will be returned to below, as it does not relate to the D_{19} vibtor levels. This ZEKE spectrum has a $\Delta(v,m)$ = 0 transition at 350 cm^{-1}, and this can be assigned to $19_1^1 m_4^4$, giving an assignment for the S_1 level of D_{19} m = 4. Owing to the signal-to-noise ratio, it is not possible to pick out the Δv = -1 and Δm = 3 transitions but based on the predicted positions of the D_{19} m = 4 levels in the S_1 and D_0^+ states, and the similarity of this region to the lower D_{20} vibtor region, the assignment is still firm. One may also note the assignment of a ZEKE band to a transition to the $D_{19}D_{20}$ level; this could be present as a symmetry-allowed transition, or alternatively, the $D_{19}D_{20}$ m = 1 level would be of the correct symmetry to couple to the D_{19} m = 4 level (a Δv = 1, Δm = 3 coupling), and these could be coupled in either (or both) electronic states. In the same vein, there is a weak band arising from a transition to $D_{19}D_{20}$ in the D_{19} m = 2 and D_{19} m = 3(-) ZEKE spectra, again possibly due to coupling.

3.B.2.4. Rationalising the intensities of transitions to vibration-torsion levels

At this point, the firm assignment of the all of the "pure" torsional levels up to and including m = 7 (excluding m = 3(-) in the S_1 state), and the D_{20} and D_{19} m = 2, m = 3(-) and m = 4 vibtor levels has been attained with the aid of ZEKE spectra recorded *via* a range of intermediate levels. One might note that the observed vibtor levels in the REMPI spectrum are those which have associated Δm = ±3 changes from the initial m = 0 and 1 levels, correlating with

the idea discussed earlier that larger Δm changes tend to be correspond to weaker transitions.

The only other vibtor level involving D_{20} or D_{19} that might be expected in this range is the D_{20} $m = 5$ level, a larger change of $\Delta m = \pm 6$, which would be expected around 240 – 250 cm^{-1} in the S_1 state, and around 240 – 245 cm^{-1} in the cation. The ZEKE spectra in Figure 3.11 shown in traces (b) and (c) were recorded at 0^0+256 and 0^0+263 cm^{-1}, and one might think to assign a transition to the D_{20} $m = 5$ level to the band assigned as m_7^7, especially considering its breadth. This was considered, but one observes what is thought to be m_7^4, i.e. the associated $m = 7$ $\Delta m = 3$ band, in that spectrum, and the associated $\Delta m = 3$ and $\Delta v = -1$ changes for D_{20} $m = 5$ are not observed. These would be expected based on observing them for $m = 7$, and so D_{20} $m = 5$ is ruled out. This is consistent with not observing a transition to M_{20} $m = 5$ in toluene,[41] but observing transitions to M_{20} $m = 2$, M_{20} $m = 3(-)$ and M_{20} $m = 4$, analogous to the observed vibtor levels here. Additionally, as discussed next, the mechanism by which a transition to the D_{20} $m = 5$ level might gain intensity is different from the other observed vibtor levels, and transitions which arise *via* this mechanism tend to be less intense.

One might ask why no vibtor levels have been observed involving D_{14} (apart from the $m = 0$ and $m = 1$ levels) in the REMPI spectrum. For this, one must look at the symmetries of the vibtor levels, recalling that D_{20} has a_2'' symmetry while D_{14} has a_2' symmetry:

D_{20} $m = 0$, D_{14} $m = 3(+)$, D_{20} $m = 6(+)$ (a_2'')

D_{14} $m = 0$, D_{20} $m = 3(+)$, D_{14} $m = 6(+)$ (a_2')

D_{20} $m = 3(-)$, D_{14} $m = 6(-)$ (a_1')

D_{20} $m = 2$, D_{14} $m = 1$, D_{20} $m = 4$, D_{14} $m = 5$ (e'')

D_{14} $m = 2$, D_{20} $m = 1$, D_{14} $m = 4$, D_{20} $m = 5$ (e')

D_{14} $m = 3(-)$, D_{20} $m = 6(-)$ (a_1'')

Note that the D_{19} levels have been omitted as these take the same symmetries as the D_{20} levels. Recalling that the transition originates in the m = 0 (a_1') or m = 1 (e'') level in the S_0 state, the a_1' and e'' vibtor levels in the S_1 state are symmetry-allowed; these are given in green above. One will note that transitions to the D_{20} m = 2, D_{20} m = 3(-) and D_{20} m = 4 levels are all symmetry-allowed, and all correspond to $\Delta m = \pm 3$ changes, and so are expected to be reasonably intense based on the torsional changes. However, for D_{14} (and other levels of a_2' symmetry), it is transitions to the m = 1, m = 5 and m = 6(-) levels which are symmetry-allowed, and these (apart from m = 1 which was thought to be observed) would arise as a result of $\Delta m = \pm 6$ changes and so be weaker. This is not to say that transitions to the other levels cannot be observed, as a_1'' and e' levels can be observed *via* vibronic coupling (given in blue above), analogous to the vibronic coupling which gives transitions to the m = 2, m = 3(+) and m = 4 levels intensity, and indeed this is likely how D_{20} m = 1 gains intensity. One might then expect to observe, for example, D_{14} m = 3(-), with an expected S_1 position of 236 cm^{-1} (based on the experimental D_{14} value already discussed and the transition to the m = 3(-) level observed in the S_1 state by Zhao *et al.*[21]), and one can see a weak feature at 232 cm^{-1} in the REMPI spectrum shown in Figure 3.10(a). This could correspond to a transition to this level, but no ZEKE spectrum was obtained *via* this feature and so this is uncertain. Regarding D_{14} m = 2 and D_{14} m = 4, there are no REMPI features near the expected positions for these, suggesting they were too weak to observe.

This symmetry analysis also helps to rationalise certain observations made earlier, such as why D_{20} m = 0 is not observed but D_{20} m = 1 is; the latter is symmetry-allowed, and the former has no obvious mechanism to gain significant intensity, being of a_2'' symmetry, the same as the m = 3(-) level. With regard to the a_2' symmetry vibtor levels (and indeed the m = 6(-) torsional level), as discussed above there is no electronic state nearby of the correct symmetry to provide intensity *via* vibronic coupling, and so these levels are observed only very weakly, if at all, with intensity likely attributable to torsion-rotation coupling.

One could do a similar analysis for the a_1' and a_1'' vibrations. The former would be simple as one would observe the same vibtor levels as the "pure" torsional levels observed in the REMPI spectrum; these have very low intensities relative to the origin band and based on this, one would only expect to see the vibtor levels of a very intense totally symmetric vibration. For the a_1'' vibrations, the m = 2, m = 3(+) and m = 4 combinations would be symmetry-allowed, with transitions to the m = 0 and m = 1 levels requiring vibronic coupling (i.e. for the pure vibration), and this would also be true for transitions to the m = 5 and m = 6(+) levels. The m = 6(-) combination would be a_2'' and so there would be no obvious mechanism for it to gain intensity, and finally the transition to the m = 3(-) combination would be a_2' and so observable in the same manner discussed above for a_2' symmetry levels.

Overall, the intensities of the observed (and the absent) transitions to vibtor levels can be rationalised based on the most intense of those observed being symmetry-allowed, with the possibility of observing weaker transitions with intensity from vibronic coupling. Within each of these subsets, one can use the rule of thumb that larger Δm changes will be weaker.

3.B.2.5. The "ripples" and the region below 400 cm^{-1}

There are a selection of very weak features leading up to the 400 cm^{-1} intense bands, and attention will now be given to these. The 400 cm^{-1} features themselves will be dealt with later in Chapter 5, alongside a similar region in *p*Xyl. The region of the REMPI spectrum under discussion is shown in Figure 3.12(a), where the excitation laser power was increased to obtain the spectrum shown. One can see that the features labelled C and D are the most intense in this region, but all of these features are extremely weak, which can be readily seen from Figure 3.4. The bands marked with asterisks are thought to be, at least in part, attributable to *p*FT.Ar or *p*FT.Ar$_2$, as discussed in reference 61. For some of these bands, attempts were made to record ZEKE spectra but these were unsuccessful. Note that the REMPI band at 320 cm^{-1} has already been assigned as $19_0^1 m_1^4$, as discussed above.

Three ZEKE spectra have been recorded over the band profile of the feature at 311 cm^{-1}, and these are shown in Figure 3.12 traces (b) – (d) corresponding to positions C_1 – C_3. The same intense feature dominates each ZEKE spectrum at 321 cm^{-1} and so is thought to be a $\Delta(v,m) = 0$ transition. This ZEKE band and the REMPI band are in good agreement with the calculated D_{30} vibrational wavenumbers, and so the $\Delta(v,m) = 0$ transition is assigned as 30_1^1; this is an a_1'' symmetry vibration, observed in the S_1 state owing to vibronic coupling. In later chapters, other a_1'' symmetry vibrations will be discussed to higher wavenumber. The band at 762 cm^{-1} in the ZEKE spectra can be assigned as $11_0^1 30_1^1$, the commonly observed combination of the $\Delta(v,m) = 0$ band with the D_{11} vibration. The 463 cm^{-1} band, also observed in all three ZEKE spectra, is not obviously any combination involving the D_{30}, and is assigned as a separate $\Delta(v,m) = 0$ band. Based on the observed D_{14} and D_{20} positions in the S_1 and D_0^+ states from the above assignments, this can be assigned as the $14_1^1 20_1^1$. This suggests that the 311 cm^{-1} REMPI band is composed of overlapping transitions 30_0^1 and $14_0^1 20_0^1$. The terminating levels are of the same symmetry, and so have the potential to interact with one another, but the near degeneracy of the $S_1 \leftarrow S_0$ transitions suggests that they are only very weakly coupled at most, and this is supported by the $\Delta v = 3$ change between the two levels. One might suggest from the ZEKE spectra that this band is the D_{30}-dominated eigenstate, and another band would correspond to the $D_{14}D_{20}$-dominated eigenstate; there is no evidence from other ZEKE spectra recorded (or attempted) *via* nearby bands for this, hence the assignment of overlapping transitions contributing to this feature.

The ZEKE spectrum recorded at position C_3 shown in Figure 3.12 trace (d) shows a feature below the 30_1^1 transition, at 301 cm^{-1}. The only obvious assignment for this is a transition to the D_{20} m = 6(-) level, and it is suggested that this is yet another $\Delta(v,m) = 0$ transition, and so D_{20} m = 6(-) is present under the high wavenumber side of the S_1 band. Note the assignment of m = 6(-) rather than m = 6(+) is based on the overall symmetry being a_1'' rather than a_2'', and so gaining intensity by vibronic coupling.

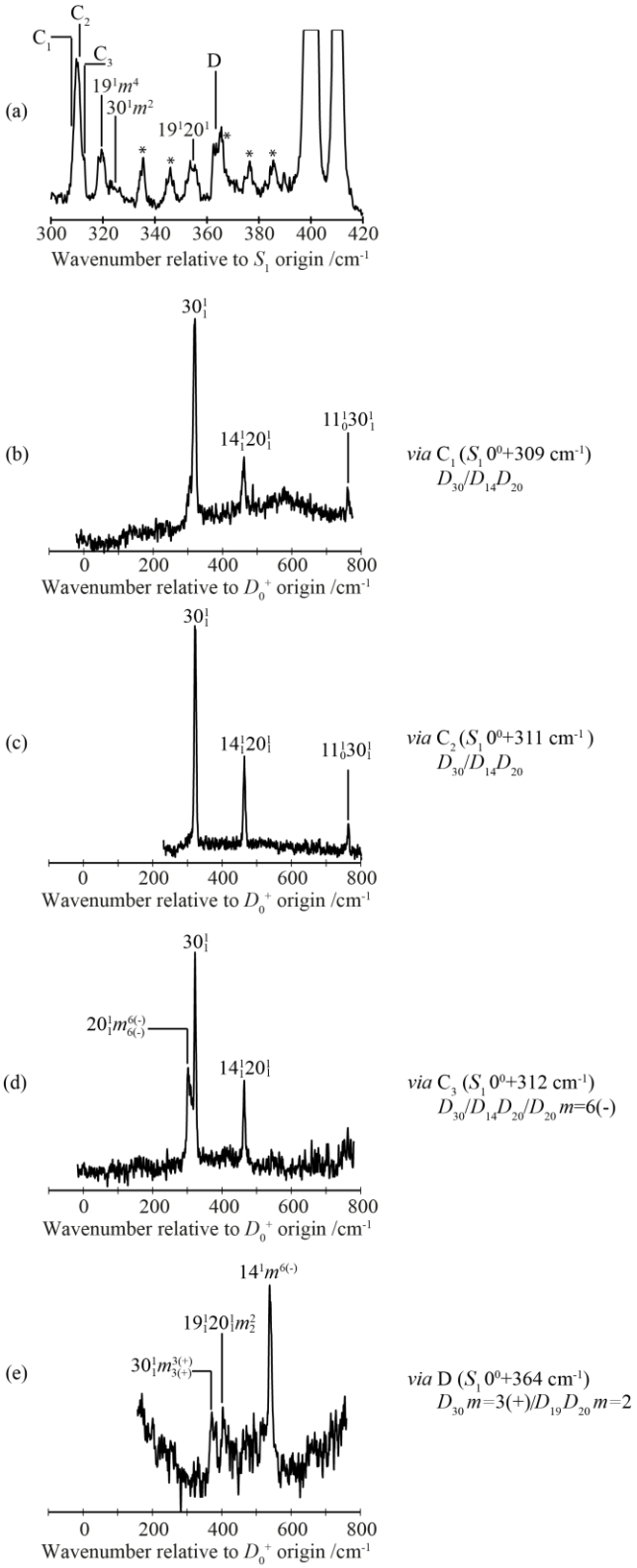


Figure 3.12 – An enhanced portion of the pFT $S_1 \leftarrow S_0$ REMPI spectrum covering the range 300 – 420 cm^{-1} is shown in trace (a) with the ZEKE spectra recorded via the labelled bands shown in traces (b) – (e). The bands marked with asterisks in the REMPI spectrum are thought to be attributable to fragmentation of the pFT.Ar and pFT.Ar$_2$ complexes.

It is notable that both Okuyama *et al.*[20] and Zhao *et al.*[21] assigned this REMPI band (LIF in those studies) in part to a transition to the m = 8 level. The band positions in the ZEKE spectra, and indeed the REMPI band position, do not agree with a simple free rotor calculation (344 cm^{-1}) of the expected position, although this would of course neglect any possible couplings. Additionally, such an m_1^8 transition would be a Δm = 9 change, and expected to be extraordinarily weak, and so it is not thought that this transition is observed. The assignment of this band to the 30_1^1 by Zhao *et al.*[21] is in agreement with the current work, albeit with other transitions also present as discussed above.

Regarding the shoulder to the band previously assigned as $19_0^1 m_1^4$ at around 323 cm^{-1}, although attempts were made, no ZEKE spectrum could be obtained, likely owing to the weakness of the feature. Based on its position however, one possible assignment is a transition to the D_{30} m = 2 level, which would be symmetry-allowed as it is of overall e'' symmetry.

The ZEKE spectrum obtained *via* the 0^0+353 cm^{-1} feature is omitted from Figure 3.12 as it shows only a single, $\Delta(v,m) = 0$, transition at 381 cm^{-1}, with poor signal-to-noise owing to the weakness of the intermediate band. This is in good agreement with a $19_1^1 20_1^1$ transition, based on the observed D_{19} and D_{20} vibtor levels discussed previously, yielding an assignment of the S_1 level as $D_{19}D_{20}$. As noted above, it is possible that the m = 1 component could be interacting weakly with the D_{19} m = 4 (and possibly the D_{19} m = 2) level, while the m = 0 component could be interacting with D_{19} m = 3(-) ; the signal-to-noise ratio in this ZEKE spectrum makes it impossible to confirm this.

Next is a slightly more intense feature at around 364 cm^{-1}, which is reasonably broad and looks like it could be composed of at least two overlapping transitions. The spectrum presented in Figure 3.12(e) was recorded at position D, 0^0+364 cm^{-1}, in the centre of the band, and shows an intense ZEKE band at 536 cm^{-1}, with weaker bands at 369 and 401 cm^{-1}. Exciting on the low wavenumber side of the feature, at 0^0+361 cm^{-1} (not shown), yields a single ZEKE band at 368 cm^{-1}, which is likely to be the same as the 369 cm^{-1} band when exciting *via* the centre. This REMPI feature is 53 cm^{-1} above the band

assigned to 30_0^1, which suggests that this feature is attributable to $30_0^1 m_0^{3(+)}$, and the 369 cm^{-1} ZEKE band can be readily assigned as $30_1^1 m_{3(+)}^{3(+)}$, supporting this assignment. The analogous $D_{14}D_{20}$ m = 3(+) band would be expected at 511 cm^{-1} in the cation, and there is some breadth in the ZEKE spectrum there, but the signal-to-noise ratio is not good enough to determine if this is present or not.

With regard to the other bands in the ZEKE spectrum *via* position D, the feature at 401 cm^{-1} can be assigned as $19_1^1 20_1^1 m_2^2$, another separate $\Delta(v,m) = 0$ transition, yielding an assignment of $19_0^1 20_0^1 m_1^2$ as one of the REMPI transitions.

The most intense ZEKE band at 536 cm^{-1} can be assigned as terminating in the totally symmetric D_{14} m = 6(-) level. This could be a $\Delta(v,m) = 0$ transition, but as discussed in Chapter 5, the S_1 level is thought to lie under the 400 cm^{-1} feature, and so this is discounted. It is not immediately apparent why this transition is observed, especially so strongly, if it is not a $\Delta(v,m) = 0$ transition. One explanation would be that D_{14} m = 6(-) is coupled to D_{30} m = 3(+), as both are totally symmetric, and this is a $\Delta v = 2$, $\Delta m = 3$ change, but there is no evidence from the ZEKE spectra *via* the 400 cm^{-1} band for this.

In summary, it appears that the 0^0+364 cm^{-1} REMPI band is composed of transitions to the D_{30} m = 3(+) and D_{19} D_{20} m = 2 levels, and perhaps also the D_{14} D_{20} m = 3(+) level.

3.B.2.6. Discussion

3.B.2.6.1. Comparison to previous work

The ZEKE spectra shown above have allowed the firm assignment of many different S_1 levels, many of which are reassigned compared to previous work. Some of the key reassignments will now be discussed.

The previous assignment of m_1^5 at 112 cm^{-1} by Okuyama *et al*.[20] and Zhao *et al*.[21] is incorrect, and this is now thought to be (predominantly) $20_0^1 m_1^2$, with m_1^5 assigned at 142 cm^{-1} in the S_1 state (although they were correct in the sense that the m = 5 zero-order level contributes to this eigenstate, albeit in a minor way). Zhao[22] later indicated that the 20_0^1 transition may contribute to the 0^0+112 cm^{-1} feature, something now shown to be correct. Similarly, $m_0^{6(-)}$ was assigned to the band at 0^0+172 cm^{-1} by Okuyama *et al*., which has now been shown to be attributable to $20_0^1 m_1^4$. This means that the *F* value generated from a fit of the torsional levels in reference 20 was incorrect, and so that *F* value should be discounted, as noted earlier.

Takazawa *et al*.[27] proposed an *F* value for the cationic ground state which was also discussed above, and the fit used to generate that contained an m = 5 value of 124 cm^{-1}. This assignment was based on a ZEKE spectrum recorded in that work *via* what they label as m = 5, but no excitation position was given. From the value used in the fit, it could be assumed that this was excitation of the D_{20} m = 2 level, and so again, this *F* value is incorrect. They also report a ZEKE spectrum *via* their assigned m = 6(-) level, but as for m = 5 do not report the excitation position. As the ZEKE spectrum looks very similar to the one reported here *via* the D_{20} m = 4 level, and the reported m = 6(-) position in the cation in reference 27 matches the observed $20_1^1 m_4^4$ position here, this also seems to be misassigned in that work.

Okuyama *et al*.[20] assigned a band at 0^0+137 cm^{-1} as Varsányi[26] mode ν_{11} (not analogous to any vibration in the current notation but energetically closest to D_{20}), and a band at 0^0+283 cm^{-1} as the first overtone of ν_{11}. Zhao[22] reassigned these to $20_0^1 m_0^{3(-)}$ and $19_0^1 m_0^{3(-)}$, which have now been confirmed by the work presented here.

Zhao *et al*.[21] assigned a band at 255 cm^{-1} in their $S_1 \leftarrow S_0$ LIF spectrum to the m_1^7 transition, from which they recorded a DF spectrum, and the same assignment was reported by Okuyama *et al*.[20], reporting the band at 254 cm^{-1}. The assignment of this band to the m_1^7 transition agrees with the current work,

although it is not the only contribution to this band, with $19_0^1 m_1^2$ contributing more significantly. Indeed, one can look at the DF spectrum shown by Okuyama *et al*. in reference 20, where it is apparent that the m_7^7 transition is not the dominating $\Delta(v,m) = 0$ transition, with a more intense band at 349 cm^{-1}. This is assignable to the D_{19} m = 2 level (using the D_{19} calculated value in the S_0 state from reference 49), consistent with the current work. Although reliance is placed on these calculated vibrational wavenumbers, the S_0 and D_0^+ values are known to be in good agreement with experiment, and one must also take care with the experimental values as the observed bands are likely perturbed by interaction with other low wavenumber levels.

3.B.2.6.2. Transition energetics and couplings

Considering now the energetics of the observed transitions, the band positions for the D_{20} vibtor levels are of higher wavenumber in the cation than in the S_1 state, even though the D_{20} vibrational wavenumber is expected to be of a similar value (~110 cm^{-1}) in both states, based on the D_{20} overtone and the D_{20} m = 2 level, and certainly not up to 18 cm^{-1} different as the D_{20} m = 3(-) level is between the two electronic states. This can be rationalised by considering that D_{19} is of a lower wavenumber in the S_1 than the D_0^+ state, and so the D_{19} vibtor levels will be interacting more strongly with the D_{20} vibtor levels in the S_1 state than in the cation, leading to the lower wavenumber of the D_{20} vibtor levels in the S_1 state. This, in theory, also means that there will stronger interactions with the "pure" torsional levels in the S_1 state than in the cation, and if one looks at the m = 4 level, it has an observed wavenumber of 76 cm^{-1} in S_1 and 79 cm^{-1} in D_0^+, compared to the expected free rotor position of 81.8 cm^{-1}, supporting the weaker interactions in the cation and approaching the expected free rotor position. The m = 2 level is effectively identical in position in the two states as it is much further removed energetically from any perturbing levels, and so the effect on this level is minimised.

The m = 5 level is found at 142 cm^{-1} in the S_1 state and 134 cm^{-1} in the D_0^+ state, which is a sizeable difference, and it was discussed above that the near degeneracy of the expected positions of the zero-order levels m = 5 and

D_{20} m = 2 in the S_1 state is responsible for the large perturbation in that case. In the cation the zero-order levels are expected at the same separation or slightly closer together (with a slightly higher D_{20} value for the cation based on the $2D_{20}$ overtone level being marginally higher in the cation), but since any interaction of the D_{20} m = 2 (or the m = 5) level with the D_{19} vibtor levels will be significantly reduced compared to the S_1 state, the net effect appears to be a reduced interaction of the m = 5 and D_{20} m = 2 levels in the cation.

This highlights that, while the couplings are discussed in a pairwise manner here, in reality the vibration-torsion coupling involves all of the levels of the correct symmetry in this low wavenumber region, and one must consider the full picture in order to predict which levels have been perturbed and by how much. To tackle this, one could fit the observed level positions to obtain V_6, F, the unperturbed vibrational wavenumbers for D_{20} and D_{19}, and the vibration-torsion coupling term, as was done for toluene by Gascooke and Lawrance[41]. It is notable that in the work of Gascooke and Lawrance, they use the S_1 band profiles to infer information on mixing between levels and to identify precise positions for band centres, and these band profiles are of a slightly higher resolution than those obtained here, making such inferences difficult in the present study. Additionally, given the FWHM of the ZEKE bands, and the several cm^{-1} uncertainty in the ZEKE band positions, it is not apparent that such a fitting procedure would be particularly precise for the cation. As such, given the focus of the current work on studying not just the low wavenumber region but also higher wavenumber regions, and comparing *p*FT to *p*Xyl, the current work will take a simpler, more qualitative, approach, using particular examples to illustrate the couplings.

For example, the eigenstates dominated by D_{20} m = 1 and D_{20} m = 2 are effectively degenerate in the S_1 state, owing to the strong interaction of the D_{20} m = 2 and m = 5 zero-order levels perturbing the D_{20} m = 2 lower in wavenumber, and the weaker interaction between D_{20} m = 1 and m = 4 perturbing the former level higher in wavenumber. As a result of this, the m = 5 level ends up higher in wavenumber than the D_{20} m = 3(-), switching order compared to any predictions made based on the calculated vibrational wavenumbers and the

free rotor energies. This is one illustration of the influence of vibration-torsion coupling on the spectra, and how it can lead to observed bands in unexpected positions.

The drawback to not deperturbing the observed levels to get the unperturbed positions is that obtaining accurate vibrational wavenumbers for the low wavenumber vibrations, D_{20} and D_{19}, becomes difficult. One approach is to look at the overtones of these, for which the m_0^0 and m_1^1 transitions are degenerate within the resolution of the current experiments. This being the case, one can assume, as a first approximation, that these levels are little shifted from their zero-order positions and, neglecting anharmonicity, one can halve the S_1 and D_0^+ band positions to obtain the vibrational wavenumbers. This yields 110 cm^{-1} and 111 cm^{-1} for D_{20} in the S_1 and D_0^+ states respectively, and for D_{19} this will be shown in Chapter 5 to yield 242 and 271 cm^{-1} for the S_1 and D_0^+ states. These are the assumed experimental values in the current work, but it should be noted that Gascooke and Lawrance have undertaken a (currently unpublished) 2D-LIF study of this region, which they have shared privately with our research group, and are carrying out a deperturbation analysis of their level positions to obtain more reliable fundamental values for these vibrations in the S_1 state.

It seems that although many levels can interact, and some are perturbed very significantly as seen for D_{20} m = 2 and m = 5, no noticeable separation of the m = 0 and m = 1 terminating levels for any vibration has been observed. This seems counterintuitive, as, for example, $2D_{20}$ can have its m = 0 component perturbed up by D_{20} vibtor levels and down by D_{19} vibtor levels, with similar perturbations from different D_{20} and D_{19} levels for the m = 1 component. Recalling that the D_{19} vibtor levels are lower in wavenumber in the S_1 state than the D_0^+ state (D_{19} is ~29 cm^{-1} lower in S_1), and that $2D_{20}$ is only 2 cm^{-1} lower in the S_1 than the D_0^+ state, this suggests that interaction with the D_{19} vibtor levels is weak overall. This will be returned to in the analogous region in *p*Xyl, discussed in Chapter 4.

3.C. Origin ZEKE spectrum

Before moving on to look at the low wavenumber region of *p*Xyl in Chapter 4, the full ZEKE spectrum recorded *via* the *p*FT S_1 origin will be discussed briefly. This is shown in Figure 3.13, where the most intense vibrational structure is assigned. This will be discussed first, followed by a discussion of the torsional and vibtor activity in the lower wavenumber region of the ZEKE spectrum.

3.C.1. Overview of vibrational activity

The assignments in Figure 3.13 come primarily from comparison with recent work by our group on *p*DFB and *p*ClFB[52,54]. In addition, the origin ZEKE spectra for *p*DFB, *p*ClFB, *p*FT and *p*Xyl were compared in reference 65, with the *p*FT and *p*Xyl ones discussed in this thesis. In both *p*DFB and *p*ClFB, most of the totally symmetric fundamentals were observed with significant intensity, and that is also the case for *p*FT, with intense transitions to D_{11}, D_9, D_7 and D_6, with weaker transitions to D_5 and D_3 (with the caveat for D_3 that the UV output of the dye laser is much less intense at that end of the spectrum, so this transition may be much more intense than it appears). Some of these assignments, such as 9^1, are confirmed by ZEKE spectra recorded *via* the same vibration in the S_1 state later in this thesis.

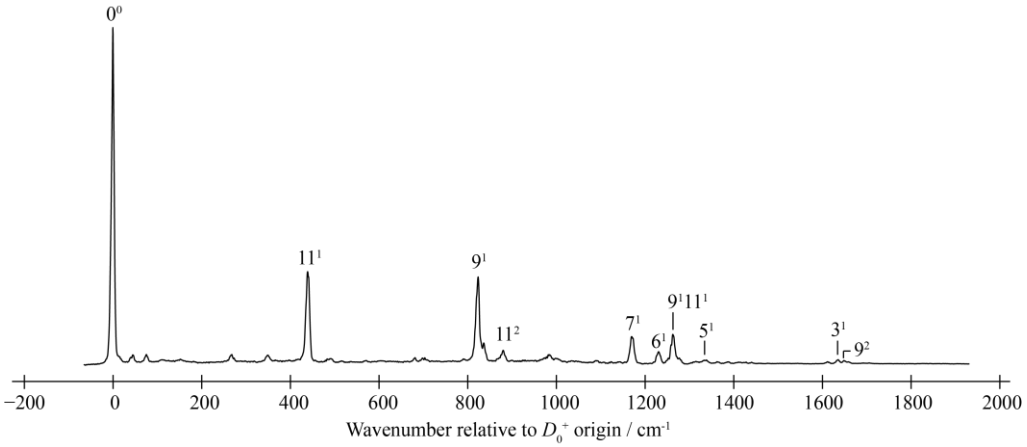


Figure 3.13 – The ZEKE spectrum recorded via the pFT S_1 origin. Assignments come from comparison to recent work on pDFB and pClFB by our group[52,54], as well as ZEKE spectra recorded via intermediate levels discussed later in this thesis.

Owing to the comparison with *p*DFB and *p*ClFB, these assignments are secure, even when it was not possible to record a ZEKE spectrum *via* the S_1 level to confirm it. This establishes most of the totally symmetric vibrational fundamentals in the D_0^+ state, and these are reported in Table B.2 in Appendix B.

3.C.2. Low wavenumber torsion and vibration-torsion activity

Figure 3.14 shows the first 600 cm^{-1} of the *p*FT origin ZEKE spectrum, but recorded with increased laser power and an increased detector voltage to pick out the torsion and vibtor structure. One can see that the origin transition and the 11^1 transition are saturating the detector, since these are both intense, symmetry-allowed, transitions.

As was discussed in section 3.A.2.6., in the ZEKE spectra recorded *via* the S_1 origin bands of *p*DFB and *p*ClFB one observes the non-totally symmetric 20^1, 19^1 and 14^1 transitions, all of which are also observed here.[j] These transitions are thought to arise owing to vibronic coupling although, as discussed in section 3.A.2.6, the precise nature of the mechanism is uncertain.[k] Perhaps *via* a similar mechanism, a transition to the a_1'' symmetry level D_{29} also appears, weakly, in this ZEKE spectrum. This is analogous to the observation of a b_2 symmetry vibration, D_{28}, in the origin ZEKE spectrum of *p*ClFB.[52]

In term of "pure" torsional structure, the transitions m_1^2, $m_0^{3(-)}$ and m_1^4 are observed, as discussed in section 3.B.1. Additionally, there is a weak ZEKE band at 186 cm^{-1} that could be assigned to $m_0^{6(+)}$, which would be

[j] In the $S_1 \leftarrow S_0$ excitation spectrum, only the $m = 1$ component of D_{20} was observed. Here, if one assumes 20^1 is observed owing to vibronic coupling, both *m* components could be present.
[k] However, the same mechanism is thought to be active in *p*DFB, *p*ClFB and *p*FT (as well as *p*Xyl, as will be seen in Chapter 4), owing to the observation of the same non-totally symmetric vibrations in all four molecules.

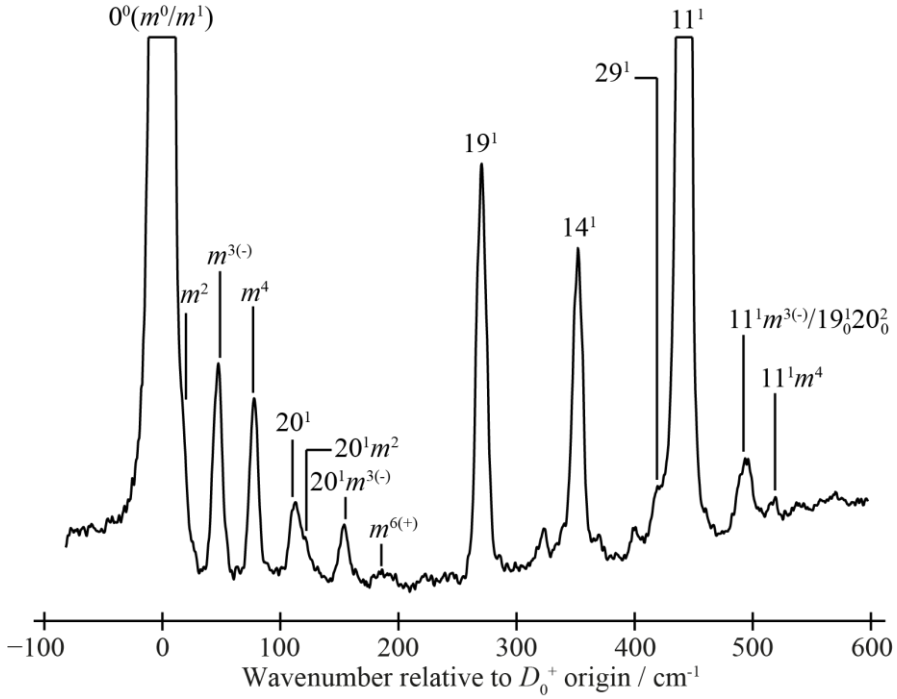


Figure 3.14 – The ZEKE spectrum recorded via the pFT S_1 origin up to 600 cm^{-1}. This was recorded with an increased detector voltage and increased laser power to resolve the torsion and vibtor structure. Assignments come primarily from ZEKE spectra recorded via the intermediate levels discussed in this chapter.

symmetry-allowed, and/or $m_0^{6(-)}$, which would be vibronically allowed. It is noted that m = 6(-) is of the same symmetry as D_{14}, a_2', and so could be observed by the same vibronic coupling mechanism as that. Since this weak ZEKE band is quite broad, and based on the discussion in section 3.B.2.2. regarding these levels, it is suggested that transitions to both of the m = 6 levels contribute to this feature.

Finally, transitions to vibtor levels are also observed, with 20^1m^2 and $20^1m^{3(-)}$, both of which are symmetry-allowed, involving D_{20}. Additionally, 20^1m^4 could contribute to the 186 cm^{-1} band, assigned above as transitions to the m = 6 levels. There is also a weak band at 324 cm^{-1}, which could be assigned to either 30^1 or $19^1m^{3(-)}$, with the latter being the current favoured assignment as it is symmetry-allowed. It appears that D_{11} vibtor levels are also observed, with $11^1m^{3(-)}$ and 11^1m^4 identified; these are thought to gain intensity from vibronic coupling, in the same way as the pure torsions $m_0^{3(-)}$ and m_1^4.

3.D. References

[1] R.A. Coveleskie, D.A. Dolson, and C.S. Parmenter, *J. Chem. Phys.*, **72**, 5774 (1980).

[2] C.S. Parmenter, *J. Phys. Chem.*, **86**, 1735 (1982).

[3] K.W. Holtzclaw and C.S. Parmenter, *J. Phys. Chem.*, **88**, 3182 (1984).

[4] R.A. Coveleskie, D.A. Dolson, and C.S. Parmenter, *J. Phys. Chem.*, **89**, 645 (1985).

[5] R.A. Coveleskie, D.A. Dolson, and C.S. Parmenter, *J. Phys. Chem.*, **89**, 655 (1985).

[6] K.W. Holtzclaw and C.S. Parmenter, *J. Chem. Phys.*, **84**, 1099 (1986).

[7] D.A. Dolson, K.W. Holtzclaw, D.B. Moss, and C.S. Parmenter, *J. Chem. Phys.*, **84**, 1119 (1986).

[8] D.A. Dolson, C.S. Parmenter, and B.M. Stone, *Chem. Phys. Lett.*, **81**, 360 (1981).

[9] D.B. Moss, C.S. Parmenter, and G.E. Ewing, *J. Chem. Phys.*, **86**, 51 (1987).

[10] C.S. Parmenter and B.M. Stone, *J. Chem. Phys.*, **84**, 4710 (1986).

[11] D.B. Moss and C.S. Parmenter, *J. Chem. Phys.*, **98**, 6897 (1993).

[12] P.J. Timbers, C.S. Parmenter, and D.B. Moss, *J. Chem. Phys.*, **100**, 1028 (1994).

[13] J.S. Baskin, T.S. Rose, and A.H. Zewail, *J. Chem. Phys.*, **88**, 1458 (1988).

[14] J.A. Davies, K.L. Reid, M. Towrie, and P. Matousek, *J. Chem. Phys.*, **117**, 9099 (2002).

[15] A.K. King, S.M. Bellm, C.J. Hammond, K.L. Reid, M. Towrie, and P. Matousek, *Mol. Phys.*, **103**, 1821 (2005).

[16] J.A. Davies and K.L. Reid, *J. Chem. Phys.*, **135**, 124305 (2011).

[17] J.A. Davies and K.L. Reid, *Phys. Rev. Lett.*, **109**, 193004 (2012).

[18] J.A. Davies, A.M. Green, A.M. Gardner, C.D. Withers, T.G. Wright, and K.L. Reid, *Phys. Chem. Chem. Phys.*, **16**, 430 (2014).

[19] J.A. Davies, L.E. Whalley, and K.L. Reid, *Phys. Chem. Chem. Phys.*, **19**, 5051 (2017).

[20] K. Okuyama, N. Mikami, and M. Ito, *J. Phys. Chem.*, **89**, 5617 (1985).

[21] Z.-Q. Zhao, C.S. Parmenter, D.B. Moss, A.J. Bradley, A.E.W. Knight, and K.G. Owens, *J. Chem. Phys.*, **96**, 6362 (1992).

[22] Z.-Q. Zhao, Ph.D. Thesis, Indiana University, 1992.

[23] Y. Hu, X. Wang, and S. Yang, *Chem. Phys.*, **290**, 233 (2003).

[24] S. Georgiev, T. Chakraborty, and H.J. Neusser, *J. Phys. Chem. A*, **108**, 3304 (2004).

[25] E.B. Wilson Jr., *Phys. Rev.*, **45**, 706 (1934).

[26] G. Varsányi, *Assignments of the Vibrational Spectra of Seven Hundred Benzene Derivatives* (Wiley, New York, 1974).

[27] K. Takazawa, M. Fujii, and M. Ito, *J. Chem. Phys.*, **99**, 3205 (1993).

[28] V.L. Ayles, C.J. Hammond, D.E. Bergeron, O.J. Richards, and T.G. Wright, *J. Chem. Phys.*, **126**, 244304 (2007).

[29] C.J. Hammond, V.L. Ayles, D.E. Bergeron, K.L. Reid, and T.G. Wright, *J. Chem. Phys.*, **125**, 124308 (2006).

[30] L.H. Spangler, *Annu. Rev. Phys. Chem.*, **48**, 481 (1997).

[31] K.-T. Lu, G.C. Eiden, and J.C. Weisshaar, *J. Phys. Chem.*, **96**, 9742 (1992).

[32] R.A. Walker, E. Richard, K.-T. Lu, E.L. Silbert, and J.C. Weisshaar, *J. Chem. Phys.*, **102**, 8718 (1995).

[33] K.-T. Lu, F. Weinhold, and J.C. Weisshaar, *J. Chem. Phys.*, **102**, 6787 (1995).

[34] R.A. Walker, E.C. Richard, K.-T. Lu, and J.C. Weisshaar, *J. Phys. Chem.*, **99**, 12422 (1995).

[35] R.A. Walker, E.C. Richard, and J.C. Weisshaar, *J. Phys. Chem.*, **100**, 7333

(1996).

[36] E.C. Richard, R.A. Walker, and J.C. Weisshaar, *J. Chem. Phys.*, **104**, 4451 (1996).

[37] K.-T. Lu and J.C. Weisshaar, *J. Chem. Phys.*, **99**, 4247 (1993).

[38] J.R. Gascooke and W.D. Lawrance, *J. Chem. Phys.*, **138**, 134302 (2013).

[39] E.A. Virgo, J.R. Gascooke, and W.D. Lawrance, *J. Chem. Phys.*, **140**, 154310 (2014).

[40] J.R. Gascooke, E.A. Virgo, and W.D. Lawrance, *J. Chem. Phys.*, **142**, 024315 (2015).

[41] J.R. Gascooke, E.A. Virgo, and W.D. Lawrance, *J. Chem. Phys.*, **143**, 044313 (2015).

[42] J.R. Gascooke and W.D. Lawrance, *J. Mol. Spectrosc.*, **318**, 53 (2015).

[43] J.R. Gascooke and W.D. Lawrance, *J. Chem. Phys.*, **138**, 084304 (2013).

[44] P.W. Atkins and R.S. Friedman, *Molecular Quantum Mechanics*, Fifth Ed. (Oxford University Press, New York, 2004).

[45] A.M. Gardner, A.M. Green, V.M. Tamé-Reyes, V.H.K. Wilton, and T.G. Wright, *J. Chem. Phys.*, **138**, 134303 (2013).

[46] A.M. Gardner, A.M. Green, V.M. Tamé-Reyes, K.L. Reid, J.A. Davies, V.H.K. Parkes, and T.G. Wright, *J. Chem. Phys.*, **140**, 114308 (2014).

[47] H.C. Longuet-Higgins, *Mol. Phys.*, **6**, 445 (1963).

[48] P.R. Bunker and P. Jensen, *Molecular Symmetry and Spectroscopy*, Second Ed. (NRC Research Press, Ottawa, 1998).

[49] A. Andrejeva, A.M. Gardner, W.D. Tuttle, and T.G. Wright, *J. Mol. Spectrosc.*, **321**, 28 (2016).

[50] J.M. Hollas, *High Resolution Spectroscopy*, Second Ed. (Wiley, Chichester, 1998).

[51] W.D. Tuttle, A.M. Gardner, and T.G. Wright, *Chem. Phys. Lett.*, **684**, 339

(2017).

[52] D.J. Kemp, L.E. Whalley, W.D. Tuttle, A.M. Gardner, B.T. Speake, and T.G. Wright, *Phys. Chem. Chem. Phys.*, **20**, 12503 (2018).

[53] G. Reiser, D. Rieger, T.G. Wright, K. Müller-Dethlefs, and E.W. Schlag, *J. Phys. Chem.*, **97**, 4335 (1993).

[54] D.J. Kemp, A.M. Gardner, W.D. Tuttle, J. Midgley, K.L. Reid, and T.G. Wright, *J. Chem. Phys.*, (submitted).

[55] C.H. Kwon, H.L. Kim, and M.S. Kim, *J. Chem. Phys.*, **118**, 6327 (2003).

[56] S.-Y. Yu and M.-B. Huang, *J. Mol. Struct. THEOCHEM*, **822**, 48 (2007).

[57] J.S. Miller, E.D. Poliakoff, T.F. Miller, A.P.P. Natalense, and R.R. Lucchese, *J. Chem. Phys.*, **114**, 4496 (2001).

[58] E.D. Poliakoff and R.R. Lucchese, *Phys. Scr.*, **74**, C71 (2006).

[59] D.J. Nesbitt and R.W. Field, *J. Phys. Chem.*, **100**, 12735 (1996).

[60] A.M. Gardner and T.G. Wright, *J. Chem. Phys.*, **135**, 114305 (2011).

[61] A.M. Gardner, W.D. Tuttle, L. Whalley, A. Claydon, J.H. Carter, and T.G. Wright, *J. Chem. Phys.*, **145**, 124307 (2016).

[62] J.P. Harris, A. Andrejeva, W.D. Tuttle, I. Pugliesi, C. Schriever, and T.G. Wright, *J. Chem. Phys.*, **141**, 244315 (2015).

[63] A. Andrejeva, W.D. Tuttle, J.P. Harris, and T.G. Wright, *J. Chem. Phys.*, **143**, 104312 (2015).

[64] A. Andrejeva, W.D. Tuttle, J.P. Harris, and T.G. Wright, *J. Chem. Phys.*, **143**, 244320 (2016).

[65] W.D. Tuttle, A.M. Gardner, L.E. Whalley, D.J. Kemp, and T.G. Wright, *Phys. Chem. Chem. Phys.*, (In press).

4. A double rotor case: the low wavenumber torsion and vibration-torsion region of *para*-xylene

Having discussed the low wavenumber region of the single rotor *para*-fluorotoluene (*p*FT) molecule in some depth in Chapter 3, attention will now be given to the analogous region of the double rotor *para*-xylene (*p*Xyl) molecule. This will start with an overview of the previous work on the molecule, followed by a summary of the appropriate molecular symmetry group (MSG) treatment, which turns out to be the G_{72} MSG here, much larger than the G_{12} group for *p*FT. The subsequent discussion of the obtained experimental spectra will utilise this symmetry treatment, and this will allow for a comparison of the activity of the single rotor *p*FT and double rotor *p*Xyl molecules.

4.A. *para*-xylene and the double rotor

4.A.1. Previous work

Ebata *et al*.[1] reported a laser-induced fluorescence (LIF) spectrum (referred to therein as a fluorescence excitation spectrum) of the S_1 state of *p*Xyl in 1984, reporting the origin transition at 36728 cm^{-1} and noting a handful of other intense transitions, assigned to ν_1 and ν_{7a} in the Wilson[2]/Varsányi[3] notation of that work. Additionally, they reported a dispersed fluorescence (DF) spectrum recorded *via* the *p*Xyl S_1 origin band. In 1988, Blease *et al*.[4] published (2+2) resonance-enhanced multiphoton ionisation (REMPI) spectra of the $S_1 \leftarrow S_0$ transition of supersonically cooled *ortho*-, *meta*- and *para*-xylene molecules. That work also included a (1+1) REMPI spectrum of *p*Xyl, and they report the S_1 origin band at 36726.7 cm^{-1}, consistent with Ebata *et al*.[1] Blease *et al*. used the comparison of one- and two-photon excitation spectra to comment on the impact of Herzberg-Teller intensity stealing on the intensities of observed transitions.

Further REMPI spectra of the $S_1 \leftarrow S_0$ transition of *p*Xyl were reported in the 1980s by Walter *et al*.[5] and Breen *et al*.[6], with the latter study being an early

focus on the low wavenumber, methyl torsion, region of the spectrum. Selco and Carrick[7] recorded jet-cooled emission spectra of *ortho*-, *meta*- and *para*-xylene, and they assigned both torsional and vibrational structure in their $S_0 \leftarrow S_1$ emission spectrum. They used the torsional assignments of Breen *et al*.[6], who suggested that the two methyl rotors were non-interacting, free, rotors, and this will be remarked upon in the below.

Schlag and co-workers have investigated *p*Xyl in a number of studies, including a REMPI study focussed on the ^{12}C-^{13}C isotopic shift[8]. Two studies focused on the cation, with the first being a zero-electron-kinetic-energy (ZEKE) photoelectron spectroscopy (PES) study of *ortho*-, *meta*- and *para*-xylene[9], with spectra recorded *via* the relevant origin bands with a focus on the cationic low wavenumber torsional region, and the second study illustrated a mass-analysed threshold ionisation (MATI) spectrum recorded *via* the S_1 origin[10]. Similarly, Gunzer and Grotemeyer have published two MATI studies of *p*Xyl[11,12], and they reported spectra *via* four intermediate levels including the S_1 origin. Although they noted the methyl torsions in the REMPI spectrum and the MATI spectrum recorded *via* the S_1 origin, no explicit assignments of these were given. Gunzer and Grotemeyer found an ionisation energy of 68,204 cm^{-1}, in fair agreement with the value of 68,186 cm^{-1} obtained by Held *et al*.[9].

Finally, there were earlier studies of the cation, such as the photoionisation study of Watanabe[13] and previous HeI photoelectron spectroscopy studies[14–17], but the resolution of those studies was relatively poor and so these have been largely superseded by the ZEKE and MATI studies mentioned above.

One may note that there have been several REMPI and ZEKE/MATI studies, but that focus has been placed on understanding either: (a) the pure torsional region of such spectra (covering only the first 150 cm^{-1} or so) or (b) selected vibrational intermediate levels, of which only three (excluding the vibrationless S_1 origin level) have been probed by ZEKE/MATI spectroscopy; as such, the present work greatly extends these previous studies. This chapter takes a comprehensive look at the *p*Xyl $S_1 \leftarrow S_0$ excitation spectrum up to ~400 cm^{-1}, with ZEKE spectra recorded *via* all intermediate levels to which $S_1 \leftarrow S_0$

transitions were observed. Comparisons to the previous chapter on *p*FT, and the extensive work on toluene by Gascooke and Lawrance[18–20] and Gardner *et al*.[21,22] are also included.

4.A.2. The double rotor

Before discussing any of the obtained spectra, it is necessary to ground the discussion for the double rotor, much as was done in Chapter 3 for the single rotor before discussing the *p*FT spectra. One may initially think of *p*Xyl by analogy to a single rotor molecule such as toluene or *p*FT, treating the two methyl groups as completely non-interacting, separable, entities, due to their spatial separation in the *para*-positions. This was the approach taken by Breen *et al*.[6], wherein they labelled the levels and transitions with a G_{12} symmetry label for each of the rotors. For example, $0a_1'0a_1'$ was used to denote the lowest torsional level, with 0 quanta in both methyl groups, while $0a_1'1e''$ denoted one methyl group with 0 quanta and the other with 1 quanta.

While at first glance the approach taken by Breen *et al*.[6] is very sensible (indeed the more complete approach taken here gives a similar overall picture), there are nonetheless a few outstanding issues. If one imagines treating *para*-xylene by the formally correct MSG, this would be G_{72} rather than G_{12}. The size of the

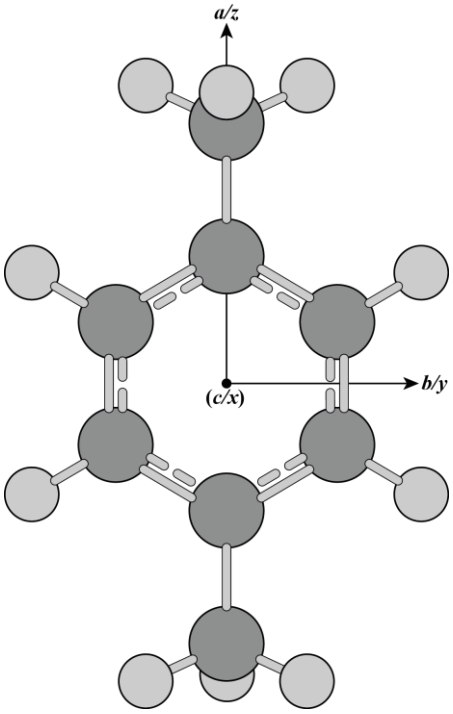


Figure 4.1 – A schematic of para-xylene showing the principal axes as well as the Cartesian axes used in this work.

group can be thought of, in part, as due to the presence of a "centre of inversion" in the *para*-xylene molecule, explicitly the case when the two methyl groups are in the staggered orientation relative to the plane of the benzene ring and staggered opposing one another; this is the orientation shown in Figure 4.1.

Continuing the comparison with the single rotor, for the *p*Xyl torsional levels to have a defined symmetry in the G_{72} MSG, they must be linear combinations of those single rotor levels. This means that care must be taken when using the G_{12} labels in the way used by Breen *et al*., and later by Held *et al*.[9] To take a particular example, Breen *et al*. assign the following transition in the excitation spectrum: $1e''0a_1' \rightarrow 2e'3a_1''$. This represents the two methyl groups undergoing transitions independently and is not in keeping with linear combinations of the single rotor levels. Bearing this in mind, in the present work, a formal approach utilising the G_{72} MSG is undertaken, and the spectral activity assigned in this way.

One might think it unusual that such a formal approach has not been used previously. Indeed, there have been many spectroscopic studies on molecules with two rotors, but traditionally the study of methyl torsions has been dominated by rotational spectroscopy, and *para*-xylene is not rotationally active since it has no permanent dipole moment. Additionally, because of the *para*-position of the substituents, the formal MSG is of a particularly high order for a double rotor system, and so *p*Xyl is the exception rather than the rule in that regard.

4.A.2.1. Molecular symmetry group treatment

Since this thesis is focused on the use of, rather than development of, the G_{72} MSG, the following section provides only a very brief summary of the G_{72} MSG treatment, which follows that of the G_{36} MSG given in Bunker and Jensen[23]. The full treatment, developed by our research group in collaboration with Professor Peter Groner from the University of Missouri-Kansas City, is provided in the published work[24] for the interested reader. In order to work out torsional level

symmetries, one can apply the same principles discussed in Chapter 3 for the G_{12} MSG, and so here the symmetries will simply be given for brevity.

4.A.2.1.1. G_{72} molecular symmetry group – key points

Table 4.1 shows the outcomes of the G_{72} MSG analysis presented in reference 24 that are relevant to this thesis. The torsional levels are shown, in the form $\{m_1,m_2\}$, where this represents a set of up to four functions: $f_{m_1,m_2}, f_{m_2,m_1}, f_{m_{-2},m_{-1}}$ and $f_{m_{-1},m_{-2}}$. This notation indicates the m value for the first methyl group as m_1 and that for the second methyl group as m_2, with the $\{m_1,m_2\}$ labels each representing a torsional level, but not necessarily a single function. The superscripted pluses and minuses derive from the behaviour of the $\{m_1,m_2\}$ levels with respect to particular operators of the G_{72} MSG, as discussed in reference 24. Here, it is sufficient to note that these superscripts distinguish levels which have effectively been split by the torsional

Table 4.1 – Transformation properties of nuclear spin, free internal rotor, asymmetric rotor and electronic dipole moment terms

G_{72}	#NS	$\{m_1,m_2\}$ sets of lowest energy	
A_1'	88	$\{0,0\}$; $\{3,3\}^{+}$; $\{3,-3\}^{+}$; $\{0,6\}^{++}$	*ee*
A_2'	0	$\{3,-3\}^{-}$; $\{0,6\}^{-+}$	*eo*, J_a
A_3'	0	$\{3,3\}^{-}$; $\{0,6\}^{+-}$	
A_4'	72	$\{0,6\}^{--}$	T_a
E_1'	24	$\{1,-1\}$; $\{-2,2\}$; $\{4,2\}^{+}$; $\{1,5\}^{+}$; $\{4,-4\}$; $\{1,-7\}^{+}$	
E_2'	16	$\{4,2\}^{-}$; $\{1,5\}^{-}$; $\{1,-7\}^{-}$	
E_3'	24	$\{1,1\}$; $\{-2,-2\}$; $\{4,-2\}^{+}$; $\{1,-5\}^{+}$; $\{4,4\}$; $\{1,7\}^{+}$	
E_4'	16	$\{4,-2\}^{-}$; $\{1,-5\}^{-}$; $\{1,7\}^{-}$	
G'	80	$\{0,2\}$; $\{-3,1\}$; $\{3,1\}$; $\{0,4\}$; $\{3,-5\}$; $\{-3,-5\}$	
A_1''	48	$\{0,3\}^{++}$	T_b
A_2''	0	$\{0,3\}^{-+}$	T_c
A_3''	0	$\{0,3\}^{+-}$	*oo*, J_b
A_4''	48	$\{0,3\}^{--}$	*oe*, J_c
E_1''	12	$\{1,2\}^{+}$; $\{1,-4\}^{+}$; $\{-5,2\}^{+}$	
E_2''	12	$\{1,2\}^{-}$; $\{1,-4\}^{-}$; $\{-5,2\}^{-}$	
E_3''	12	$\{1,-2\}^{+}$; $\{1,4\}^{+}$; $\{-2,-5\}^{+}$	
E_4''	12	$\{1,-2\}^{-}$; $\{1,4\}^{-}$; $\{-2,-5\}^{-}$	
G''	48	$\{0,1\}$; $\{3,-2\}$; $\{-3,-2\}$; $\{-3,4\}$; $\{0,5\}$; $\{3,4\}$; $\{6,1\}$; $\{-6,1\}$; $\{0,7\}$	

barrier(s) and so are no longer quadruply degenerate.

There are simple rules one can follow to determine the number of degenerate functions for a given $\{m_1,m_2\}$ level. These are:

- If both m_1 and m_2 are multiples of three and $m_1 \neq m_2$, four separate levels are formed which are linear combinations of the four initial functions. Each level is singly degenerate and belongs to one of the *A* symmetry species. This is subtly different when $m_1 = m_2$, but one still ends up with singly degenerate levels.
- If neither m_1 or m_2 are multiples of three, two doubly degenerate levels are formed, with each level composed of two functions which are linear combination of the four initial functions. These levels belong to one of the *E* symmetry species.
- If one of m_1 and m_2 is divisible by three and the other is not, the four functions are degenerate and so belong to a *G* symmetry G_{72} species.

One might ask how this compares to the single rotor, and this is best illustrated with an example. In the single rotor, the $m = 2$ level was of e' symmetry and was doubly degenerate, i.e. composed of the functions +2 and -2. In the double rotor *p*Xyl, one starts with effectively twelve functions that are comparable to those of the $m = 2$ level. These can be separated as:

- $f_{0,2}, f_{2,0}, f_{-2,0}, f_{0,-2}$, which are effectively "$m = 2$" on one rotor and "$m = 0$" on the other. These correspond to a single level, {0,2}, which is of g' symmetry, since one of the levels is a multiple of three.
- $f_{1,2}, f_{2,1}, f_{-2,-1}, f_{-1,-2}$, which are effectively "$m = 2$" on one rotor and "$m = 1$" on the other. Neither *m* level here is a multiple of three, and so two doubly degenerate levels arising from linear combinations of the functions are formed. The resulting levels are $\{1,2\}^+$ and $\{1,2\}^-$, which take e_1" and e_2" symmetries respectively.
- $f_{-1,2}, f_{2,-1}, f_{-2,1}, f_{1,-2}$, which are again effectively "$m = 2$" on one rotor and "$m = 1$" on the other, but with opposite rotation of one of the rotors

compared to the above case. Neither *m* level here is a multiple of three, and so two doubly degenerate levels arising from linear combinations of the functions are formed. The resulting levels are $\{1,\text{-}2\}^{+}$ and $\{1,\text{-}2\}^{-}$, which take e_3" and e_4" symmetries respectively.

Thus, what was a single, doubly degenerate, level in *p*FT is now five levels with various degeneracies in *p*Xyl.

For the analogues to the single rotor "*m* = 3" levels, one finds four, separate, singly degenerate levels (since both m_1 and m_2 are divisible by three): $\{0,3\}^{++}$, $\{0,3\}^{+-}$, $\{0,3\}^{-+}$ and $\{0,3\}^{--}$. These are linear combinations of the four functions:

$$\frac{(f_{0,3} + f_{3,0} + f_{-3,0} + f_{0,-3})}{2} = \{0,3\}^{++}$$

$$\frac{(f_{0,3} + f_{3,0} - f_{-3,0} - f_{0,-3})}{2} = \{0,3\}^{+-}$$

$$\frac{(f_{0,3} - f_{3,0} + f_{-3,0} - f_{0,-3})}{2} = \{0,3\}^{-+}$$

$$\frac{(f_{0,3} - f_{3,0} - f_{-3,0} + f_{0,-3})}{2} = \{0,3\}^{--}$$

Thus, one ends up with four energetically distinct "{0,3}" levels, in a similar way to the splitting of the $\underline{m} = 3$ to the *m* = 3(+) and *m* = 3(-) linear combinations in the single rotor, i.e. splitting owing to the torsional barrier. The labels assigned to differentiate these levels are indicated above. As for *m* = 2, there will also be the "{1,3}" levels, which will be quadruply degenerate, and these will be discussed later in this chapter.

These "{0,3}" linear combinations can be conveniently thought of as combinations of the single rotor *m* = 3 levels, and to facilitate easy comparison with the G_{12}, single rotor, *p*FT molecule, these are re-expressed as follows:

$$\{0,3(+)\}^{+} = \{0,3\}^{++} = 3(+)_1 + 3(+)_2$$

$$\{0,3(-)\}^{+} = \{0,3\}^{+-} = 3(-)_1 + 3(-)_2$$

$$\{0,3(-)\}^{-} = \{0,3\}^{-+} = 3(-)_2 - 3(-)_1$$

$$\{0,3(+)\}^{-} = \{0,3\}^{--} = 3(+)_2 - 3(+)_1$$

Here, the 3(+)/3(-) notation indicates the linear combination of single rotor m = 3 levels, while the superscript plus and minus signs indicate whether the combination is an addition or subtraction. One can also do the same with the $\{0,6\}^{++}$, $\{0,6\}^{-+}$, $\{0,6\}^{+-}$ and $\{0,6\}^{--}$ levels, all of which are again singly degenerate and each represent the various ways of combining the $f_{0,6}, f_{6,0}, f_{-6,0}$ and $f_{0,-6}$ functions.

It is notable, as mentioned briefly above, that the lowering in the degeneracies of the levels is caused by the torsional barrier(s). It will not be discussed in detail in this thesis, but for *p*Xyl the barrier has multiple terms, with the equivalent to the single rotor "V_6" barrier still thought to dominate, as discussed in our

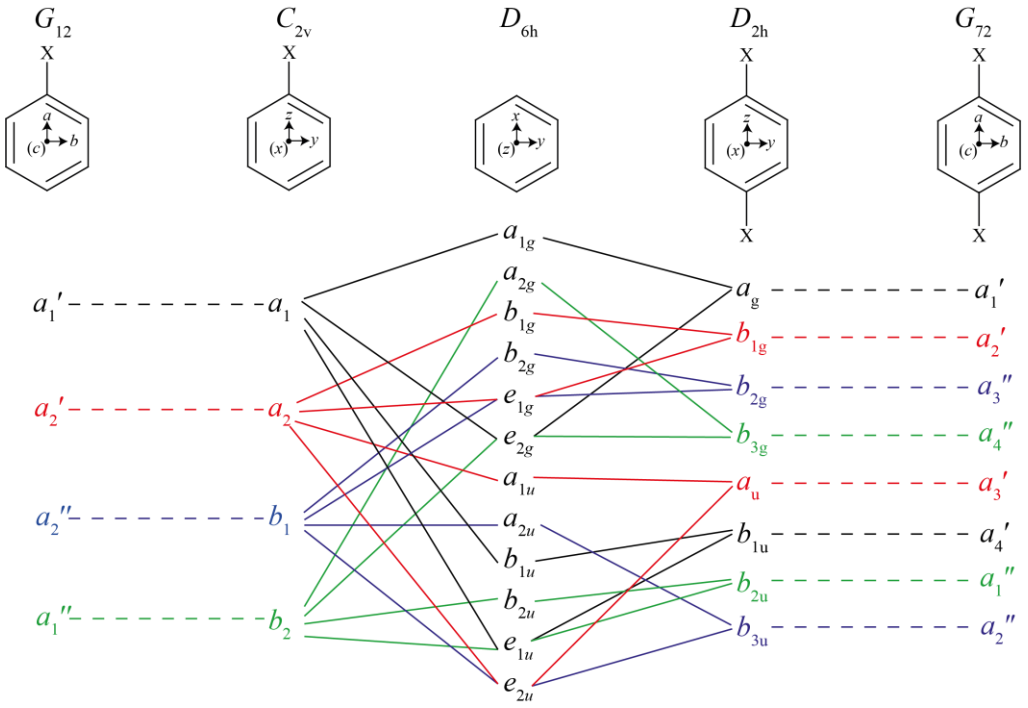


Figure 4.2 – Correlation of the G_{12} and G_{72} molecular symmetry groups. Also included are the point group symmetries of D_{6h} (for benzene), D_{2h} (for pDFB and pXyl, treating the methyl groups as point masses) and C_{2v} (for pClFB, pFT and toluene, treating the methyl groups as point masses). This allows easy comparison of the irreducible representations of the different groups. Note that the Cartesian and principal axes are also given for reference.

publication.[24] Using the {0,3} levels as an example, this "V_6" term splits the "{0,3(+)}" and "{0,3(-)}" levels in the same way as the single rotor, but additional terms separate these into $\{0,3(+)\}^+$ and $\{0,3(+)\}^-$ for the former and $\{0,3(-)\}^+$ and $\{0,3(-)\}^-$ for the latter. As will be seen later in this chapter, based on the *p*Xyl REMPI spectrum, it seems that the V_6 term is dominant, and for the purposes of this thesis the other terms are assumed to be much smaller, such that, for example, $\{0,3(+)\}^+$ and $\{0,3(+)\}^-$ are effectively degenerate (within the resolution of the current experiments), but separated from $\{0,3(-)\}^+$ and $\{0,3(-)\}^-$ by the V_6 term. In the same vein, while there are technically five energetically distinct "m = 2" levels as discussed above – {0,2}, $\{1,2\}^+$, $\{1,2\}^-$, $\{1,-2\}^+$ and $\{1,-2\}^-$ – observed transitions to these will be seen to be degenerate, suggesting that the splitting of the {1,2} and {1,-2} levels is very small.

In summary, for *p*Xyl the torsional levels take G_{72} *a*, *e* and *g* symmetries (with a total of eighteen different symmetries), each being singly, doubly or quadruply degenerate respectively.[a] One can consider these, loosely, as two sets of single rotor m levels, one on each rotor, with m_1 and m_2 quanta of excitation. For example, the {0,1} level is composed of the functions $f_{0,1}$, $f_{1,0}$, $f_{-1,0}$ and $f_{0,-1}$, which loosely represent one methyl group with one quantum of excitation rotating clockwise or anticlockwise in each case. In reality, these $\{m_1, m_2\}$ states do not represent the two rotors moving completely independently of one another, but rather indicate linear combinations of the two single rotor torsional m_i levels. In the above example of {0,1} then, both methyl groups are actually rotating, as required by the molecular symmetry of *p*Xyl, and {0,1} represents a set of four degenerate functions.

To ease the reader into comparisons between the G_{12} and G_{72} MSGs, as well as comparisons with the *para*-chlorofluorobenzene (*p*ClFB) C_{2v} and *para*-difluorobenzene (*p*DFB) D_{2h} point groups, Figure 4.2 shows the correlation between these.

[a] This contrasts with only *a* and *e* symmetries in *p*FT, with a total of six different symmetries.

4.A.2.1.2. "Cold" torsional levels

Continuing the above, one can pick out the energetic ordering of the torsional levels from Table 4.1, simply by virtue of their m_1 and m_2 values and analogy to the single rotor. However, this alone does not aid in determining which levels will have population in the supersonic jet expansion conditions of the experiment. For the single rotor in Chapter 3 it was established that, under jet expansion conditions, there would essentially only be torsional population in the $m = 0$ and $m = 1$ levels, and that these could not be interconverted due to their differing nuclear spin symmetries. One can carry out the corresponding analysis for the double rotor *p*Xyl molecule, and again one must split the total wavefunction into its various components:

$$\Phi_{tot} = \phi_{evr}\phi_{tor}\phi_{ns}$$

As for the single rotor in Chapter 3, Φ_{tot} must be antisymmetric with respect to the exchange of odd numbers of pairs of the fermionic hydrogen nuclei, and symmetric with respect to exchange of an even numbers of pairs. The relevant operators for this are discussed in reference 24, which showed that the allowed Φ_{tot} symmetries, Γ_{tot}, are A_2' and A_4'.

Also as for the single rotor, ϕ_{evr} will take the same symmetries as the asymmetric rotor functions, as the electronic and vibrational components will both be totally symmetric under the supersonic jet conditions employed in the current experiments. In the G_{72} MSG, the asymmetric rotor functions take the symmetries A_1', A_2', A_3'' and A_4'', as given in Table 4.1, and these can be derived in the same way as they are for the single rotor. As the torsional symmetries have already been given above, that leaves only the nuclear spin symmetries. The derivation of these for the (G_{12}) *p*FT molecule was discussed in Chapter 3, and the nuclear spin symmetries can be obtained in an analogous way here and are included in Table 4.1. These can be summarised as:

$$88\ A_1' + 72\ A_4' + 24\ E_1' + 16\ E_2' + 24\ E_3' + 16\ E_4' + 80\ G'$$

$$48\ A_1'' + 48\ A_4'' + 12\ E_1'' + 12\ E_2'' + 12\ E_3'' + 12\ E_4'' + 48\ G''$$

Table 4.2 – Component wavefunctions, ϕ, which together give an overall allowed symmetry, Γ_{tot}, for Φ_{tot}.[a]

Φ_{tot} symmetry (Γ_{tot})	ϕ_{evr}	ϕ_{tor}	ϕ_{ns}[b]
		a_1'	$[a_2']$
		g''	g''
A_2'		e_3'	e_4'
		e_1'	e_1'
		g'	g'
	A_1'	a_1''	$[a_2'']$
		a_1'	a_4'
		g''	g''
A_4'		e_3'	e_4'
		e_1'	e_2'
		g'	g'
		a_1''	a_4''
		a_1'	a_1'
		g''	g''
A_2'		e_3'	e_3'
		e_1'	e_1'
		g'	g'
	A_2'	a_1''	a_1''
		a_1'	$[a_3']$
		g''	g''
A_4'		e_3'	e_3'
		e_1'	e_2'
		g'	g'
		a_1''	$[a_3'']$
		a_1'	$[a_3'']$
		g''	g'
A_2'		e_3'	e_3''
		e_1'	e_2''
		g'	g''
	A_4''	a_1''	$[a_3']$
		a_1'	a_1''
		g''	g'
A_4'		e_3'	e_3''
		e_1'	e_1''
		g'	g''
		a_1''	a_1'
		a_1'	a_4''
		g''	g'
A_2'		e_3'	e_4''
		e_1'	e_2''
		g'	g''
	A_3''	a_1''	a_4'
		a_1'	$[a_2'']$
		g''	g'
A_4'		e_3'	e_4''
		e_1'	e_1''
		g'	g''
		a_1''	$[a_2']$

[a] Note that this table illustrates only six of the possible torsional symmetries, but one can work through the same analysis for the others. For the interested reader, the lowest torsional levels (up to $\Delta\{m_1, + m_2\} = 6$ from the "cold" levels) are given in Table 4.1, and one can use these to work through the same analysis for the other symmetries.

[b] The square brackets indicate that these nuclear spin symmetries do not exist and so the combination corresponding to these is not an allowed combination.

Using all of these component wavefunction symmetries allows for the construction of Table 4.2. This shows some of the possible combinations of $\phi_{evr,}$ $\phi_{tor,}$ and ϕ_{ns} that can give allowed Φ_{tot} symmetries. One can then consider each of the low energy torsional levels in turn to see if they can be interconverted in the jet expansion. For example, the {0,0} level is of a_1' symmetry, which can combine with an a_4', a_1', a_1'' or a_4'' nuclear spin symmetry depending on whether ϕ_{evr} is of A_1', A_2', A_4'' or A_3'' symmetry respectively. Note all of these are A symmetries.

The {1,1} level is of e_3' symmetry and can combine with nuclear spin symmetries of e_4', e_3', e_3'' or e_4'' depending on whether ϕ_{evr} is of A_1', A_2', A_4'' or A_3'' symmetry respectively. The {1,-1} level is of e_1' symmetry and can combine with nuclear spin symmetries of e_1', e_2', e_1'' or e_2''. So far, the {0,0}, {1,1} and {1,-1} levels have been found to have differing nuclear spin symmetries, and so cannot be interconverted in the supersonic jet expansion.

Continuing this analysis, the {0,1} level is of g'' symmetry and can combine with g'' or g' nuclear spin symmetries, giving a fourth level which cannot interconvert with the other three. One may note at this point that all of the nuclear spin symmetries which actually exist for *p*Xyl have been exhausted, and so any other torsional level must take a nuclear spin symmetry shared by one of these four levels. This leads directly to the conclusion that in *p*Xyl, excited torsional population will be cooled into one of the lowest four torsional levels, {0,0}, {0,1}, {1,1} and {1,-1}, and populations in these levels cannot be interconverted within this set. This is twice the number of "cold" levels than in the G_{12} toluene and *p*FT molecules, and as such one expects more allowed transitions than in those cases.

Note that technically, one would refer to only the lowest, $m = 0$ or {0,0} level of a vibration, i.e. the one which involves no torsional excitation, as a "pure" vibration. However, since the four "cold" levels in the S_0 state are all populated in the jet expansion and, in the absence of coupling, the transitions to these four torsional levels for a particular vibration are expected to be at the same energy, in this thesis the word vibration will often be used to refer to a vibration with the

{0,0}, {0,1}, {1,1} and {1,-1} component torsional levels. If the vibration is not observed with all four of these levels, for example if it is a non-totally symmetric vibration, the torsional levels will be given explicitly. Following on from this definition, a vibration-torsion (vibtor) level is then any vibration in combination with a torsional level, usually in reference to higher torsional excitation, or observing only one (rather than all four) of these torsional levels in combination with a vibration.

In *p*FT, each vibration has an $m = 0$ (a_1') level and an $m = 1$ (e'') level. The $m = 1$ level effectively reduces the number of different vibrational symmetries from the four C_{2v} symmetries for a C_{2v} substituted benzene molecule with monatomic substituents, to only two (e' or e''). The a_1', $m = 0$, level does not have the same effect, and one still obtains four different vibtor symmetries in that case. Here, in *p*Xyl, there are more than two different *e* symmetries, and so the same does not occur here. However, one of the four "cold" torsional levels, {0,1}, has g'' symmetry, and so this reduces the eight D_{2h} vibrational symmetries down to only two symmetries (g' or g''). In both *p*FT and *p*Xyl this effect is important as it means that potentially more vibrational levels can be coupled to one another (and to vibtor levels), than in a molecule without the methyl group(s). This can occur either *via* vibration-vibration[b] or vibration-torsional coupling, as the levels are now all of one of two rather than one of four (in *p*FT) or eight (in *p*Xyl) symmetries. It is particularly interesting that for the higher symmetry *p*Xyl molecule this represents a fourfold reduction in the number of vibrational symmetries, as opposed to a twofold reduction in the case of *p*FT.

4.A.2.2. Allowed and forbidden torsional excitations accompanying electronic excitation

Having dealt with the G_{72} MSG formalism and the issue of what levels will be populated in the supersonic jet expansion, attention can now be given to the expected transitions in the excitation spectrum. In Chapter 1, a general overview

[b] Although a vibration-vibration coupling would strictly only occur between the $m = 0$ levels of the vibrations.

of transition intensities was given, and this was expanded for the relevant single rotor systems in Chapter 3. The following discussion builds on those sections.

One can start by framing the discussion in terms of the Born-Oppenheimer (BO) approximation, with separable electronic, vibrational, torsional and rotational motions of the *p*Xyl molecule. In this framework, one can use the concept of Franck-Condon factors (FCFs) in relation to the intensity of vibrational bands in the electronic excitation and photoelectron spectra reported here. Additionally, as with most substituted benzene molecules, the geometries of the S_0, S_1 and D_0^+ states are similar, and so a $\Delta v = 0$ propensity rule is expected to hold. Similarly, based on the previous work of Gascooke and Lawrance on the S_0 and S_1 states of toluene[19,20], and the discussions in this work from Chapter 3 for *p*FT, it can be reasonably assumed that the internal rotation constant is similar in all three electronic states, and the torsional potential is likely small in all three states. As such, one also expects a $\Delta\{m_1, m_2\} = 0$ propensity rule to hold, where both m_1 and m_2 remain unchanged.

One may expect to see vibrations in the $S_1 \leftarrow S_0$ excitation spectrum that are seen in other substituted benzene molecules, and if one treated the methyl groups as point masses, *p*Xyl would be a D_{2h} molecule. As such, comparison to the vibrational activity of *p*DFB is a sensible choice, where one sees Franck-Condon allowed totally symmetric vibrations, as well as b_{3g} symmetry vibrations which are allowed by vibronic coupling.

With regard to torsional transitions, it was established in Chapter 3, from an expansion of the electronic transition moment in terms of the torsional angle, that for the single rotor one expects $\Delta m = 0$, $\Delta m = 3$ and $\Delta m = 6$ transitions with progressively weaker intensities. Here, one can carry out the same analysis, but expanding the electronic transition moment in terms of the two torsional angles:

$$\boldsymbol{M} = \langle\{m_1', m_2'\}|\langle\psi'(\boldsymbol{q}; \alpha_1, \alpha_2)|\boldsymbol{\mu}|\psi''(\boldsymbol{q}; \alpha_1, \alpha_2)\rangle|m_1'', m_2''\}\rangle$$

Here, α_1 and α_2 are the two torsional angles, m_1' and m_2' are the internal rotor quantum numbers in the upper electronic state and m_1'' and m_2'' are the internal

rotor quantum numbers in the lower electronic state. As for the single rotor, ψ' and ψ'' are the electronic wavefunctions in the upper and lower electronic states, $\boldsymbol{q}$ are the electronic coordinates and $\boldsymbol{\mu}$ is the electric dipole moment operator. Table 4.1 shows that the components of $\boldsymbol{\mu}$ along the principal axes *a*, *b* and *c* transform as the G_{72} symmetries A_4', A_1'' and A_2'' respectively, which correlate with the symmetries of the components in G_{12} for *p*FT. The S_0 state is of A_1' symmetry and the S_1 state of A_1'' symmetry, analogous to the A_g and B_{2u} states of the *p*DFB molecule, and again correlating with the states of *p*FT. As such, the middle integral will transform as a_4'', a_1' or a_2' for the *a*, *b* and *c* components of $\boldsymbol{\mu}$ respectively. With this information, one can solve the following for allowed transitions:

$$\{m_1', m_2'\} \times \psi' \times \boldsymbol{\mu} \times \psi'' \times \{m_1'', m_2''\} \supseteq A_1'$$

Where it follows that:

$$\{m_1', m_2'\} \times \{m_1'', m_2''\} \supseteq a_4'', a_1' \text{ or } a_2'$$

One must now identify the symmetries of the terms in the Fourier expansion of the electronic transition moment in terms of the torsional angles. This two-dimensional expansion is discussed in reference 24, but in this thesis only the outcomes are of interest. As such, the lowest order terms of the expansion are simply given below, with their symmetries:

$$\mu^a(\alpha_1, \alpha_2) = M_3(\cos(3\alpha_1) - \cos(3\alpha_2)) \quad a_4''$$

$$\mu^b(\alpha_1, \alpha_2) = M_0 + M_{33}(\cos(3\alpha_1)\cos(3\alpha_2)) + M_{33}'(\sin(3\alpha_1)\sin(3\alpha_2)) \quad a_1'$$

$$\mu^c(\alpha_1, \alpha_2) = M_{33}''(\sin(3\alpha_1)\cos(3\alpha_2) - \cos(3\alpha_1)\sin(3\alpha_2)) \quad a_2'$$

Note that lack of a superscript, superscript prime and double prime symbols serve to differentiate the various M_{33} terms from one another, as one involves purely cosine components, one purely sine components, and the third a mixture of the sine and cosine components.

It can be seen that $\Delta\{m_1, m_2\} = 0$ transitions will be *b*-type, and expected to be most intense, followed by $\Delta\{m_1, m_2\} = 3$ transitions, given by an M_3 term, which will be *a*-type and less intense. Finally, $\Delta\{m_1, m_2\} = 6$ transitions, given by the various M_{33} terms, will be the weakest and will be *b*-type and *c*-type, with different mechanisms for their intensities depending on the type, discussed further in the below. This is analogous to the single rotor case discussed for *p*FT in Chapter 3.

With all of this information, it is now possible to determine the *a*-, *b*- and *c*-type transitions from all four "cold" levels, as was done for *p*FT in Chapter 3. This will be done for the lowest m' levels, such that only changes up to and including $\Delta\{m_1 + m_2\} = 6$ are considered, as such transitions are already expected to be very weak.

For the $\{m_1'', m_2''\} = \{0,0\}$ level, which is of a_1' symmetry, the following will combine to give an overall totally symmetric electronic transition moment:

a-type: $\{0,3\}^{--}$, i.e. $\{0,3(+)\}^{-}$ (a_4'')
b-type: **{0,0}**, $\{3,3\}^{+}$, $\{3,-3\}^{+}$, $\{0,6\}^{++}$, i.e. $\{0,6(+)\}^{+}$ (a_1')
c-type: $\{3,-3\}^{-}$, $\{0,6\}^{-+}$, i.e. $\{0,6(-)\}^{-}$ (a_2')

For the $\{m_1'', m_2''\} = \{1,1\}$ level, which is of e_3' symmetry, the following will combine to give an overall totally symmetric electronic transition moment:

a-type: $\{1,-2\}^{-}$, $\{1,4\}^{-}$ and $\{-2,-5\}^{-}$ (e_4'')
b-type: **{1,1}**, $\{-2,-2\}$, $\{4,-2\}^{+}$, $\{1,-5\}^{+}$ and $\{4,4\}$ (e_3')
c-type: $\{4,-2\}^{-}$ and $\{1,-5\}^{-}$ (e_4')

For the $\{m_1'', m_2''\} = \{1,-1\}$ level, which is of e_1' symmetry, the following will combine to give an overall totally symmetric electronic transition moment:

a-type: $\{1,2\}^{-}$, $\{1,-4\}^{-}$ and $\{-5,2\}^{-}$ (e_2'')
b-type: **{1,-1}**, $\{-2,2\}$, $\{4,2\}^{+}$, $\{1,5\}^{+}$ and $\{4,-4\}$ (e_1')

c-type: **{1,-1}**, {-2,2}, {4,2}$^+$, {1,5}$^+$ and {4,-4} (e_1')

For the {m_1'', m_2''} = {0,1} level, which is of g'' symmetry, the following will combine to give an overall totally symmetric electronic transition moment:

a-type: {0,2}, {-3,1}, {3,1}, {0,4}, {3,-5} and {-3,-5} (g')
b-type: **{0,1}**, {3,-2}, {-3,-2}, {-3,4}, {0,5} and {3,4} (g'')
c-type: **{0,1}**, {3,-2}, {-3,-2}, {-3,4}, {0,5} and {3,4} (g'')

In the above, a bold blue level indicates a $\Delta\{m_1, m_2\} = 0$ change, and a non-bold blue level indicates a $\Delta\{m_1, m_2\} = 3$ change. These are expected to be the only ones with significant intensity, based on analogy with the single rotor cases, and the order of the terms in the Fourier expansion. Note that although a change of three must be a change in either m_1 or m_2, a change of six could be a change of m_1 by six, m_2 by six, or m_1 and m_2 both by three. All of these are expected to give rise to, at best, very weak transitions.

Working initially within the BO approximation, the purely electronic transition for *p*Xyl ($S_1 \leftarrow S_0$, $^1A_1'' - {}^1A_1'$) must be polarised along the *b* axis. This means that any symmetry-allowed torsional transition must all be *b*-polarised, i.e. *b*-type transitions. One can see that this only allows access to {0,0}, {0,1}, {1,1} and {1,-1} levels in the S_1 state with any appreciable intensity, i.e. only the various $\Delta\{m_1, m_2\} = 0$ torsional components of the electronic origin transition. This is analogous to *p*FT, and the $\Delta m = 0$ m_0^0 and m_1^1 components of the electronic origin in that molecule. Note that one may, in theory, observe symmetry-allowed transitions to, for example, the {0,5} or {0,6(+)}$^+$ levels as weak, *b*-type, $\Delta\{m_1, m_2\} = 6$ transitions, analogous to the observed transitions to the $m = 5$ and $m = 6$ levels in *p*FT discussed in Chapter 3. One can think of these *b*-type transitions as analogous to Franck-Condon allowed vibrational structure in the electronic excitation spectrum, as they arise from transitions to levels of the same symmetry as the initial level, and indeed this is how Weisshaar and co-workers[25] have referred to these transitions for the single rotor. In this thesis, such structure will often be referred to as "symmetry-allowed" when it takes the same symmetry as the initial level, whether it be torsion, vibration, or

vibtor structure. This is because the term Franck-Condon strictly only applies to vibrations and, in any case, the magnitude of the Franck-Condon factors is not known, and other mechanisms, such as torsion-electronic coupling (referred to under the general umbrella term vibronic coupling in this thesis to avoid unnecessary terminology), could contribute to transition intensity.

As was seen for *p*FT, there are far more transitions than just the *b*-type ones observed in the excitation spectrum. As such, one must look to the *a*-type and *c*-type transitions, which are allowed by different mechanisms and are not symmetry-allowed.

The *a*-type transitions arise from a vibronic coupling mechanism, analogous to the Herzberg-Teller intensity stealing mechanism[c] which gives rise to $b_2(a_1'')$ and b_{3g} vibrations in the excitation spectra of *p*FT and *p*DFB respectively, as well as transitions to the a_1'' and e' symmetry torsional levels, m_1^2, $m_0^{3(+)}$ and m_1^4, in *p*FT.

Working through an example, the $\{1,2\}^-$ level has e_2'' symmetry, and the S_1 state is of A_1'' symmetry, giving a vibronic symmetry of E_2'. This is the same symmetry as the {1,-1} level of the S_2 A_4' state ($e_1' \times A_4' = E_2'$), and so the transition from the {1,-1} level in the S_0 state to $\{1,2\}^-$ level in the S_1 state could steal intensity from the allowed transition from the {1,-1} level in the S_0 state to the {1,-1} level in the S_2 state.

The *c*-type transitions could again derive intensity from a vibronic coupling mechanism, but in *p*FT these transitions were always weak, and no state of the correct symmetry was thought to be nearby for a Herzberg-Teller mechanism to be applicable. As such, and as suggested for *p*FT, these transitions may gain intensity through another mechanism, such as torsion-rotation coupling.

[c] The states involved are analogous to *p*FT and *p*DFB, with symmetry correlations showing transitions to a_4'' levels in the S_1 state (A_1''), i.e. vibronically A_4' levels, can gain intensity by stealing from the allowed electronic transition to the S_2 (A_4') state.

Finally, one might also note that there were no transitions of any type in the above analysis which could terminate in a level akin to m = 3(-) in the single rotor: either $\{0,3(-)\}^-$ or $\{0,3(-)\}^+$. In the single rotor case, the Fourier expansion does not give any terms which allow access to the m = 3(-) level, and it is an effectively identical scenario here. Since, based on the above analysis, it is the $\{0,3(+)\}^-$ level rather than the $\{0,3(+)\}^+$ level which is expected to be observed, the partner would be the $\{0,3(-)\}^-$ level, and it is assumed that transitions to it can gain intensity by the same mechanism as transitions to m = 3(-) in the single rotor; incomplete mixing of the free rotor levels and a torsion-rotation coupling mechanism.

4.A.2.3. Vibrations and torsions accompanying the $D_0^+ \leftarrow S_1$ transition

The $D_0^+ \leftarrow S_1$ transition will now be briefly considered, where the D_0^+ state of *p*Xyl is of A_3'' symmetry (analogous to the B_{2g} symmetry of the D_0^+ state of *p*DFB and the A_2'' symmetry of the D_0^+ state of *p*FT and toluene). When exciting *via* a vibrational, torsional or vibtor level, one expects primarily Δv = 0, $\Delta\{m_1,m_2\}$ = 0 and $\Delta v\{m_1,m_2\}$ = 0 behaviour to give the most intense structure in the ZEKE spectra, with other symmetry-allowed transitions also giving significant features. One must recall that a ZEKE spectrum recorded at a particular excitation wavenumber may be exciting from multiple initial levels; for example, the origin ZEKE spectrum is recorded *via* the {0,0}, {0,1}, {1,1} and {1,-1} levels. There will be symmetry-allowed structure from all of these initial levels, although not all will be resolved.

As discussed for *p*FT in Chapter 3, one also observes transitions to non-totally symmetric levels which are not symmetry-allowed. In Chapter 3, these were proposed to arise from a combination of vibronic coupling mechanisms, such as Herzberg-Teller intensity stealing (also termed interchannel coupling) and intrachannel coupling, as discussed in recent work by our group[26] as an extension of the ideas of Poliakoff, Lucchese and co-workers[27,28]. Since the same activity is observed in a range of molecules, such as seeing transitions to D_{20}, D_{19} and D_{14} in the origin ZEKE spectra of *p*ClFB[29], *p*DFB[26,30] and *p*FT (Chapter 3), whatever mechanism is responsible is thought to be active in all of these

systems, and thus likely also active in *p*Xyl. As such, one expects to see transitions to D_{20}, D_{19} and D_{14} in the origin ZEKE spectrum. Additionally, this spectrum could be further complicated by vibronic coupling not just involving the {0,0} ladder, but also the {0,1}, {1,1} and {1,-1} ladders, with transitions arising from each of these "cold" levels.

It should be noted that if one records a ZEKE spectrum *via* a non-totally symmetric vibrational (or vibtor) level, the symmetry-allowed structure will be different to that *via* a totally symmetric level. Similarly, the structure owing to vibronic coupling will also be different and can again be thought of by analogy to *p*DFB (and *p*FT).

4.A.2.4. Vibration-torsion bands

As for *p*FT, and as discussed above, it is possible for vibtor levels to be observed in the spectra of *p*Xyl. One can assign a symmetry to a vibtor level by correlating the vibrational point group symmetries (in D_{2h}) with the correct G_{72} MSG symmetries. The calculated and experimental vibrational wavenumbers for *p*Xyl in the S_1 and D_0^+ states are given, with their D_{2h} symmetries, in Tables B.1 and B.2 in Appendix B. These can be correlated with the appropriate G_{72} MSG symmetries using Figure 4.2. One can then simply combine the torsional and vibrational symmetries and look at the resulting symmetry. While the relevant symmetries for this thesis are given when required, and the low wavenumber torsion and vibtor level symmetries are provided in Appendix C, for the particularly interested reader, the G_{72} direct product table is available as supplementary material to reference 24.

Having established the symmetry of the vibtor level, one can treat it in the usual way. For example, in the $S_1 \leftarrow S_0$ excitation spectrum, if the vibtor level is totally symmetric then it is symmetry-allowed and can have intrinsic oscillator strength, either Franck-Condon intensity or intensity from a vibronic coupling mechanism, in the same way that pure torsions or pure vibrations can gain intensity. Alternatively, it may not have intrinsic oscillator strength, but may be observed because it is coupled to another level, such as in a Fermi resonance.

If it is non-totally symmetric, it may still have the correct symmetry to gain intensity from a vibronic coupling mechanism. The same arguments apply in the cation, where the symmetry of the intermediate level will dictate whether the transition to the vibtor level in the cation is symmetry-allowed, or whether it requires a coupling mechanism to gain intensity, with the possible coupling mechanisms discussed briefly in the previous section.

Finally, now that there are four "cold" torsional levels, as opposed to the two in *p*FT, there is an interesting side effect. In *p*FT, a transition to the D_{20} $m = 2$ level was observed in the $S_1 \leftarrow S_0$ excitation spectrum. Such a transition had to originate from the $m = 1$ level in the S_0 state, as the $m = 0$ level cannot undergo a transition to the $m = 2$ level. Here, the analogues of the $m = 2$ level are the $\{0,2\}$, $\{1,2\}^+$, $\{1,2\}^-$, $\{1,-2\}^+$ and $\{1,-2\}^-$ levels, which loosely represent the various ways of exciting $m = 2$ on an individual rotor (but of course in reality represent linear combinations of this excitation with the $m = 0$ or $m = 1$ character of the other rotor in each case). Here then, one can access the $\{0,2\}$ level from the $\{0,1\}$ level, the $\{1,-2\}^-$ level from the $\{1,1\}$ level, and the $\{1,2\}^-$ level from the $\{1,-1\}$ level, all of which are *a*-type transitions (observed through a vibronic coupling mechanism). In theory, these three transitions would occur at the same energy, assuming that the internal rotation constant[d], F, is the same in both the S_0 and S_1 states. However, there is a possibility of one of these $m = 2$ analogues interacting with another level and being perturbed, while the others are not, due to their differing symmetries. Such selective interactions will be observed in the spectra below, although not involving $m = 2$; this just represents a simple example case. Note that none of these "$m = 2$" levels can be accessed from the $\{0,0\}$ "cold" torsional level, and this can be rationalised in the same way as in the single rotor; it is not possible to get to $m = 2$ from $m = 0$ due to the differing nuclear spin symmetries.

[d] It may seem odd to use a single F value rather than a separate internal rotation constant for each rotor. This could be thought of loosely as the symmetry of the molecule effectively keeping this constant for both rotors, or as owing to both methyl groups rotating for any torsional level, allowing a single definition of F.

Before continuing, some notation used throughout this chapter should be explained. While for the single rotor *p*FT molecule denoting a vibtor level is relatively straightforward, for example D_{20} m = 4, it is more complex in the double rotor *p*Xyl molecule. This is because there are multiple levels analogous to the single rotor m = 4 level; {0,4}, $\{1,4\}^+$, $\{1,4\}^-$, $\{1,-4\}^+$ and $\{1,-4\}^-$, as discussed above for m = 2. As such, torsional or vibtor levels for *p*Xyl will often be referred to by analogy to their single rotor equivalent, in inverted commas, such as "D_{20} m = 4" representing multiple of the "m = 4" *p*Xyl levels in combination with D_{20}, analogous to the D_{20} m = 4 level in *p*FT.

Additionally, in the single rotor system, a transition to an m = 4 level in the S_1 state must initiate in the m = 1 level of the S_0 state, while in the double rotor system, a transition to one of these "m = 4" levels can initiate in the {0,1}, {1,1} or {1,-1} level depending on which "m = 4" level is being accessed. As such, transitions to *p*Xyl torsional and vibtor levels will also be referred to by analogy to their single rotor equivalents, such as "m_1^2" indicating the observed transitions to "m = 2" levels for *p*Xyl that are analogous to the m_1^2 transition for *p*FT.

4.B. The low wavenumber region of the S_1 state of *para*-xylene

Having dealt with the relevant background material for understanding the torsional levels and transitions of *para*-xylene, attention can now be turned to the spectra. As for *p*FT, the *p*Xyl REMPI spectrum is presented with the $S_1 \leftarrow S_0$ transition (found to be at 36724 ± 2 cm^{-1}, in agreement with previous work[1,4]) offset to 0 cm^{-1} to give an internal energy scale. Similarly, the ZEKE spectra are offset such that the adiabatic ionisation energy (AIE) is at 0 cm^{-1}, and the AIE has been determined from the origin ZEKE spectrum to be 68200 ± 5 cm^{-1}, in agreement with earlier work[12–14].

Reference will be made to the assignments of the single rotor *p*FT spectra from Chapter 3, as well as the calculated vibrational wavenumbers for the S_1 and D_0^+

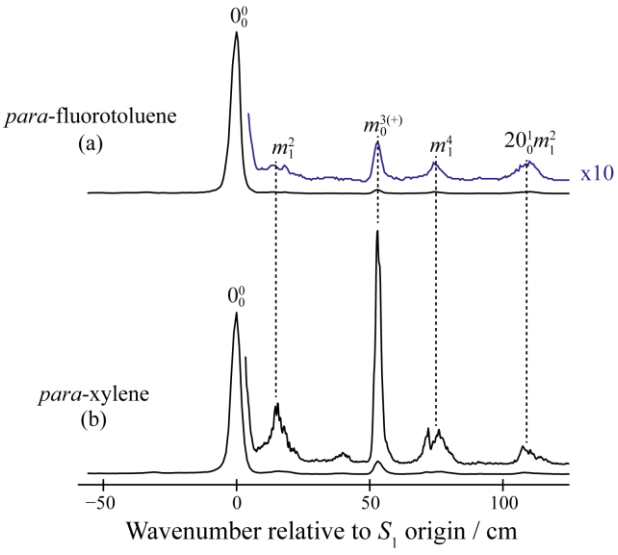


Figure 4.3 – The pFT (a) and pXyl (b) $S_1 \leftarrow S_0$ REMPI spectra up to 125 cm^{-1}. Note the expanded trace in the pXyl case is an expanded trace of a spectrum recorded with a finer laser step size than the primary trace. The transitions are labelled in the pFT case based on the discussion in Chapter 3.

states of *p*Xyl, given in Tables B.1 and B.2 in Appendix B, to aid in assigning and understanding the recorded REMPI and ZEKE spectra.

4.B.1. Below 100 cm^{-1}: the pure torsional region

4.B.1.1. Spectra and assignments

The low wavenumber part of the REMPI spectrum where the torsions were observed in *p*FT will be considered first. This region covers the first 100 cm^{-1}, as that is where all $\Delta m = 3/\Delta\{m_1,m_2\} = 3$ transitions are expected to occur, and these will have the most intensity after the $\Delta m = 0/\Delta\{m_1,m_2\} = 0$ transitions. Figure 4.3 shows a comparison of this region in *p*Xyl and *p*FT. It is apparent that the band positions are almost identical in the two cases but that some of the band profiles are quite different, for example the band at 76.0 cm^{-1} in the *p*Xyl spectrum has an additional intense spike at 72.0 cm^{-1}. This suggests that the transitions observed in this region are likely analogous to the torsional transitions observed in *p*FT; m_1^2, $m_0^{3(+)}$ and m_1^4. Initially, some of the possible torsional transitions in this region will be determined before moving on to the ZEKE spectra to confirm the assignments.

For *p*FT, the S_1 origin band consisted of both the m_0^0 and m_1^1 transitions, i.e. $\Delta m = 0$ transitions from both of the "cold" torsional levels populated in the jet expansion. These were degenerate within the resolution of the experiment due to the similarity of F in the two electronic states. For *p*Xyl then, one would expect the origin band to consist of $\Delta\{m_1,m_2\} = 0$ transitions from all four of the "cold" torsional levels; $m_{\{0,0\}}^{\{0,0\}}$, $m_{\{0,1\}}^{\{0,1\}}$, $m_{\{1,1\}}^{\{1,1\}}$ and $m_{\{1,-1\}}^{\{1,-1\}}$. In Figure 4.3(b), the origin band is not particularly broad, with a full-width at half-maximum (FWHM) of ~4 cm^{-1}, the same as for the *p*FT S_1 origin band. This suggests that these four transitions are degenerate within the current resolution, and as such, it is not possible to differentiate them here.

Next, one might consider the m_1^2 transition of *p*FT, which was observed at 0^0+16.5 cm^{-1}. This represents a $\Delta m = 3$ transition from an $m = 1$ to an $m = 2$ level. Note that in *p*FT this transition is not symmetry-allowed and is thought to be observed owing to a vibronic coupling mechanism. This is expected to be the same for the analogous "$m = 1$ to $m = 2$", $\Delta\{m_1,m_2\} = 3$, transitions in *p*Xyl, and there is a band observed with a maximum at 15.6 cm^{-1}. Here, this could be $m_{\{0,1\}}^{\{0,2\}}$, $m_{\{1,1\}}^{\{1,-2\}^-}$ and/or $m_{\{1,-1\}}^{\{1,2\}^-}$, which are all *a*-type transitions. Although $\{1,-2\}^+$ and $\{1,2\}^+$ are also analogous to $m = 2$ in the single rotor, these levels are not of the correct symmetry to be observed by the same mechanism (they are not *a*-, *b*- or *c*-type in the electronic transition moment analysis given earlier in this chapter) and so can be thought of as forbidden, with no mechanism to gain significant intensity. Finally, as in *p*FT, there is no way to get from $m = 0$ to $m = 2$, and so no transitions can arise from the $\{0,0\}$ level to an "$m = 2$" level.

Before continuing down the current line of argument, the ZEKE spectra will be inspected for confirmation of the suggested assignments. Figure 4.4 shows a series of ZEKE spectra recorded *via* the S_1 origin and *via* the low wavenumber bands above it. Figure 4.4(b) shows the ZEKE spectrum recorded *via* the S_1 origin, which shows an intense cationic origin band (here off-scale to illustrate other structure in the spectrum, but the full spectrum is shown in Figure 4.12). This origin is no wider than usual for a ZEKE band, and is expected to be

composed of the $\Delta\{m_1,m_2\} = 0$ transitions $m^{\{0,0\}}_{\{0,0\}}$, $m^{\{0,1\}}_{\{0,1\}}$, $m^{\{1,1\}}_{\{1,1\}}$ and $m^{\{1,-1\}}_{\{1,-1\}}$, where the lower levels here are those of the S_1 state and the upper levels those of the D_0^+ state. The other low wavenumber structure in this ZEKE spectrum will be discussed with reference to the other transitions below.

It is noted here that the overlap of these four transitions in the REMPI spectrum suggests that the internal rotation constant, F, is very similar in the S_0 and S_1 states, and the overlap of these transitions in the ZEKE spectrum recorded *via* the S_1 origin suggests that the constant also takes a very similar value in the D_0^+ state.

For the ZEKE spectrum *via* the 15.6 cm^{-1} band, Figure 4.4(c), an intense ZEKE band is observed at 14.6 cm^{-1}, consistent with the position of a shoulder on the origin band at around 15 cm^{-1} in the origin ZEKE spectrum. In this ZEKE spectrum, the intense band is expected to correspond to the $\Delta\{m_1,m_2\} = 0$ transitions, i.e. $m^{\{0,2\}}_{\{0,2\}}$, $m^{\{1,-2\}^-}_{\{1,-2\}^-}$ and $m^{\{1,2\}^-}_{\{1,2\}^-}$. There is also a weak shoulder in the ZEKE spectrum corresponding to the position of the cationic origin. This must arise from the {0,2}, {1,-2}$^-$ or {1,2}$^-$ levels in the S_1 state, and so at most one expects to observe transitions to the terminating levels {0,1}, {1,1} and {1,-1}, with intensity from vibronic coupling in the cation.

Moving on to the next bands in the REMPI spectrum in Figure 4.3, there is a weak band at 0^0+40 cm^{-1} and a more intense band at 0^0+53 cm^{-1}. Only one band was observed in *p*FT in this region, assigned as the $m_0^{3(+)}$ transition, which was observed at 0^0+53.5 cm^{-1}, with a similar band profile to the intense band in *p*Xyl at 0^0+53 cm^{-1}. Note that in toluene there were two bands, with a weaker one at 41 cm^{-1} and a more intense one at 53 cm^{-1}, assigned as the transitions $m_0^{3(-)}$ and $m_0^{3(+)}$ respectively[18,19,21]. As such, comparison to the single rotor, employed above for the "m_1^2" band, would suggest that these bands are the analogues of the single rotor "$m_0^{3(-)}/m_0^{3(+)}$" transitions, where here the analogous levels are the {0,3} ones.

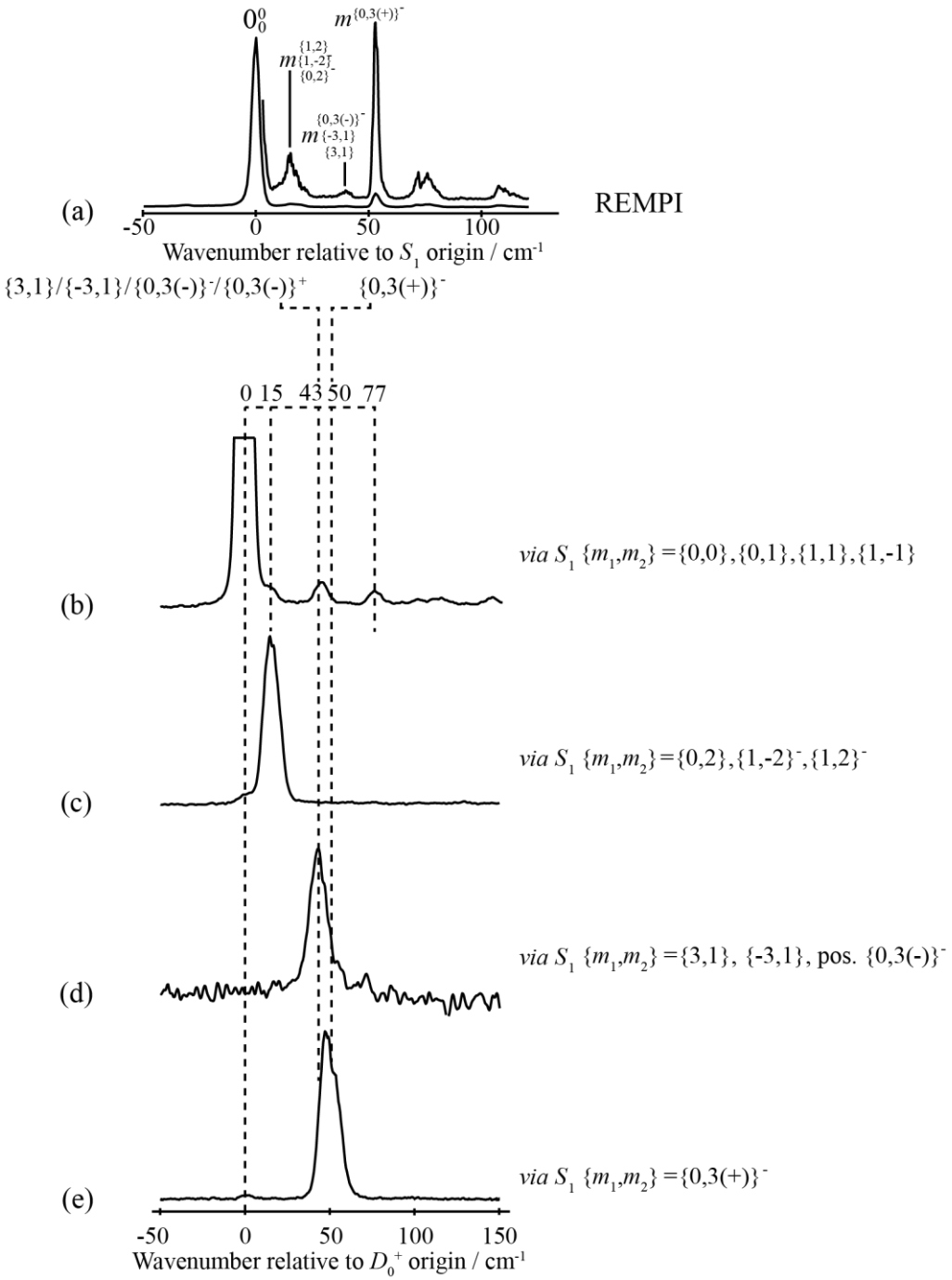


Figure 4.4 – The pXyl $S_1 \leftarrow S_0$ REMPI spectrum up to 125 cm^{-1} is shown in (a). Traces (b) – (e) show ZEKE spectra recorded via the S_1 origin, the $\{m_1,m_2\} = \{0,2\},\{1,-2\}^-$ and $\{1,2\}^-$ levels, the $\{m_1,m_2\} = \{3,1\},\{-3,1\}$ and $\{0,3(-)\}^-$ levels and the $\{m_1,m_2\} = \{0,3(+)\}^-$ level. On the REMPI spectrum, only the terminating levels are labelled, owing to the complexity of the labels if the initial "cold" levels for the transitions are also shown. The initial levels are obvious from the symmetries of the terminating levels and can be found with reference to section 4.A.2.2. on allowed transitions.

It was discussed in Chapter 3 that the intense band in the $S_1 \leftarrow S_0$ excitation spectra for *p*FT and toluene is the $m_0^{3(+)}$, as this is of the correct symmetry to be observed with intensity owing to vibronic coupling. Following through the same logic here, the vibronic coupling induced transition would be from the {0,0} to the $\{0,3\}^{--}$, i.e. the $\{0,3(+)\}^{-}$, level, which is an *a*-type transition. One can thus assign the intense band at 0^0+53 cm^{-1} to $m_{\{0,0\}}^{\{0,3(+)\}^-}$. The ZEKE spectrum recorded *via* this band is shown in Figure 4.4(e), where there is an intense band centred around 50 cm^{-1}, which could then be assigned to the $m_{\{0,3(+)\}^-}^{\{0,3(+)\}^-}$ transition, i.e. the $\Delta\{m_1,m_2\} = 0$ transition. There is also a weak feature corresponding to the cationic origin in this ZEKE spectrum, and since the S_1 level is thought to be solely the $\{0,3(+)\}^{-}$ level, this must be due to accessing the {0,0} level.

Regarding the weaker feature in the REMPI spectrum, it follows that this is the companion, "$m_0^{3(-)}$" band, which arose in the single rotor from incomplete mixing of the free rotor $\underline{m} = 3$ levels and torsion-rotation coupling. As such, the appropriate S_1 level would be the $\{0,3\}^{-+}$, i.e. the $\{0,3(-)\}^{-}$ level, and so the REMPI transition can be assigned as $m_{\{0,0\}}^{\{0,3(-)\}^-}$. A ZEKE spectrum recorded *via* this intermediate level is shown in Figure 4.4(d), and shows a $\Delta\{m_1,m_2\} = 0$ transition at 43 cm^{-1}, assigned as $m_{\{0,3(-)\}^-}^{\{0,3(-)\}^-}$, with additional contributions discussed in the below.

One can see that the $\{0,3(-)\}^{-}$ and $\{0,3(+)\}^{-}$ levels in the cation are at different wavenumbers, 43 and 50 cm^{-1} respectively. For the single rotor, it was the case that the transition to the $m = 3(+)$ level was intense in the $S_1 \leftarrow S_0$ REMPI spectra of toluene and *p*FT, but that in the ZEKE spectra *via* the origin bands, it was the transition to the $m = 3(-)$ level which carried more intensity. This was thought to be due to vibronic coupling, which could give intensity to a transition to $m = 3(+)$ in the S_1 state but $m = 3(-)$ in the D_0^+ state.

In *p*FT, the $m = 3(-)$ level is of a_2'' symmetry, the same as the D_{19} and D_{20} vibrations, also observed in the origin ZEKE spectrum owing to vibronic

coupling. Here, the $\{0,3(-)\}^+$ and $\{0,3(-)\}^-$ levels are of a_3'' and a_2'' symmetry respectively, the same symmetries as D_{19} and D_{20}. As such, based on comparison to *p*FT, *p*DFB[26,30] and *p*ClFB[29], either (or both) terminating {0,3(-)} levels could be observed on vibronic grounds in the origin ZEKE spectrum, and if both are present, they appear to be degenerate within the resolution of the current experiments.

Returning to the REMPI spectrum, although it has not yet been discussed, to higher wavenumber in the S_1 state are the D_{20} vibtor levels, some of which could perturb the $\{0,3(-)\}^-$ level. These are closer in wavenumber to the $\{0,3(-)\}^-$ than the M_{20} vibtor levels were to the m = 3(-) in toluene (and also closer than the D_{20} vibtor levels to the expected position of the m = 3(-) in *p*FT) and so one might expect the transition to $\{0,3(-)\}^-$ to be observed to lower wavenumber than m = 3(-) in those molecules. However, it is almost the same place. This suggests there may be other possible contributors to the band at 0^0+40 cm^{-1} in *p*Xyl.

Indeed, the above discussion deals with the {0,3} levels, but not the {3,1} and {-3,1} levels, which are not split by the torsional potential(s) in *p*Xyl, and so retain their fourfold degeneracy and take g' symmetries. These do not have a true analogue in *p*FT but could be observed in the S_1 state *via* the same mechanism as the $\{0,3(+)\}^-$: here, the vibronic symmetry would be G'', and the transitions to the {3,1} and {-3,1} levels could gain intensity from vibronic coupling, stealing intensity from the allowed transition to the {0,1} level (g'') of the S_2 state (A_4', G'' overall). These levels can be perturbed by levels around them, as discussed later, and so their position is hard to determine, but one would expect the transitions to be observed around the unperturbed free rotor "{0,3}" position.

As such, it is proposed that the 0^0+40 cm^{-1} REMPI band also has contributions from the transitions $m_{\{0,1\}}^{\{3,1\}}$ and $m_{\{0,1\}}^{\{-3,1\}}$, and it may even be solely these rather than the $m_{\{0,0\}}^{\{0,3(-)\}^-}$ transition. This then suggests that the band in the ZEKE spectrum recorded *via* this level is due to the $m_{\{3,1\}}^{\{3,1\}}$ and $m_{\{-3,1\}}^{\{-3,1\}}$ transitions, and that in the cation these are coincident with the $m_{\{0,0\}}^{\{0,3(-)\}^+}/m_{\{0,0\}}^{\{0,3(-)\}^-}$ transitions

thought to be observed in the origin ZEKE spectrum. Indeed, transitions to the {3,1} and {-3,1} levels may also be present in the origin ZEKE spectrum due to vibronic coupling, and so it is possible that there, one is observing transitions to all four levels, {3,1}, {-3,1}, $\{0,3(-)\}^+$ and $\{0,3(-)\}^-$, and that these transitions are degenerate within the resolution of the ZEKE spectra.

In summary, the current favoured assignment of the 0^0+40 cm^{-1} band in the REMPI spectrum is to transitions to the {3,1} and {-3,1} levels, with a possible contribution from the $\{0,3(-)\}^-$ level.

There is one final band below 100 cm^{-1}, which looks like it has two components at 0^0+72 and 0^0+76 cm^{-1}. As such, ZEKE spectra were recorded at three positions over the band, and these are given in Figure 4.5(c), (d) and (e). The S_1 position of the REMPI band suggests something analogous to the m_1^4 transition in *p*FT, but the splitting of the band profile is unique to *p*Xyl. The allowed transitions to levels analogous to m = 4 in the REMPI spectrum are $m_{\{0,1\}}^{\{0,4\}}$, $m_{\{1,1\}}^{\{1,4\}^-}$ and $m_{\{1,-1\}}^{\{1,-4\}^-}$, and as with the "$m$ = 2" case, there are other levels ($\{1,-4\}^+$ and $\{1,4\}^+$) which are not thought to be able to gain any significant intensity.

The ZEKE spectra in Figure 4.5 show an intense $\Delta\{m_1,m_2\} = 0$ transition at 77 cm^{-1} regardless of excitation position across the band, and this suggests that all of the band is composed of "m = 4" character. The ZEKE band maximum appears in the same position in all three spectra, although the spectrum in Figure 4.5(e) shows a broader band. This is thought to be due to exciting different parts of the rotational profile, and also manifested in the ZEKE spectra for *p*FT discussed in Chapter 3. As such, it seems that in the ZEKE spectra *via* this intermediate feature, one observes the $m_{\{0,4\}}^{\{0,4\}}$, $m_{\{1,4\}^-}^{\{1,4\}^-}$ and $m_{\{1,-4\}^-}^{\{1,-4\}^-}$ transitions at effectively the same transition energy. Within the resolution of the ZEKE spectra, it is not obvious that any of these levels is perturbed more than any other in the cation, and so it is not possible to say from the ZEKE spectra if part of the S_1 profile is dominated by one particular "m = 4" level. As such, the REMPI transitions are assigned as $m_{\{0,1\}}^{\{0,4\}}$, $m_{\{1,1\}}^{\{1,4\}^-}$ and $m_{\{1,-1\}}^{\{1,-4\}^-}$, and the unusual profile will be returned to later in relation to perturbation by vibtor levels in the S_1 state,

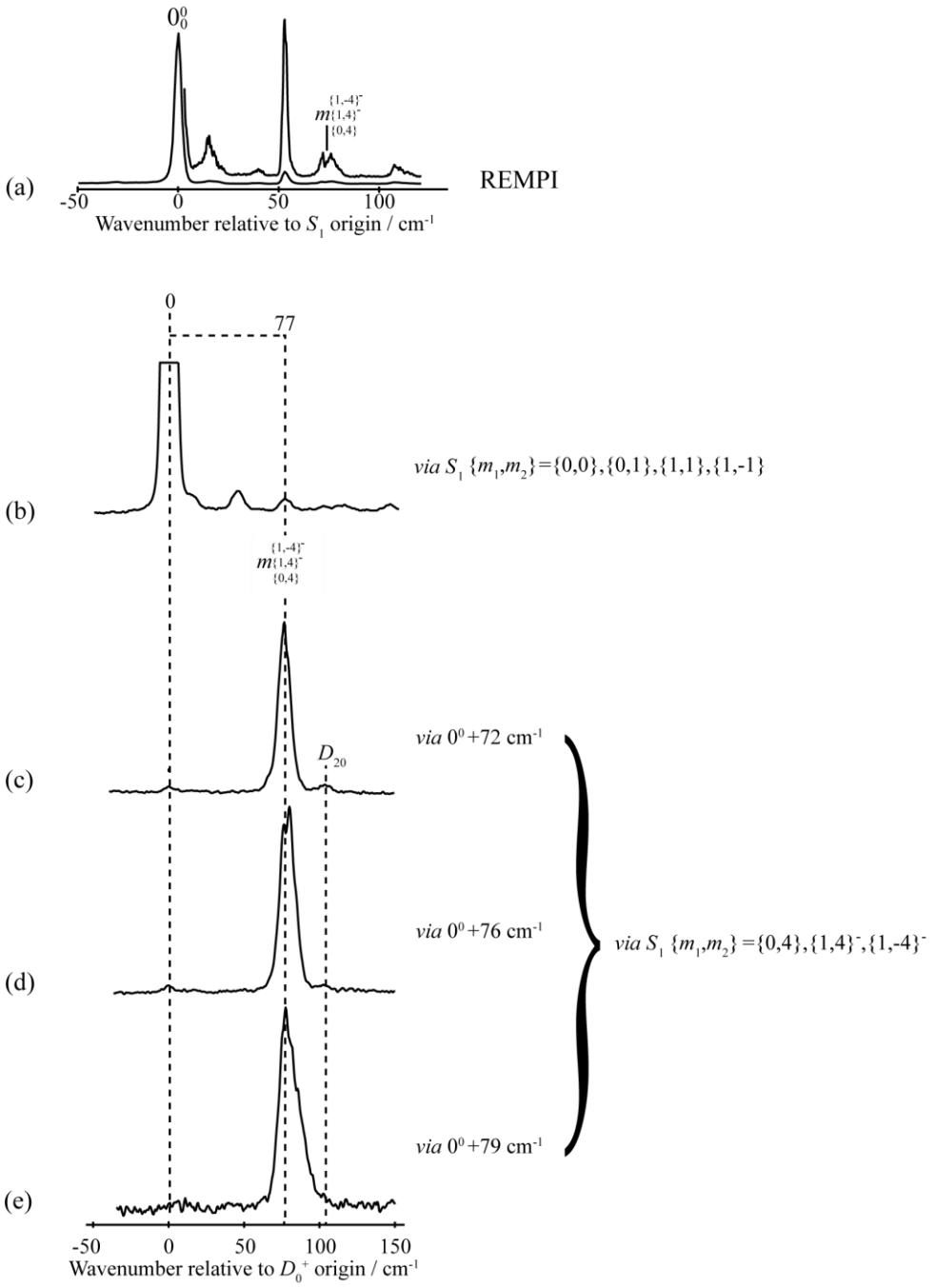


Figure 4.5 – The pXyl $S_1 \leftarrow S_0$ REMPI spectrum up to 125 cm^{-1} is shown in (a). Traces (b) – (e) show ZEKE spectra recorded via the S_1 origin and the $\{m_1,m_2\}$ = {0,4},{1,4}$^-$ and {1,-4}$^-$ levels. Note that on the REMPI spectrum, only the terminating levels are labelled, owing to the complexity of the labels if the initial "cold" levels for the transitions are also shown. The initial levels are obvious from the symmetries of the terminating levels and can be found with reference to section 4.A.2.2. on allowed transitions.

where one can use the symmetries of the levels to deduce which transitions contribute to the lower and upper parts of the band profile based on possible perturbing levels.

Finally, as for the ZEKE spectrum recorded at 0^0+15.6 cm^{-1} *via* the "m = 2" levels, one observes a weak origin band in the ZEKE spectra *via* the "m = 4" levels. The possible transitions, based on the initial S_1 levels, are to the terminating levels {0,1}, {1,1} and {1,-1}, with intensity deriving from vibronic coupling in the cation.

4.B.1.2. Discussion

Having assigned all of the torsional transitions up to $\Delta\{m_1,m_2\} = 3$, one can reflect on the nature of the internal rotation constant, F. In *p*FT, the m_1^2, $m_0^{3(+)}$ and m_1^4 transition were observed at 0^0+16.5, 0^0+53.5 and 0^0+76.0 cm^{-1} in the REMPI spectrum. For *p*Xyl, the analogous transitions were observed with maxima at 0^0+15.6 cm^{-1}, 0^0+52.6 cm^{-1} and 0^0+76.0 cm^{-1}, although the latter of these has a different, broader, band profile than in *p*FT. Noting the similarities of these positions in the two spectra, illustrated in Figure 4.3, one can conclude that F takes a similar value in *p*Xyl to *p*FT. One might suggest that it takes a slightly lower value in *p*Xyl, due to the "m_1^2" band having a maximum to slightly lower wavenumber, and this band is also expected to be the least perturbed of those just discussed owing to being the furthest energetically from levels of the same symmetry with which it can interact. However, the band profile is broad, and so it is not possible to conclude this definitively, but F appears to be very close to the value in the S_1 state of *p*FT, which itself was shown in Chapter 3 to be almost identical to the value found for the S_1 state of toluene by Gascooke and Lawrance[19]. Also as for *p*FT, it appears that the F value is very similar in the cation, where transitions in the *p*Xyl ZEKE spectrum recorded *via* the S_1 origin to the "m = 2" and "m = 4" levels occur at 0^0+15 cm^{-1} and 0^0+77 cm^{-1} respectively.

No attempt will be made to ascertain the torsional barriers of *p*Xyl, since, as was discussed for *p*FT, even with the "m = 3" level positions, a correlation with the

barrier height is still tricky due to potential couplings with these levels. However, based on the assumption of a similar internal rotation constant to that of *p*FT, the "*m* = 3" splitting appears similar to that in *p*FT or toluene, i.e. a low "V_6" barrier.

4.B.2. Vibration-torsion levels

4.B.2.1. The D_{20} vibration-torsion levels and the "*m* = 5" levels

Transitions observed above 0^0+100 cm^{-1} will now be considered. Comparing the *p*FT and *p*Xyl REMPI spectra from 100 to 240 cm^{-1}, as shown in Figure 4.6, there is a remarkable similarity in the band positions, as for the pure torsional region. As such, one might suggest that the assignments are the same, and that the transitions in *p*Xyl are to the analogous D_{20} vibtor levels. The B3LYP/aug-cc-pVTZ calculated S_1 vibrational wavenumber for D_{20} is 110 cm^{-1} for *p*FT, while for *p*Xyl it is 104 cm^{-1}. The closeness of these values would suggest, based on the similarity of the pure torsional regions of *p*Xyl and *p*FT,

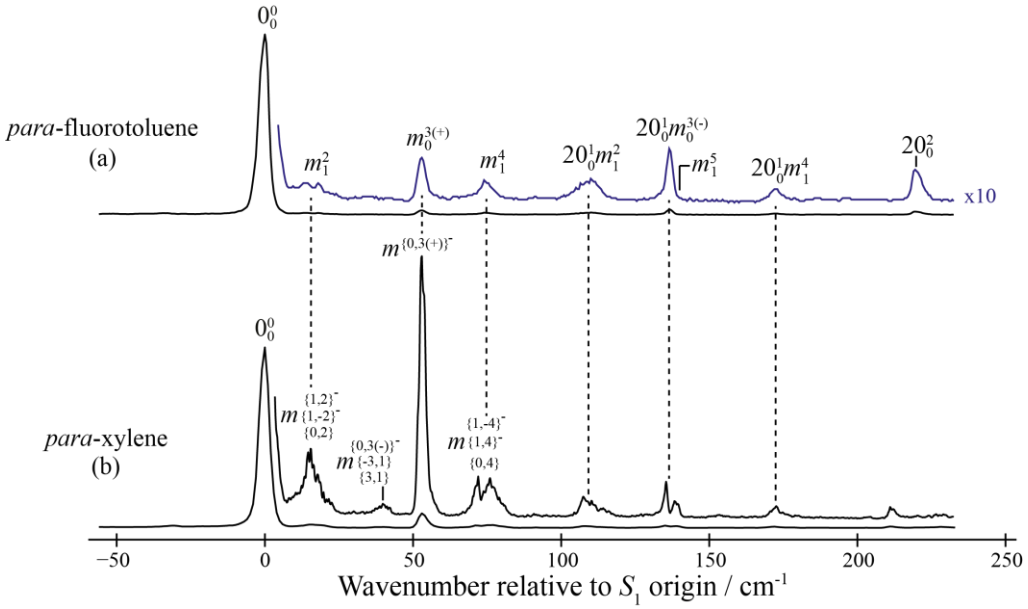


Figure 4.6 – The pFT (a) and pXyl (b) $S_1 \leftarrow S_0$ REMPI spectra up to ~240 cm^{-1}. Note the expanded trace in the pXyl case is not a x10 multiplication, but rather a spectrum recorded with a finer laser step size. The transitions are labelled in the pFT case based on the discussion in Chapter 3. For para-xylene, the terminating levels of the torsional transitions discussed in section 4.B.1. are labelled.

that the D_{20} vibtor levels would be expected in similar positions here. Again, as with the pure torsional region, there are some significant differences in the band profiles.

Starting with the band which has a maximum at 107.4 cm^{-1}, this would be expected to be composed of transitions to the vibtor levels analogous to the D_{20} m = 2 level, although in *p*FT it was thought that a transition to the D_{20} m = 1 level was also under the band. In *p*Xyl then, the possible transitions from the "cold" torsional levels are:

$20_0^1 m_{\{0,1\}}^{\{0,1\}}$ and $20_0^1 m_{\{1,1\}}^{\{1,1\}}$ for the "D_{20} m = 1" levels

$20_0^1 m_{\{0,1\}}^{\{0,2\}}$, $20_0^1 m_{\{1,1\}}^{\{1,-2\}^-}$, $20_0^1 m_{\{1,1\}}^{\{1,-2\}^+}$ and $20_0^1 m_{\{1,-1\}}^{\{1,2\}^+}$ for the "D_{20} m = 2" levels

Both of the transitions to the "D_{20} m = 1" levels are *a*-type, and so require vibronic coupling to gain any intensity, with the terminating levels taking the same symmetries as the {0,2}/{0,4} and $\{1,-2\}^-/\{1,4\}^-$ levels. For the transitions to the "D_{20} m = 2" levels, three of them are *b*-type, symmetry-allowed transitions, while $20_0^1 m_{\{1,1\}}^{\{1,-2\}^+}$ is a *c*-type transition, and so not symmetry-allowed and thus expected to be a weaker contribution, if present at all.

This means that the expected transitions to the "D_{20} m = 2" levels could gain intensity in a way analogous to Franck-Condon allowed transitions, although one might not expect the Franck-Condon factors to be very significant, and so vibronic coupling could still be responsible for intensity in these transitions. One might also note that is not possible to access the $D_{20}\{0,0\}$ or $D_{20}\{1,-1\}$ levels with any *a*-, *b*- or *c*-type transitions, and so they are not expected to have any significant intensity.

Having postulated on the nature of the transitions, one may now look at the ZEKE spectra recorded *via* this feature, shown in Figure 4.7 traces (b) – (d). The first of these, recorded at 0^0+107.4 cm^{-1}, shows two features, the most intense at

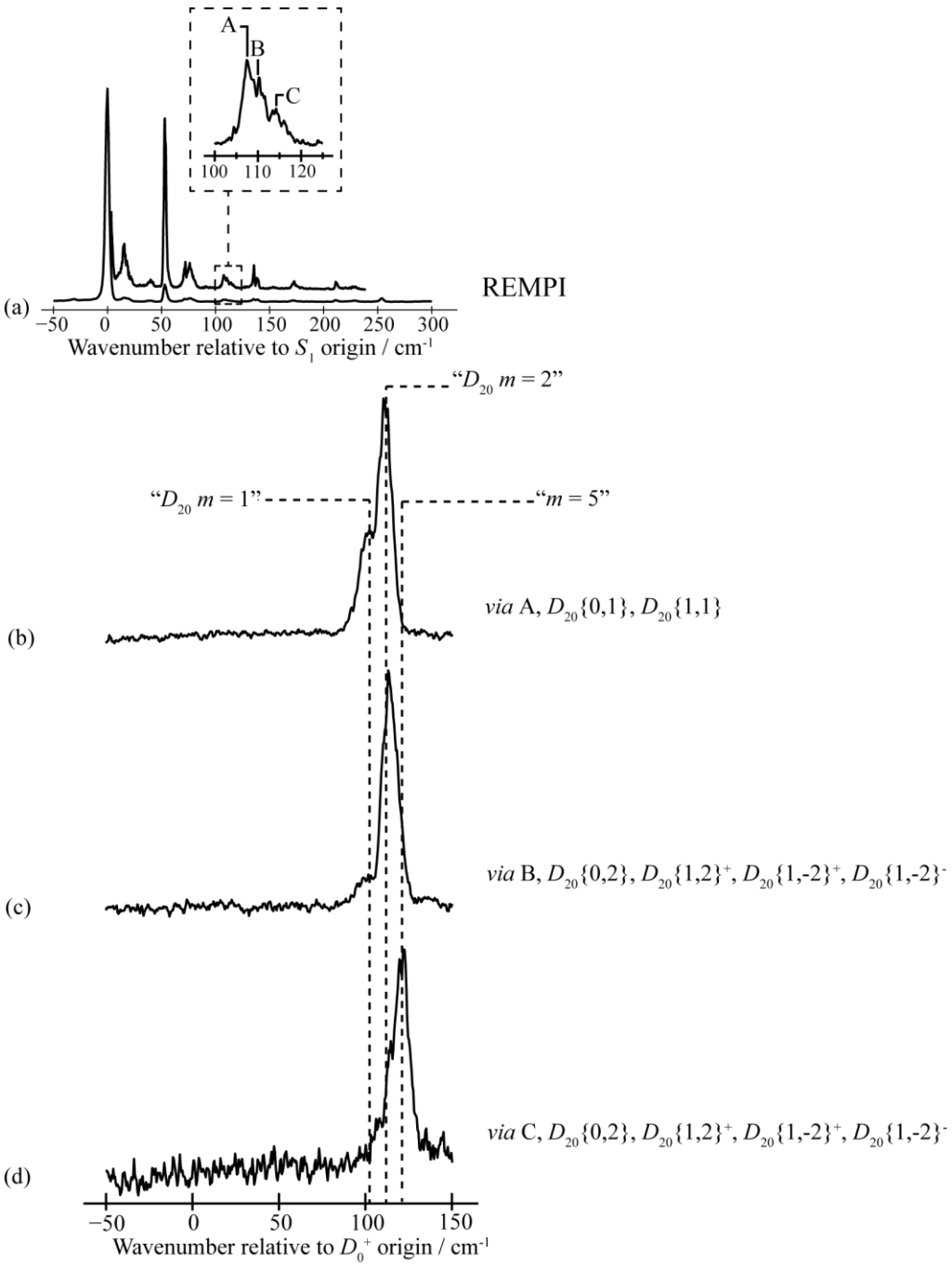


Figure 4.7 – The pXyl $S_1 \leftarrow S_0$ REMPI spectrum up to 300 cm^{-1} is shown in trace (a), with excitation positions where ZEKE spectra were recorded labelled A – C. Traces (b) – (d) show the ZEKE spectra recorded at these positions. Note that on the ZEKE spectra, only one, general, terminating level is labelled for the $\Delta v\{m_1,m_2\} = 0$ transitions to avoid clutter, but one can see from the excitation level labels the number of different terminating levels.

111 cm^{-1} with a weaker, but still intense, shoulder at 102 cm^{-1}. The position of this shoulder matches a band observed in the ZEKE spectra recorded *via* the "m = 4" levels and can be assigned to 20^1 based on the calculated vibrational

wavenumbers and similarity with the case of *p*FT. Based on the preceding discussion, it is likely that position A has contributions from transition to the $D_{20}\{0,1\}$ and $D_{20}\{1,1\}$ levels, the only two which are expected to have intensity in the excitation spectrum, and the 102 cm^{-1} ZEKE band is thus assigned specifically to these. Note that these are of the same symmetry as the $\{0,4\}$ and $\{1,4\}^-$ levels respectively, and so the appearance of a D_{20} band in those ZEKE spectra is suggestive of a (weak) interaction between the levels, such that the S_1 levels would be better represented as $D_{20}\{0,1\}\ldots\{0,4\}$ and $D_{20}\{1,1\}\ldots\{1,4\}^-$ here, and as $\{0,4\}\ldots D_{20}\{0,1\}$ and $\{1,4\}^-\ldots D_{20}\{1,1\}$ for the 0^0+76 cm^{-1} band, where the … indicates eigenstates of mixed character. These D_{20} levels are also of the correct symmetry to interact with the $\{0,2\}$ and $\{1,-2\}^-$ levels, but there is no evidence for this in the ZEKE spectra, presumably because of the larger energetic separation of the levels. Note also that the $\{0,2\}$, $\{0,4\}$ and $D_{20}\{0,1\}$ levels are all of g' symmetry, i.e. the same symmetry as the $\{3,1\}$ and $\{-3,1\}$ levels, and so could interact with those too. This is particularly interesting as it represents what, in the single rotor, would have been "$m = 1$" and "$m = 0$" levels coupling, which would in that case have been impossible due to the different symmetries, but here is possible owing to "$m = 0$" character on one rotor and "$m = 1$" character on the other.

In trace (c), recorded at 0^0+110 cm^{-1}, this shoulder is much reduced in intensity, while the intense 111 cm^{-1} band still dominates this spectrum. This suggests that the $20_0^1 m_{\{0,1\}}^{\{0,1\}}$ and $20_0^1 m_{\{1,1\}}^{\{1,1\}}$ contributions are present on the low wavenumber side of the REMPI band only. From the previous assignment of the 102 cm^{-1} ZEKE band as the $\{0,1\}$ and $\{1,1\}$ torsional components of D_{20} in the cation, it is possible that the 111 cm^{-1} band could be due to "D_{20} $m = 2$" levels. It is a little low based on simply adding the "$m = 2$" to the observed D_{20} $\{0,1\}/\{1,1\}$ levels, which could suggest interaction with a higher level or levels.

Trace (d), recorded at 0^0+114.2 cm^{-1}, shows an intense band at 122 cm^{-1}, with a weaker shoulder in the position of the 111 cm^{-1} band. In Chapter 3 it was discussed that the D_{20} $m = 2$ and $m = 5$ were interacting, and as such one possible assignment of this band is transitions to the "$m = 5$" levels. As for the single

rotor, transitions to the "m = 5" levels will be weaker than those to the torsions discussed so far, as they are $\Delta\{m_1,m_2\}$ = 6 changes, rather than the changes of 0 and 3 observed so far.

At position B then, the REMPI spectrum is dominated by transitions to "D_{20} m = 2" levels, i.e. $20_0^1 m_{\{0,1\}}^{\{0,2\}}$, $20_0^1 m_{\{1,1\}}^{\{1,-2\}^-}$, $20_0^1 m_{\{1,-1\}}^{\{1,2\}^+}$ and perhaps $20_0^1 m_{\{1,1\}}^{\{1,-2\}^+}$, while at position C, the spectrum appears to be dominated by transitions to "m = 5" levels, which take the same symmetries as the "D_{20} m = 2" levels; $m_{\{0,1\}}^{\{0,5\}}$, $m_{\{1,1\}}^{\{1,-5\}^+}$, $m_{\{1,-1\}}^{\{1,5\}^+}$ and perhaps $m_{\{1,1\}}^{\{1,-5\}^-}$. This suggests an interaction between the two sets of levels, akin to the situation in *p*FT, such that:

Position B: $D_{20}\{0,2\}\ldots\{0,5\}$, $D_{20}\{1,\text{-}2\}^{\text{-}}\ldots\{1,\text{-}5\}^{+}$, $D_{20}\{1,2\}^{+}\ldots\{1,5\}^{+}$, $D_{20}\{1,\text{-}2\}^{+}\ldots\{1,\text{-}5\}^{\text{-}}$

Position C: $\{0,5\}\ldots D_{20}\{0,2\}$, $\{1,\text{-}5\}^{+}\ldots D_{20}\{1,\text{-}2\}^{\text{-}}$, $\{1,5\}^{+}\ldots D_{20}\{1,2\}^{+}$, $\{1,\text{-}5\}^{\text{-}}\ldots D_{20}\{1,\text{-}2\}^{+}$

This leads to the conclusion that the 111 cm^{-1} ZEKE band is composed of the $\Delta v\{m_1,m_2\}$ = 0 transitions from the "D_{20} m = 2" levels, and the 122 cm^{-1} band is the $\Delta\{m_1,m_2\}$ = 0 transitions from the "m = 5" levels. The interaction between the levels is analogous to *p*FT, although in that case the m = 5 level was thought to be at a higher internal energy in the S_1 state of 0^0+142 cm^{-1}, while here it is would be at 0^0+114.2 cm^{-1}. Based on the similarity of the rest of the spectrum in this region, this difference is rather striking, and suggests that this is not the full story.

Indeed, if one looks at the ZEKE spectrum recorded *via* the feature at 0^0+138 cm^{-1} (discussed below), one can see a shoulder at ~125 cm^{-1}, which could also be assigned as the $\Delta\{m_1,m_2\}$ = 0 transitions to the "m = 5" levels. If this is assigned as the $\Delta\{m_1,m_2\}$ = 0, then this in much better agreement with the *p*FT case, which is more consistent with the striking resemblance of the rest of this region of the REMPI spectrum.

Thus, the conclusion is that the 0^0+110 cm^{-1} position is dominated by transitions to the "D_{20} m = 2" levels, which are interacting with the "m = 5" levels: $D_{20}\{0,2\}\ldots\{0,5\}$, $D_{20}\{1,-2\}^-\ldots\{1,-5\}^+$, $D_{20}\{1,2\}^+\ldots\{1,5\}^+$ and $D_{20}\{1,-2\}^+\ldots\{1,-5\}^-$. The transitions to the "m = 5" partner levels ($\{0,5\}\ldots D_{20}\{0,2\}$, $\{1,-5\}^+\ldots D_{20}\{1,-2\}^-$, $\{1,5\}^+\ldots D_{20}\{1,2\}^+$ and $\{1,-5\}^-\ldots D_{20}\{1,-2\}^+$) could be found at either 0^0+114.2 cm^{-1} or 0^0+138 cm^{-1}, based on the above evidence, with the higher position favoured based on the discussion above.

One might note the $\Delta v = 1$, $\Delta\{m_1,m_2\} = 3$ change between the "D_{20} m = 2" and "m = 5" levels, and the same between the "D_{20} m = 1" and "m = 4" levels. This represents a reasonably strong vibration-torsion coupling, analogous to the $\Delta v = 1$, $\Delta m = 3$ changes discussed for *p*FT for these levels. Additionally, this can explain the unusual band profile observed for the "m_1^4" band in the REMPI spectrum, as only two of the three levels can be perturbed downwards by interaction with the two observed "D_{20} m = 1" levels, leaving the third (effectively) unperturbed to higher wavenumber.

Moving to slightly higher wavenumber, there is a double feature in the REMPI spectrum with maxima at 0^0+135.4 and 0^0+138.4 cm^{-1}. Since the "$20_0^1m_1^1$" and "$20_0^1m_1^2$" transitions appear in effectively the same place energetically as their *p*FT counterparts, this double band would be expected to be the analogue of the $20_0^1m_0^{3(-)}$ transition in *p*FT.

Figure 4.8 traces (b) and (c) show the ZEKE spectra recorded *via* the two maxima of this double band, and they show remarkably similar activity. One would perhaps expect only a single transition terminating in a level analogous to "D_{20} m = 3(-)" in *p*FT, and that would be $20_0^1m_{\{0,0\}}^{\{0,3(-)\}^-}$, as this terminating level is totally symmetric and therefore the transition to it is symmetry-allowed, and can have, effectively, Franck-Condon intensity, as in the *p*FT case.

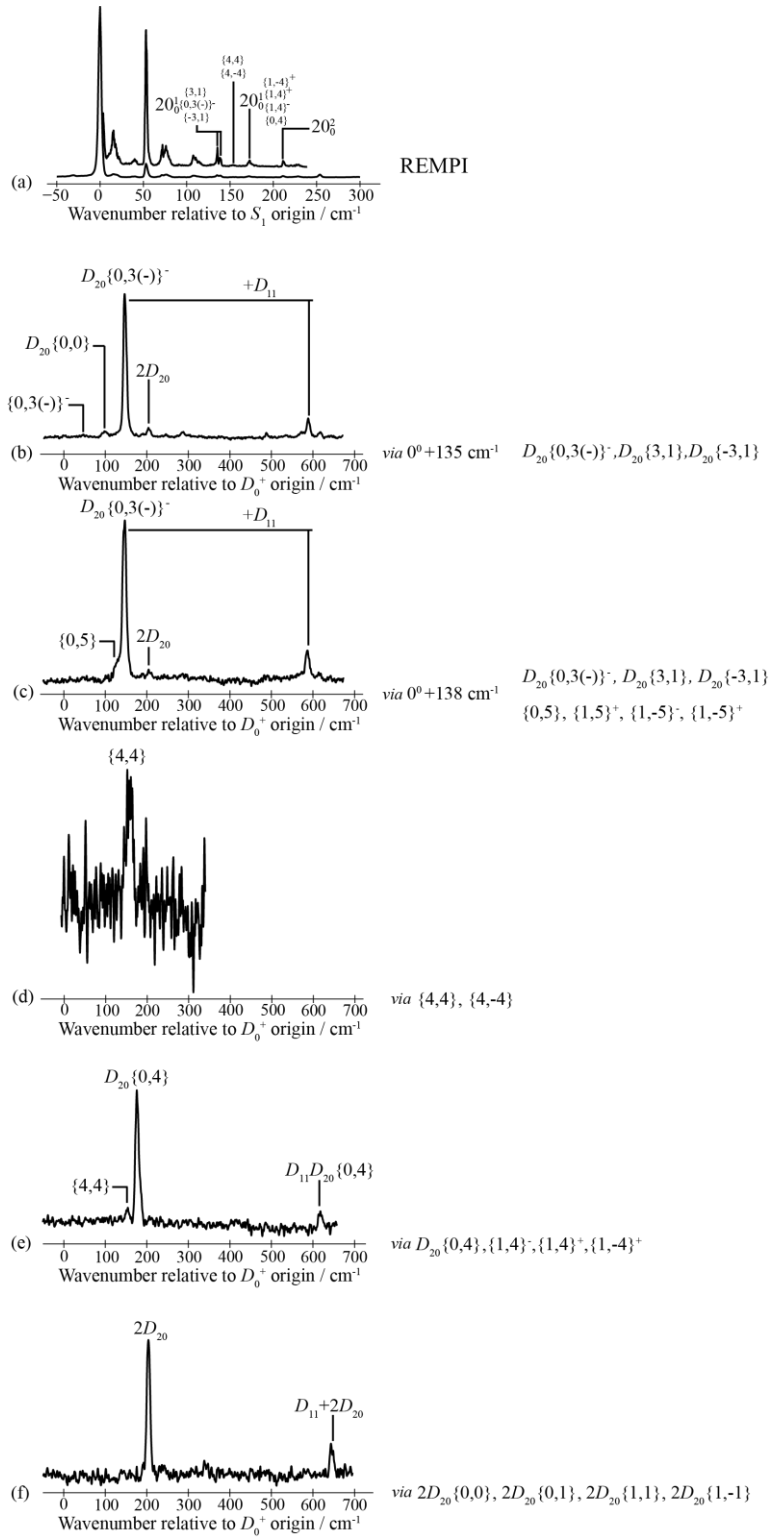


Figure 4.8 – The pXyl $S_1 \leftarrow S_0$ REMPI spectrum up to 300 cm^{-1} is shown in trace (a). Traces (b) – (f) show the ZEKE spectra recorded via (primarily) D_{20} vibtor levels over this region. On the REMPI spectrum, only the terminating levels are labelled, and on the ZEKE spectra, only one terminating level is labelled for the $\Delta v\{m_1,m_2\} = 0$ transitions to avoid clutter, but one can see from the excitation level labels the number of different terminating levels.

As such, the $\Delta v\{m_1,m_2\}$ = 0 transition that dominates both ZEKE spectra at 146 cm^{-1} can be assigned to the $20_1^1 m_{\{0,3(-)\}^-}^{\{0,3(-)\}^-}$, suggesting both components of the double REMPI feature are due to transitions to the same "D_{20} m = 3(-)" level.

However, this does not seem sensible based on the obvious doubled structure, and while this could be rotational, it is not akin to rotational profiles that have been noted previously for *p*FT. As such, one looks to other allowed transitions from the other "cold" torsional levels, and in doing this, finds that $20_0^1 m_{\{0,1\}}^{\{3,1\}}$ and $20_0^1 m_{\{0,1\}}^{\{-3,1\}}$ are also symmetry-allowed, and transitions to the {3,1} and {-3,1} were assigned in the torsional region of the REMPI spectrum. All three of these transitions to "D_{20} m = 3" levels can in theory have "Franck-Condon" like intensity (although only one level is "D_{20} m = 3(-)" like), and they take a_1', g'' and g'' symmetries, such that the g'' levels can interact with different vibration/vibtor/torsional levels to the a_1' level, and this could be the cause of the split band profile.

Although the split band profile could be explained by the contribution of the "m = 5" levels to the higher component, proposed above, the intense "D_{20} m = 3" bands in both ZEKE spectra suggests that "D_{20} m = 3" character contributes to (and dominates) both parts of the profile.

Note also that $D_{20}\{3,1\}$ and $D_{20}\{-3,1\}$ are the same symmetry as the {0,5} level, and so these could potentially be interacting with one another. This is an alternative explanation as to why a transition to {0,5} is observed in the 0^0+138 cm^{-1} ZEKE spectrum (as opposed to being a $\Delta\{m_1,m_2\}$ = 0 transition), but if a strong interaction were the case one might expect $m_{\{0,1\}}^{\{0,5\}}$ to be perturbed from the other allowed "m_1^5" transitions in the REMPI spectrum, and there is no evidence of any separation. As such, it still seems sensible to assign the transitions to the "m = 5" levels as underneath the higher wavenumber 0^0+138 cm^{-1} band, as discussed above.

Also observed in the ZEKE spectrum recorded at 0^0+135 cm^{-1} are a transition/transitions to the D_{20} terminating level(s). This could be either the

$D_{20}\{0,0\}$, accessible from the $D_{20}\{0,3(-)\}^-$ level, or the $D_{20}\{0,1\}$, accessible from the $D_{20}\{3,1\}$ and $D_{20}\{-3,1\}$ levels. Either option would require a vibronic coupling mechanism in the cation, and so this does not help deduce which part of the REMPI band profile is due to which symmetry levels.

In a similar vein, a weak band is observed at 46 cm^{-1} in that ZEKE spectrum, assignable to a transition terminating in one of these "m = 3" levels. As for the band observed in the origin ZEKE spectrum, this terminating level could be $\{0,3(-)\}^-$, $\{0,3(-)\}^+$, {3,1} or {-3,1}, in any case requiring vibronic coupling in the cation for any intensity. The assignments of $\{0,3(-)\}^-$ and {3,1}/{-3,1} are favoured, since these are analogous to the commonly observed "Δv = -1" transitions in *p*FT.

These two ZEKE spectra also contain the $\Delta v\{m_1,m_2\} = 0$ band in combination with D_{11}, a common feature observed in the *p*FT spectra, as well as here a transition to the $2D_{20}$ level(s) , which could be either symmetry-allowed or coupled to these levels. This could be $2D_{20}\{0,0\}$, which would be symmetry-allowed from the $D_{20}\{0,3(-)\}^-$ level, or it could be $2D_{20}\{0,1\}$, which could arise as a transition from the $D_{20}\{3,1\}$ and $D_{20}\{-3,1\}$ intermediate levels, and would again be symmetry-allowed.

Figure 4.8(f) shows the ZEKE spectrum recorded at 0^0+211.2 cm^{-1}, which shows two ZEKE bands, one intense one at 203 cm^{-1} (the $\Delta v\{m_1,m_2\} = 0$ one), and one at 643 cm^{-1} (the $\Delta v\{m_1,m_2\} = 0$ in combination with D_{11}). This S_1 band might be expected to involve D_{19}, but the ZEKE band does not match that, and so it is assigned as a transition to $2D_{20}$, giving the REMPI transitions: $20_0^2 m_{\{0,0\}}^{\{0,0\}}$, $20_0^2 m_{\{0,1\}}^{\{0,1\}}$, $20_0^2 m_{\{1,1\}}^{\{1,1\}}$ and $20_0^2 m_{\{1,-1\}}^{\{1,-1\}}$. The 203 cm^{-1} ZEKE band is then just composed of the $\Delta v\{m_1,m_2\} = 0$ transitions. There is no evidence of any D_{20} vibtor levels in the ZEKE spectrum, suggesting any interactions are weak. Finally, it is interesting to note that, unlike the D_{20} vibtor levels, the position of $2D_{20}$ is lower than in *p*FT. This will be returned to in the discussion later.

4.B.2.2. The "double excitation" torsional levels and the "D_{20} m = 4" levels

A ZEKE spectrum was recorded *via* a very weak feature at 0^0+153.4 cm^{-1}, shown in Figure 4.8(d), and it shows a single band (presumably the $\Delta v\{m_1,m_2\} = 0$ transition) at 156 cm^{-1}. Such a band was not present in the REMPI spectrum of *p*FT, and at such a low wavenumber there are very few possibilities. It does not correspond to the expected position for any torsional transitions which are analogous to the single rotor, and the only vibtor transitions this low in wavenumber involve D_{20} (indeed, that is the only vibration this low in wavenumber). As such, it could be assigned to the $20_0^1 m_{\{0,0\}}^{\{0,3(+)\}^+}$ transition, which is a *c*-type transition. In *p*FT such *c*-type transitions were weak, and although could be observed owing to vibronic coupling, there is not thought to be a nearby electronic state of the correct symmetry. For observed *c*-type transitions in *p*FT, other mechanisms (such as torsion-rotation coupling) were thought to be involved, such as for the observed $m_0^{6(-)}$ transition. The analogous "$m_0^{6(-)}$" transition does not appear to be observed in *p*Xyl, which suggests that this REMPI band is likely not attributable to the *c*-type $20_0^1 m_{\{0,0\}}^{\{0,3(+)\}^+}$ transition.

The keen observer may note that this 0^0+153.4 cm^{-1} band is in approximately the right position in the S_1 state for a transition to one (or both) of the {4,4} levels: {4,4} and {4,-4}. If one assumes that these would be at double the "m = 4" position, they would be expected somewhere around 150 cm^{-1} in the REMPI spectrum, and 154 cm^{-1} in the cation. The transition to the {4,4} would be *b*-type (symmetry-allowed) from the {1,1} level, and that to the {4,-4} would also be *b*-type (symmetry-allowed) from the {1,-1} level. Such a "double excitation" transition is a $\Delta\{m_1 + m_2\}$ change of six, and so expected to be weak, as the REMPI transition is. If this assignment is correct, one might also expect to observe transitions to the {2,2} and {3,3} levels.

The transitions to the {2,2} levels, {-2,-2} and {-2,2}, would be expected at 32 cm^{-1} in the S_1 state and 30 cm^{-1} in the D_0^+ state, and these would also be symmetry-allowed in the REMPI spectrum. However, there is no obvious band at this position in the REMPI spectrum, and these do not appear to be observed.

In a similar vein, the transitions to the {3,3} levels – $\{3,3\}^-$, $\{3,3\}^+$, $\{3,-3\}^-$ and $\{3,-3\}^+$ - would be expected somewhere between 80 and 106 cm^{-1} in the S_1 state and between 86 and 100 cm^{-1} in the D_0^+ state (based on the observed "m = 3" levels). Note that only the $\{3,3\}^+$ and $\{3,-3\}^+$ are symmetry allowed. A ZEKE spectrum was recorded *via* a band at 107 cm^{-1}, which contained a reasonably intense band at 102 cm^{-1}, and this could be assigned to such a {3,3} transition, but was instead assigned to a transition to the "D_{20} m = 1" level, in analogy to *p*FT.

Finally, the {4,2} levels are also a $\Delta\{m_1 + m_2\}$ change of six, and these are the $\{4,-2\}^+$, $\{4,-2\}^-$, $\{4,2\}^+$ and $\{4,2\}^-$ levels, of which only transitions to $\{4,2\}^+$ and $\{4,-2\}^+$ would be symmetry-allowed. Transitions to these would be expected at around 176 – 184 cm^{-1} in the S_1 state, and around 184 cm^{-1} in the cation. Although a band was observed at 173 cm^{-1} in the REMPI spectrum, this will be assigned to transitions to "D_{20} m = 4" levels below, again in analogy to *p*FT, and there is no transition at 184 cm^{-1} in the ZEKE spectrum, with the closest being 176 cm^{-1}, which is assigned as $\Delta v\{m_1,m_2\}$ = 0 transitions to the "D_{20} m = 4" terminating levels. Additionally, this 173 cm^{-1} band is reasonably intense in the REMPI spectrum (for a transition in this torsion/vibtor region), and so is unlikely to correspond to a $\Delta\{m_1 + m_2\}$ = 6 transition.

One could conclude from the lack of observation of the {2,2}, {3,3} and {4,2} levels that the 0^0+153.4 cm^{-1} band is not the {4,4} terminating level. Indeed, it appears that such "double excitations" do not appear to be observed in the REMPI and ZEKE spectra of *p*Xyl, likely owing to their $\Delta\{m_1 + m_2\}$ = 6 nature, meaning that they are likely to be weak at best. This is analogous to a single "m" change of six being weaker than a change of three; for example, in *p*FT, the transitions to the m = 6 and m = 7 levels were observed only very weakly, with the m_1^7 one found somewhat fortuitously as it was overlapping another transition. However, if one of these "double excitation" terminating levels was to be coupled to a level arising from a more intense, bright, transition, it might be observed. With this, and the possible assignment of this 153.4 cm^{-1} REMPI band to the {4,4} levels, in mind, this point will be returned to very shortly.

Continuing to higher wavenumber, there is a feature with a maximum at 0^0+172.6 cm^{-1}, which is in the correct place to be due to "$20_0^1 m_1^4$" transitions based on the comparison to *p*FT. The expected transitions from the "cold" torsional levels here are: $20_0^1 m_{\{0,1\}}^{\{0,4\}}$, $20_0^1 m_{\{1,1\}}^{\{1,4\}^-}$, $20_0^1 m_{\{1,1\}}^{\{1,4\}^+}$ and $20_0^1 m_{\{1,-1\}}^{\{1,-4\}^+}$. As for the "$D_{20}$ m = 2" levels discussed earlier, three of these transitions are *b*-type, and so are symmetry-allowed. The ZEKE spectrum is shown in Figure 4.8(e), and shows an intense $\Delta v\{m_1,m_2\}$ = 0 band at 176 cm^{-1}, assigned to $20_1^1 m_{\{0,4\}}^{\{0,4\}}$, $20_1^1 m_{\{1,4\}^-}^{\{1,4\}^-}$, $20_1^1 m_{\{1,4\}^+}^{\{1,4\}^+}$ and $20_1^1 m_{\{1,-4\}^+}^{\{1,-4\}^+}$. Additionally, one observes the $\Delta v\{m_1,m_2\}$ = 0 band in combination with D_{11}, and a feature at 155 cm^{-1}. This feature is in the same position as the $\Delta v\{m_1,m_2\}$ = 0 transition from the 0^0+153.4 cm^{-1} REMPI band. If it was assignable to a transition to the $D_{20}\{0,3(+)\}^+$ level discussed above, such a transition would have to arise from a torsional level in the {0,0} "ladder", and none of the levels here are from that "ladder", suggesting that would be an incorrect assignment.

The only other possible assignment to this would be to the terminating levels {4,4} (e_3') and {4,-4} (e_1'), which would be of the correct symmetry to observed as symmetry-allowed transitions from the $D_{20}\{1,4\}^-$ (e_3') and $D_{20}\{1,-4\}^+$ (e_1') levels, although as discussed above such transitions are expected to be weak. However, the {4,4} and {4,-4} levels could be coupled to the $D_{20}\{1,4\}^-$ and $D_{20}\{1,-4\}^+$ levels; this is, effectively, a $\Delta\{m_1,m_2\}$ = 3 and Δv = 1 coupling, analogous to the couplings observed in *p*FT; such coupling would explain the presence of these unusual "double excitation" levels in the REMPI spectrum.

Bearing this in mind, one can return to the 0^0+153.4 cm^{-1} REMPI band, which showed a (weak) $\Delta v\{m_1,m_2\}$ = 0 transition at 156 cm^{-1}, the same place as the weak ZEKE feature when exciting *via* the "D_{20} m = 4" levels. One can assign the 0^0+153.4 cm^{-1} REMPI band as the $m_{\{1,1\}}^{\{4,4\}}$ and $m_{\{1,-1\}}^{\{4,-4\}}$ transitions (and thus the $\Delta\{m_1,m_2\}$ = 0 transition as $m_{\{4,4\}}^{\{4,4\}}$ and $m_{\{4,-4\}}^{\{4,-4\}}$), and then the weak band in the "D_{20} m = 4" ZEKE spectrum recorded at 0^0+172.6 cm^{-1} arises owing to the coupling of the {4,4} and {4,-4} levels to the $D_{20}\{1,4\}^-$ and $D_{20}\{1,-4\}^+$ levels in the S_1 state. While the levels could also be coupled in the D_0^+ state, the presence

of the $m^{\{4,4\}}_{\{1,1\}}$ and $m^{\{4,-4\}}_{\{1,-1\}}$ transitions in the excitation spectrum, when none of the other "double excitation" torsional transitions were observed, suggests that they must be coupled in the S_1 state. Since only two of the four "D_{20} m = 4" levels are involved in this coupling, one might expect these to separate energetically, and the REMPI band is somewhat asymmetric and "spread out" on the high wavenumber side, supporting this, although this could also be its rotational profile. This can be seen in Figure 4.9.

4.B.2.3. The D_{19} vibration-torsion levels

Figure 4.9 shows a comparison of the *p*FT and *p*Xyl REMPI spectra up to 350 cm^{-1}, extending another 100 cm^{-1} higher than the regions discussed so far. In the 250 – 350 cm^{-1} region of the *p*FT REMPI spectrum, the D_{19} vibtor levels dominate, with the most intense band in that range due to the $19^1_0 m_0^{3(-)}$ transition, in the same way that the $20^1_0 m_0^{3(-)}$ was the most intense of the transitions involving the D_{20} vibtor levels. If one expects the same activity in

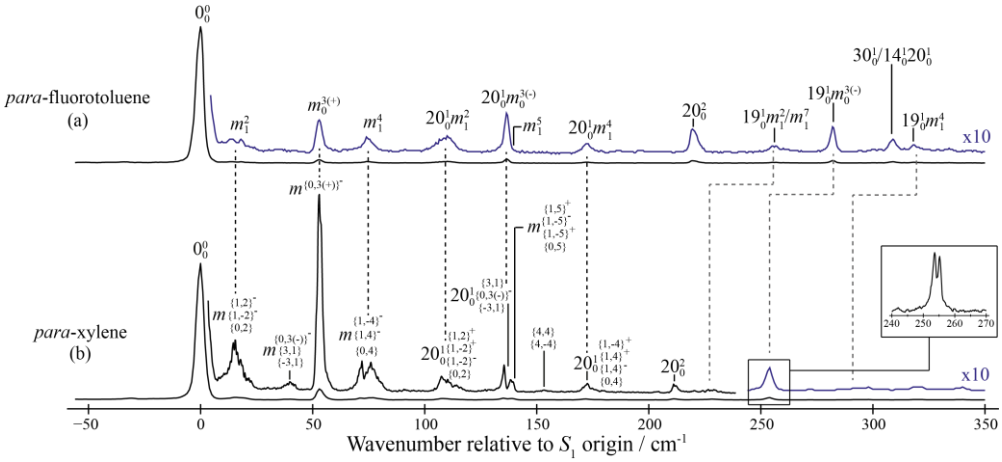


Figure 4.9 – The pFT (a) and pXyl (b) $S_1 \leftarrow S_0$ REMPI spectra up to 350 cm^{-1}. Note that the black expanded trace in the pXyl case is not a x10 multiplication, but rather a spectrum recorded with a finer laser step size, while the blue expanded trace is a x10 multiplication. The transitions are labelled in the pFT case based on the discussion in Chapter 3. For pXyl, the terminating levels of the torsional transitions and D_{20} vibtor transitions already discussed are labelled. The grey dashed lines indicate the expected shifts of the D_{19} vibtor levels from pFT to pXyl, as discussed in the text, and the inset spectrum from 240 – 270 cm^{-1} shows a higher resolution scan across that range.

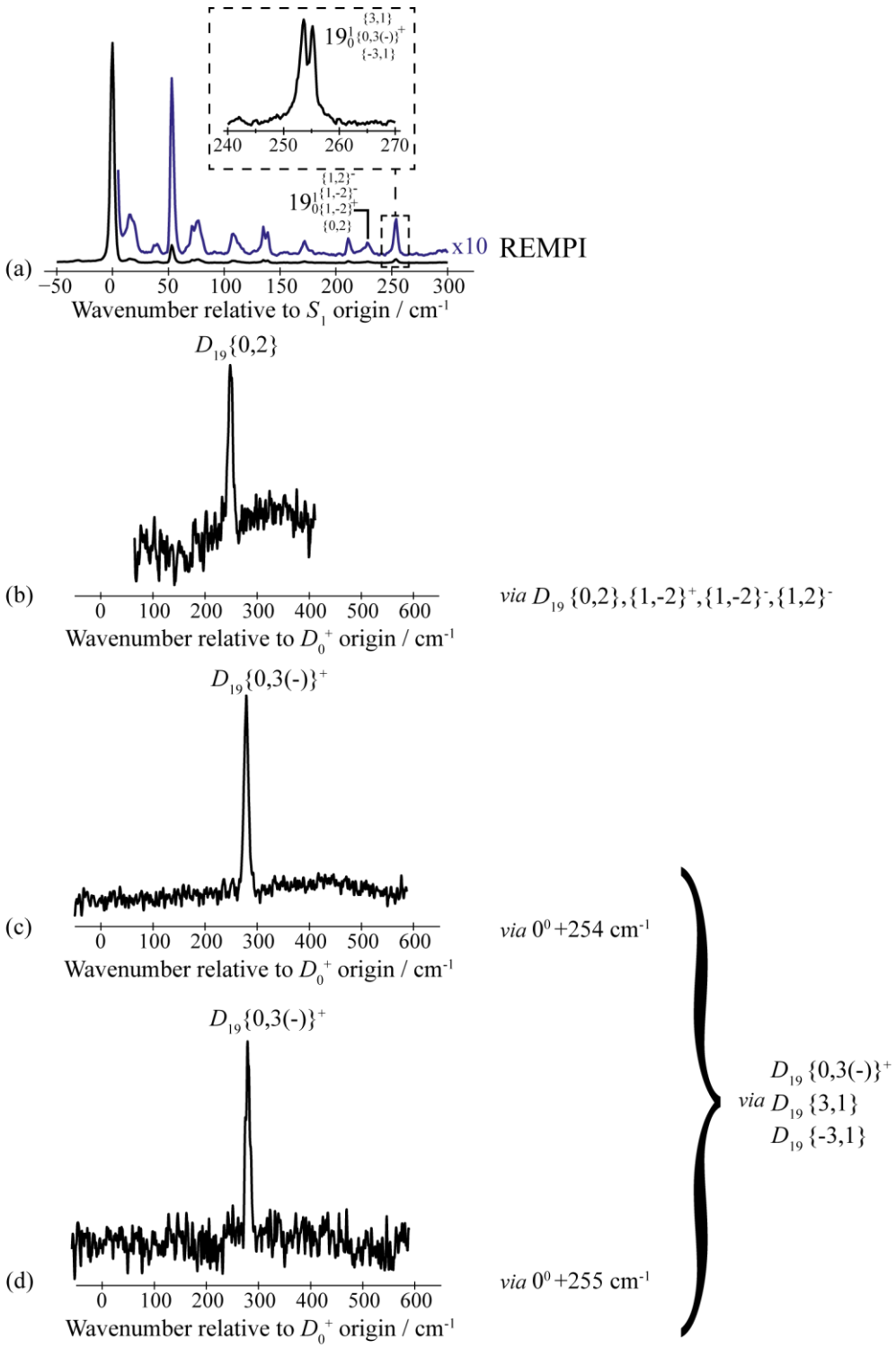


Figure 4.10 – The pXyl $S_1 \leftarrow S_0$ REMPI spectrum up to 300 cm^{-1} is shown in trace (a), with a higher resolution trace from 240 – 270 cm^{-1} inset. Traces (b) – (d) show the ZEKE spectra recorded via D_{19} vibtor levels over this region. On the REMPI spectrum, only the terminating levels are shown, and on the ZEKE spectra, only one terminating level is shown for each $\Delta v\{m_1,m_2\} = 0$ transition to avoid clutter, but one can see from the excitation level labels the number of different terminating levels.

*p*Xyl, the double band at 254 cm^{-1} is expected to be analogous to the $19_0^1 m_0^{3(-)}$ transition, and this doubled feature looks similar to the doubled feature observed for the "$20_0^1 m_0^{3(-)}$" transitions in *p*Xyl, discussed earlier.

For *p*FT, D_{19} was calculated (B3LYP/aug-cc-pVTZ) to be at 243 cm^{-1} in the S_1 state, while for *p*Xyl this was calculated to be 203 cm^{-1}. Owing to this, one would expect the "D_{19} *m* = 3(-)" levels in *p*Xyl to be to lower wavenumber than in *p*FT, simply owing to a lower D_{19} fundamental value, and this double band is in approximately the right position.

A ZEKE spectrum was recorded *via* each of the two maxima of this double feature, and these are shown in Figure 4.10 traces (c) and (d). The activity in both cases is almost identical, with only a single feature observed at 279 cm^{-1}. This increase in wavenumber of ~25 cm^{-1} on going to the cation is suggestive of involvement of D_{19} (based on the calculated vibrational wavenumbers in the S_1 and D_0^+ states), and so one concludes that the S_1 band is due to transitions to the "D_{19} *m* = 3(-)" level(s). In this case, the expected $S_1 \leftarrow S_0$ transition from the {0,0} "cold" level is $19_0^1 m_{\{0,0\}}^{\{0,3(-)\}^+}$ (compared to $20_0^1 m_{\{0,0\}}^{\{0,3(-)\}-}$ for the D_{20} equivalent). This is due to the differing symmetries of the D_{19} and D_{20} vibrations in the G_{72} MSG, which were both the same symmetry (a_2'') in the lower symmetry *p*FT molecule. In *p*Xyl both of these terminating "D_{20}/D_{19} *m* = 3(-)" levels are totally symmetric but contain different "*m* = 3(-)" components. As for the D_{20} analogue, the splitting of the band could be due to other contributions, and $19_0^1 m_{\{0,1\}}^{\{3,1\}}$ and $19_0^1 m_{\{0,1\}}^{\{-3,1\}}$ are both symmetry-allowed as they were for D_{20}. This leads to the assignment of the ZEKE band at 279 cm^{-1} as the transitions $19_1^1 m_{\{0,3(-)\}^+}^{\{0,3(-)\}^+}$, $19_1^1 m_{\{3,1\}}^{\{3,1\}}$ and $19_1^1 m_{\{-3,1\}}^{\{-3,1\}}$, but it is not possible to deduce which component of the REMPI band is dominated by which levels from these spectra.

With this in mind, one explanation for the splitting of the D_{20} and D_{19} "*m* = 3" vibtor bands in the REMPI spectrum is that the $D_{19}\{3,1\}/D_{19}\{-3,1\}$ levels are interacting with the $D_{20}\{3,1\}/D_{20}\{-3,1\}$ levels (all of g'' symmetry), and that the $D_{19}\{0,3(-)\}^+$ level is interacting with the $D_{20}\{0,3(-)\}^-$ level (both of a_1'

symmetry), but that these interactions are subtly different for the two different symmetries. This could be due to slightly different zero-order level energies, and exacerbated by the involvement of other levels, such as {0,5} potentially interacting with $D_{20}\{3,1\}$ and $D_{20}\{-3,1\}$. Alternatively, rather than direct interactions, these couplings could be mediated by intermediate levels, such as the $2D_{20}\{0,1\}$ (g'') and the $2D_{20}\{0,0\}$ (a_1'), but there is no evidence for a splitting of the $2D_{20}$ band profile, and so it seems unlikely that this is the case. In any case, one must remember that effectively all of the levels discussed so far are perturbed to some degree, and one would need to account for all of these interactions together for a true depiction of the coupling; these pairwise interaction arguments simply serve to illustrate the likely dominant couplings.

Having assigned the "$19_0^1 m_0^{3(-)}$", one can, to a first approximation, use the shift between that band in *p*FT and *p*Xyl to estimate the positions of "$19_0^1 m_1^2$" and "$19_0^1 m_1^4$"; this is indicated by the dashed grey lines in Figure 4.9. There is a weak feature at 227 cm^{-1}, and an even weaker one at around 294 cm^{-1}, which could correlate with these transitions. A ZEKE spectrum was obtained *via* the former, and is shown in Figure 4.10(b), which shows a single transition at 248 cm^{-1}. Following on from this being analogous to "D_{19} m = 2", one expects the following levels to be accessible in the S_1 state from the "cold" torsional levels: $D_{19}\{0,2\}$, $D_{19}\{1,2\}^-$, $D_{19}\{1,-2\}^+$ and $D_{19}\{1,-2\}^-$. Assuming all are present to some degree in the REMPI spectrum (the first three are *b*-type transitions and the final one *c*-type, so at least three of these are expected), the ZEKE band can be assigned as $19_1^1 m_{\{0,2\}}^{\{0,2\}}$, $19_1^1 m_{\{1,2\}^-}^{\{1,2\}^-}$, $19_1^1 m_{\{1,-2\}^+}^{\{1,-2\}^+}$ and $19_1^1 m_{\{1,-2\}^-}^{\{1,-2\}^-}$.

No ZEKE spectrum was attempted *via* the very weak feature at around 294 cm^{-1}, but this could be due to the "$19_0^1 m_1^4$", with the expected $S_1 \leftarrow S_0$ transitions in this case being $19_0^1 m_{\{0,1\}}^{\{0,4\}}$, $19_0^1 m_{\{1,1\}}^{\{1,4\}^+}$, $19_0^1 m_{\{1,1\}}^{\{1,4\}^-}$ and $19_0^1 m_{\{1,-1\}}^{\{1,-4\}^-}$, with all except $19_0^1 m_{\{1,1\}}^{\{1,4\}^-}$ being *b*-type transitions and so symmetry-allowed.

4.B.3. Other possible transitions

In *p*FT, transitions to the D_{30}, D_{14}, $D_{14}D_{20}$, m = 6 and m = 7 levels were also observed, and these have not been assigned here. Considering each in turn, D_{30} was of a_1'' symmetry in *p*FT, and is still of a_1'' symmetry here for *p*Xyl. In terms of the D_{2h} point group one would use for *p*Xyl (treating the methyl groups as point masses for pure vibrations) this is a b_{2u} symmetry vibration, rather than the b_{3g} vibrations which are usually observed owing to vibronic coupling/Herzberg-Teller intensity stealing, and so it is not expected to be observed. In *p*FT, it is of b_2 symmetry, and so can be observed by this mechanism. Indeed, the transition to D_{30} was observed in *p*FT (see Chapter 3), but not in the D_{2h} *p*DFB molecule[26,31]. If one explicitly considers the four torsional components of D_{30}, only $30_0^1 m_{\{0,1\}}^{\{0,1\}}$ might be expected, as an *a*-type transition with any intensity due to vibronic coupling, and so with only one of the four components expected (and thus reliant on vibration-torsion coupling) it seems possible that such a transition will be weak and so not seen in the REMPI spectrum.

$D_{14}D_{20}$ takes a b_{3g} D_{2h} symmetry and so could have intensity on vibronic coupling grounds in an analogous way to the Herzberg-Teller intensity stealing for b_{3g} vibrations in *p*DFB, and here all four torsional components would be expected as *a*-type transitions. In the next chapter, the D_{14} fundamental is established as 217 cm^{-1} in the S_1 state, and so in the absence of anharmonicity (and depending on the value taken for D_{20}), one would expect $D_{14}D_{20}$ in the range 315 – 325 cm^{-1}. There is a weak band at 321 cm^{-1}, but no ZEKE spectrum was recorded *via* this. Nonetheless, it is certainly possible that this band arises from transitions to $D_{14}D_{20}$.

The transition involving D_{14} itself, expected around 217 cm^{-1}, does not appear to be observed. It is expected in the cation at 340 cm^{-1} (from Chapter 5), and the only S_1 features near to its expected position have had ZEKE spectra recorded *via* them and have already been discussed; these were those recorded at 0^0+211 and 0^0+227 cm^{-1}. However, in the 0^0+211 cm^{-1} case, there is (possibly) a weak

band at 338 cm^{-1} which could be due to D_{14}. It should be noted that transitions to $D_{14}\{0,1\}$ and $D_{14}\{1,1\}$ from the "cold" torsional levels would be symmetry-allowed in the REMPI spectrum. The signal-to-noise ratio in the 0^0+211 cm^{-1} ZEKE spectrum is not good enough to say with any certainty whether the transition to D_{14} is present, but if it is it could be present as a $\Delta v\{m_1,m_2\} = 0$ transition, by Franck-Condon overlap with the $2D_{20}\{0,1\}$ and $2D_{20}\{1,1\}$ levels, or by virtue of coupling to those levels. In summary, it is not possible to say definitively whether a transition to D_{14} is present in the REMPI spectrum.

Based on the similarity of the low wavenumber torsional region of the *p*Xyl REMPI spectrum with that of *p*FT, one can assume a similar internal rotation constant, *F*, value of ~5.45 cm^{-1}, yielding expected positions for the "*m* = 6" and "*m* = 7" levels of ~196 and 267 cm^{-1}, with the transitions then expected at 196 and 262 cm^{-1} respectively. In *p*FT, the $m_0^{6(+)}$ was thought to be observed at 0^0+198 cm^{-1}, with the m_1^7 observed overlapping with the $19_0^1m_1^2$ at 0^0+256 cm^{-1}. There is a very weak band at 0^0+204 cm^{-1} which could be due to transitions to the "*m* = 6" levels, but no ZEKE spectrum was recorded *via* it and so it is not possible to say with any certainty (although not much else is expected around this position). Transitions to the "*m* = 7" levels would then be expected around the position of the "$19_0^1m_0^{3(-)}$" band, and no evidence of "*m* = 7" character was observed in the two ZEKE spectra recorded there, so it appears that transitions to the "*m* = 7" levels do not appear with any significant intensity in *p*Xyl.

4.B.4. Comparison to previous work

There is now a complete set of assignments up to 0^0+350 cm^{-1} in the REMPI spectrum, supported by the ZEKE spectra, and these assignments can be compared to previous work.

Breen *et al.*[6] assigned a transition at 109.5 cm^{-1} in their $S_1 \leftarrow S_0$ excitation spectrum to an excitation of the *m* = 3(+) on both rotors. This "double" excitation would correlate with one of the "{3,3}" levels in the true G_{72} MSG of *p*Xyl, with

a transition to this level expected to be weak owing to a $\Delta\{m_1 + m_2\}$ change of six, as discussed above. The evidence from the REMPI and ZEKE spectra suggest a reassignment of this, and given the good agreement between the *p*Xyl and *p*FT REMPI spectra, this band has been reassigned in the present work to be due to overlapping transitions to "D_{20} m = 1" and "D_{20} m = 2" levels, with vibtor levels not considered in the work of Breen *et al*.

The "double" band at 0^0+72 and 0^0+76 cm^{-1} was assigned to different components by Breen, with the upper assigned to a transition to "m = 4", as it is here, but the lower assigned to excitation of "m = 2" on one rotor and "m = 3(+)" on the other. Only one such "double excitation" has been assigned in the current work, and that appeared only to be present by virtue of coupling. Additionally, there is no ZEKE transition in the appropriate place for such an excitation, and once one considers the full symmetry of *p*Xyl it is seen that the unusual REMPI band profile can be explained by different interactions between the "D_{20} m = 1" and the various "m = 4" levels. In general, the assignments here agree with the torsional assignments of Breen *et al*. when they were localised to a single rotor, with the caveat that in the current full MSG treatment, there are multiple degenerate transitions for each of these bands.

Gunzer and Grotemeyer[12] assigned bands at 18, 44, 76, 113 and 144 cm^{-1} in their MATI spectrum *via* the *para*-xylene origin to "methyl torsion". As will be seen later when discussing the origin ZEKE spectrum recorded for the current work, the 113 and 144 cm^{-1} bands are actually due to transitions to "D_{20} m = 2" and "D_{20} m = 3" levels, in agreement with the observation of such transitions in the ZEKE spectra already discussed *via* the respective intermediate levels.

Finally, Held *et al*.[9] also reported a MATI spectrum of the *para*-xylene origin, and in general the current assignments agree with theirs, although in the current MSG treatment one obtains four "cold" levels rather than the three reported therein. However, they assigned a band at 44 cm^{-1} in the MATI spectrum to transitions to "m = 3(+)" levels, which are now thought to be due to "m = 3(-)" levels based on the vibronic coupling mechanism by which they are thought to gain intensity. Additionally, a band at 112 cm^{-1} in the cation (here assigned as

transitions to "D_{20} m = 2" levels) was assigned as a transition from "m = 0,2" to "m = 0,5" and coincidentally a transition from "m = 0,2" to "m = 3,4". These require starting in an excited torsional level, and so would only be expected if the spectrum was torsionally warm. Finally, the band at 144 cm^{-1}, assigned here to transitions to "D_{20} m = 3" levels, was assigned therein as a transition from "m = 0,3(+)" to "m = 0,6(+)", and under supersonic jet conditions, one would not expect significant "m = 0,3(+)" population, so this assignment has also been discounted.

4.B.5. Discussion

The similarity of the torsion and low wavenumber vibration-torsion regions of the REMPI spectra of *p*FT and *p*Xyl is quite remarkable. While the similarity of the torsional regions is perhaps unsurprising, as the value of the internal rotation constant, F, is largely unaffected by other substituents, and the methyl groups are far apart in the *para*- positions in *p*Xyl (and so perturbing interactions would be expected to be weak), the similarity in positions of the D_{20} vibtor levels in the two cases is interesting. Based on the B3LYP calculated vibrational wavenumbers, these would be expected to be slightly different owing to a small difference in D_{20} vibrational fundamental, and so the similarity in the appearance of the spectra suggests a D_{20} value in the S_1 state for *p*Xyl that is very close to that in *p*FT. This is different to the D_{19} vibtor levels, which are observed in different places in *p*FT and *p*Xyl owing to different fundamental values.

While the $S_1 \leftarrow S_0$ transitions to the D_{20} vibtor levels are energetically similar between the two molecules, that is not the case for $2D_{20}$, perhaps because of different interactions with the D_{19} vibtor levels, which are lower in wavenumber in *p*Xyl than in *p*FT. This makes it difficult to extract an "unperturbed" D_{20} value, since all D_{20} vibtor levels and $2D_{20}$ are expected to interact to some extent with nearby levels.

Simply subtracting the torsions from the D_{20} vibtor levels suggests D_{20} is within the range 94 – 101 cm^{-1}, while taking the $D_{20}\{0,1\}/D_{20}\{1,1\}$ position as D_{20}

Table 4.3 – Experimental band positions for torsion and vibtor bands

Terminating Level[a]	*p*FT		*p*Xyl	
	S_1	D_0^+	S_1	D_0^+
"m = 2"	17	17	16	15
"m = 3(-)"	-	45	40	43
"m = 3(+)"	54	48	53	50
"m = 4"	76	79	72/76	77
"m = 5"	142	134	138	122
"D_{20} m = 1"	112	112	107	102
"D_{20} m = 2"	110	121	110	111
"D_{20} m = 3(-)"	137	155	135/138	146
"D_{20} m = 4"	172	188	173	176
"2D_{20}"	220	222	211	203
"D_{19} m = 2"	260	287	227	248
"D_{19} m = 3(-)"	283	319	254/255	279
"D_{19} m = 4"	320	350	294	-

[a] The single rotor levels are given, which correspond with the analogous double rotor levels for *p*Xyl.

suggests 107 cm^{-1}, and half of 2D_{20} suggests 106 cm^{-1}. This latter value is taken as the S_1 D_{20} fundamental in the current work, since this is consistent with both 2D_{20} (expected to be perturbed to lower energy) and D_{20}{0,1}/D_{20}{1,1} (expected to be perturbed to higher energy). Taking the value from the same levels in the cation, the D_{20} fundamental there is 102 cm^{-1}. These are in good agreement with the calculated values of 104 and 100 cm^{-1} for the S_1 and D_0^+ states respectively.

Since the current work does not attempt a full deperturbation analysis, only a few comments regarding the couplings will be made in the below. To aid in this discussion, Table 4.3 gives the band positions for torsional and vibtor bands in both *p*FT and *p*Xyl, for both the S_1 and D_0^+ states. Although the couplings will

be discussed in a pairwise fashion, really one needs to treat all of the levels together to investigate the vibration-torsion coupling, as demonstrated by Gascooke and Lawrance for toluene.[18,19]

One finds the observed D_{20} vibtor bands in the REMPI spectra are lower in wavenumber than would be predicted from the obtained D_{20} fundamental for both *p*FT and *p*Xyl. For example, the "D_{20} $m = 2$" levels are coupled to the "$m = 5$" levels to higher wavenumber, thus perturbing them to lower wavenumber. Both components of the band profile of the "D_{20} $m = 3$" levels at 135.4 and 138.4 cm^{-1} are lower than predicted, suggesting both have been perturbed down in wavenumber, and some components more than others, again consistent with their perturbation by the "D_{19} $m = 3$" levels from above. The "D_{20} $m = 4$" levels are also observed lower in wavenumber than their expected position, perhaps perturbed downward by interaction with "$2D_{20}$ $m = 1$" or the "D_{19} $m = 2$"/"D_{19} $m = 4$" vibtor levels.

Based upon the obtained D_{20} S_1 fundamental of 110 cm^{-1} for *p*FT and 106 cm^{-1} for *p*Xyl, it might appear strange that the vibtor levels are observed in the same place in both species. This suggests a complex picture, where the D_{19} vibtor levels in *p*Xyl perturb the D_{20} vibtor levels (and $2D_{20}$) lower in wavenumber than they were perturbed in *p*FT. This places them closer to the torsional levels than in *p*FT, and so they are perturbed upward more strongly in *p*Xyl than in *p*FT, with the balance of these interactions (i.e. the vibration-torsion coupling prevalent across this region) placing the D_{20} vibtor levels in the same positions in the two molecules. This is consistent with the observed, slightly lower, positions for the torsional levels in *p*Xyl compared to *p*FT.

The situation is more nuanced than this direct comparison between the molecules, owing to the larger number of levels in *para*-xylene taking a larger range of symmetries. For example, just looking at the pure torsional region, one can see that the {0,2} level is of the same symmetry as the {3,1} and {-3,1} levels, as well as the {0,4} level, whereas in *p*FT only the $m = 2$ and $m = 4$ levels had the same symmetries; there was no equivalent of the "{3,1}" levels. This could significantly change the low wavenumber coupling, and so one must take

care in comparing the two spectra for information on the internal rotation constant, F, or the torsional barrier.

One might attempt to extract the D_{19} fundamental in the S_1 state, as was done for D_{20}. Subtracting the "m = 2" torsional position from the "D_{19} m = 2" position yields 211 cm^{-1}, while doing the same with the "m = 3" levels and "D_{19} m = 3(-)" yields 214 cm^{-1}, suggesting a value for D_{19} between 211 and 214 cm^{-1}. This agrees with the value of ~213 cm^{-1} that can be obtained from the $2D_{19}$ level, which itself is perturbed, as discussed in the next chapter, and is in reasonable agreement with the calculated D_{19} value of 203 cm^{-1}. In the cation, the same approach suggests a value between 233 and 236 cm^{-1}, again in good agreement with the value obtained from the $2D_{19}$ level in the next chapter and with the calculated value of 232 cm^{-1}. Note that the value obtained from $2D_{19}$ in the cation is 236 cm^{-1}, and the value of D_{19} is likely somewhere between this and 233 cm^{-1}; owing to possible coupling in the cation (specifically for the vibtor levels discussed here) and anharmonicity, it is not possible to be more precise than this in the current study.

A qualitative illustration of some of the interactions between the torsion, vibtor and vibrational levels is shown in Figure 4.11, based on the above discussion. This aids the reader in visualising what are thought to be some of the stronger interactions, with arrows on the spectrum to indicate which levels are thought to have significantly perturbed one another, with many of the couplings analogous to those discussed for *p*FT. One can see from the diagram the sheer number of possible interactions by looking for all of the levels of the same colour (neglecting other mechanisms which could couple levels of different symmetry), and so this serves to illustrate only a snippet of the complexity of the couplings. Note that there are no other observed levels which can perturb the $\{0,3(+)\}^-$ level in this region, suggesting that it is effectively unperturbed from its hindered rotor position (although obviously perturbed from its free rotor position by the torsional barrier(s) of *p*Xyl) – this is analogous to m = 3(+) in *p*FT.

As a general note, and as summarised nicely by Figure 4.11, there are many cases where multiple transitions, from the different "cold" torsional levels, have

been assigned as degenerate. For these, as the bands generally do not appear unusually broad in either the REMPI or the ZEKE spectra, it is not possible to confirm that all of the components suggested are present. However, band profile splittings due to different coupling of the component levels – such as with the band profile of the "m_1^4", and the transitions to the "D_{20} m = 3" and "D_{19} m = 3" levels – is evidence that these different transitions are all present and are simply degenerate within the current resolution in most cases. One rationale for this is that the components are equally perturbed by interactions, and this appears to be the case with the "D_{20} m = 2" and "m = 5" coupling. Alternatively (or alongside this), it could be that the couplings perturbing levels both higher and lower in wavenumber simply cancel out within the current resolution. A higher resolution experiment picking out overlapping bands from their rotational profiles would be required to understand this aspect in any further depth.

Finally, it is worth noting explicitly that although certain transitions occur at different wavenumbers in *p*FT and *p*Xyl, comparable activity is seen across the whole region, with explanations on symmetry grounds for bands that were observed in *p*FT and not in *p*Xyl. This similarity in activity between these single and double rotor systems will also be seen to higher wavenumber. Bearing this in mind, the two systems form an interesting basis for comparison, with a lower symmetry, single rotor, and (perhaps unusually) a higher symmetry, double rotor, molecule.

4.C. Origin ZEKE spectrum

4.C.1. Overview

Before giving attention to the ZEKE spectrum recorded *via* the S_1 origin of *p*Xyl, shown in Figure 4.12, it is important to recall what activity might be expected. So far, the ZEKE spectra shown (barring an earlier instance showing a portion of the origin ZEKE spectrum in Figures 4.4 and 4.5) have been recorded *via* torsional levels, vibtor levels or vibrational levels, and so have been assigned primarily on the basis of the $\Delta v\{m_1,m_2\} = 0$ propensity rule, with activity being predominantly symmetry-allowed based upon the symmetries of the initial

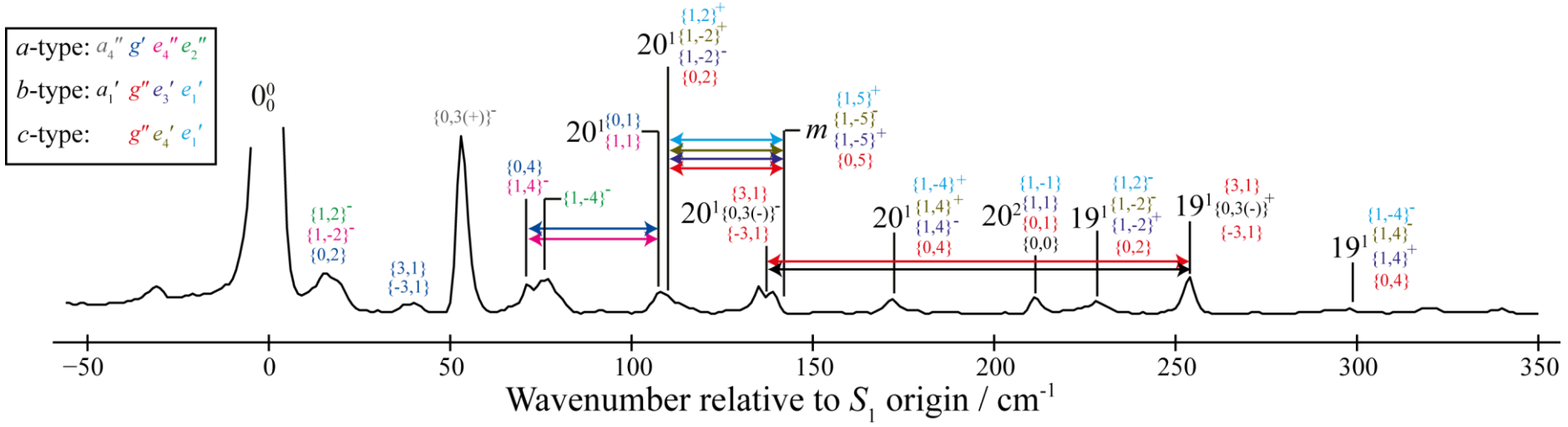


Figure 4.11 – The pXyl $S_1 \leftarrow S_0$ REMPI spectrum up to 350 cm^{-1} is shown, with the terminating levels colour coded to indicate the symmetries of the various levels and the types of transition. Arrows are used to indicate particular couplings between sets of levels discussed in the text; not all of the (potential) couplings are shown but the complexity of the couplings can be observed by simply looking for all levels of the same colour.

levels. Here, a similar approach can be taken, based upon the symmetries of the four "cold" torsional levels which are expected to be present as part of the S_1 origin band. Transition to levels in the cation which are of the same symmetry as these "cold" torsional levels – {0,0}, {0,1}, {1,1} and {1,-1} – are symmetry-allowed and can potentially have Franck-Condon intensity. Any other transitions that are observed that do not meet this criterion must occur due to some other mechanism, which is currently thought to be a vibronic coupling mechanism of some sort, as discussed in Chapter 3 for *p*FT.

Figure 4.12 labels any terminating levels which are symmetry-allowed in blue. For the remaining transitions, it is assumed that one can observe the same non-totally symmetric vibrations as in *p*DFB, which is to say D_{20} (a_2''), D_{19} (a_3'') and D_{14} (a_3'), and one then expects to see any level which takes the same symmetry as each of these non-totally symmetric vibrations. This can, in theory, also be extended to the four "cold" torsional levels being observed for each of these vibrations, and thus anything which takes any of those product vibration-torsion symmetries could potentially be observed, i.e.:

$$D_{20}\{0,0\}\ (a_2''),\ D_{20}\{0,1\}\ (g'),\ D_{20}\{1,1\}\ (e_4''),\ D_{20}\{1,-1\}\ (e_1'')$$

$$D_{19}\{0,0\}\ (a_3''),\ D_{19}\{0,1\}\ (g'),\ D_{19}\{1,1\}\ (e_3''),\ D_{19}\{1,-1\}\ (e_2'')$$

$$D_{14}\{0,0\}\ (a_3'),\ D_{14}\{0,1\}\ (g''),\ D_{14}\{1,1\}\ (e_3'),\ D_{14}\{1,-1\}\ (e_2')$$

In this analysis, it is assumed that anything in the D_0^+ state of one of these product vibtor symmetries is "vibronically allowed", and such terminating levels are given in red in Figure 4.12.

4.C.2. Discussion

Many of the transitions (labelled as terminating levels) in Figure 4.12 can be assigned based upon the ZEKE spectra recorded *via* other intermediate levels discussed above. For example, there is a band at 145 cm^{-1} in the origin ZEKE spectrum, which is the same position as the $\Delta v\{m_1,m_2\} = 0$ transitions from the 0^0+135 and 0^0+138 cm^{-1} ZEKE spectra, assigned there as transitions to the

$D_{20}\{3,1\}$, $D_{20}\{-3,1\}$ and $D_{20}\{0,3(-)\}^-$ levels. Transitions to these levels are symmetry-allowed here, and so the same terminating levels are assigned.

Although the other ZEKE spectra assist in the assignments, the terminating levels are not always identical between the two cases. For example, the ZEKE spectrum recorded at 0^0+15.6 cm^{-1} had a $\Delta\{m_1,m_2\} = 0$ transition at 15 cm^{-1}, and this was assigned as (degenerate within the current resolution) transitions to the terminating levels $\{0,2\}$, $\{1,2\}^-$ and $\{1,-2\}^-$, based on that propensity rule. There is also a band at 15 cm^{-1} in the origin ZEKE spectrum, but the assigned levels here are $\{0,2\}$, $\{1,2\}^-$, $\{1,2\}^+$, $\{1,-2\}^-$ and $\{1,-2\}^+$, i.e. all transitions to all five "$m = 2$" levels are potentially observed from one of the four initial $\{0,0\}$, $\{0,1\}$, $\{1,1\}$ and $\{1,-1\}$ levels, although no comment can be made on the relative

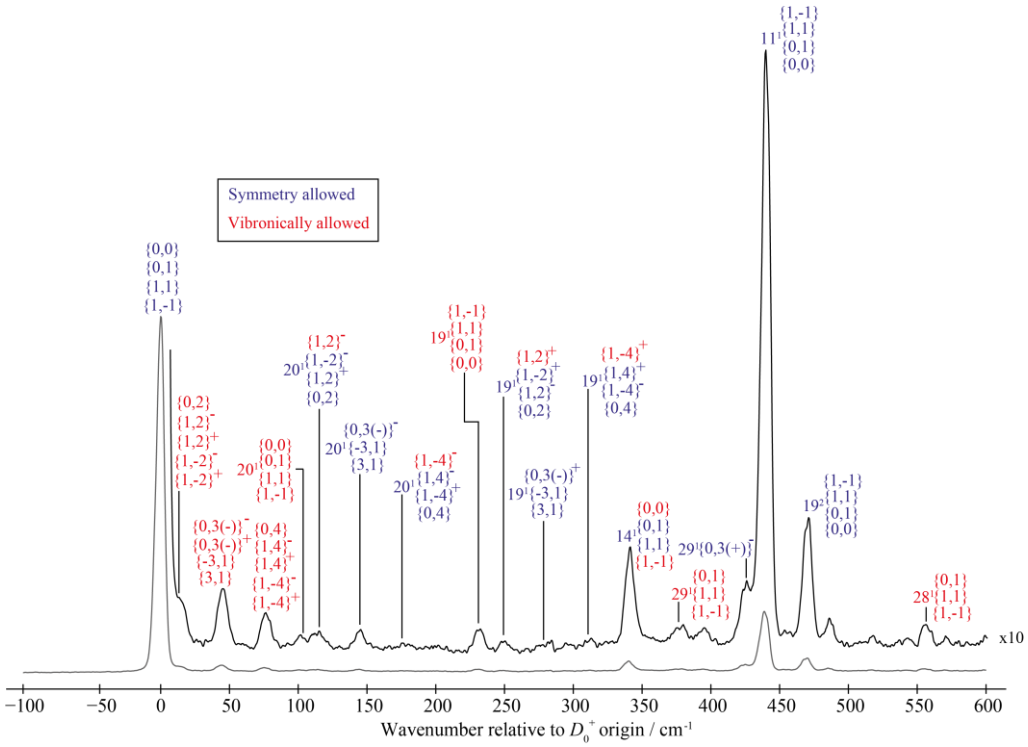


Figure 4.12 – The ZEKE spectrum recorded via the pXyl S_1 origin band is shown. Transitions will initiate in one of the torsional levels {0,0}, {0,1}, {1,1} and {1,-1}, which are all expected at this excitation position. Only the terminating levels of the transitions are labelled on the spectrum, due to the number of them. In blue are the terminating levels which are of the same torsion/vibtor symmetry as the initial torsional levels and are thus symmetry-allowed and can potentially have Franck-Condon intensity. In red are the terminating levels which are thought to be observed on vibronic coupling grounds in the cation.

intensities of each of these. In the 0^0+15.6 cm^{-1} ZEKE spectrum, the transitions were based upon the levels observed in the S_1 state, appearing in the ZEKE spectrum effectively by Franck-Condon overlap, whereas here the transitions occur on vibronic grounds. In either case, one is observing levels analogous to $m = 2$ in *p*FT, but the precise nature of the levels is (or could be) different.

The above two examples illustrate how one arrives at the set of assignments in Figure 4.12. It should be noted that all observed transitions to torsional levels (here only observing up to $\Delta\{m_1,m_2\} = 3$ transitions) require vibronic coupling to be observed (as $\Delta\{m_1,m_2\} = 3$ transitions to torsional levels did in the REMPI spectrum). One also observes transitions to D_{20}, D_{19} and D_{14}, thought to arise owing to vibronic coupling, the same reason for their observation in *p*FT in Chapter 3, as well as in *p*DFB[26,30] and *p*ClFB[29].

4.D. References

[1] T. Ebata, Y. Suzuki, N. Mikami, T. Miyashi, and M. Ito, *Chem. Phys. Lett.*, **110**, 597 (1984).

[2] E.B. Wilson Jr., *Phys. Rev.*, **45**, 706 (1934).

[3] G. Varsányi, *Assignments of the Vibrational Spectra of Seven Hundred Benzene Derivatives* (Wiley, New York, 1974).

[4] T.G. Blease, R.J. Donovan, P.R.R. Langridge-Smith, and T. Ridley, *Laser Chem.*, **9**, 241 (1988).

[5] K. Walter, K. Scherm, and U. Boesl, *Chem. Phys. Lett.*, **161**, 473 (1989).

[6] P.J. Breen, J.A. Warren, E.R. Bernstein, and J.I. Seeman, *J. Chem. Phys.*, **87**, 1917 (1987).

[7] J.I. Selco and P.G. Carrick, *J. Mol. Spectrosc.*, **173**, 262 (1995).

[8] B. Zhang, U. Aigner, H.L. Selzle, and E.W. Schlag, *Opt. Commun.*, **183**, 95 (2000).

[9] A. Held, H.L. Selzle, and E.W. Schlag, *J. Phys. Chem. A*, **102**, 9625 (1998).

[10] B. Zhang, U. Aigner, H.L. Selzle, and E.W. Schlag, *Chem. Phys. Lett.*, **380**, 337 (2003).

[11] F. Gunzer and J. Grotemeyer, *Phys. Chem. Chem. Phys.*, **4**, 5966 (2002).

[12] F. Gunzer and J. Grotemeyer, *Int. J. Mass Spectrom.*, **228**, 921 (2003).

[13] K. Watanabe, *J. Chem. Phys.*, **22**, 1564 (1954).

[14] K. Watanabe, T. Nakayama, and J. Mottl, *J. Quant. Spectrosc. Radiat. Transf.*, **2**, 369 (1962).

[15] T.P. Debies and J.W. Rabalais, *J. Electron Spectros. Relat. Phenomena*, **1**, 355 (1972).

[16] M. Klessinger, *Angew. Chemie Int. Ed.*, **11**, 525 (1972).

[17] T. Koenig, M. Tuttle, and R.A. Wielesek, *Tetrahedron Lett.*, **15**, 2537 (1974).

[18] J.R. Gascooke and W.D. Lawrance, *J. Chem. Phys.*, **138**, 134302 (2013).

[19] J.R. Gascooke, E.A. Virgo, and W.D. Lawrance, *J. Chem. Phys.*, **143**, 044313 (2015).

[20] J.R. Gascooke, E.A. Virgo, and W.D. Lawrance, *J. Chem. Phys.*, **142**, 024315 (2015).

[21] A.M. Gardner, A.M. Green, V.M. Tamé-Reyes, V.H.K. Wilton, and T.G. Wright, *J. Chem. Phys.*, **138**, 134303 (2013).

[22] A.M. Gardner, A.M. Green, V.M. Tamé-Reyes, K.L. Reid, J.A. Davies, V.H.K. Parkes, and T.G. Wright, *J. Chem. Phys.*, **140**, 114308 (2014).

[23] P.R. Bunker and P. Jensen, *Molecular Symmetry and Spectroscopy*, Second Ed. (NRC Research Press, Ottawa, 1998).

[24] A.M. Gardner, W.D. Tuttle, P. Groner, and T.G. Wright, *J. Chem. Phys.*, **146**, 124308 (2017).

[25] R.A. Walker, E. Richard, K.-T. Lu, E.L. Silbert, and J.C. Weisshaar, *J. Chem. Phys.*, **102**, 8718 (1995).

[26] D.J. Kemp, A.M. Gardner, W.D. Tuttle, J. Midgley, K.L. Reid, and T.G. Wright, *J. Chem. Phys.*, (submitted).

[27] J.S. Miller, E.D. Poliakoff, T.F. Miller, A.P.P. Natalense, and R.R. Lucchese, *J. Chem. Phys.*, **114**, 4496 (2001).

[28] E.D. Poliakoff and R.R. Lucchese, *Phys. Scr.*, **74**, C71 (2006).

[29] D.J. Kemp, L.E. Whalley, W.D. Tuttle, A.M. Gardner, B.T. Speake, and T.G. Wright, *Phys. Chem. Chem. Phys.*, **20**, 12503 (2018).

[30] G. Reiser, D. Rieger, T.G. Wright, K. Müller-Dethlefs, and E.W. Schlag, *J. Phys. Chem.*, **97**, 4335 (1993).

[31] A.E.W. Knight and S.H. Kable, *J. Chem. Phys.*, **89**, 7139 (1988).

5. Low wavenumber region of *para*-fluorotoluene and *para*-xylene (350 – 600 cm^{-1})

Figure 5.1 shows the resonance-enhanced multiphoton ionisation (REMPI) spectra of *para*-difluorobenzene (*p*DFB), *para*-fluorotoluene (*p*FT) and *para*-xylene (*p*Xyl), with assignments for *p*FT from reference 1 and for *p*DFB from reference 2. In Chapters 3 and 4, the lowest wavenumber regions were discussed for *p*FT and *p*Xyl, with assignments proposed for transitions to

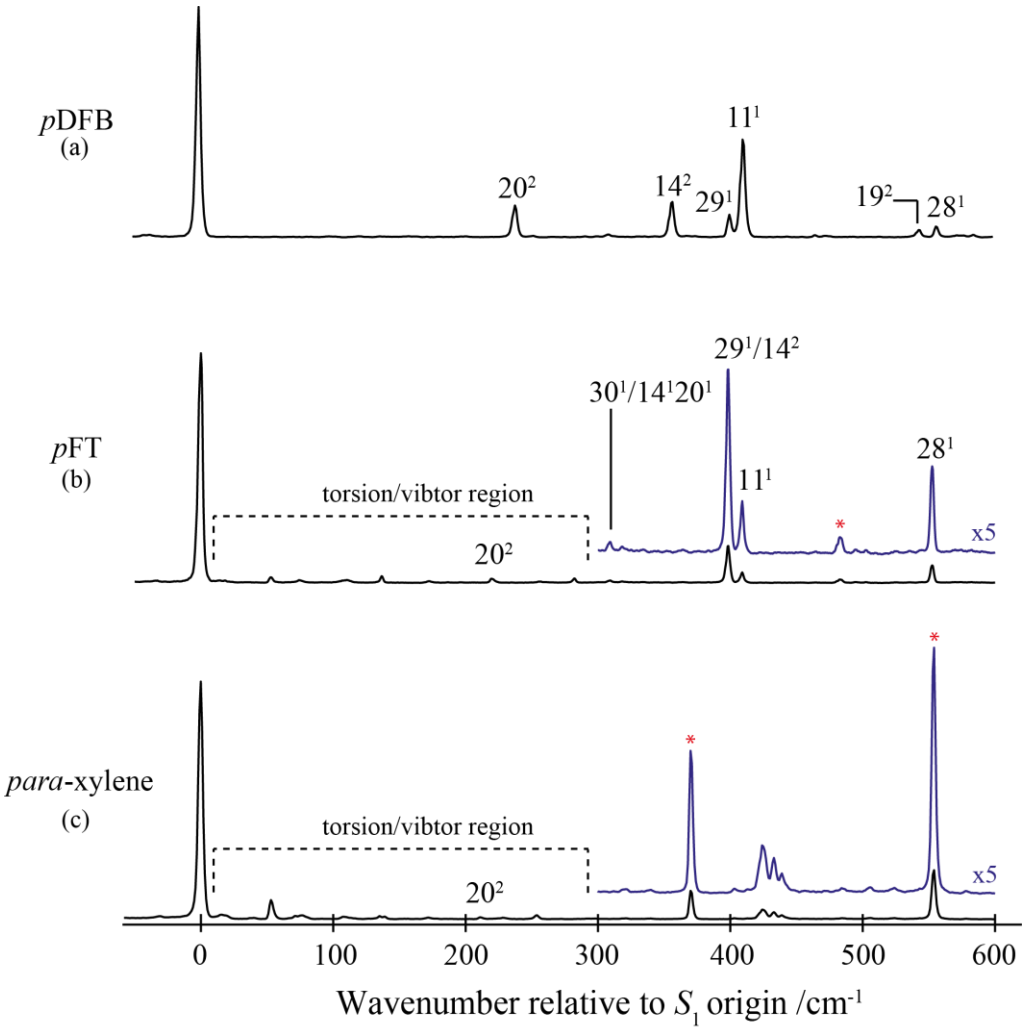


Figure 5.1 – The (a) pDFB, (b) pFT and (c) pXyl $S_1 \leftarrow S_0$ REMPI spectra up to 600 cm^{-1} are shown. Only vibrations, rather than vibtor levels, are labelled. For the region considered in this chapter, assignments are given for pFT based on the previous ZEKE study of Ayles et al.[1], and have been converted to ^pD_i labels from the Wilson labels given in that work. The pDFB assignments have been converted to ^pD_i labels from the Mulliken assignments given by Knight and Kable[2].

torsional levels, vibration-torsion (vibtor) levels involving the D_{20} and D_{19} vibrations, and in the case of *p*FT, additional assignments such as the D_{30} vibration, which is not expected in *p*Xyl owing to its symmetry. In the present chapter, the focus shifts to this higher wavenumber region, covering the 350 – 600 cm^{-1} region for these two molecules.

Previously, Ayles *et al.*[1] employed zero-electron-kinetic-energy (ZEKE) photoelectron spectroscopy (PES), with spectra recorded *via* a number of S_1 intermediate levels over this wavenumber range in *p*FT. One such spectrum was recorded *via* D_{28} (ν_{6b} in the Wilson[3]/Varsányi[4] notation used in that work), one *via* D_{11} (ν_{6a} in that work), and at three positions over a REMPI feature at 0^0+400 cm^{-1}, assigned in that work as two overlapped bands corresponding to 29_0^1 and 14_0^2 ($9b_0^1$ and $16a_0^2$ in that work).

For *p*Xyl, Gunzer and Grotemeyer[5] reported a single mass-analyzed threshold ionisation (MATI) spectrum, recorded *via* 0^0+553 cm^{-1}, but this spectrum was only recorded over a short range, and no assignment was provided. Ebata *et al.*[6] reported a laser-induced fluorescence (LIF) spectrum of *p*Xyl, which looks very similar to the REMPI spectrum presented in this thesis. They labelled a band at 0^0+553 cm^{-1} in their LIF study, but this was unassigned. As such, a ZEKE spectrum has been recorded *via* this feature in the current study. Additional previous work on *p*Xyl was carried out by Blease *et al.*[7] who assigned bands at 370 ($9b_0^1$), 425 ($6a_0^1$), 433 ($16a_0^2$) and 553 cm^{-1} ($6b_0^1$) in a REMPI study. In the D_i notation of this thesis, these most closely correlate with 29_0^1, 11_0^1, 14_0^2 and 28_0^1 respectively. These will be discussed at the appropriate points throughout this chapter. Walter, Scherm and Boesl[8] recorded a REMPI spectrum of *p*Xyl, and provided the same assignments of the 370, 425 and 553 cm^{-1} bands as Blease *et al.*, as well as employing PES *via* different intermediate levels to study the cation. However, the resolution in their PE spectra is low, and the current ZEKE study allows for more precise values of fundamentals to be obtained in the cation.

In this chapter, since comparisons will be made between *p*FT and *p*Xyl throughout, some of the level and transition labels will be slightly different to

Chapters 3 and 4. In the energetic regions of the REMPI spectra discussed in those chapters, torsion and vibration-torsion (vibtor) levels were particularly dominant, and so even for transitions to vibrational levels such as 20_0^2 the appropriate associated torsional levels were explicitly stated: $m = 0$ and $m = 1$ in the *p*FT case, and {0,0}, {0,1}, {1,1} and {1,-1} in the *p*Xyl case. Since this has been discussed in some depth in the previous two chapters, for brevity, the torsional labels have generally been omitted from the vibrational transitions here, although obviously overlapped transitions involving such levels are still present. The torsional labels will only be used when explicitly required, but their omission for the vibrational transitions should clarify the comparison of the spectra, having already shown their similarity in the lower wavenumber region (see Chapters 3 and 4).

5.A. Overview of vibrational wavenumber trends

One can use the assignments of the *p*DFB REMPI spectrum, where the assignments were confirmed in a thorough LIF/dispersed fluorescence (DF) study by Knight and Kable[2], to aid in understanding what structure might be expected in this region of the *p*FT and *p*Xyl REMPI spectra. The trends in vibrational wavenumber from *p*DFB to the other species will form a useful starting point for the subsequent analysis, which will refer to the ZEKE spectra.

It can be seen from Figure 5.1 that in *p*DFB, the 14_0^2, 29_0^1 and 11_0^1 transitions dominate this region of the spectrum, with 19_0^2 and 28_0^1 to higher wavenumber. Note that the D_{29} and D_{28} vibrations are of b_{3g} symmetry in *p*DFB, and so their intensity derives from vibration-electronic (vibronic) coupling. Table B.1 in Appendix B shows the calculated and experimental S_1 vibrational wavenumbers for *p*DFB, *p*FT and *p*Xyl and comparison of these illustrates how particular vibrations change between the molecules. For example, the D_{28} vibrational wavenumber is almost unchanged between the species, suggesting that the REMPI band at ~550 cm^{-1} in all three species is due to a transition to this vibration. In *p*FT, this band was assigned by Ayles *et al.*[1] based on ZEKE spectroscopy as the $6b_0^1$ transition; this Wilson label would be best represented

by D_{28}, consistent with the assignment in *p*DFB. This evidence suggests that the band at this position in *p*Xyl is likely 28_0^1.

One can carry out a similar analysis of trends for the 19_0^2 transition, with it being observed at 0^0+545 cm^{-1} in *p*DFB. The trend in calculated wavenumbers, and the approximate D_{19} fundamentals extracted from the vibtor levels in *p*FT and *p*Xyl, suggests that the band in *p*FT at around 480 cm^{-1} is likely the 19_0^2 transition, and in *p*Xyl it would be expected within the triplet of features in the range 410 – 440 cm^{-1}.

The 11_0^1 band appears in *p*DFB at 0^0+411 cm^{-1}, and was assigned in *p*FT (as $6a_0^1$) by Ayles *et al.*[1] to a band at 0^0+408 cm^{-1}. That these transitions are so close in wavenumber between the two species suggests that the 11_0^1 transition will be observed at a similar wavenumber in *p*Xyl, and the calculated vibrational wavenumber supports this, being only a little lower at 402 cm^{-1}.

The 29_0^1 transition appears in *p*DFB at 0^0+401 cm^{-1}, and the calculated wavenumbers suggest a similar position in *p*FT, supported by the ZEKE spectra of Ayles *et al.* which place it as part of the 0^0+400 cm^{-1} overlapped feature. The calculated wavenumber for *p*Xyl is lower, 367 cm^{-1}, suggesting that it is likely the relatively intense transition at 0^0+370 cm^{-1} in that case. Finally, the 14_0^2 transition was observed in *p*DFB at 0^0+358 cm^{-1}, while it is underneath the 0^0+400 cm^{-1} overlapped feature in *p*FT; this vibration increases in wavenumber from *p*DFB to *p*FT, in contrast to the others discussed. Based upon this trend, it is expected in *p*Xyl at 430 – 440 cm^{-1}, placing it within the triplet of bands where the 19_0^2 is expected. Note that for the 14_0^2 transition emphasis has not been placed on the trends in calculated vibrational wavenumber, as the calculated B3LYP/aug-cc-pVTZ values for this vibration in the S_1 state have been found to be highly unreliable.[9–11]

In the remainder of this chapter, ZEKE spectra recorded over this region will be presented to probe these assignments and ascertain if there are any couplings. Owing to the slightly more complex picture of the overlapping feature at 0^0+400 cm^{-1} in *p*FT, previously investigated by Ayles *et al.*[1] and briefly

reinvestigated here, and the triplet of bands from 410 – 440 cm^{-1} in *p*Xyl, these will be discussed later, with the isolated features being discussed first; these are marked with red asterisks in Figure 5.1.

5.B. Selected ZEKE spectra and S_1 assignments

5.B.1. The D_{28} vibration in *para*-fluorotoluene and *para*-xylene

The 28_0^1 transition is considered first; it is reasonably isolated and is expected at an almost identical position in all three molecules. Owing to the good quality of the ZEKE spectrum recorded *via* the 0^0+549 cm^{-1} band in *p*FT, this has not been re-recorded in the current work, but the one reported in reference 1 shows a dominant $\Delta(v,m) = 0$ transition, and a reasonably intense band corresponding to a transition to the terminating level $D_{28}D_{11}$, i.e. the commonly observed $\Delta(v,m) = 0$ plus D_{11} combination band; in addition, there are a handful of weak features.

For *p*Xyl, a ZEKE spectrum was recorded *via* the REMPI feature at 0^0+554 cm^{-1}, which is expected to be the 28_0^1 transition; this ZEKE spectrum is shown in Figure 5.2. It shows an intense $\Delta v\{m_1,m_2\} = 0$ transition at 556 cm^{-1}, and an

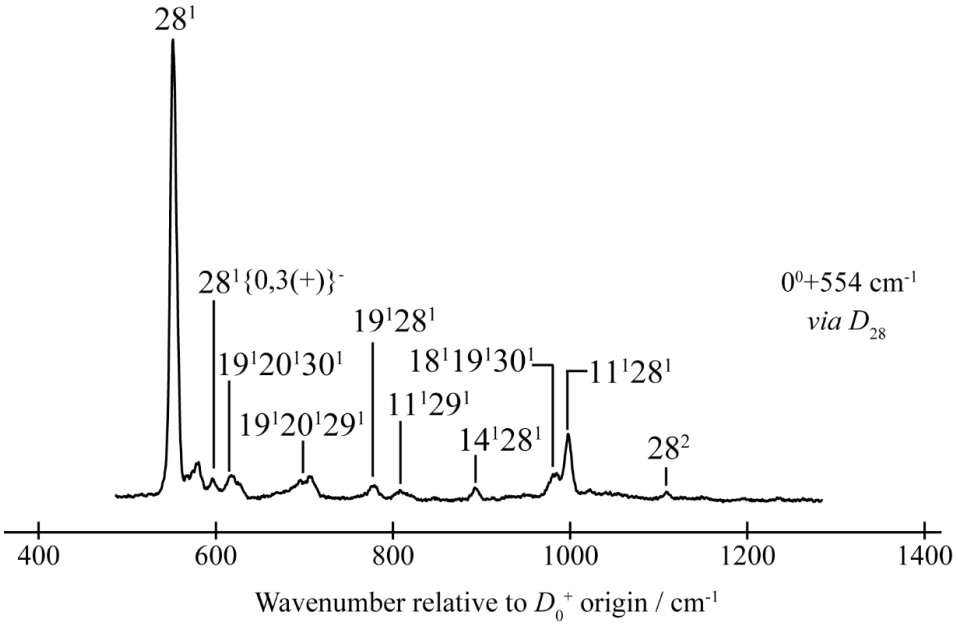


Figure 5.2 – A ZEKE spectrum recorded via the band at 0^0+554 cm^{-1} in pXyl is shown.

assortment of weaker structure. Based on the calculated D_{28} cationic wavenumber of 553 cm^{-1}, the $\Delta v\{m_1,m_2\} = 0$ transition can be readily assigned as 28_1^1, confirming the identity of the initial S_1 level as D_{28}. Other assignments of note in this ZEKE spectrum are to the terminating levels $D_{11}D_{28}$, the $D_{14}D_{28}$ and $D_{19}D_{28}$. These are the $\Delta v\{m_1,m_2\} = 0$ transition in combination with the D_{11}, D_{14} and D_{19} vibrations, which appear in many of the ZEKE spectra of *p*Xyl.

The D_{11} combination is symmetry-allowed and observed on, effectively, Franck-Condon grounds, while the D_{14} and D_{19} combinations are expected on vibronic coupling grounds. While one could look at each of the four "cold" torsional levels of these, it is assumed that the transitions to both the $D_{14}D_{28}$ and $D_{19}D_{28}$ levels are vibronically induced, analogous to the observation of the 14^1 and 19^1 transitions in the *p*DFB[12,13], *para*-chlorofluorobenzene (*p*ClFB)[14], *p*FT and *p*Xyl origin ZEKE spectra, albeit here in combination with the D_{28} level.

Other assignments have been given in Figure 5.2, such as weak bands assigned to the terminating levels $D_{11}D_{29}$, $D_{19}D_{20}D_{30}$ and $D_{19}D_{20}D_{29}$; $D_{11}D_{29}$ and $D_{19}D_{20}D_{30}$ are of the same symmetry as D_{28} (a_4'') and so transitions from all four torsional components are symmetry-allowed, whereas the $D_{19}D_{20}D_{29}$ is of a different (a_1'') symmetry, and so would need another mechanism, such as vibronic coupling, to be observed.

The first overtone of the D_{28} vibration is observed, and this is totally symmetric, suggesting that totally symmetric vibrational levels can be observed *via* a non-totally symmetric intermediate level on vibronic grounds. This then leads to the assignment of a transition to $D_{28}\{0,3(+)\}^-$, which is also a totally symmetric terminating level. One may also note that there is weak structure just above the 28_1^1 transition, which can be assigned to "D_{28} $m = 2$" terminating levels, which could be observed on vibronic grounds.

This ZEKE spectrum confirms that the transition to D_{28} is in effectively the same S_1 position in *p*FT (Ayles *et al.*[1]), *p*Xyl (current work) and *p*DFB (Knight and Kable[2]), and so one might expect it to be in a similar position in other such

molecules, such as *p*ClFB; recent work by our research group[14,15] has shown it to be in a similar position for that molecule.

It should be noted that Blease *et al.*[7] assigned this *p*Xyl REMPI band to a transition to v_{6b} in their study, which is analogous to D_{28}, and so the presented ZEKE spectrum confirms their assignment.

5.B.2. The D_{29} vibration in *para*-xylene

The 29_0^1 transition is observed in the REMPI spectra of *p*DFB and *p*FT in Figure 5.1; for *p*FT, it was found to be overlapping with the 14_0^2 transition, and this will be returned to later in this chapter. In *p*Xyl, based on the calculated vibrational wavenumbers, the 29_0^1 transition is expected at 367 cm^{-1}, and there is an intense band at 0^0+370 cm^{-1}. Additionally, this band was assigned as a transition to v_{9b} by Blease *et al.*[7], and the 9*b* motion is closest to that of D_{29}. A ZEKE spectrum recorded *via* this feature is presented in Figure 5.3.

The ZEKE spectrum shows an intense $\Delta v\{m_1,m_2\} = 0$ transition at 378 cm^{-1}, in good agreement with the calculated vibrational wavenumber for D_{29} in the cation of 376 cm^{-1}, confirming the assignment of the REMPI band as 29_0^1. Similar to the ZEKE spectrum recorded *via* D_{28}, combination bands involving the D_{19}, D_{14} and D_{11} vibrations are all observed with D_{29}. By analogy to the D_{28} case, the

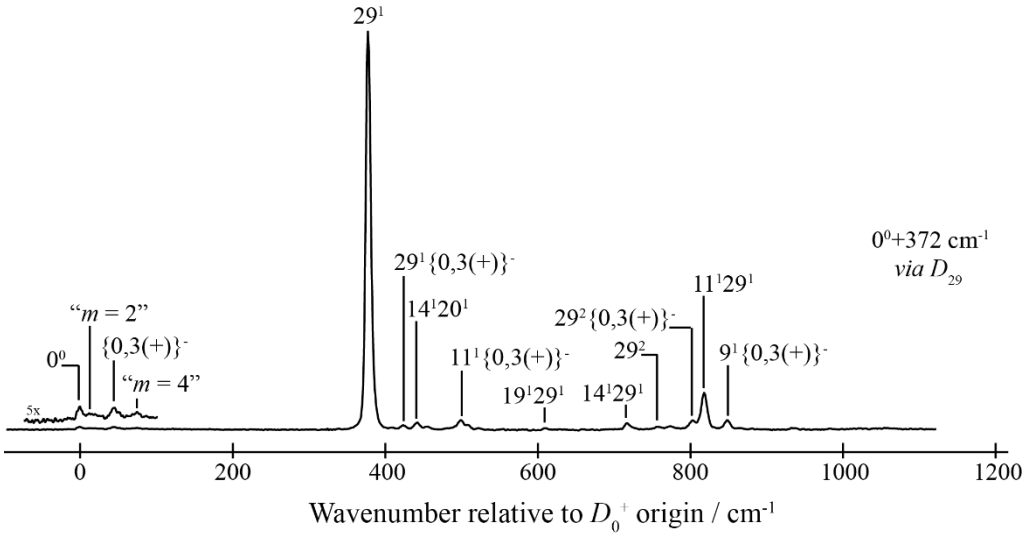


Figure 5.3 – A ZEKE spectrum recorded via the band at 0^0+372 cm^{-1} in pXyl is shown.

transition to $D_{11}D_{29}$ is symmetry-allowed, as it is the same symmetry as D_{29} itself, while the transitions to $D_{14}D_{29}$ and $D_{19}D_{29}$ are expected to be observed on vibronic coupling grounds.

Transitions to the totally symmetric terminating levels $2D_{29}$ and $D_{29}\{0,3(+)\}^-$ are observed, for the same reason that the D_{28} equivalents were observed in that ZEKE spectrum. A transition to D_{11} with an "m = 3" level was also assigned; this could be either a symmetry-allowed transition to $D_{11}\{0,3(+)\}^-$ or symmetry-allowed transitions to $D_{11}\{3,1\}$ and $D_{11}\{-3,1\}$. Similarly, a transition to D_9 with an "m = 3" level is observed and symmetry-allowed. In both cases the energetics suggest that it is the $\{0,3(+)\}^-$, rather than $\{3,1\}/\{-3,1\}$ levels, which are observed, with the $\{0,3(+)\}^-$ combination expected to slightly higher wavenumber than the alternative based on the discussions of the "m = 3" levels in Chapter 4.

There is also some weak structure in the ZEKE spectrum to low wavenumber, and the origin, "m = 3" and "m = 4" terminating levels are identified. The observed "m = 3" level is expected to be $\{0,3(+)\}^-$, as this is symmetry-allowed, and the band is in the correct position for this. The "m = 4" levels are expected

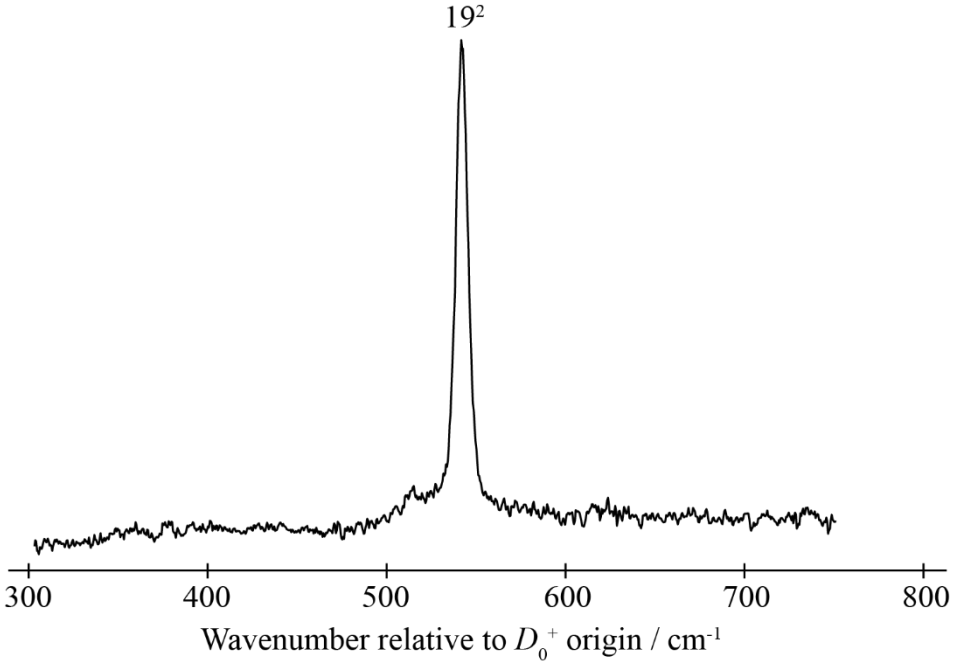


Figure 5.4 – A ZEKE spectrum recorded via the band at 0^0+484 cm^{-1} in pFT is shown.

to be {0,4}, {1,4}$^-$ and {1,-4}$^-$, since these are also symmetry-allowed. The origin is then expected on vibronic grounds, consistent with the observation of the totally symmetric $2D_{29}$ level, and so potentially all four torsional levels expected at this position could be contributing. Transitions to "m = 2" levels with the terminating levels {0,2}, {1,2}$^-$ and {1,-2}$^-$ are also symmetry-allowed, although if they are present it is only weakly.

5.B.3. The $2D_{19}$ vibration in *para*-fluorotoluene

Based on the calculated wavenumber for D_{19} in the S_1 state, the 19_0^2 transition is expected at 486 cm^{-1}, and there is a band at 0^0+484 cm^{-1}. A ZEKE spectrum recorded *via* this feature is presented in Figure 5.4, and it shows a single band at 542 cm^{-1}, in good agreement with the value of $2D_{19}$ calculated in the cation. This confirms the assignment of the REMPI band as 19_0^2, and allows the D_{19} fundamental to be established as 242 cm^{-1} in the S_1 state and 271 cm^{-1} in the D_0^+ state.

5.C. *para*-fluorotoluene: 400 cm^{-1} features

Having dealt with the isolated structure, it is now time to turn to the more complex regions of the *p*FT and *p*Xyl REMPI spectra in this region, starting with the two features ~400 cm^{-1} in *p*FT. As already mentioned, Ayles *et al*.[1] assigned the first of these as overlapping 29_0^1 and 14_0^2 transitions, with 29_0^1 dominating the high wavenumber side of the band and 14_0^2 dominating the low wavenumber side. The higher wavenumber feature at ~410 cm^{-1} was then assigned as 11_0^1.

Ayles *et al*. recorded three ZEKE spectra exciting at positions in the first band, illustrating how the observed activity changed when exciting at different points across it. In this thesis, a similar approach has been taken for several features in *p*FT and *p*Xyl, stepping across their band profiles and recording ZEKE spectra, in what will be termed a "2D-ZEKE" spectrum. This approach allows overlapping features to be unravelled and aids in elucidating possible couplings between levels.

5.C.1. Overview

As the assignments of the S_1 bands in *p*FT are already understood for this region, it provides a good test case to illustrate a "2D-ZEKE" spectrum, and the one recorded across this region for *p*FT is shown in Figure 5.5. This shows six spectra recorded *via* the 0^0+400 cm^{-1} band (band A) and three spectra recorded *via* the 410 cm^{-1} band (band B). On the right of the figure, presented vertically, is a REMPI spectrum over this region, with the ZEKE spectra linked to their excitation positions with dashed lines, giving the two dimensions of the term "2D-ZEKE".

The ZEKE spectra recorded at positions A_1, A_2 and A_3 show a strong $\Delta(v,m) = 0$ band at 697 cm^{-1}, assigned to the 14_2^2 transition, while the ZEKE spectra recorded at positions A_4, A_5 and A_6 show a strong $\Delta(v,m) = 0$ band at 414 cm^{-1}, assigned to the 29_1^1 transition. This suggests that 14_0^2 dominates the low wavenumber side of band A in the REMPI spectrum, while 29_0^1 dominates the high wavenumber side; in trace A_4, recorded at the maximum of band A, the character of both is observed. This is in agreement with the study of Ayles *et al*.[1] and the positions of $2D_{14}$ and D_{29} in the cation are in agreement with the B3LYP/aug-cc-pVTZ calculated values of this thesis (Table B.2 in Appendix B).

Other features in these ZEKE spectra support the $\Delta(v,m) = 0$ assignments. For example, in spectra *via* the lower wavenumber, $2D_{14}$ side of the band, the 14_2^1 band is observed, and this gets progressively weaker and then becomes absent moving to the D_{29} side of the band. This is consistent with seeing D_{14} in the cation *via* a totally symmetric intermediate level, owing to vibronic coupling in the cation. Transitions to the D_{11} level are also seen in these ZEKE spectra, again in the ZEKE spectra recorded *via* $2D_{14}$, suggesting a Franck-Condon overlap between these levels.

The three ZEKE spectra recorded *via* band B show much more consistent character between excitation positions, suggesting that band B is dominated by only a single vibration.

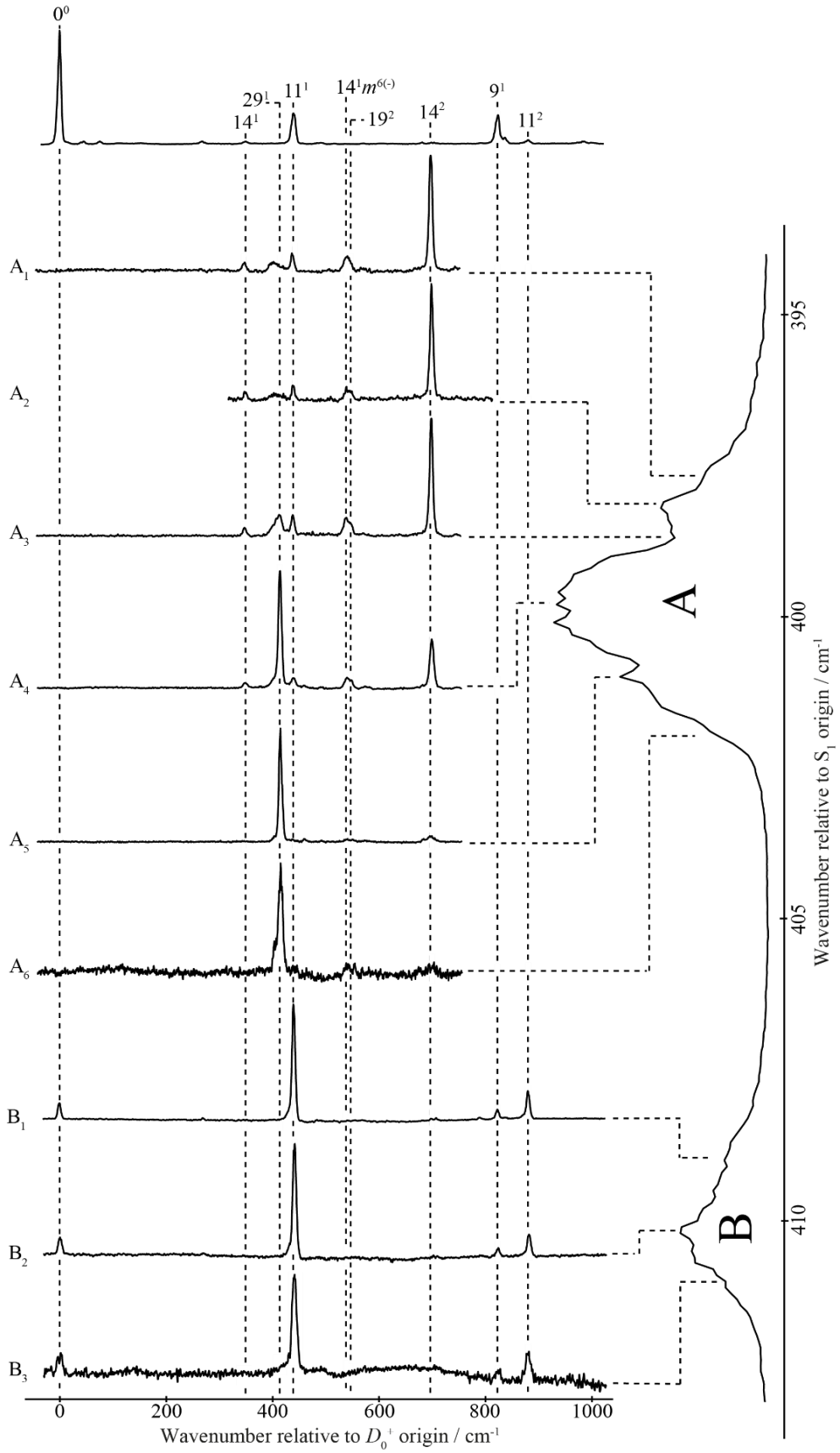


Figure 5.5 – A "2D-ZEKE" spectrum, comprising ZEKE spectra recorded at different excitation wavenumbers across the range 395 – 415 cm^{-1} for pFT. The top ZEKE spectrum was recorded via the S_1 origin and is shown for comparison purposes.

The $\Delta(v,m) = 0$ transition lies at 440 cm^{-1}, and is easily assigned as 11_1^1, in agreement with the B3LYP/aug-cc-pVTZ calculations of this thesis and the previous work of Ayles *et al*. Also observed are the 11_1^2 and $11_1^0 9_0^1$ transitions, both of which are symmetry-allowed and match the observed positions of 11_0^2 and 9_0^1 in the origin ZEKE spectrum, which is presented at the top of Figure 5.5 for reference.

These confirmed assignments allow the fundamentals of D_{14}, D_{29} and D_{11} to be confirmed in the S_1 state as 199, 401 and 410 cm^{-1} respectively. For D_{14} and D_{29}, positions on either side of the 0^0+400 cm^{-1} REMPI band are chosen as the $2D_{14}$ and D_{29} positions, and anharmonicity is neglected in obtaining D_{14} from $2D_{14}$. The extracted fundamentals are in good agreement with the calculated values for D_{29} and D_{11}. No comparison with the calculated B3LYP/aug-cc-pVTZ S_1 value for D_{14} is possible, as already discussed. These spectra also allow the D_{14}, D_{29} and D_{11} wavenumbers to be confirmed in the D_0^+ state, supporting earlier evidence from the origin ZEKE spectrum and the work of Ayles *et al*.[1]

5.C.2. Discussion

In the ZEKE spectra recorded *via* band A, a ZEKE band is observed at 541 cm^{-1}, primarily in the spectra recorded *via* the D_{14} side of the band. This agrees well with the position of the $2D_{19}$ level in the cation established earlier, and so this can be assigned to this. The transition to $2D_{19}$ is symmetry-allowed from $2D_{14}$, but it could also be coupled to the $2D_{14}$ level as they are of the same symmetry. This seems unlikely, as there is a change of four vibrational quanta between these levels and they are reasonably energetically separated in both the S_1 and D_0^+ states, so any coupling would be expected to be weak.

This 541 cm^{-1} ZEKE band is broad compared to other bands in this spectrum, with a full-width at half-maximum (FWHM) of 15 cm^{-1} (compared to 7 cm^{-1} for the $\Delta(v,m) = 0$ transition(s)). This suggests that this band may arise due to two overlapping transitions, and so another assignment was sought. The proposed assignment is to the terminating level D_{14} m = 6(-), which is totally symmetric and could be observed here for one or more of three reasons:

(i) it is symmetry-allowed from $2D_{14}$

(ii) it is coupled to $2D_{14}$

(iii) it is a $\Delta(v,m) = 0$ transition, and the $14^1m^{6(-)}$ transition is overlapping band A in the S_1 state

Although the $m_0^{6(-)}$ transition was not observed in the REMPI spectrum of *p*FT, one expects the transitions to $m = 6$ levels at 196 cm^{-1} in the S_1 state based on a simple free rotor calculation, and the expected splitting of the $m = 6(-)$ and $6(+)$ levels is expected to be small as these levels are significantly above the expected torsional barrier height. This is consistent with the observation of $m_0^{6(+)}$ at 198 cm^{-1}, as discussed in Chapter 3. Thus, one would expect $14^1m^{6(-)}$ at 397 cm^{-1} in the REMPI spectrum, based on the fundamental wavenumber established for D_{14} above, and this could lie underneath band A. The fact that this ZEKE band appears to correlate with the excitation positions dominated by $2D_{14}$ does not help elucidate which mechanism(s) is/are at work.

It is tentatively concluded that the $14_0^1m_0^{6(-)}$ transition is found under the low wavenumber side of band A and is thus coincidental with 14_0^2, suggesting at most a weak coupling. An alternative however, is that the two are interacting and D_{14} $m = 6(-)$ is perturbed to lower wavenumber. It is not possible to deduce this from the current study, but ongoing 2D-LIF work in our group and the group of Professor Warren Lawrance (shared privately with our research group) has suggested that $14_0^1m_0^{6(-)}$ is indeed coincident with 14_0^2.

One observes a transition to D_{11} when exciting $2D_{14}$, and a weak transition to $2D_{14}$ when exciting D_{11}. This could imply that the two levels are coupled, as they are reasonably close energetically and of the same symmetry. However, this could also just be Franck-Condon activity, as 14^2 is also observed weakly in the origin ZEKE spectrum. Again, it is not possible to be definitive here, but if these levels are coupled, it is expected to be only very weakly, and so both the 14_0^2 and 11_0^1 transitions are concluded to be intrinsically bright in the REMPI spectrum. Owing to the separation of these levels being only around 10 cm^{-1} in the S_1 state, a time-resolved experiment that could coherently excite both

eigenstates could shed more light on this, such as a picosecond time-resolved photoelectron spectroscopy (tr-PES) experiment.

Finally, it is worth pointing out that the overlapping $2D_{14}$ and D_{29} levels are not expected to be strongly coupled, owing to their different symmetries, although they could couple through vibronic interactions.

5.D. *para*-xylene: 400 – 450 cm^{-1} features

5.D.1. Overview

To recap what has been discussed so far in the excitation spectra of these *para*-disubstituted benzene molecules, for *p*DFB, in the range 350 – 600 cm^{-1}, Knight and Kable[2] assigned the 14_0^2, 29_0^1, 11_0^1, 19_0^2 and 28_0^1 transitions with significant intensity, and these same transitions have all been assigned in *p*FT with significant intensity. In *p*Xyl, so far 29_0^1 and 28_0^1 have been assigned, with the other three transitions expected in the range 400 – 450 cm^{-1}, where there is a weak band followed by a triplet of reasonably intense ones. It is this region where the remainder of this chapter will focus.

A "2D-ZEKE" spectrum, over the triplet of features, is presented in Figure 5.6. This shows four ZEKE spectra recorded *via* the first band of the triplet (band C), three *via* the second band (D) and one *via* the third band (E). At the top of the figure, the ZEKE spectrum recorded *via* the S_1 origin is presented, which aids in assignment of bands in these ZEKE spectra. Vertically, on the right of the figure, the REMPI spectrum over this region is presented, with the ZEKE spectra linked to their excitation positions with dashed lines.

Band D has a maximum at 0^0+434 cm^{-1} and shows the same activity in all three ZEKE spectra recorded *via* it; this suggests that it is due to a single vibration or vibtor level. There is an obvious $\Delta v\{m_1,m_2\} = 0$ transition at 683 cm^{-1}, and with such a large S_1 to D_0^+ shift, this is expected to be an out-of-plane vibration. Based on *p*DFB and *p*FT, $2D_{14}$ would have a large shift such as this, and the $\Delta v\{m_1,m_2\} = 0$ transition is in pretty good agreement with the calculated

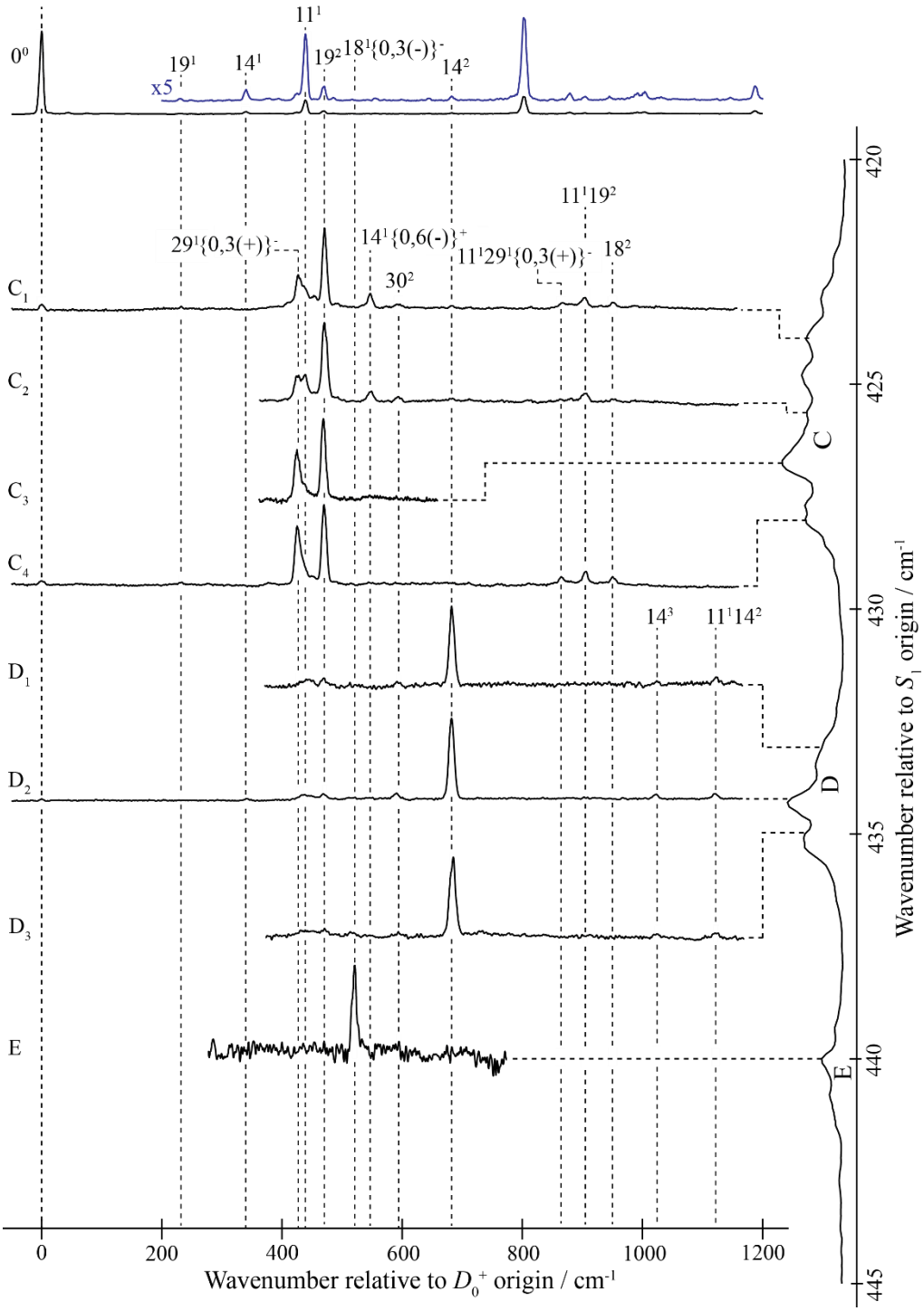


Figure 5.6 – A "2D-ZEKE" spectrum, comprising ZEKE spectra recorded at different excitation wavenumbers across the range 420 – 445 cm^{-1} for pXyl. The top ZEKE spectrum was recorded via the S_1 origin and is shown for comparison purposes.

position of $2D_{14}$ in the cation. This allows the intense ZEKE band to be assigned as 14_2^2, establishing that REMPI band D is the 14_0^2 transition, in agreement with the assignment of $16a_0^2$ given to this band by Blease *et al.*[7] in their REMPI study.

Band E, at 0^0+440 cm^{-1}, has not been discussed by any previous workers, and the ZEKE spectrum shows only the $\Delta v\{m_1,m_2\} = 0$ band at 521 cm^{-1}. All vibrational fundamentals (apart from D_{18}) below this wavenumber are now known for both the S_1 and D_0^+ states, from the REMPI and ZEKE spectra of bands to lower wavenumber, and so this makes it relatively simple to check vibrational assignments. It transpires that this band is not readily assignable to any vibration, and so must involve a vibtor level.

Since this ZEKE spectrum does not show any other bands, and this $\Delta v\{m_1,m_2\} = 0$ band does not appear in any of the ZEKE spectra recorded *via* bands C and D, it appears that the level(s) giving rise to band E are not coupled to the levels giving rise to bands C or D, and therefore band E must be intrinsically bright. Looking at the low wavenumber torsion and vibtor region discussed in Chapter 4, one will note that the most intense, intrinsically bright, bands are those arising from the "D_{20} m = 3" and "D_{19} m = 3" levels. As such, one might expect vibrations of the same symmetry as D_{20} and D_{19} to be observed with their "m = 3" levels, and D_{18} is of the same symmetry. Here then, "D_{18} m = 3" is a possible assignment, but D_{18} is calculated at 443 cm^{-1} in the S_1 state, suggesting that "D_{18} m = 3" would be too high in wavenumber for band E. However, D_{18} is calculated at 470 cm^{-1} in the cation, and so "D_{18} m = 3" would be expected at 513 cm^{-1} in the cation (for $D_{18}\{0,3(-)\}^-$, with the {3,1} and {-3,1} combinations expected at approximately the same position). This is reasonably close to the observed ZEKE band position.

Thus, the $\Delta v\{m_1,m_2\} = 0$ of band E is assigned as $18_1^1 m_{\{0,3(-)\}^-}^{\{0,3(-)\}^-}$ (with $18_1^1 m_{\{3,1\}}^{\{3,1\}}$ and $18_1^1 m_{\{-3,1\}}^{\{-3,1\}}$ also expected). This gives the assignment of band E in the REMPI spectrum as the terminating levels "D_{18} m = 3". Although the D_{18} fundamental in the S_1 state extracted from this approach (400 cm^{-1}) is not in good agreement with the B3LYP calculated value (443 cm^{-1}), it will be shown in the next chapter that it agrees with the value obtained from the D_{18} overtone band to higher wavenumber, and so this assignment is secure.

Band C was assigned by Blease *et al*. to $6a_0^1$, with the D_i label which most closely corresponds to this being D_{11}. As 11^1 has significant intensity in the origin ZEKE spectrum, its cationic wavenumber is already known to be 440 cm^{-1}, and thus it is easy to identify it in the ZEKE spectra C_1 – C_4. The transition to D_{11} is not the most intense transition in any of those ZEKE spectra, and it does not appear to be a $\Delta v\{m_1,m_2\} = 0$ transition, so the assignment of 11^1 to this S_1 feature seems to be incorrect.

The most intense ZEKE transitions in traces C_1 – C_4 are at 471 cm^{-1} and 427 cm^{-1}. Based on the earlier comparison to *p*DFB and *p*FT, a transition to $2D_{19}$ is expected in the region of band C, and a $\Delta v\{m_1,m_2\} = 0$ transition from this would be expected to be at 464 cm^{-1} in the ZEKE spectrum (based on the calculated D_{19} wavenumber[a]). This is in agreement with the 471 cm^{-1} band which dominates all four of these ZEKE spectra, and matches a band in the origin ZEKE spectrum which was assigned to 19^2 in Chapter 4. This allows 19_0^2 to be assigned as a contributor to band C. However, it can be seen from the REMPI spectrum in Figure 5.6 that band C is much broader than band D. Band D was assigned to a single vibrational eigenstate ($2D_{14}$, albeit with its four expected torsional levels), and so this suggests that there is another contribution to band C.

So, what other contributions could be present? Based on the ZEKE spectra, another contribution is likely to be giving rise to the band at 427 cm^{-1}, which appears to change intensity across band C. Since all vibrational fundamentals below the S_1 position of band C are now known, one can look at all possible vibrational assignments and as for band E, conclude that there are none which fit this band and the remaining ZEKE activity. This means that a vibtor level is expected. The simplest way to check for vibtor levels is to subtract the observed "*m* = 2", "*m* = 3(-)", "*m* = 3(+)" and "*m* = 4" positions from the band C position and look for vibrations at those wavenumbers. In doing this, it becomes apparent that "D_{29} *m* = 3(+)" would be expected at 425 cm^{-1} in the S_1 state, matching the

[a] Although D_{19} is, in theory, known from the D_{19} vibtor levels discussed in Chapter 4, since these are all expected to be at least somewhat perturbed, the B3LYP/aug-cc-pVTZ calculated value is still being used to estimate the position of $2D_{19}$.

position of band C, and at 428 cm^{-1} in the D_0^+ state, in agreement with the remaining intense ZEKE transition. Thus, band C appears to be composed of both 19_0^2 and $29_0^1 m_{\{0,0\}}^{\{0,3(+)\}^-}$, both of which are totally symmetric.

In summary, band C has been assigned as having terminating levels $D_{29}\{0,3(+)\}^-$ and $2D_{19}$ (with all four "cold" torsional levels), band D has been assigned as terminating level $2D_{14}$ (with all four "cold" torsional levels) and band E has been assigned as terminating levels $D_{18}\{0,3(-)\}^-$, $D_{18}\{3,1\}$ and $D_{18}\{-3,1\}$. The possible couplings will be discussed in the next section.

5.D.2. Discussion

One might note that the 11_0^1 transition has not yet been assigned in the REMPI spectrum, having been discounted from band C where it was previously[7,8] assigned. For *p*DFB and *p*FT, the calculated S_1 wavenumber for D_{11} was in excellent agreement with the observed position, and here the calculated D_{11} S_1 wavenumber is 402 cm^{-1}, and there is a weak band at 404 cm^{-1} in the REMPI spectrum, just below the triplet of bands C – E. This can be seen in Figure 5.1 and can thus be assigned as the 11_0^1 transition, although unfortunately no ZEKE spectrum was attempted *via* this weak intermediate. The weakness of this transition is similar to the weakness of the M_{11} vibration in the excitation spectra of fluorobenzene[9,16,17]; this is analogous to ν_{6a} and D_{11}. It appears that M_{11} in monosubstituted benzene species and D_{11} in *para*-disubstituted benzene species change intensity between molecules. At first sight this seems unusual, since the S_0 to S_1 geometry change is expected to be similar between the different substituted benzene molecules, and the vibrations are expected to be similar within the monosubstituted and *para*-disubstituted sets. Indeed, the similarity in the REMPI activity of different monosubstituted benzene molecules[9–11] (and *para*-disubstituted benzene molecules as discussed in this thesis) supports this. As such, it seems plausible that the activity of D_{11} (and M_{11}) is not just Franck-Condon, but also has a contribution from vibronic coupling. This would then give rise to differing intensities for 11_0^1 between molecules as the proximity of the relevant electronic state to the S_1 state changes. Such a mechanism was

proposed by Blease *et al.*[7] to explain the intensity of band C, which changed between their 1+1 and 2+2 REMPI spectra. Although band C has been reassigned in this thesis, this mechanism could still be important to the intensities of transitions to totally symmetric levels.

Within band C, the ZEKE spectra allowed two contributions to be assigned: $D_{29}\{0,3(+)\}^-$ and $2D_{19}$. However, the $\Delta v\{m_1,m_2\} = 0$ intensities vary in the ZEKE spectra C_1 – C_4 recorded across this feature. The 19_2^2 is always the most intense transition in these ZEKE spectra, perhaps owing to a higher photoionisation cross section than for $29_1^1 m_{\{0,3(+)\}^-}^{\{0,3(+)\}^-}$, but the $29_1^1 m_{\{0,3(+)\}^-}^{\{0,3(+)\}^-}$ band grows in intensity from C_1 – C_4. One must be careful in interpreting these intensity changes, as these spectra are all normalised to the most intense peak in the spectrum, which is the 19_2^2 in each case, rather than to, for example, a total number of detected electrons. As such, it seems that in trace C_4, the $29_1^1 m_{\{0,3(+)\}^-}^{\{0,3(+)\}^-}$ band is (relatively) much more dominant than in C_1, even though 19_2^2 is the most intense transition in both cases. This then suggests that the lower

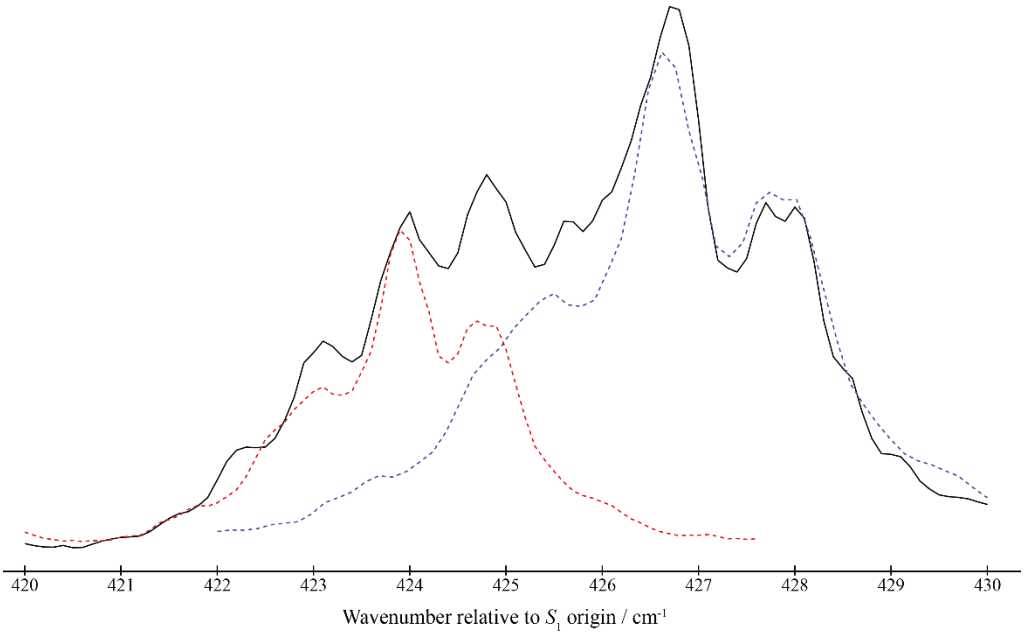


Figure 5.7 – A schematic representation of how the $2D_{19}$ (red) and $D_{29}\{0,3(+)\}^-$ (blue) eigenstates contribute to the profile of band C. The black trace is the band C profile from the REMPI spectrum, while the coloured traces use the band D profile, vertically scaled, as a typical rotational profile for these totally symmetric eigenstates.

wavenumber side of the REMPI band is dominated by 19_0^2 while the higher wavenumber side of the band is dominated by $29_0^1 m_{\{0,0\}}^{\{0,3(+)\}^-}$. This is illustrated in Figure 5.7, where the profile of band D (which was found to be a single vibrational eigenstate) is used as a guide as to the positions of the $2D_{19}$ and $D_{29}\{0,3(+)\}^-$ eigenstates.

A handful of other, weaker, features are observed in the ZEKE spectra. The spectra recorded *via* band C show D_{11} in combination with the two $\Delta v\{m_1,m_2\} = 0$ transitions, as well as a band assigned as terminating with $2D_{18}$; this likely arises owing to Franck-Condon overlap with $2D_{19}$, hence its appearance in ZEKE spectra across the whole feature, following the $2D_{19}$ contributions.

Additionally, a band is observed with reasonable intensity in traces C_1 and C_2 at 548 cm^{-1}. The most sensible assignment found for this was the terminating level $D_{14}\{0,6(-)\}^+$, which would be expected at around 540 cm^{-1} based on the known D_{14} fundamental and a free rotor "$m = 6$" position. This seems a little low, but it is possible that it could be coupled to $2D_{19}$ in the cation, which would perturb the $D_{14}\{0,6(-)\}^+$ level to higher wavenumber. It is also suggested that this band is observed in the REMPI spectrum, with the expected position there being 413 cm^{-1}. A weak band is observed at 414 cm^{-1}, and it is suggested that is due to $14_0^1 m_{\{0,0\}}^{\{0,6(-)\}^+}$. Thus, it is postulated that there is a weak coupling between the $D_{14}\{0,6(-)\}^+$ and $2D_{19}$ levels in the S_1 state, and this is why a transition to $D_{14}\{0,6(-)\}^+$ is observed in the ZEKE spectra recorded *via* the $2D_{19}$ side of band C. Unfortunately, no ZEKE spectrum was attempted *via* the weak band at 414 cm^{-1}, so this cannot be confirmed. However, the observation of $14_0^1 m_{\{0,0\}}^{\{0,6(-)\}^+}$ in the REMPI spectrum would be consistent with the observation of $14_0^1 m_0^{6(-)}$ in *p*FT, discussed above, and so its appearance here is not unexpected.

The ZEKE spectra also suggest other possible couplings. Indeed, the observation of transitions to $D_{29}\{0,3(+)\}^-$ and $2D_{19}$ in all ZEKE spectra recorded across

feature C suggests that these levels are coupled, and that the low wavenumber side of band C is an eigenstate dominated by $2D_{19}$ with a $D_{29}\{0,3(+)\}^-$ contribution, while the high wavenumber side is due to an eigenstate dominated by $D_{29}\{0,3(+)\}^-$ with a $2D_{19}$ contribution. This is also supported by the predicted positions of the transitions to these levels in the S_1 state, with both $29_0^1 m_{\{0,0\}}^{\{0,3(+)\}^-}$ and 19_0^2 expected around the centre of band C, with their observed positions consistent with them being pushed apart by coupling to one another. It is a little more complex than this, since $D_{29}\{0,3(+)\}^-$ is of a_1' symmetry and can therefore interact only with the $2D_{19}\{0,0\}$ level, leaving the $2D_{19}\{0,1\}$, $2D_{19}\{1,1\}$ and $2D_{19}\{1,-1\}$ levels effectively unperturbed (assuming no other couplings). This could explain why the 19_2^2 ZEKE transition dominates so many of the ZEKE spectra recorded *via* band C. Since the $D_{29}\{0,3(+)\}^-$ and $2D_{19}$ levels are more energetically separated in the cation, any coupling would be weaker there, explaining why the $2D_{19}$ ZEKE band is not obviously split by the coupling.

Comparing to *p*FT, it is notable that the analogous $29_0^1 m_0^{3(+)}$ band was not observed there, but that 19_0^2 was. This suggests that 19_0^2 is bright, and $29_0^1 m_0^{3(+)}$ is dark, with intensity in the $29_0^1 m_{\{0,0\}}^{\{0,3(+)\}^-}$ band arising only due to its proximity to (and therefore coupling to) 19_0^2 in *p*Xyl.

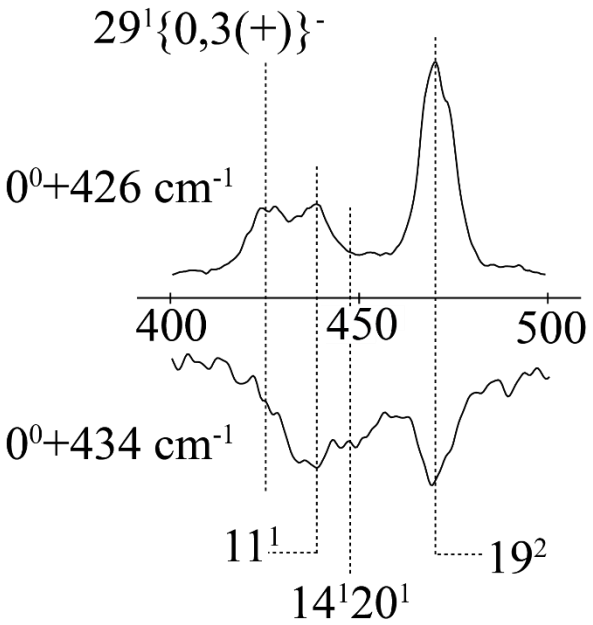


Figure 5.8 – An expanded view of the 400 – 500 cm^{-1} region of ZEKE spectra C_2 and D_2, recorded at the centres of bands C and D respectively.

It is also possible that D_{11} is coupled to the levels which give rise to band C, since it also appears (weakly) in all ZEKE spectra recorded across that band. This could alternatively be Franck-Condon activity and since a ZEKE spectrum was not recorded *via* the assigned 11_0^1 band at 0^0+403 cm^{-1}, it is not possible to say much more than this. Further work, such as tr-PES spectroscopy exciting (ideally) the D_{11}, $D_{14}\{0,6(-)\}^+$, $2D_{19}$ and $29\{0,3(+)\}^-$ eigenstates simultaneously, would be useful in shedding further light on possible couplings here.

Finally, the question arises as to whether the $2D_{14}$ level is coupled to the two levels that comprise band C. To establish this, one can look at the 400 – 500 cm^{-1} region of a ZEKE spectrum recorded at the centre of band C (0^0+426 cm^{-1}) and the same region of a ZEKE spectrum recorded at the centre of band D (0^0+434 cm^{-1}). This comparison is presented in Figure 5.8.

One can see that when exciting either band C or band D, 19^2 is observed, and indeed, one can see from Figure 5.6 that the 14^2 is observed weakly when exciting band C, suggesting either a Franck-Condon overlap or a weak coupling of the $2D_{19}$ and $2D_{14}$ levels in the S_1 state. However, $29^1m^{\{0,3(+)\}^-}$ is not observed *via* $2D_{14}$, and 11^1 is observed more prominently *via* $2D_{14}$. This suggests that the $2D_{14}$ intermediate level is not coupled to $D_{29}\{0,3(+)\}^-$, but

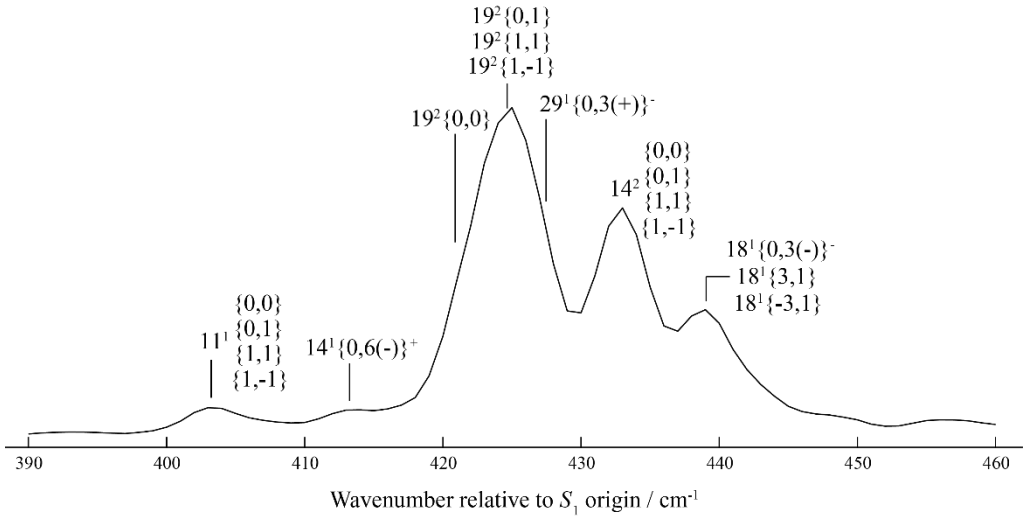


Figure 5.9 – An expanded view of the 390 – 460 cm^{-1} region of the pXyl REMPI spectrum, with the assignments of the current work shown. Note that the separation of {0,0} from the other three $2D_{19}$ $\{m_1,m_2\}$ levels is not quantitative, but a qualitative, postulated, separation based on the proposed coupling with $D_{29}\{0,3(+)\}^-$.

could be coupled to $2D_{19}$ and/or D_{11}. Regarding a possible $2D_{14}…D_{11}$ coupling, this is analogous to the situation in *p*FT discussed earlier in this chapter, and it is currently thought that Franck-Condon overlap is the more likely explanation in both molecules.

Figure 5.9 summarises the assignments of the REMPI bands from 390 – 460 cm^{-1} discussed in this section. The expected bright transitions, deduced from the ZEKE spectra and comparison to other molecules, are 11_0^1, 19_0^2 and 14_0^2. The transitions to the "D_{18} m = 3" levels are also expected to be intrinsically bright, as there is no evidence of coupling in the ZEKE spectrum recorded *via* that band. $D_{14}\{0,6(-)\}^+$ is thought to be coupled to $2D_{19}$ based on the ZEKE spectra[b], and so could be a dark state gaining its intensity in this manner, or it could be inherently (weakly) bright, and coupled. Finally, $D_{29}\{0,3(+)\}^-$ is proposed to be a dark state, with all of its intensity arising from coupling to the $2D_{19}\{0,0\}$ level, since the analogous D_{29} m = 3(+) was not observed in *p*FT.

5.E. Summary

Having now assigned all observed structure up to 600 cm^{-1} in *p*FT and *p*Xyl to transitions to torsions, vibrations and vibtor levels, it seems sensible to reflect on how the REMPI activities of these molecules compare to that of *p*DFB. Figure 5.10 shows a comparison of the REMPI activities of these three molecules up to 600 cm^{-1}, excluding the low wavenumber torsion and vibtor structure for *p*FT and *p*Xyl which was discussed in Chapters 3 and 4. This figure also includes *p*ClFB as an additional comparison, and this molecule shows effectively the same bright structure as *p*DFB in its REMPI spectrum. One can see very similar activities in the bright transitions observed, with intense 14_0^2 and reasonably intense 20_0^2 and 19_0^2 transitions observed for all four molecules, as well as intensity in 29_0^1 and 28_0^1 transitions, suggesting that the S_2 electronic state is at a similar energetic separation from the S_1 state in each case (for the

[b] It is notable that there is a significant quanta change between $D_{14}\{0,6(-)\}^+$ and $2D_{19}$, and on the grounds of quanta changes it would be more likely to be coupled to $2D_{14}$, but the ZEKE spectra show no evidence of this.

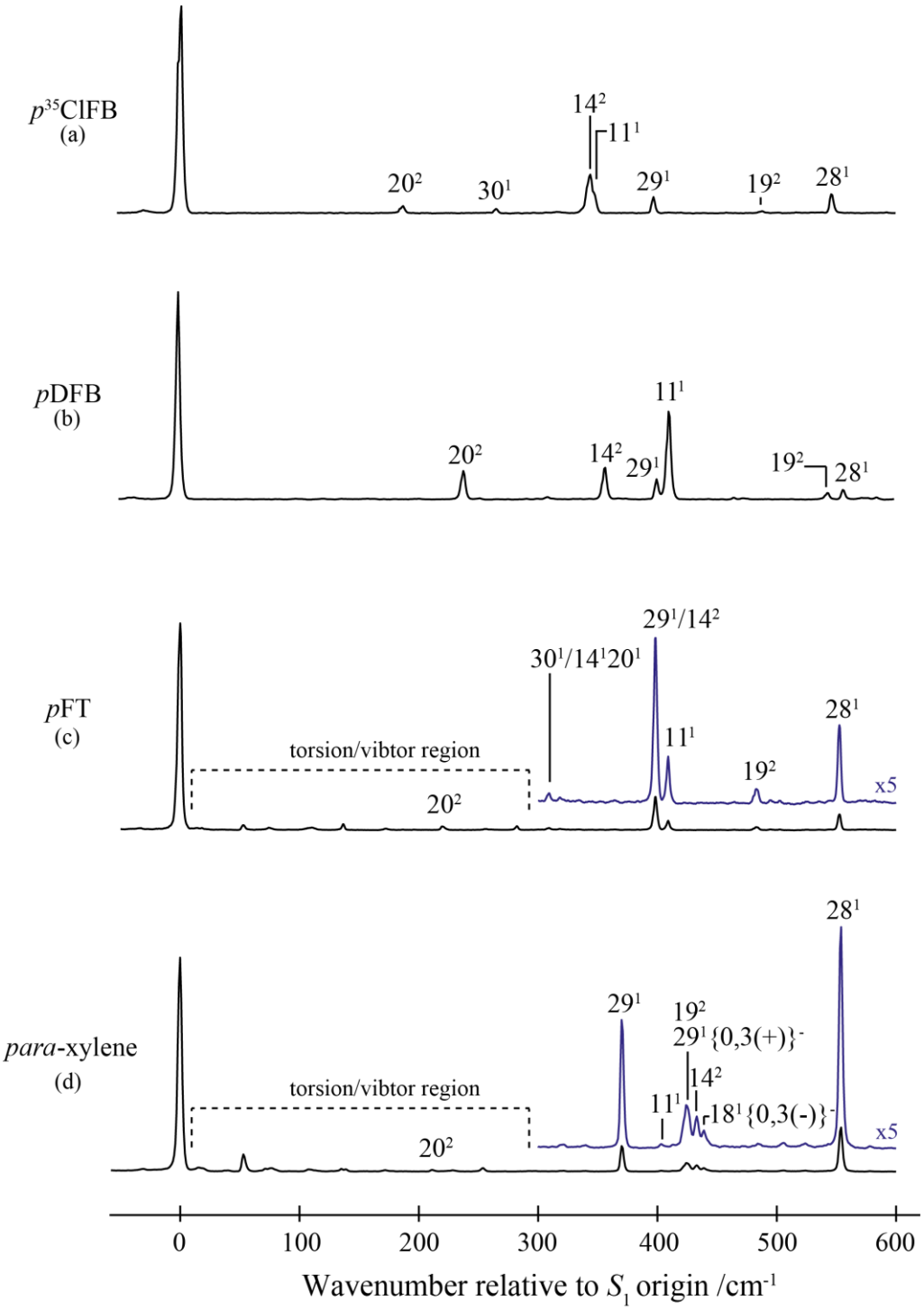


*Figure 5.10 – The (a) p[35]ClFB, (b) pDFB, (c) pFT and (d) p*Xyl $S_1 \leftarrow S_0$ *REMPI spectra up to 600 cm^{-1} are shown. The assignments are those of Figure 5.1, with the addition of those from ZEKE spectra discussed in this chapter. The assignments for the pClFB REMPI spectrum come from recent REMPI and ZEKE work by our research group.*[14,15]

intensity stealing mechanism for these vibrations). Additionally, the 11_0^1 band is observed in all four spectra, but with quite different intensities, being quite

intense in *p*DFB but very weak in *p*Xyl. This is thought to be due to another vibronic coupling mechanism with a different, higher, electronic state, and this state would then be changing energetically between the systems, modulating the intensity stealing mechanism from molecule to molecule, with the most stealing in *p*DFB and the least in *p*Xyl.

In *p*DFB, none of the levels in this region are thought to be coupled to one another, and the same is true in *p*ClFB. In *p*FT, it is possible that $2D_{14}$ and D_{11} are coupled (with perhaps some involvement of D_{14} m = 6(-)), although the activity in the spectra suggests this could alternatively be Franck-Condon activity, which is thought to be the case. However, for *p*Xyl, the $2D_{19}$ level is coupled to the $D_{29}\{0,3(+)\}^-$ level, which is thought to be intrinsically dark. Additionally, the $2D_{19}$ level may also be coupled to the $D_{14}\{0,6(-)\}^+$ level, and perhaps also to the D_{11} level; future studies using techniques such as 2D-LIF or tr-PES would aid in clarifying these proposed couplings.

In *p*Xyl, degenerate transitions to three "D_{18} m = 3" levels are also observed, and as these transitions are symmetry-allowed and there is no evidence for coupling, it is thought that these transitions have intrinsic intensity. The analogous transition for *p*FT would be expected at 460 cm^{-1} (based on a D_{18} fundamental extracted in Chapter 6 from the first overtone of D_{18} , and the S_1 m = 3(-) position of 37 cm^{-1} from the work of Zhao *et al*.[18]), and if one records a REMPI spectrum over this region with the laser power turned up, a band can be seen at 464 cm^{-1}. No ZEKE spectrum was recorded *via* this feature, but it is tentatively assigned as $18_0^1 m_0^{3(-)}$, consistent with the observation of the analogous transition(s) in *p*Xyl discussed in this chapter.

Similarly, there is a weak shoulder to the low wavenumber side of the 28_0^1 *p*FT REMPI transition, at 0^0+545 cm^{-1}, and based on the D_{17} S_1 fundamental extracted from other transitions in Chapter 6, this can be assigned as $17_0^1 m_0^{3(-)}$, although again no ZEKE spectrum was recorded *via* this intermediate. Thus, all of the a_2'' symmetry fundamentals (b_1 in the C_{2v} point group) up to 600 cm^{-1} (the region covered up to this chapter) have been observed in combination with the

m = 3(-) level (itself a_2''), suggesting that these totally symmetric vibtor levels are intrinsically bright and an expected sight in these molecules.

For *p*Xyl, the D_{20}, D_{19} and D_{18} "m = 3(-)" combinations have been observed, and the higher energy combinations of these a_2''/a_3'' (b_{3u}/b_{2g} in the D_{2h} point group) symmetry vibrations with the "m = 3(-)" levels (themselves a_2''/a_3'') will be touched upon in the next chapter, as will the remaining *p*FT combinations with D_{15} and D_{16}.

The fundamentals obtained from this low wavenumber region will be of great use in assigning more complex structure to higher wavenumber, and the general trend of more coupled levels being observed for the methyl rotor species than for *p*DFB and *p*ClFB will continue to be demonstrated in the ZEKE spectra recorded to higher wavenumber. This will be discussed further in Chapter 7, where the density of states for these four molecules will be examined and compared.

5.F. References

[1] V.L. Ayles, C.J. Hammond, D.E. Bergeron, O.J. Richards, and T.G. Wright, *J. Chem. Phys.*, **126**, 244304 (2007).

[2] A.E.W. Knight and S.H. Kable, *J. Chem. Phys.*, **89**, 7139 (1988).

[3] E.B. Wilson Jr., *Phys. Rev.*, **45**, 706 (1934).

[4] G. Varsányi, *Assignments of the Vibrational Spectra of Seven Hundred Benzene Derivatives* (Wiley, New York, 1974).

[5] F. Gunzer and J. Grotemeyer, *Int. J. Mass Spectrom.*, **228**, 921 (2003).

[6] T. Ebata, Y. Suzuki, N. Mikami, T. Miyashi, and M. Ito, *Chem. Phys. Lett.*, **110**, 597 (1984).

[7] T.G. Blease, R.J. Donovan, P.R.R. Langridge-Smith, and T. Ridley, *Laser Chem.*, **9**, 241 (1988).

[8] K. Walter, K. Scherm, and U. Boesl, *Chem. Phys. Lett.*, **161**, 473 (1989).

[9] J.P. Harris, A. Andrejeva, W.D. Tuttle, I. Pugliesi, C. Schriever, and T.G. Wright, *J. Chem. Phys.*, **141**, 244315 (2015).

[10] A. Andrejeva, W.D. Tuttle, J.P. Harris, and T.G. Wright, *J. Chem. Phys.*, **143**, 104312 (2015).

[11] A. Andrejeva, W.D. Tuttle, J.P. Harris, and T.G. Wright, *J. Chem. Phys.*, **143**, 244320 (2016).

[12] D.J. Kemp, A.M. Gardner, W.D. Tuttle, J. Midgley, K.L. Reid, and T.G. Wright, *J. Chem. Phys.*, (submitted).

[13] G. Reiser, D. Rieger, T.G. Wright, K. Müller-Dethlefs, and E.W. Schlag, *J. Phys. Chem.*, **97**, 4335 (1993).

[14] D.J. Kemp, L.E. Whalley, W.D. Tuttle, A.M. Gardner, B.T. Speake, and T.G. Wright, *Phys. Chem. Chem. Phys.*, **20**, 12503 (2018).

[15] W.D. Tuttle, A.M. Gardner, and T.G. Wright, *Chem. Phys. Lett.*, **684**, 339 (2017).

[16] P. Butler, D.B. Moss, H. Yin, T.W. Schmidt, and S.H. Kable, *J. Chem. Phys.*, **127**, 094303 (2007).

[17] I. Pugliesi, N.M. Tonge, and M.C.R. Cockett, *J. Chem. Phys.*, **129**, 104303 (2008).

[18] Z.-Q. Zhao, C.S. Parmenter, D.B. Moss, A.J. Bradley, A.E.W. Knight, and K.G. Owens, *J. Chem. Phys.*, **96**, 6362 (1992).

6. Intermediate wavenumber region of *para*-fluorotoluene and *para*-xylene (600 – 900 cm^{-1})

Moving up in internal energy from the previous chapters, this chapter covers what will be termed the "intermediate" wavenumber range in this thesis. This region contains an expected bright transition, 9_0^1, and this chapter will discuss the assignment of other vibrations and vibration-torsion (vibtor) levels in this region, with the aid of zero-electron-kinetic-energy (ZEKE) photoelectron spectra recorded *via* many different intermediate levels. 9_0^1 is expected at around 790 – 820 cm^{-1} in the resonance-enhanced multiphoton ionisation (REMPI) spectra for the molecules discussed in this thesis (from the B3LYP/aug-cc-pVTZ calculations given in Table B.1 in Appendix B). Significant emphasis will be given to this region around the 9_0^1 transition, but first several much weaker features in *para*-fluorotoluene (*p*FT) will be considered, with the assignment of these being key to understanding higher wavenumber activity.

Before discussing any ZEKE spectra, consideration will be given to what might be expected in this wavenumber range for *p*FT and *para*-xylene (*p*Xyl), based on comparison to *para*-difluorobenzene (*p*DFB), *para*-chlorofluorobenzene (*p*ClFB) and the lower wavenumber spectra.

6.A. Expected vibrations in this wavenumber range

Figure 6.1 shows the REMPI spectra of *p*ClFB, *p*DFB, *p*FT and *p*Xyl up to 900 cm^{-1}, with the assignments below 600 cm^{-1} discussed in previous chapters. From 600 – 900 cm^{-1}, the assignments of the *p*ClFB spectrum come from the REMPI and ZEKE spectroscopy studies of our group[1,2]. The assignments of the *p*DFB spectrum come from the laser-induced fluorescence (LIF) and dispersed fluorescence (DF) work of Knight and Kable[3], as well as recent ZEKE work carried out by our group[4], with ZEKE spectra recorded *via* a larger number of S_1 intermediate levels than earlier ZEKE work[5].

In the *p*ClFB and *p*DFB cases, the activity in this region is dominated by the 9_0^1 transition, with 11_0^2 and 29_0^2 transitions also observed (overtones of the lower wavenumber ~400 cm^{-1} region discussed in the last chapter), as well as the 18_0^2 transition. Additionally, some combinations of lower wavenumber structure are observed, such as $11_0^1 14_0^2$. Based on the similarity of the lower wavenumber vibrational activity in all four of these REMPI spectra, one would then expect to observe the same activities in this region for *p*FT and *p*Xyl, with more observed transitions owing to the addition of the torsional levels in these cases.

For *p*FT, Okuyama *et al.*[6] reported an LIF spectrum over this region, labelling the two intense bands at ~800 cm^{-1} both as 9_0^1 (1_0^1 in the Wilson[7]/Varsányi[8] labelling schemes of that work), and the two weaker bands to higher wavenumber as 11_0^2 and 8_0^1 ($6a_0^2$ and $18a_0^1$ in that work). The D_8 vibration is expected at 954 cm^{-1}, based on the B3LYP/aug-cc-pVTZ calculations provided in Table B.1 in Appendix B, and so the latter assignment seems unlikely. In the REMPI and ZEKE study of Ayles *et al.*[9], these same assignments were given, but with the second of the two bands at ~800 cm^{-1} assigned as 10_0^1 (12_0^1 in that work, with D_{10} being the best correlation, from reference 10). This would be expected at ~700 cm^{-1} from the calculated vibrational wavenumbers, and so again seems unlikely. This band was assigned to 29_0^2 in the LIF and DF study of Zhao and Parmenter[11] and later, independently, by Davies and Reid[12] in their picosecond time-resolved photoelectron spectroscopy (tr-PES) study, and this reassignment will be confirmed herein.

Regarding the analogous region of *p*Xyl, there are two intense transitions at 0^0+775 cm^{-1} and 0^0+804 cm^{-1}. Walter *et al.*[13] and Zhang *et al.*[14] assigned both as these as 9_0^1 in their REMPI studies (1_0^1 in the Wilson[7]/Varsányi[8] notation of those papers), while Ebata *et al.*[15] assigned the 0^0+775 cm^{-1} band as 1_0^1 in their LIF study, again in the Wilson/Varsányi notation, and left the other band unassigned. Blease *et al.*[16], in their (1+1) REMPI spectrum, assigned the lower band as 9_0^1 (1_0^1 in their paper) and the higher one as 18_0^2 ($16b_0^2$ in their paper), and Gunzer and Grotemeyer[17] assigned the lower band as 9_0^1 (1_0^1 in their paper) on the basis of a mass-analysed threshold ionisation (MATI) spectrum recorded *via* this

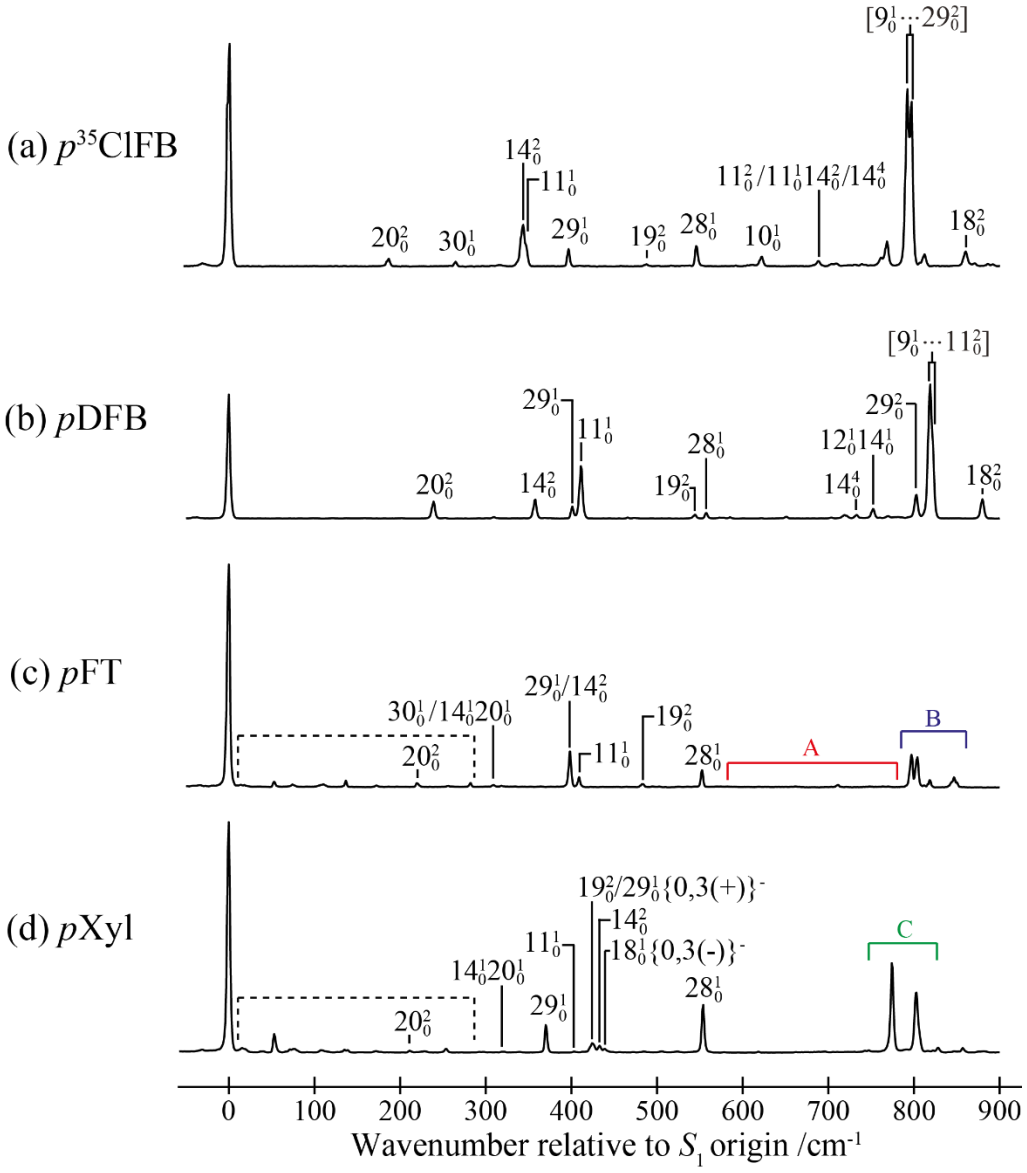


Figure 6.1 – The (a) p^{35}ClFB (b), pDFB (c) pFT and (d) pXyl $S_1 \leftarrow S_0$ REMPI spectra up to 900 cm^{-1} are shown. Below 600 cm^{-1}, the assignments are those discussed in the previous chapters, with the region from 600 – 900 cm^{-1} considered in this chapter for pFT and pXyl. For pDFB, the assignments are taken from Knight and Kable[3], and have been converted to ^pD_i labels from the Mulliken assignments given therein, as well as ZEKE work by our group[4]. For p^{35}ClFB, the assignments are taken from the published REMPI and ZEKE studies of our group[1,2].

feature, but left the higher band unassigned. Looking at the MATI spectra they recorded *via* these two features suggests that the two S_1 levels may be coupled.

Although there is substantial previous work on these reasonably intense $S_1 \leftarrow S_0$ transitions for both *p*FT and *p*Xyl, there is still some ambiguity regarding the

assignments of the transitions, and whether the S_1 levels are coupled. In *p*ClFB, there is some evidence that D_9 and $2D_{29}$ are coupled in the S_1 state[2] (a Fermi resonance), while for *p*DFB, Knight and Kable[3] suggested D_9 is in Fermi resonance with $2D_{11}$, a conclusion supported by our recent ZEKE study[4]. For *p*FT and *p*Xyl, the previous studies suggest that D_9 and $2D_{29}$ are coupled in *p*FT, while for *p*Xyl, combining the findings of the previous work, one would conclude that D_9 is in Fermi resonance with $2D_{18}$. This was proposed by Blease *et al.*[16], and will be confirmed in this thesis. This apparent difference in couplings between the molecules is an interesting point, as it suggests that the same vibration couples rather differently in different molecules, owing to the changing energetic proximities of the nearby levels. This will be returned to later in this chapter.

In this chapter, 2D-ZEKE spectra of the ~800 cm^{-1} region of *p*FT will be presented (labelled region B in Figure 6.1) and a selection of ZEKE spectra over the same region of *p*Xyl will be presented (labelled region C in Figure 6.1). Before that, however, there are some very weak features just below this in the *p*FT REMPI spectrum, from 580 – 780 cm^{-1}, for which assignments should be discussed (region A in Figure 6.1).

6.B. Region A: *para*-fluorotoluene 580 – 800 cm^{-1} features

6.B.1. Overview of ZEKE spectra

Figure 6.2 shows the REMPI spectrum recorded over the range 580 – 800 cm^{-1} for *p*FT, with increased laser power and under very cold conditions. One can see several very weak features, labelled a – i; for scale, band g is the one which is barely visible at 711 cm^{-1} in Figure 6.1(c). One might question the significance of such weak bands in understanding the couplings in *p*FT. However, it should be noted that most of these bands do not fit any expected fundamentals or combinations of intense lower wavenumber structure, and so it is expected that these bands arise owing to transitions to vibrational combinations and vibtor levels. As such, assigning these transitions may give more experimentally deduced vibrational fundamentals, thus making it easier to assign structure to

higher wavenumber accurately. Which vibtor levels are intrinsically bright in the $S_1 \leftarrow S_0$ excitation is a particularly important question, as it can help to predict the observed structure to higher wavenumber, or in other molecules. Briefly, it is noted that similar (although fewer) weak features were observed for *p*DFB in a similar spectral region by Knight and Kable[3], and in recent work by our group[4].

Before continuing, since this structure is found below, and relatively close in wavenumber to, the ~800 cm^{-1} intense features, it is possible that some of it is due to complexation with the argon carrier gas. However, REMPI spectra recorded around the S_1 origin under these conditions suggest that complexation is not significant in the presented REMPI trace, and thus the bands are due to the cold *p*FT molecule.

To assign these spectra, the vibrational fundamentals extracted from the lower wavenumber region (D_{11}, D_{14}, D_{19}, D_{20}, D_{28}, D_{29} and D_{30}, as well as the D_{18} value from the D_{18} m = 3(-) vibtor level, and later in this chapter from $2D_{18}$) for both the S_1 and D_0^+ states were used to look for simple overtone and combination bands. These experimental fundamentals were also combined with methyl torsion positions and the other (calculated) vibrational wavenumbers to estimate band positions for other transitions, and this list was used to assign the ZEKE spectra and thus the REMPI bands.

Finally, one should note that the baselines in these spectra are not flat – this is a manifestation of the UV changing over the range scanned and is particularly noticeable here owing to the weakness of the $S_1 \leftarrow S_0$ transitions being probed.

6.B.1.1. The uncoupled levels

Considering the ZEKE spectra in turn, the one recorded *via* the band at 0^0+606 cm^{-1} (labelled a) shows only a single transition with significant intensity, suggesting only a single $\Delta(v,m) = 0$ transition, and thus only a single contribution to the REMPI band. This ZEKE transition is at the correct wavenumber for $28^1 m^{3(+)}$, leading to an assignment of the REMPI band of $28_0^1 m_0^{3(+)}$, which is

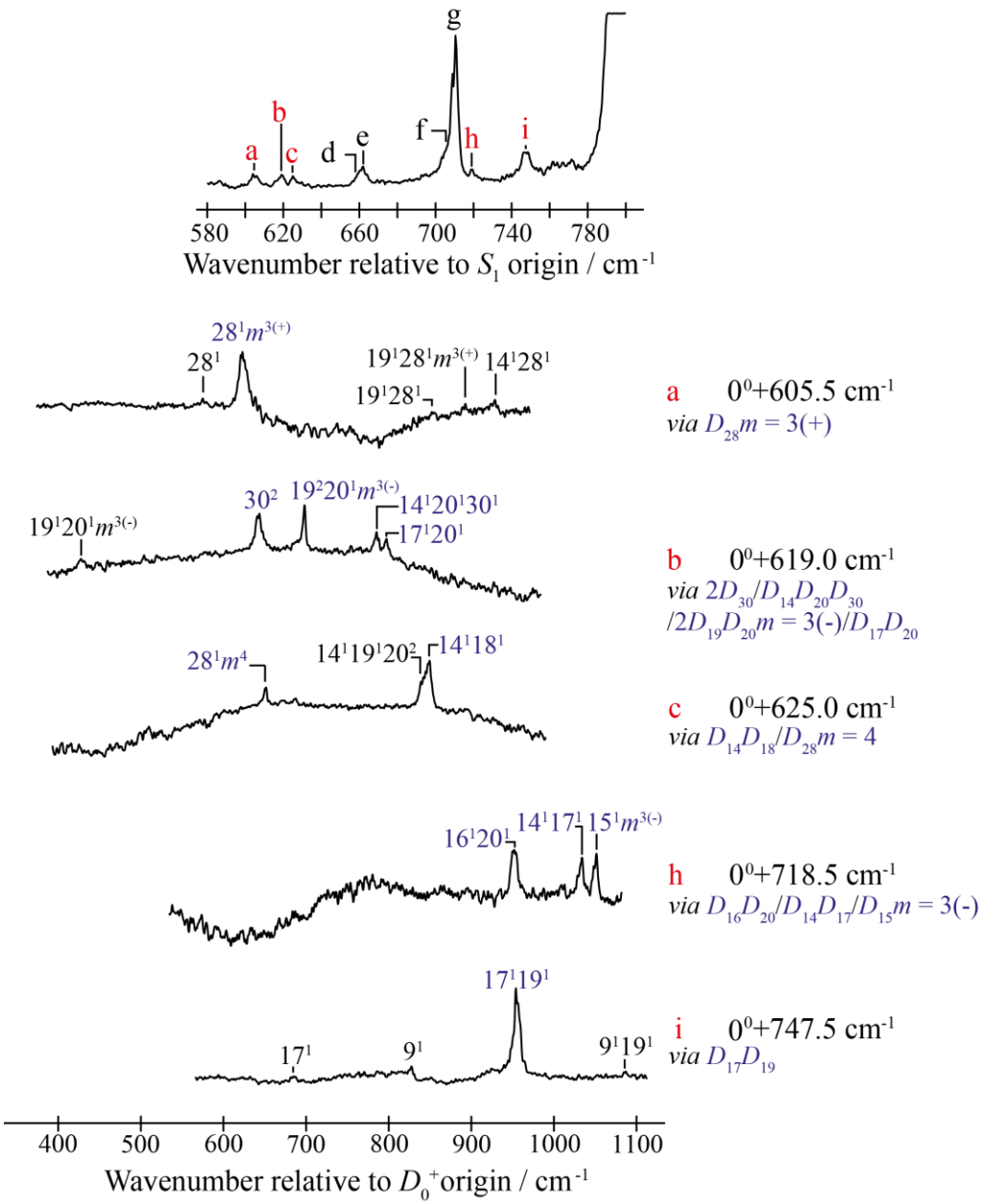


Figure 6.2 – The top trace shows the pFT REMPI spectrum, recorded with increased laser power, over the region 580 – 800 cm^{-1}. The letters indicate excitation positions at which ZEKE spectra were recorded, with ZEKE spectra recorded via the positions a, b, c, h and i shown in this figure. Those recorded via d, e, f and g are shown in Figure 6.3. The blue transitions labels on the ZEKE spectra indicate proposed Δ(v,m) = 0 transitions.

totally symmetric and therefore symmetry-allowed. Also observed in this ZEKE spectrum are a selection of other transitions involving D_{28}, such as $19^128^1m^{3(+)}$.

Interestingly, the analogous $29_0^1 m_0^{3(+)}$, expected at 455 cm^{-1} in the REMPI spectrum, does not appear to be observed, although the $29_0^1 m_{\{0,0\}}^{\{0,3(+)\}^-}$ was observed for *p*Xyl in Chapter 5, where $D_{29}\{0,3(+)\}^-$ was postulated to be a dark state gaining intensity through coupling to $2D_{19}$. As to whether the analogous $28_0^1 m_{\{0,0\}}^{\{0,3(+)\}^-}$ is observed in *p*Xyl, no attempt was made to record ZEKE spectra *via* the weak features between the intense bands at 554 and 775 cm^{-1}, owing to the increased difficulty in obtaining the *p*Xyl spectra, and so no definitive conclusion can be drawn, but there is no obvious band at the correct wavenumber to be assigned to this.

Owing to the weakness of the $28_0^1 m_0^{3(+)}$ band here in *p*FT (and the absence of $29_0^1 m_0^{3(+)}$), it seems that transitions to these a_1''/a_4'' symmetry vibrations for *p*FT/*p*Xyl, in combination with "m = 3(+)", are usually very weak, with the exception being the $29_0^1 m_{\{0,0\}}^{\{0,3(+)\}^-}$ transition in *p*Xyl with its intensity owed to coupling to a much brighter level.

Moving on to the band at 0^0+619 cm^{-1} (labelled b), there are now multiple transitions with reasonable intensity, suggesting multiple $\Delta(v,m) = 0$ transitions. The ZEKE transition at 644 cm^{-1} may be assigned as 30^2, which would be expected ~622 cm^{-1} in the S_1 state, suggesting that this is a $\Delta(v,m) = 0$ transition. There is another intense ZEKE band at 698 cm^{-1}, which fits well the position of 14^2, but this would not fit a $\Delta(v,m) = 0$ transition, and this band appears to be too intense to simply be symmetry-allowed, suggesting an alternative assignment is required. Somewhat surprisingly, this ZEKE band matches the transition $19^2 20^1 m^{3(-)}$, and this is also in reasonable agreement with the S_1 band position[a], suggesting another $\Delta(v,m) = 0$ transition. Supporting this is the observation of the $19^1 20^1 m^{3(-)}$ band in the ZEKE spectrum, i.e. a Δv = -1 transition, with such transitions observed in many ZEKE spectra for *p*FT. Note that both of these $\Delta(v,m) = 0$ assignments are totally symmetric, but there is no

[a] Note that the precise value for this this depends on how one estimates the S_1 position; using the obtained D_{20} and free rotor m = 3(-) values or using the D_{20} m = 3(-) band position.

evidence that they are interacting significantly, in line with the large difference in vibrational (and torsional) quanta between the two levels.

Finally, there are two weak bands at 786 and 798 cm^{-1} in this ZEKE spectrum. No symmetry-allowed assignments that would be expected to have significant intensity could be found for these, suggesting yet more $\Delta(v,m) = 0$ transitions. For the 786 cm^{-1} band, the assignment $14^1 20^1 30^1$ is proposed, with the wavenumber for $D_{14}D_{20}D_{30}$ in good agreement with the experimental values in both the S_1 and D_0^+ states. Thus, it appears that this REMPI band comprises a combination and overtones of the coincident features at 0^0+311 cm^{-1}, which were assigned as 30_0^1 and $14_0^1 20_0^1$. Since the 30^2 and $14^1 20^1 30^1$ have been observed in the ZEKE spectrum, one may also expect $14^2 20^2$ at ~920 cm^{-1}. There is an inkling of a feature at 926 cm^{-1}, but it is extremely weak and so its assignment is very tentative.

The 798 cm^{-1} band fits reasonably well an assignment to the transition $17^1 20^1$, with the obtained experimental D_{17} value being 685 cm^{-1} for D_0^+, compared to 671 cm^{-1} for the B3LYP/aug-cc-pVTZ calculated value. It should be noted that the agreement of the experimental values with the calculations for the out-of-plane vibrations appears to be poorer than for the in-plane vibrations, perhaps owing to stronger vibration-torsion coupling for the out-of-plane vibrations. The $17_0^1 20_0^1$ assignment would also fit in the S_1 state, with a difference between the experimental D_{17} (obtained from this band as 509 cm^{-1}) and the calculated value (538 cm^{-1}); this value for D_{17} agrees with the proposed $17_0^1 m_0^{3(-)}$ assignment discussed at the end of Chapter 5, and it will be shown later that this assignment also agrees with the value for D_{17} obtained from another transition, putting this assignment on a surer footing.

In summary, the band at 0^0+619 cm^{-1} appears to be composed, remarkably, of four different contributions: 30_0^2, $19_0^2 20_0^1 m_0^{3(-)}$, $14_0^1 20_0^1 30_0^1$ and $17_0^1 20_0^1$, with $\Delta(v,m) = 0$ transitions observed for all of these in the ZEKE spectrum.

In the ZEKE spectrum recorded *via* the band at 0^0+625 cm^{-1} (labelled c in Figure 6.2), there is a band at 652 cm^{-1}, and a broad feature at 842 – 850 cm^{-1}. Although the REMPI band would match the position of 11^120^2, none of the ZEKE bands do, negating this assignment. The 652 cm^{-1} ZEKE band matches most closely the 28^1m^4 transition, which would also be consistent with the S_1 wavenumber of $28_0^1m_1^4$. The transition 14^118^1 is expected within the broad ZEKE feature, based on the D_{18} fundamental extracted in the S_1 and D_0^+ states from $2D_{18}$ later in this chapter, and in agreement with the D_{18} value in the S_1 state from D_{18} m = 3(-)[b]. Accepting this assignment means that this is then a $\Delta(v,m) = 0$ transition, implying the REMPI band has a $14_0^118_0^1$ contribution, similar to the observation of $14_0^120_0^1$ in the low wavenumber region of *p*FT (and possibly *p*Xyl). The breadth of the 842 – 850 cm^{-1} ZEKE band is proposed to come from another transition, $14^119^120^2$, alongside 14^118^1. This does not match a $\Delta(v,m) = 0$ transition as it would not be in the correct place in the S_1 state, but the transition appears particularly intense in the ZEKE spectrum, suggesting it is not simply symmetry-allowed from the $D_{14}D_{18}$ initial level. Thus, it is hypothesised that these two levels could be coupled in the cation. In summary, it is proposed that the REMPI band at 0^0+625 cm^{-1} is composed of the symmetry-allowed transition $28_0^1m_1^4$ and the vibronically allowed transition $14_0^118_0^1$.

Skipping the ZEKE spectra *via* position d – g for now, as these are all related and discussed together in the next section, the ZEKE spectrum recorded *via* the very weak band at 0^0+719 cm^{-1} (labelled h) shows three transitions of similar intensity at 952, 1034 and 1052 cm^{-1}. In the ZEKE spectrum *via* the weak band at 0^0+748 cm^{-1} (labelled i), the 952 cm^{-1} band dominates the activity, suggesting that these two S_1 levels could be coupled. However, this single ZEKE band would be the only shared activity between the spectra, and it is thus suggested that the band being in the same position is coincidental, and the intermediate levels are unrelated. In the case of the ZEKE spectrum at position i, this 952 cm^{-1}

[b] Although the value for D_{18} in the S_1 state is not in good agreement with the calculated value, the same value can be obtained from multiple REMPI bands which have D_{18} contributions, and the bands observed match the activity in other molecules and the low wavenumber regions, suggesting that the experimental value is secure.

$\Delta(v,m) = 0$ band can be readily assigned as $17^1 19^1$, which fits in both the S_1 and D_0^+ states, suggesting that REMPI band is dominated by $17_0^1 19_0^1$. This assignment gives very similar values for D_{17} in the S_1 and D_0^+ states as extracted earlier from $17^1 20^1$ when exciting at 0^0+619 cm^{-1}.

The 952 cm^{-1} band in the ZEKE spectrum at position h is then assigned as a different $\Delta(v,m) = 0$ transition, $16^1 20^1$, which gives a value of D_{16} in the S_1 state of 609 cm^{-1} and in the D_0^+ state of 841 cm^{-1}, in reasonable agreement with the calculated value for the cation but with poorer agreement in the S_1 state. This is likely for the same reasons discussed for D_{17} above, and it seems to be the case for most of the out-of-plane modes. The other two bands in this ZEKE spectrum then match $14^1 17^1$ and $15^1 m^{3(-)}$. $14^1 17^1$ fits the 1034 cm^{-1} band very well in the cation, but from the D_{17} fundamental obtained earlier, would be expected ~10 cm^{-1} lower than this excitation position in the S_1 state. However, such an intense transition would not be expected unless it were a $\Delta(v,m) = 0$, and so it is tentatively assigned as such, possibly interacting with a level to lower wavenumber perturbing it to this higher position. Finally, the 1052 cm^{-1} band can be readily assigned to $15^1 m^{3(-)}$, and again this is not expected to have significant intensity in the ZEKE spectrum solely on the grounds of it being symmetry-allowed, and it is suggested that this is another $\Delta(v,m) = 0$ band. This would give D_{15} in the S_1 state as 682 cm^{-1} and in D_0^+ as 1007 cm^{-1}, in good agreement with the calculated values.

In summary, the REMPI band at 0^0+719 cm^{-1} is thought to be composed of three transitions, $16_0^1 20_0^1$, $14_0^1 17_0^1$ and $15_0^1 m_0^{3(-)}$, while the REMPI band at 0^0+748 cm^{-1} is thought to arise owing to $17_0^1 19_0^1$. Note that the assignment of $15_0^1 m_0^{3(-)}$, while the only current assignment containing D_{15}, is thought to be secure owing to the observation of all of the other a_2'' vibrations with m = 3(-); the only one not assigned so far, $16_0^1 m_0^{3(-)}$, will be discussed in the next section.

6.B.1.2. The coupled levels

Figure 6.3 shows the ZEKE spectra recorded at positions d – g, *via* two bands, 0^0+662 cm^{-1} and 0^0+711 cm^{-1}. Traces d and e were recorded *via* the 0^0+662 cm^{-1} band and show similar activity, while traces f and g were recorded *via* the 0^0+711 cm^{-1} band and show similar activity. Additionally, there seems to be shared structure across all four spectra, suggesting the terminating levels of the two REMPI bands are interacting.

Treating traces d and e first, the primary difference is the increased intensity of the ~719 cm^{-1} and ~728 cm^{-1} ZEKE bands in trace d relative to trace e. However, the overall activities seem very similar, with the broadening of bands in trace d compared to trace e thought to be attributable to excitation a different part of the rotational profile, similar to the broadening discussed in Chapter 3 when exciting *via* the m = 3(+) level. Thus, trace e will be discussed, with the derived assignments applicable to both.

The two most intense ZEKE features, at 684 cm^{-1} and 769 cm^{-1}, are of almost equal intensity, suggesting they are both $\Delta(v,m) = 0$ transitions, and/or the initial levels could be coupled to one another. The lower one can be assigned as $20^2 29^1 m^{3(+)}$, which fits well the position in the cation, but would be expected at 675 cm^{-1} in the S_1 state, rather than the 662 cm^{-1} excitation position. This is indicative of being coupled to a higher level and being perturbed to lower wavenumber, which would also be a possible explanation for observing $20^2 29^1 m^{3(+)}$ for *p*FT but not obviously observing $29^1 m^{3(+)}$, as the current assignment could be a dark state gaining its intensity through coupling. The 769 cm^{-1} ZEKE band can be assigned readily as $18^1 19^1$, which again might be expected to slightly higher wavenumber in the S_1 state, but is assigned as a second $\Delta(v,m) = 0$ transition. The 18^1 band is also observed in traces d and e, which would be the commonly observed $\Delta v = -1$ component band, supporting this assignment.

The 719 cm^{-1} ZEKE band is in reasonable agreement with the position for 10^1 in the cation, but its wavenumber in the S_1 state does not match a $\Delta(v,m) = 0$

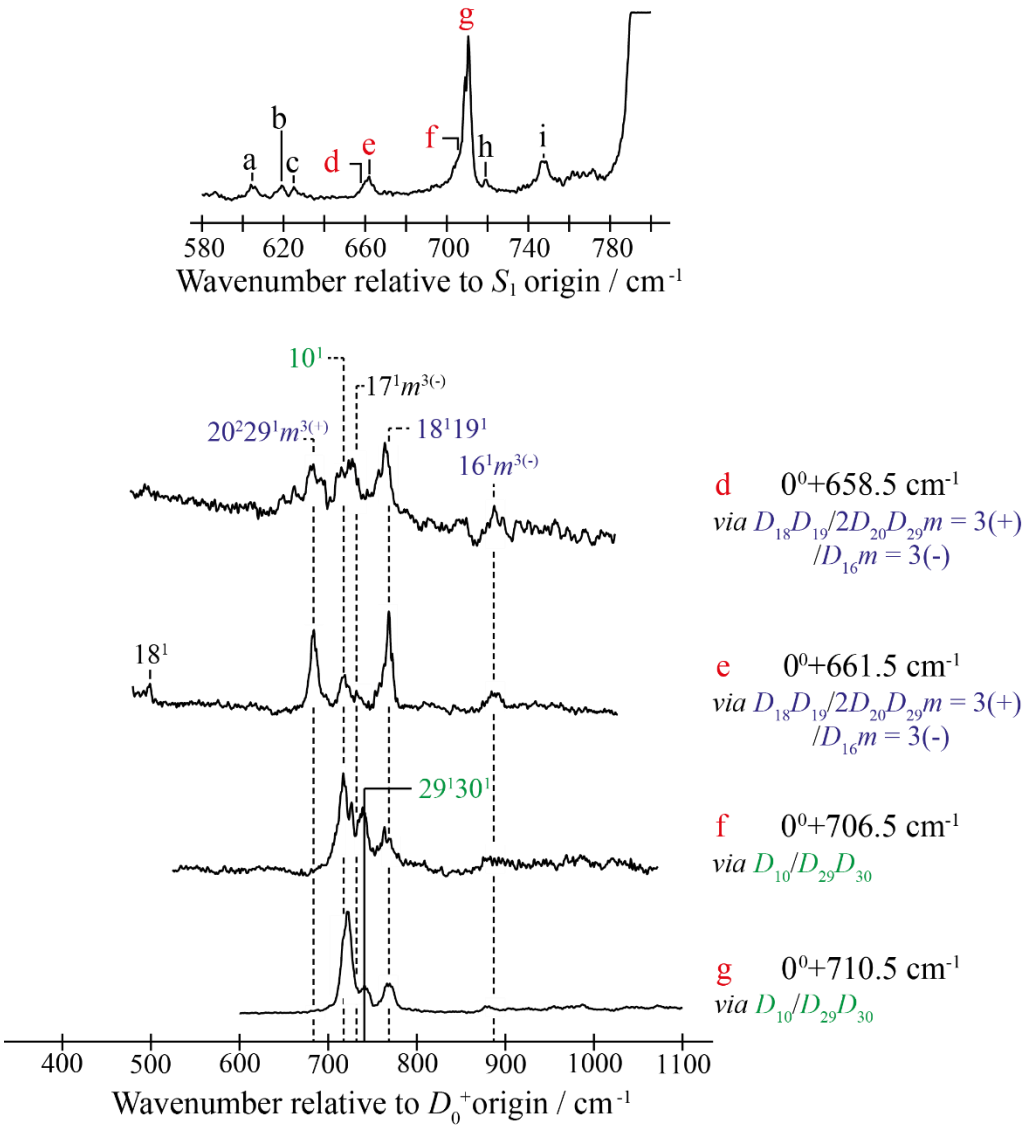


Figure 6.3 – The top trace shows the REMPI spectrum, recorded with increased laser power, over the region 580 – 800 cm^{-1} in pFT. The letters indicate excitation positions at which ZEKE spectra were recorded, with ZEKE spectra recorded via the positions d, e, f and g shown in this figure. Those recorded via a, b, c, h and i are shown in Figure 6.2. The blue and green transitions labels on the ZEKE spectra indicate proposed Δ(v,m) = 0 transitions, with the blue being Δ(v,m) = 0 transitions from the 0^0+662 cm^{-1} REMPI band and the green being Δ(v,m) = 0 transitions from the 0^0+711 cm^{-1} REMPI band.

transition; this will be returned to shortly. The 728 cm^{-1} ZEKE band assignment is less certain, and is thought to arise owing to symmetry-allowed activity from

one of the initial levels, $2D_{20}D_{29}$ m = 3(+) or $D_{18}D_{19}$. One possible assignment is $17^1m^{3(-)}$.[c]

Finally, the feature at 885 cm^{-1} fits a transition to 11^2 at first glance, but this is thought to be at ~881 cm^{-1} from other ZEKE spectra, discussed later in this chapter; indeed, the band to slightly lower wavenumber at ~881 cm^{-1} in Figure 6.3 traces f and g is thought to be 11^2, and clearly does not line up with the ZEKE band under discussion. As such, an alternative assignment was sought, with $16^1m^{3(-)}$ being the most sensible assignment found, as a $\Delta(v,m) = 0$ transition, and this agrees with the value of D_{16} obtained in the cation from $D_{16}D_{20}$. However, based on the previously obtained S_1 value, $16_0^1m_0^{3(-)}$ would be expected in the REMPI spectrum at ~646 cm^{-1}, significantly below this band.

There are two obvious explanations for this. Either D_{16} m = 3(-) is coupled to the $D_{18}D_{19}$ (or $2D_{20}D_{29}$ m = 3(+)) level and is actually to lower wavenumber in the S_1 state, or $D_{16}D_{20}$ is perturbed in the S_1 state. As there is no evidence of another REMPI band to lower wavenumber that would match $16_0^1m_0^{3(-)}$, it is suggested that $D_{16}D_{20}$ is perturbed to lower wavenumber and thus gives an artificially low D_{16} value; it could be perturbed by the intense D_9 transition to higher wavenumber, but the signal-to-noise ratio of the ZEKE spectrum does not allow any further conclusions to be drawn.

In summary, the suggested assignments for the 0^0+662 cm^{-1} REMPI band are $18_0^119_0^1$, $20_0^229_0^1m_0^{3(+)}$ and $16_0^1m_0^{3(-)}$, based on the ZEKE activity, with $17^1m^{3(-)}$ also observed in the ZEKE spectrum, perhaps as symmetry-allowed activity from D_{16} m = 3(-).

Moving on to traces f and g, recorded *via* the 0^0+711 cm^1 band, one can again see similar activity in the two traces, with slightly broader features in trace f, likely owing to exciting high-lying rotational levels, and an additional narrow, sharp, ZEKE feature at 727 cm^{-1}, again thought to be due to rotational effects.

[c] Note that this was thought to be observed to much lower wavenumber in the S_1 state, as discussed in Chapter 5, and so must be symmetry-allowed and not a $\Delta(v,m) = 0$ transition.

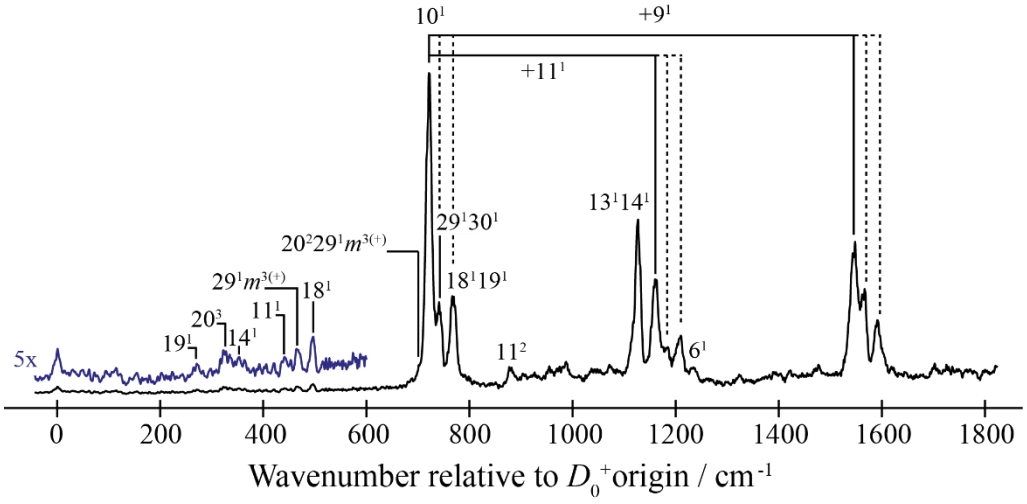


Figure 6.4 – pFT ZEKE spectrum recorded at 0^0+710.5 cm^{-1} (trace g in Figure 6.3), showing the dominant structure.

Both spectra are dominated by the ZEKE band at 721 cm^{-1}, which was assigned as 10^1 in the traces d and e above, where it was weaker. Here, it fits as a $\Delta(v,m) = 0$ transition, and so the REMPI band is assigned as 10^1_0. It is notable that in *p*ClFB, a REMPI band was also assigned to 10^1_0, and this is consistent with that, while in *p*DFB and *p*Xyl, D_{10} is no longer totally symmetric, which explains its absence in those molecules.

The ZEKE transition at 739 cm^{-1} matches the 29^130^1 transition, which would also fit in the S_1 state, and so be another $\Delta(v,m) = 0$ transition. The band at 770 cm^{-1} matches 18^119^1, as assigned in traces d and e. Note that in traces f and g, 10^1 dominates while 18^119^1 is weaker, while in traces d and e 18^119^1 dominates, with a weaker 10^1 transition. This suggests that D_{10} and $D_{18}D_{19}$ are in Fermi Resonance in the S_1 state. It is possible that $2D_{20}D_{29}$ m = 3(+) is also coupled to D_{10}, but it appears only weakly (if at all) in the ZEKE spectra *via* D_{10}, suggesting this coupling is, at most, small. This Fermi resonance is somewhat complicated by the overlap of $D_{29}D_{30}$ with D_{10} in the S_1 state, which does not appear to be involved in the coupling, and by the overlap of D_{16} m = 3(-) with $D_{18}D_{19}$, which again doesn't appear to be involved in the coupling.

Owing to the good signal-to-noise ratio of the ZEKE spectrum recorded at 0^0+711 cm^{-1}, a spectrum was recorded over a higher wavenumber range, and this is shown in Figure 6.4. The most intense structure is labelled, and is mostly the

expected $\Delta(v,m) = 0$ bands, plus combinations with D_{11} and D_9 to higher wavenumber. However, a reasonably intense transition is observed at 1127 cm^{-1}, with the most sensible assignment being to the $13^1 14^1$ transition, which fits as a $\Delta(v,m) = 0$ transition, yielding a D_{13} value of 512 cm^{-1} and 778 cm^{-1} in the S_1 and D_0^+ states respectively. This is tentative currently, as it is not known how reliable the D_{13} calculated value is in the S_1 state, and the agreement with the calculation is poor.

To lower wavenumber in Figure 6.4, there are some very weak transitions. One can see the 19^1 and 14^1 transitions, which were observed in the origin ZEKE spectrum, as well as 18^1 (perhaps a $\Delta v = -1$ band, owing to the coupling between D_{10} and $D_{18}D_{19}$). 11^1 is observed weakly, presumably on Franck-Condon grounds (one might note that D_{10} was not observed in the ZEKE spectrum recorded *via* D_{11}, suggesting the Franck-Condon overlap for these vibrations is poor), and apparently the totally symmetric $29^1 m^{3(+)}$ is also observed, a potential indicator of coupling between D_{10} and $2D_{20}D_{29}$ $m = 3(+)$.

To summarise the surprisingly complex finding for the REMPI bands at 0^0+662 cm^{-1} and 0^0+711 cm^{-1}, the former is composed of $18_0^1 19_0^1$, $20_0^2 29_0^1 m_0^{3(+)}$ and $16_0^1 m_0^{3(-)}$, while the latter is composed of 10_0^1, $29_0^1 30_0^1$ and $13_0^1 14_0^1$. The ZEKE spectra suggest that $D_{18}D_{19}$ and D_{10} are coupled, and perhaps also that $2D_{20}D_{29}$ $m = 3(+)$ forms part of this coupling.

6.B.2. Discussion

One might immediately note the sheer number of $\Delta(v,m) = 0$ transitions found *via* some of these very weak bands. A simple density of states calculation over the range 580 – 780 cm^{-1} (using the same method as in Chapter 7, including up to 4 quanta of vibration and up to $m = 7$) suggests that there are 54 a_1' symmetry levels in this range, and 100 e'' symmetry levels, all of which would (in theory) be accessible from the S_0 $m = 0$ (a_1') or $m = 1$ (e'') levels. Of course, not all of these will have intensity, and additionally there will be the a_1'' levels (of which there are 52) and e' levels (of which there are 101) observable by vibronic

coupling. This gives 307 theoretically accessible S_1 terminating levels in this region, and only a handful of these are observed, owing to a combination of intrinsic intensities, coincident transitions, and couplings.

As to the nature of the transitions observed, they involve many out-of-plane vibrational combinations, $D_{17}D_{20}$, $D_{17}D_{19}$, $D_{16}D_{20}$, $D_{14}D_{18}$, $D_{14}D_{17}$, $D_{18}D_{19}$ and $D_{13}D_{14}$, which are either symmetry-allowed or vibronically allowed, and this mirrors similar combinations observed for other molecules such as *p*DFB and *p*ClFB.[1–4] Additionally, transitions to D_{16} m = 3(-) and D_{15} m = 3(-) were assigned in the REMPI spectrum, consistent with the assignment of D_{20} m = 3(-) and D_{19} m = 3(-) in the low wavenumber region. Although no ZEKE spectra were recorded *via* them, D_{17} m = 3(-) and D_{18} m = 3(-) were assigned in the REMPI spectrum in Chapter 5; thus, all a_2'' vibrations with the m = 3(-) (totally symmetric overall) have now been observed. This is an observation to bear in mind for future studies looking at methyl rotor-containing systems, as these transitions appear to have intrinsic intensity. Additionally, the observation of these vibtor bands, and combination bands containing out-of-plane vibrations, has allowed all a_2'' vibrational fundamentals and one additional a_2' fundamental to be obtained experimentally. These are of importance in accurately assigning the higher wavenumber structure, where coupling is more prevalent, and illustrate the importance of persevering with the recording of these ZEKE spectra *via* very weak intermediates.

Although this section discussed such transitions in *p*FT, it should be noted that fewer of the analogous transitions have been assigned in *p*Xyl. It was more difficult to record the *para*-xylene ZEKE spectra, and the signal-to-noise ratio of those recorded is often poorer than for *p*FT. As such, it seems likely that such transitions to D_{14} through D_{20} vibrational combination bands, and D_{15} through D_{17} combinations with "m = 3(-)", could also be present in *p*Xyl, but they are harder to discern in the present study.

6.C. Region B: *para*-fluorotoluene 800 – 850 cm^{-1} features

Having discussed the weak features which comprise Region A, the intense features in Region B, shown in Figure 6.1, will now be addressed. Summarising the previous work discussed above, the two intense transitions at 0^0+797 cm^{-1} and 0^0+804 cm^{-1} have previously been assigned as 9^1 and 29^2 (with an earlier assignment of 10^1 for the latter, which has been assigned elsewhere in this thesis), the 0^0+818 cm^{-1} feature as 11^2, and the 0^0+846 cm^{-1} band as 8^1. Each of these bands will be discussed in turn.

6.C.1. Overview of ZEKE spectra

6.C.1.1. The 0^0+797 cm^{-1} and 0^0+804 cm^{-1} bands

6.C.1.1.1 Dominant transitions

Starting with the two bands previously assigned as 9^1 and 29^2, Figure 6.5 shows a "2D-ZEKE" spectrum comprising five ZEKE spectra (j – n) recorded over the 0^0+797 cm^{-1} band from 793.8 to 798.6 cm^{-1}. At the top of the figure is an overview of this region of the REMPI spectrum, illustrating the band being excited, and on the right of the figure this REMPI band is again presented, with the ZEKE spectra linked to their excitation positions with dashed lines.

Figure 6.6 shows a "2D-ZEKE" spectrum comprising six ZEKE spectra (o – t) recorded over the 0^0+804 cm^{-1} band from 800.6 to 810.8 cm^{-1}. At the top of the figure is an overview of this region of the REMPI spectrum, illustrating the band being excited, and on the right of the figure this REMPI band is again presented, with the ZEKE spectra linked to their excitation positions with dashed lines.

All of the traces (j – n) recorded *via* the 0^0+797 cm^{-1} band show very similar dominating, $\Delta(v,m) = 0$, structure in the ZEKE spectra, with two intense bands at 824 and 837 cm^{-1}. In the cation, D_9 is expected at 811 cm^{-1} based on the calculated value, while the fundamental for D_{29} is known experimentally as 414 cm^{-1}, placing the $2D_{29}$ overtone at 828 cm^{-1}. Based on the comparison to

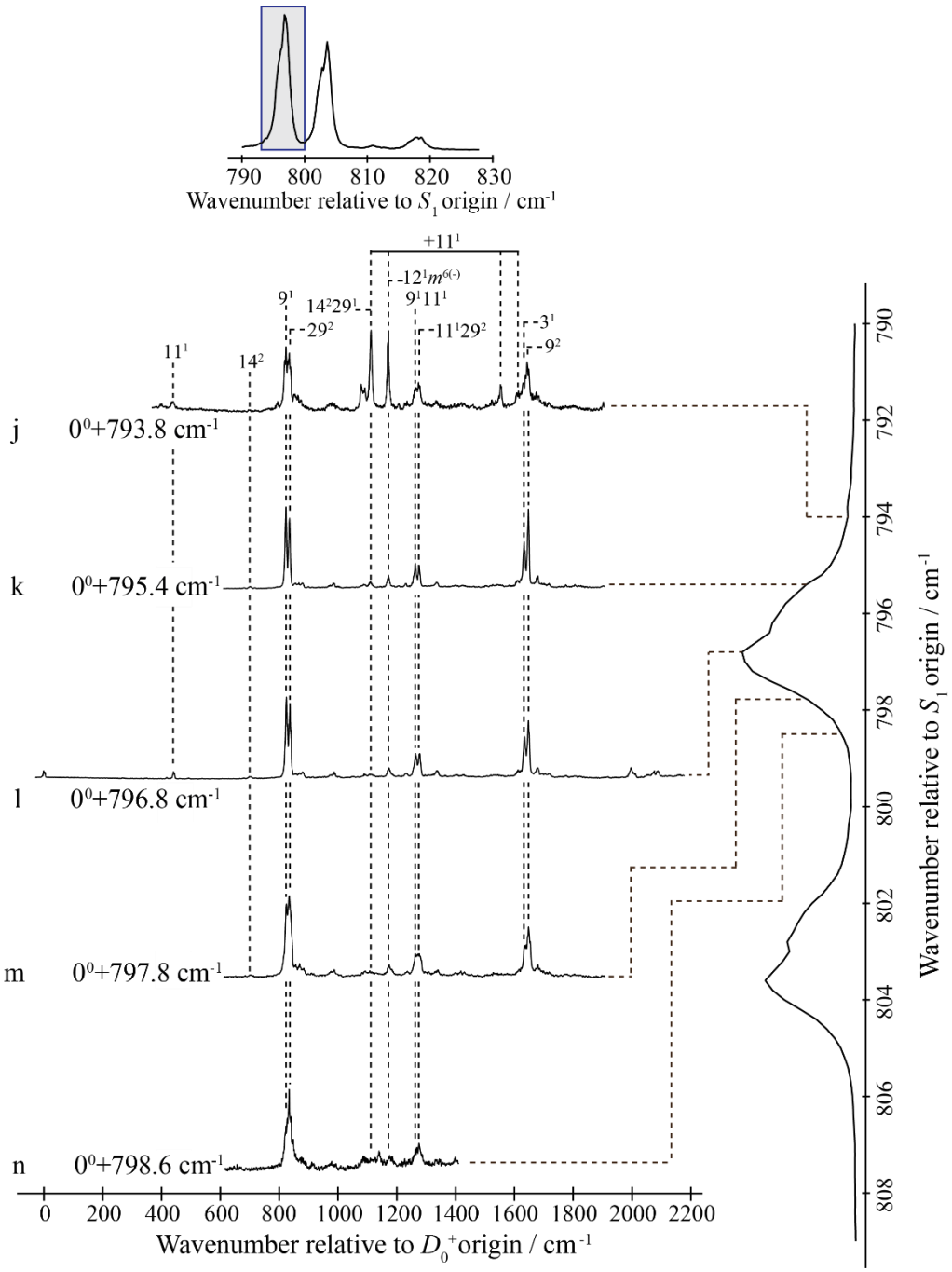


Figure 6.5 – A "2D-ZEKE" spectrum comprising ZEKE spectra recorded at excitation wavenumbers across the range 792 to 800 cm^{-1}, with the individual ZEKE spectra given in traces j – n. The right hand vertical trace and the top trace illustrate the relevant region of the REMPI spectrum. Each ZEKE trace is normalised to the most intense feature in that trace.

*p*DFB and *p*ClFB, 9_0^1 is expected to have significant intensity in the REMPI spectrum, and the previous work from Zhao and Parmenter[11] and Davies and Reid[12] suggest that the 29_0^2 transition is also contributing in this region. As such, these two ZEKE bands are assigned as 9^1 (at 824 cm^{-1}) and 29^2 (at 837 cm^{-1}).

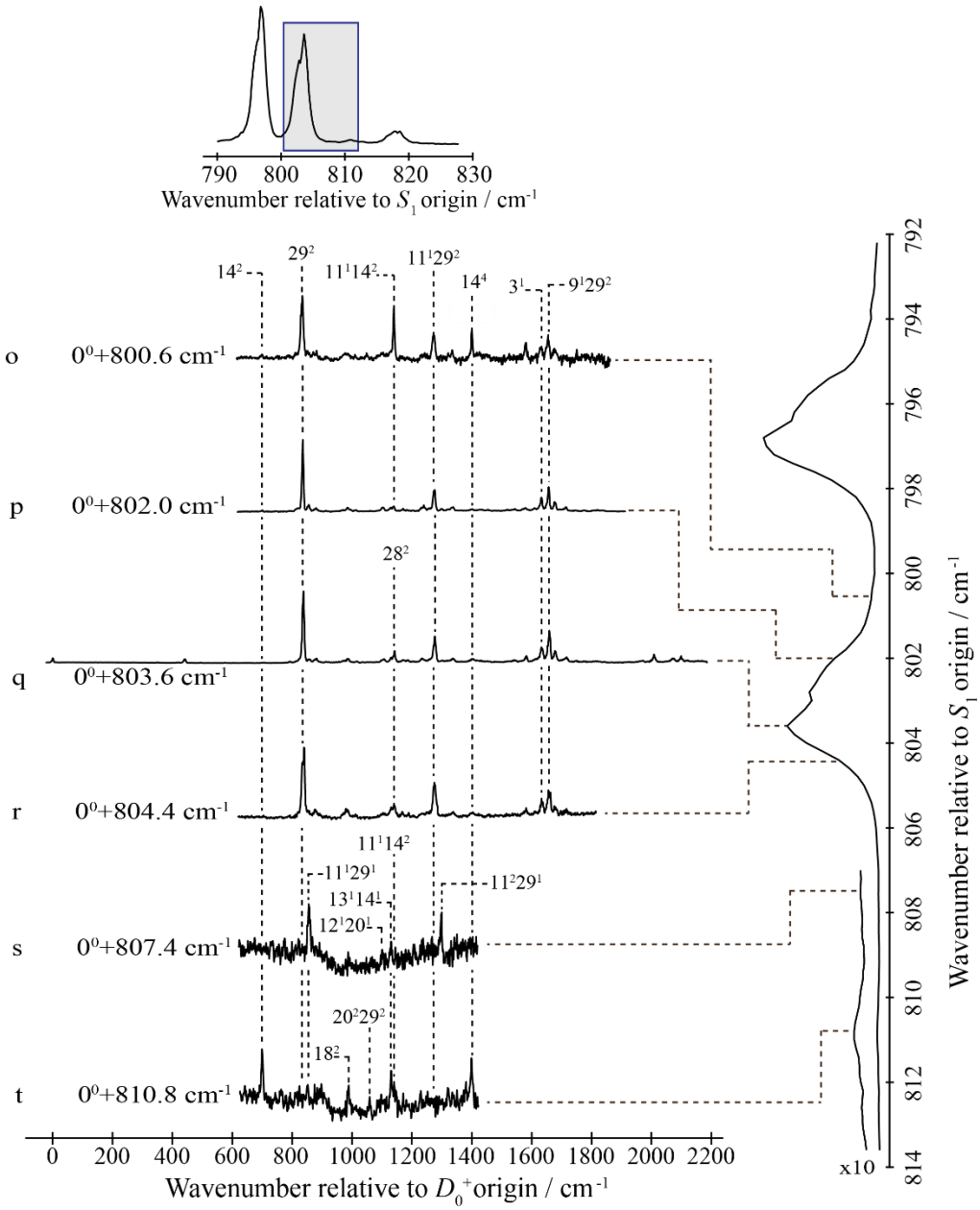


Figure 6.6 – A "2D-ZEKE" spectrum comprising ZEKE spectra recorded at excitation wavenumbers across the range 800 to 812 cm^{-1}, with the individual ZEKE spectra given in traces o – t. The right hand vertical trace and the top trace illustrate the relevant region of the REMPI spectrum. Each ZEKE trace is normalised to the most intense feature in that trace.

Thus, $2D_{29}$ is higher than predicted in the cation from its fundamental, perhaps owing to interaction with D_9 in the cation. At this point, the appearance of both 9^1 and 29^2 ZEKE bands with significant intensity when exciting *via* the 0^0+797 cm^{-1} band could imply that the two levels are overlapped in the S_1 state and so both are being excited, or that the two levels are coupled in the S_1 state (or the cation).

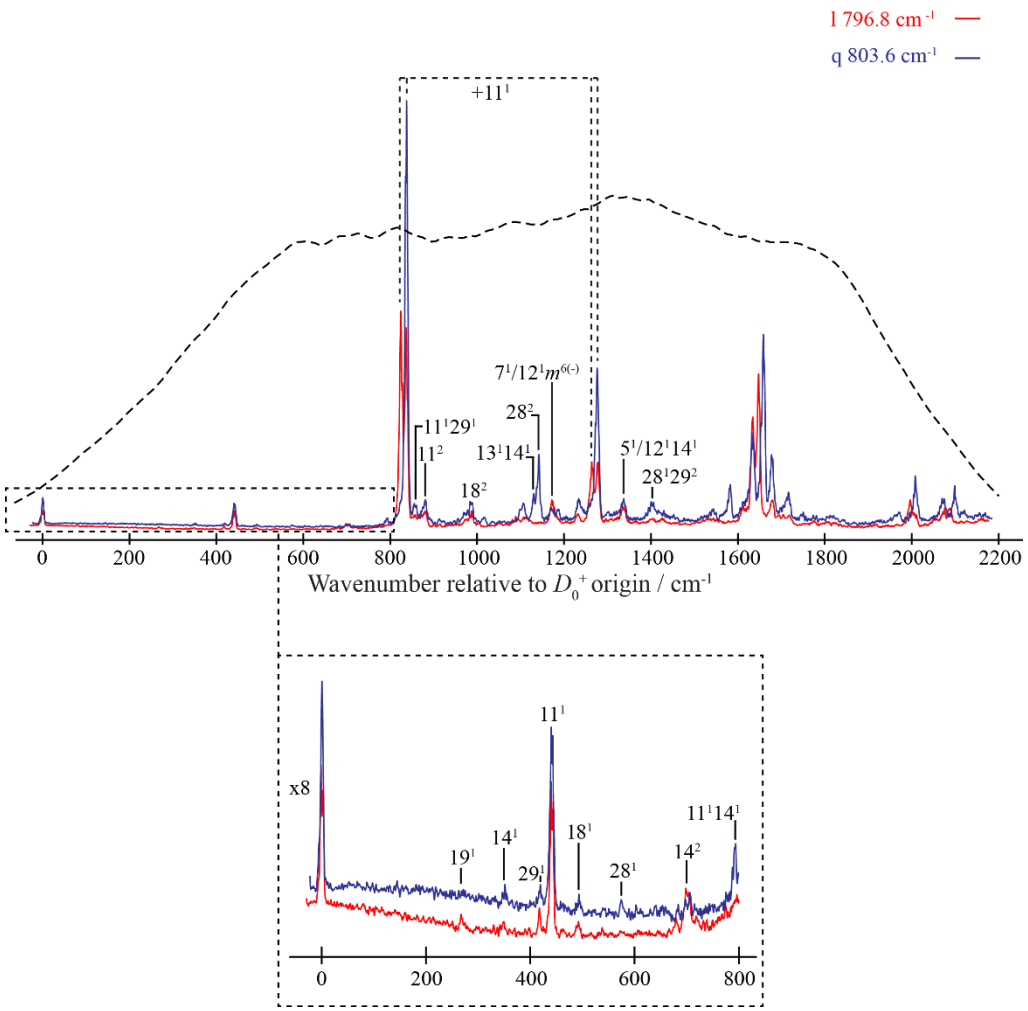


Figure 6.7 – Comparison of the ZEKE spectra recorded via the centres of the 797 and 804 cm^{-1} REMPI bands, showing the unnormalized traces. These were recorded on the same day under the same conditions, and so the relative intensities between the two traces are representative. Additionally, the changing UV intensity as the laser is scanned over this region is presented as a black dashed line.

Considering the ZEKE spectra recorded *via* the 0^0+804 cm^{-1} band shown in Figure 6.6, here only one intense transition rather than two dominates all of the ZEKE spectra, and this is at 837 cm^{-1}, i.e. the 29^2 transition. The 824 cm^{-1} ZEKE band assigned to 9^1 appears, at best, only very weakly as a shoulder on the low wavenumber side of this 29^2 band. At first glance then, these ZEKE spectra give a confusing picture, suggesting that the REMPI band at 0^0+797 cm^{-1} is dominated by both D_9 and $2D_{29}$ and the one at 0^0+803 cm^{-1} is dominated only by $2D_{29}$. This implies that $2D_{29}$ contributes to both bands, something it could only do if coupled to D_9, and in that case one would expect D_9 to appear in both

ZEKE spectra too. To shed some light on this, one can look at the unnormalized ZEKE spectra, rather than the normalised ones presented in Figures 6.5 and 6.6.

Figure 6.7 shows two unnormalized and unscaled ZEKE traces recorded at the centres of the 0^0+797 cm^{-1} and 0^0+804 cm^{-1} bands. As these two ZEKE spectra were recorded on the same day under the same expansion conditions, it is expected that the relative intensities between the two traces are representative. The trace recorded *via* the 0^0+797 cm^{-1} band shows that the two intense features, 9^1 and 29^2, have roughly half of the intensity of the 29^2 transition in the 0^0+804 cm^{-1} trace. Figure 6.8 shows key sections of this comparison of the two ZEKE traces, alongside the origin ZEKE spectrum. From these, one can draw out some useful information: for example, trace (a) in Figure 6.8 shows that in the origin ZEKE spectrum, the 29^2 transition is observed, albeit weakly compared to the 9^1 transition. The 29^2 transition would not be expected to have significant Franck-Condon intensity in that spectrum, and so this could be interpreted as coupling between D_9 and $2D_{29}$ in the cation, as suggested above based on the energetics.

Figure 6.8(b) then shows the region of the $\Delta(v,m) = 0$ bands in combination with the D_{11} vibration, where one can see effectively a repeat of the $\Delta(v,m) = 0$ region structure: when exciting at 0^0+796.8 cm^{-1}, one sees both $9^1 11^1$ and $11^1 29^2$ with roughly equal intensities, while when exciting at 0^0+803.6 cm^{-1}, one sees $11^1 29^2$ with around twice the intensity as in the other trace. There, the $9^1 11^1$ band appears as a weak shoulder. In the origin ZEKE spectrum, one can see $9^1 11^1$ and $11^1 29^2$, with similar relative intensities to 9^1 and 29^2 in the origin trace given in Figure 6.8(a), suggesting again that D_9 and $2D_{29}$ are coupled in the cation. As an aside, it appears that transitions to D_7 and D_6 are observed in this region based on their calculated vibrational wavenumbers and agreement with the origin ZEKE spectrum (shown in Chapter 3), where many totally symmetric vibrational fundamentals were observed.

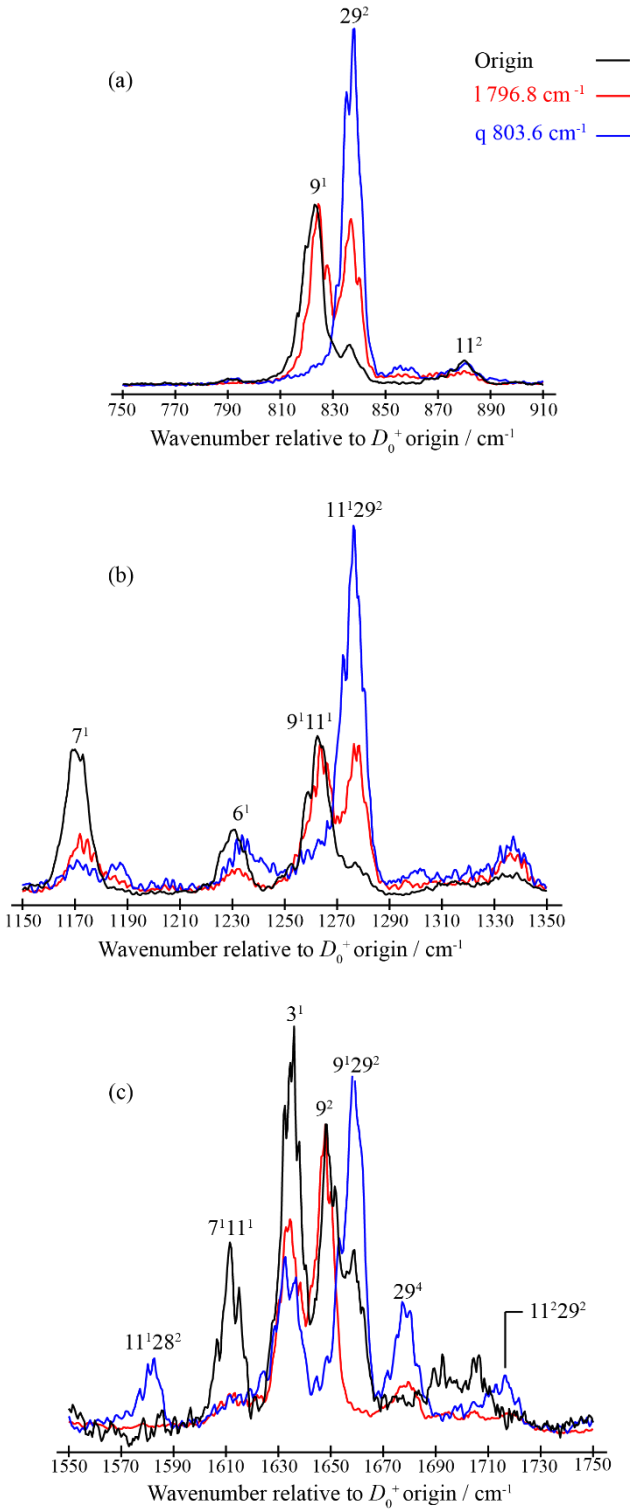


Figure 6.8 – Sections of the ZEKE spectra recorded via the centres of the 797 and 804 cm^{-1} REMPI bands, showing the unnormalized traces, as well as the origin ZEKE spectrum. The origin ZEKE spectrum has been normalised such that in traces (a) – (c), the 9^1, $9^1 11^1$ and 9^2 transitions respectively are the same intensity as in the 0^0+796.8 cm^{-1} trace. This was necessary as this spectrum was recorded on a different day, and with different UV intensity across the spectrum.

The region corresponding to the expected overtones of the ~800 cm^{-1} features is shown in Figure 6.8(c), and here the behaviour is different to the regions shown in (a) and (b). The ZEKE spectrum recorded at 0^0+803.6 cm^{-1} shows the expected behaviour, with an intense $9^1 29^2$ transition and a reasonably intense 29^4 transition. However, the ZEKE spectrum recorded at 0^0+796.8 cm^{-1} shows an intense 9^2 transition, but the $9^1 29^2$ transition appears to be completely absent, even though the 29^2 and $11^1 29^2$ bands had the same intensity as 9^1 and $9^1 11^1$ respectively. This suggests that when exciting *via* the 0^0+796.8 cm^{-1} band, significant ZEKE intensity occurs to both 9^1 and 9^2 in the ZEKE spectrum, i.e. the behaviour is not $\Delta(v,m) = 0$ like, but rather a progression is formed in the D_9 coordinate (there is also some intensity at the origin, a Δv = -1 transition, possibly owing to this). Thus, to get a "true" representation of the "$\Delta(v,m) = 0$" intensity when exciting the D_9 intermediate, the intensities for 9^1 and 9^2 (as well as the origin, and possibly higher overtone) transitions should be summed, suggesting that the D_9 character is very much dominating the spectrum over $2D_{29}$ for this band. Based on this, one would conclude that the 0^0+797 cm^{-1} band arises from an eigenstate largely dominated by the D_9 zero-order state, and that the 0^0+804 cm^{-1} band is an eigenstate largely dominated by the $2D_{29}$ zero-order state, an apparent contradiction to the previous time-resolved study[12].

6.C.1.1.2. Comparison to time-resolved studies

Davies and Reid[12] used the technique of picosecond tr-PES, coherently exciting the two S_1 eigenstates under consideration here with a 1 ps pulse (full-width at half-maximum (FWHM) of ~13 cm^{-1}) and observing the time-dependence by carrying out a series of experiments with ionisation at different picosecond time delays after the initial excitation. Specifically, they recorded slow-electron velocity-map imaging (SEVI) spectra, which allowed them to achieve a resolution of ~40 cm^{-1}, which although is good for such a study, did not allow them to resolve the two photoelectron bands in the range 820 – 840 cm^{-1} (specifically at 824 and 837 cm^{--1} in the ZEKE spectra of this thesis).

The time-dependent behaviour suggested that the origin band in their SEVI spectra was present at a 0 ps delay, but effectively absent when ionising after a

2.5 ps delay, suggesting that it arose only from what they termed the bright zero-order state (the D_9 vibration) and not from the dark zero-order state (the $2D_{29}$ vibration). As such, they investigated the time-dependence of the origin band, and observed a long quantum beating pattern, the Fourier transform of which gave two eigenstate separations of 6.22 and 6.69 cm^{-1}. It is noted that the maxima of the bands in the REMPI spectrum of this thesis are separated by 6.8 cm^{-1}, within error of the higher eigenstate separation given by Davies and Reid. From this time-dependence, Davies and Reid suggested that the two eigenstates were an almost equal mixture of the D_9 and $2D_{29}$ zero-order states, and that it was likely that other zero-order states were present and coupled to D_9 and $2D_{29}$. This latter point is important, as they noted that some signal was lost over the first ~30 ps, but the signal was then constant for 500 ps, suggesting that population of one of the $m = 0$ or $m = 1$ torsional levels was rapidly lost, implying selective coupling of one of those levels.

From the current study, it is not possible to conclude whether population of $m = 0$ or $m = 1$ is being selectively lost, as no torsional or vibtor structure is observed in the ZEKE spectra[d], with one exception, discussed in the next section, but it is notable that it is more likely that population would be lost from $m = 1$ than $m = 0$, on the grounds that the e'' symmetry $m = 1$ level can couple to more levels than the a_1' symmetry $m = 0$ level. This concept will be returned to briefly later in this chapter, with reference to a recently published ZEKE/2D-LIF study[18] by our group that is not the subject of this thesis.

Regarding other zero-order states, several other levels are assigned close to these REMPI bands in the next section, and thus could be involved in the coupling. More important for the current analysis is the conclusion from the tr-PES study that the eigenstates which dominate the two REMPI bands under discussion are almost equal mixtures of the D_9 and $2D_{29}$ zero-order states, as the ZEKE spectra appear to contradict this. However, if the levels are coupled in both the S_1 and D_0^+ states to the same (or to a very similar) extent, then one would expect to observe $\Delta(v,m) = 0$ behaviour even though the vibrations are coupled. Here, the

[d] This is perhaps not surprising, as the 9^1 and 29^2 REMPI bands are significantly weaker than the S_1 origin band.

two REMPI bands are separated by 6.8 cm^{-1}, and the ZEKE bands by 12 cm^{-1}, and so it is certainly possible that they are coupled (albeit to different extents) in both states, as suggested by the appearance of 29^2 in the origin ZEKE spectrum, discussed above and shown in Figure 6.8(a).

With the time-resolved work of Davies and Reid[12] suggesting that the two REMPI bands are eigenstates that are very strong mixtures of D_9 and $2D_{29}$, the conclusion drawn above from the ZEKE spectra that the D_9 and $2D_{29}$ are effectively uncoupled must be reconsidered. Following the above discussion, it is instead concluded that the levels are coupled in both the S_1 and D_0^+ states, and this coupling in the cation obscures any evidence of coupling in the S_1 state when analysing the ZEKE spectra. It is suggested that D_9 contributes most strongly to the lower S_1 eigenstate, owing to the progression formed in that mode in the ZEKE spectra recorded *via* it, and thus the higher eigenstate has its largest contribution from $2D_{29}$, but with significant mixing of the two zero-order states. It is notable that any evidence of coupling in the ZEKE spectra is further obscured by the non-diagonal Franck-Condon Factors (FCFs) implied by the formation of a progression in the D_9 coordinate, as well as the aforementioned probable coupling of D_9 and $2D_{29}$ in the cation.

These are points worth bearing in mind when carrying out a study such as the current one, where one projects the S_1 eigenstates onto the D_0^+ levels (photoelectron spectroscopy) or the S_0 levels (dispersed fluorescence). Indeed, previous ZEKE studies[5] and recent ZEKE work[4,19] by our group on *p*DFB suggest a similar progression is formed in D_9 in that molecule, and Knight and Kable[3] observed a similar effect in their DF spectrum recorded *via* the S_1 D_9 level, suggesting that this non-$\Delta(v,m) = 0$ behaviour for D_9 is not exclusive to *p*FT or to photoelectron spectroscopy.

6.C.1.1.3. Other $\Delta(v,m) = 0$ transitions

Having discussed the make-up of the eigenstates which dominate the 0^0+797 cm^{-1} and 0^0+804 cm^{-1} REMPI bands, it is time to consider the other structure in these ZEKE spectra. The above discussion implies that D_9 dominates

the lower eigenstate and $2D_{29}$ the upper eigenstate, and this is supported by the observation of the transitions 28^1 and 28^2 in the ZEKE spectra *via* the upper eigenstate but not the lower eigenstate, as illustrated in Figure 6.7. This figure also shows a zoom of the low wavenumber region of the ZEKE spectra recorded *via* the centres of the bands, where weak non-totally symmetric structure is observed such as 19^1, 14^1 and 18^1, as well as the expected transition to the totally symmetric 11^1. This structure is observed in the ZEKE spectra recorded *via* both eigenstates.

Figure 6.5 shows the ZEKE spectra recorded *via* the 0^0+797 cm^{-1} band, and although the general activity is very similar in all of the spectra, there are some significant differences. Trace n, recorded at 0^0+798.6 cm^{-1}, shows broader structure than the other spectra, thought to be due to exciting high lying rotational levels, as discussed for several other cases throughout this thesis. Trace j, recorded at 0^0+793.8 cm^{-1}, on the low wavenumber side of the band, shows two additional very intense transitions at 1112 and 1171 cm^{-1}. The intensity of these, and their drop off in the other ZEKE spectra recorded across the band, suggests that they must be $\Delta(v,m) = 0$ transitions at this excitation position. In considering assignments for these, one must remember that $2D_{29}$ has been assigned, i.e. an overtone of the lower wavenumber D_{29}, and so overtones of $2D_{14}$ and D_{11} (i.e. $4D_{14}$ and $2D_{11}$) are also expected in this region of the REMPI spectrum, as well as the "cross-terms", i.e. $D_{11}2D_{14}$, $D_{11}D_{29}$ and $2D_{14}D_{29}$. The band at 1112 cm^{-1} fits the $14^2 29^1$ transition, and this also fits the excitation position, and so it is assigned as a $\Delta(v,m) = 0$ transition.

The expected positions of these overtones and combinations of the lower 400 – 410 cm^{-1} vibrations are as follows:

Vibration	S_1 wavenumber	D_0^+ wavenumber
$4D_{14}$	796	1396
$2D_{14}D_{29}$	799	1112
$2D_{29}$	802	828
$D_{11}2D_{14}$	808	1138
$D_{11}D_{29}$	811	854
$2D_{11}$	820	880

The 1171 cm^{-1} band fits none of these assignments but can instead be assigned as $12^1m^{6(-)}$, as a $\Delta(v,m) = 0$ transition. This assignment gives reasonable agreement with the B3LYP/aug-cc-pVTZ calculated wavenumber for D_{12} in the cation. In the next section, $D_{12}D_{14}$ will be assigned, and this will yield a higher S_1 value for D_{12} than here; it is thought that here, D_{12} m = 6(-) is interacting with D_9 (as it appears weakly in other ZEKE spectra recorded across the 0^0+797 cm^{-1} band), and so is perturbed down in energy.

Turning now to the 0^0+804 cm^{-1} band, trace o in Figure 6.6 (recorded at 0^0+800.6 cm^{-1}) shows two intense ZEKE bands at 1140 and 1400 cm^{-1}, which fit transitions to 11^114^2 and 14^4 respectively. $D_{11}2D_{14}$ is expected slightly higher than this in the S_1 state, a point returned to in the below. $4D_{14}$ is expected to lower wavenumber, suggesting it has been perturbed up in wavenumber by coupling to D_9. There is a very weak band at ~1400 cm^{-1} in the ZEKE spectra recorded *via* the D_9 dominated band, which could support this coupling.

To slightly higher wavenumber than these two intense REMPI features are two weak REMPI features at 0^0+807.4 and 0^0+810.8 cm^{-1}, with ZEKE spectra recorded *via* these also shown in Figure 6.6. Trace s, recorded at 0^0+807.4 cm^{-1}, shows an intense band at 856 cm^{-1} and another at 1299 cm^{-1}. The former can be assigned as a $\Delta(v,m) = 0$ transition, 11^129^1, with the latter being this plus another quanta of D_{11}. Trace t, recorded at 0^0+810.8 cm^{-1}, shows intense bands at 699 and 1400 cm^{-1}, readily assigned as 14^2 and 14^4. Note that the transition to 14^4 is not a $\Delta(v,m) = 0$ transition, with this already assigned above, but $11_0^114_0^2$ would be expected at around this excitation position. There is a band at

1130 cm^{-1}, with a shoulder at 1138 cm^{-1}, and $11^1 14^2$ would best fit the shoulder position. The 1130 cm^{-1} band is thought to be the symmetry-allowed $13^1 14^1$ transition.

Thus, the appearance of the 14^2 and 14^4 ZEKE bands in trace t is taken as an indicator of the S_1 level being $D_{11}2D_{14}$ and could imply a coupling of $D_{11}2D_{14}$ with $4D_{14}$ in the S_1 state, hence the observation of $11^1 14^2$ in the ZEKE spectrum recorded when exciting $4D_{14}$. However, it is noted that $2D_{14}$ and D_{11} were thought not to be coupled in the lower wavenumber region, and so any potential coupling of $4D_{14}$ and $D_{11}2D_{14}$ here is unclear. Ongoing 2D-LIF studies by our research group will hopefully aid in clarifying this.

One might also note the appearance of a weak, non-$\Delta(v,m) = 0$, transition to 18^2 in trace t, perhaps suggesting a coupling to the $2D_{18}$ level in the S_1 state, found to slightly higher wavenumber as discussed later in this chapter.

With these assignments in hand, the S_1 activity over the range 792 – 814 cm^{-1} can be summarised as dominated by two strongly coupled levels, D_9 and $2D_{29}$, but with the involvement of many other zero-order states, including overtone and combination "cross-terms" of the lower wavenumber 400 – 410 cm^{-1} structure, as well as the D_{12} $m = 6(-)$ vibtor level. This agrees with the conclusion of the time-resolved study[12], that more zero-order states than just D_9 and $2D_{29}$ are involved in the coupling.

6.C.1.2. The 0^0+818 cm^{-1} band

Moving on to slightly higher wavenumber, Figure 6.9 shows a "2D-ZEKE" spectrum composed of 6 individual ZEKE spectra recorded when exciting across the band profile of the 0^0+818 cm^{-1} REMPI band. This band was previously assigned[6,9] as 11_0^2, expected at around this S_1 position and at ~880 cm^{-1} in the cation based on the experimental fundamentals obtained from the lower wavenumber region in Chapter 5. There is a reasonably intense band at 880 cm^{-1} in these spectra, but it is not the most intense band, with significant bands at

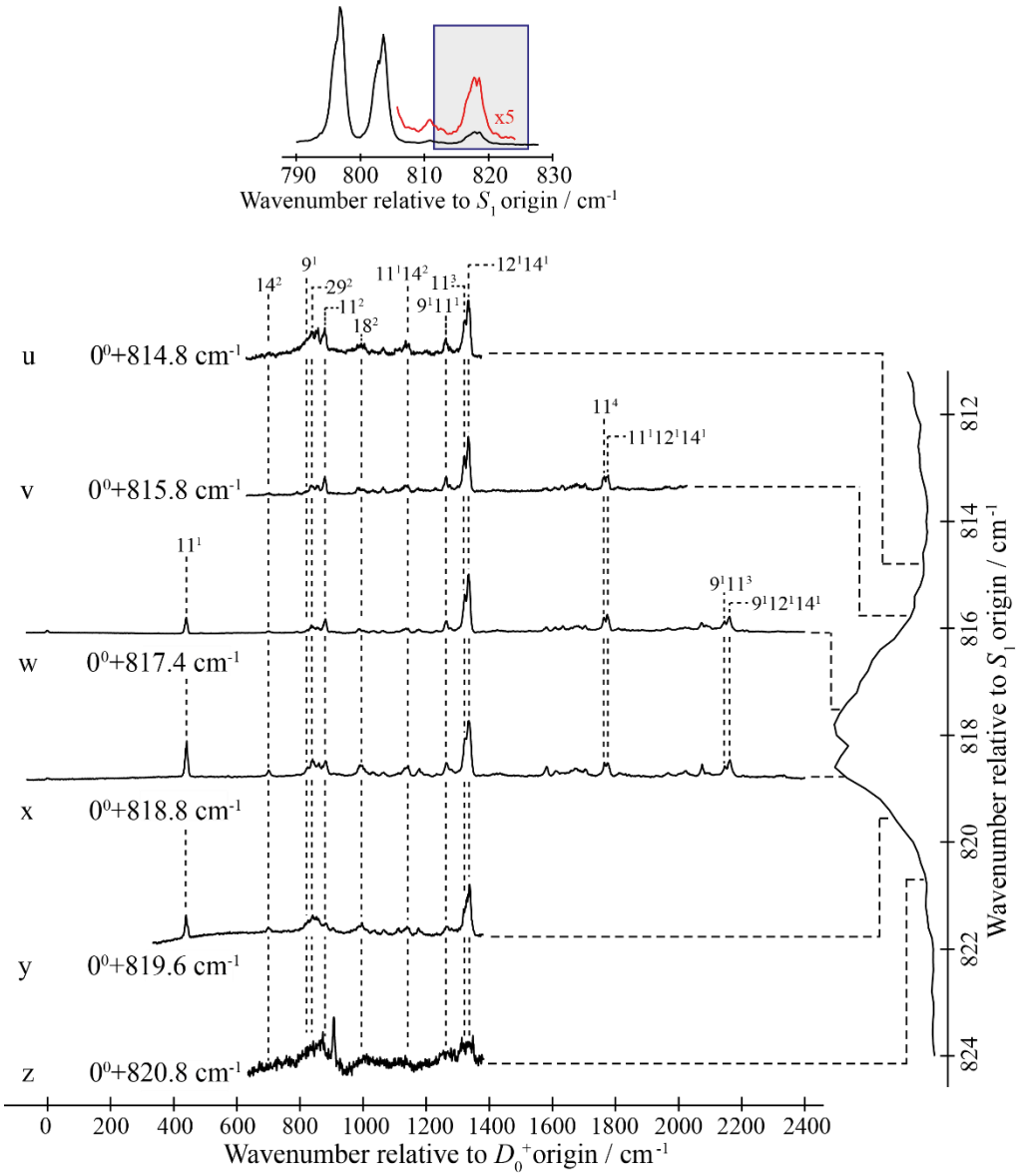


Figure 6.9 – A "2D-ZEKE" spectrum comprising ZEKE spectra recorded at excitation wavenumbers across the range 814 to 822 cm^{-1}, with the individual ZEKE spectra given in traces u – z. The right hand vertical trace and the top trace illustrate the relevant region of the REMPI spectrum. Each ZEKE trace is normalised to the most intense feature in that trace.

440 cm^{-1} and a double feature at 1322/1335 cm^{-1}. This suggests that the 440 cm^{-1} band is 11^1, the 880 cm^{-1} band is 11^2 and the 1322 cm^{-1} band is 11^3, with the 11^4 transition also observed to higher wavenumber at 1763 cm^{-1}, and thus it is apparent that D_{11} is a progression forming mode (i.e. not $\Delta(v,m) = 0$ like, with non-diagonal FCFs) upon ionisation. Ayles *et al.*[9] also presented a ZEKE spectrum recorded *via* this band, and commented on the non-$\Delta(v,m) = 0$ nature of the spectrum. They assigned the 1335 cm^{-1} ZEKE feature as 5^1 ($7a^1$ in the

Wilson[7]/Varsányi[8] notation used in that work), and suggested that D_5 and D_{11} were coupled, although presumably they were actually referring to a Duschinsky mixing between these vibrations, as these vibrational modes are significantly energetically separated in both the S_1 and D_0^+ states.

In looking at the current ZEKE spectra, such a Duschinsky mixing argument seems unlikely as this 1335 cm^{-1} feature is the most intense transition in all of the spectra recorded *via* the 0^0+818 cm^{-1} REMPI band, and so an alternative assignment was sought. It is suggested that the 1335 cm^{-1} band arises from a $\Delta(v,m) = 0$ transition, and with such a large S_1 to D_0^+ shift in wavenumber, likely involves significant out-of-plane vibrational character. It can be assigned as a transition to $12^1 14^1$, consistent with the D_{12} value obtained from D_{12} m = 6(-) earlier (with the caveat that the D_{12} m = 6(-) appears to be coupled to D_9 in the S_1 state, introducing uncertainty into the value of D_{12} from that state). This $12^1 14^1$ assignment yields a D_{12} S_1 value of 619 cm^{-1} (taking the centre of the REMPI band) and a D_0^+ value of 986 cm^{-1}. It is notable that Knight and Kable[3] assigned an intrinsically bright band in their LIF spectrum of *p*DFB to $12^1 14^1$, and so its apparent intrinsic brightness in the REMPI spectrum presented here is not entirely surprising.

Thus, one concludes that the 0^0+818 cm^{-1} band is composed of two contributions, 11_0^2 and $12_0^1 14_0^1$, with these seeming to be completely overlapped with no obvious interaction between the two. One might note, again, the broadening in the ZEKE spectra when exciting the higher lying rotational levels at the edges of the band profile.

6.C.1.3. The 0^0+846 cm^{-1} band

In the REMPI spectrum presented in Figure 6.1, one can see another band to slightly higher wavenumber, at 0^0+846 cm^{-1}. This band was assigned as 8_0^1 by Okuyama *et al.*[6], an assignment which was propagated by Ayles *et al.*[9] and Davies and Reid[20].

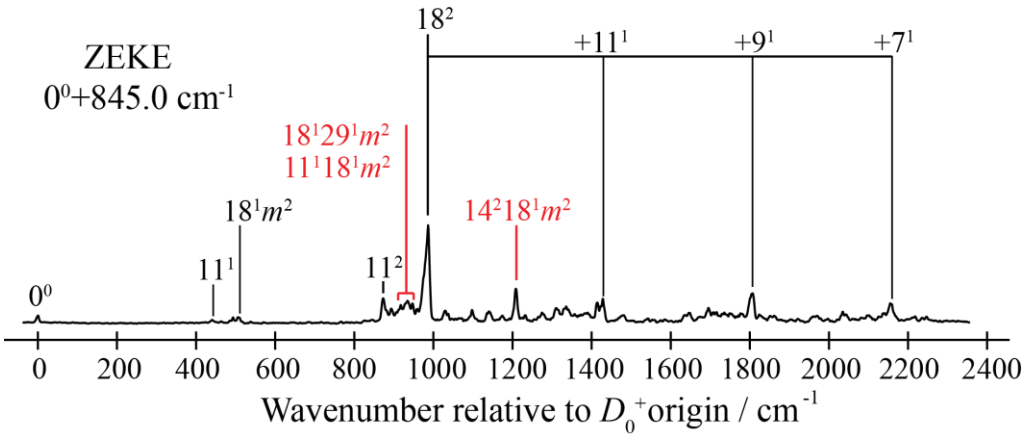


Figure 6.10 – A ZEKE spectrum recorded when exciting via the centre of the 0^0+846 cm^{-1} REMPI band.

Although a "2D-ZEKE" spectrum was recorded *via* this band, it is not presented in its entirety here; this band is very complex and has been the subject of its own ZEKE/2D-LIF study recently by our group[18], which does not form part of this thesis. Instead, a single ZEKE spectrum recorded at the centre of the band will be presented, to assign the dominant bright state character, and this is shown in Figure 6.10.

The spectrum is dominated by an intense transition at 987 cm^{-1}, which can be readily assigned as a $\Delta(v,m) = 0$ transition, 18^2, in excellent agreement with the previously derived S_1 and D_0^+ values for D_{18}, and consistent with the observation of a relatively isolated band in the REMPI spectra of both *p*DFB and *p*ClFB which was assigned as 18_0^2. One observes the $\Delta(v,m) = 0$ band in combination with D_{11}, D_9 and D_7 in the ZEKE spectrum, and 11^2 is also observed, either on grounds of being symmetry-allowed or owing to weak coupling of $2D_{18}$ with the $2D_{11}$ level to lower wavenumber in the S_1 state.

To briefly summarise our recent publication[18] for the interested reader, the $2D_{18}$ m = 1 level was shown (by 2D-LIF) to couple strongly to $D_{11}D_{18}$ m = 2, $D_{18}D_{29}$ m = 2 and $2D_{14}D_{18}$ m = 2 (i.e. the 400 – 410 cm^{-1} region bands in combination with D_{18} m = 2). These were proposed as doorway states, as there is evidence that there is further coupling from these to the underlying bath of states, and some of the (many) transitions in this ZEKE spectrum could be to those levels. Note the importance of torsional/vibtor levels, since $2D_{18}$ m = 0

appeared to be effectively unperturbed, suggesting an $m = 1$ specific coupling, likely owing to the increased number of e'' levels that $2D_{18}$ $m = 1$ can couple to relative to the number of a_1' levels that $2D_{18}$ $m = 0$ can couple to, and the proximity of these levels energetically.

As this band is not going to be discussed further in this thesis, only brief remarks will be made regarding the picosecond tr-PES study of Davies and Reid[20]. In that work, they assigned the bright state as 8_0^1 ($18a_0^1$ in the Wilson/Varsányi notation of that work) which has now been reassigned as 18_0^2. They also suggested a doorway state assignment of D_{12} $m = 6(-)$, a level that has now been assigned to lower wavenumber, close to (and seemingly coupled to) D_9. Interestingly, their doorway state assignment would require coupling to the $m = 0$ level of the bright state, rather than the $m = 1$ level as was proposed by our group. It seems, based on density of states argument for levels of each symmetry, that the $m = 1$ level couplings would be far more likely to lead to widespread coupling/statistical intramolecular vibrational redistribution (IVR) than $m = 0$ ones. As such, our study is consistent with their observed 50% population loss but suggests that this is from the $m = 1$ level rather than the $m = 0$ level.

6.C.2. Discussion

Figure 6.11 summarises the assignments of the *p*FT REMPI spectrum discussed here, from 790 – 860 cm^{-1}. Assignments given in blue are symmetry-allowed from either the $m = 0$ or $m = 1$ level, being totally symmetric or of e'' symmetry, respectively; the assignments in red are of a_1'' vibrational symmetry and may be observed by vibronic coupling. It appears that D_9 and $2D_{29}$ are strongly coupled, with $2D_{11}$ only weakly involved in the coupling. One can compare this to our recent study[1,2] of *p*ClFB, where it was shown that D_9 and $2D_{29}$ also appear to be coupled, with $2D_{11}$ significantly lower in wavenumber in that case. This contrasts with *p*DFB, where Knight and Kable[3] (and our recent ZEKE study[4]) suggested D_9 and $2D_{11}$ were strongly coupled, and D_9 was not coupled to $2D_{29}$, with $2D_{29}$ being slightly further away energetically in that case. This supports the idea that the couplings observed depend heavily on serendipity, with the

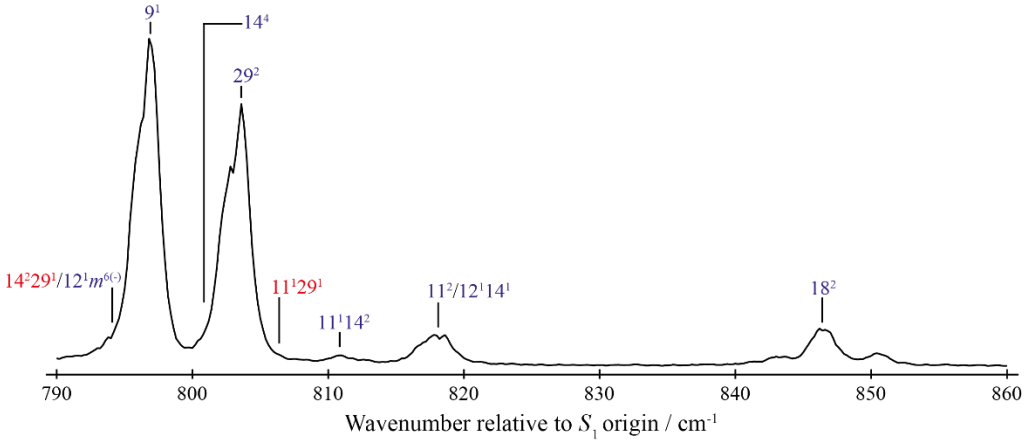


Figure 6.11 – The pFT REMPI spectrum from 790 – 860 cm^{-1} is shown, indicating the assigned levels. These assignments are effectively the different dominant zero-order level contributions at each position, with the eigenstate makeup being some combination of these, as discussed in the previous sections. Note that assignments in blue are totally symmetric while those in red are of a_1" symmetry, and that for 18^2, the coupled levels are omitted here as they do not form part of the discussion - see reference 18 for details.

levels needing to be in close proximity energetically, and this will be returned to after discussing the *p*Xyl spectra in the next section.

One might also note the similar spectral activity here compared to that in *p*DFB and *p*ClFB, with 9_0^1, 11_0^2, $12_0^1 14_0^1$ and 18_0^2 bands observed in all three molecules (with $12_0^1 14_0^1$ more difficult to identify in *p*ClFB, as discussed in reference 2) and so thought to be intrinsically bright in all of these molecules. It is debatable whether 29_0^2 is intrinsically bright, at its intensity appears to depend on its proximity to the 9_0^1 transition. In *p*DFB, the D_9 and $2D_{11}$ coupling was effectively the only coupling noted in this region, and that is a simple Fermi resonance between only those two levels. Here, in *p*FT, there are five other zero-order level contributors close to D_9 and $2D_{29} - 2D_{14}D_{29}$, D_{12} m = 6(-), $4D_{14}$, $D_{11}D_{29}$ and $D_{11}2D_{14}$ – with some evidence of their involvement in the couplings, particularly for the D_{12} m = 6(-) level.

It has also been noted that, although not the subject of this thesis, vibtor levels have been shown[18] to lead to widespread couplings (effectively statistical IVR) by acting as doorway states for the $2D_{18}$ m = 1 level in *p*FT, while in *p*DFB, $2D_{18}$ was isolated in the S_1 state, with a very clean DF spectrum recorded by Knight

and Kable[3], and a clean ZEKE spectrum presented in reference 4, suggesting no coupling. This contrast illustrates the importance of energetic coincidences in couplings, aided by the build-up of the density of states caused by the existence of the vibtor levels for *p*FT. This will be discussed again in Chapter 7 of this thesis, where some calculated densities of states will be shown for *p*DFB, *p*ClFB, *p*FT and *p*Xyl to rationalise the general observations of this thesis.

6.D. Region C: *para*-xylene 770 – 810 cm^{-1} features

6.D.1. Overview of ZEKE spectra

Having noted the consistency in the observed bright structure in this wavenumber region for *p*DFB, *p*ClFB and *p*FT, this information can be used to aid in assigning corresponding features in the *p*Xyl REMPI spectrum. Figure 6.12 presents ZEKE spectra recorded *via* the two intense features at 0^0+775 cm^{-1} and 0^0+804 cm^{-1}, and two ZEKE spectra recorded *via* the shoulders to these bands. Note that the *p*Xyl ZEKE spectra were more difficult to obtain than those of *p*FT, restricting the number of good-quality spectra that could be obtained, likely owing to a combination of the lack of a permanent dipole moment in *p*Xyl and a lower vapour pressure for *p*Xyl (and perhaps also owing to increased IVR in *p*Xyl at similar internal energies compared to the other molecules – see below).

Starting with the intense REMPI band (B) at 0^0+775 cm^{-1}, the ZEKE spectrum recorded *via* this intermediate shows an intense transition at 806 cm^{-1}, which is expected to be 9^1. Since this is the most intense transition in this ZEKE spectrum, it is suggested that this REMPI band is 9_0^1, in agreement with the activity in the other molecules discussed above. However, there is also an intense ZEKE transition at 947 cm^{-1}. This can be assigned as 18^2, in agreement with the value of D_{18} obtained from D_{18} $\{0,3(-)\}^-$ in Chapter 5. The S_1 position for 18_0^2 is expected ~800 cm^{-1}, and if one looks at the ZEKE spectrum recorded *via* the intense REMPI band at 0^0+803 cm^{-1} (band C), one can see the same two intense transitions as *via* band B, but now with the 18^2 band dominating the ZEKE spectrum and the 9^1 band being the weaker one.

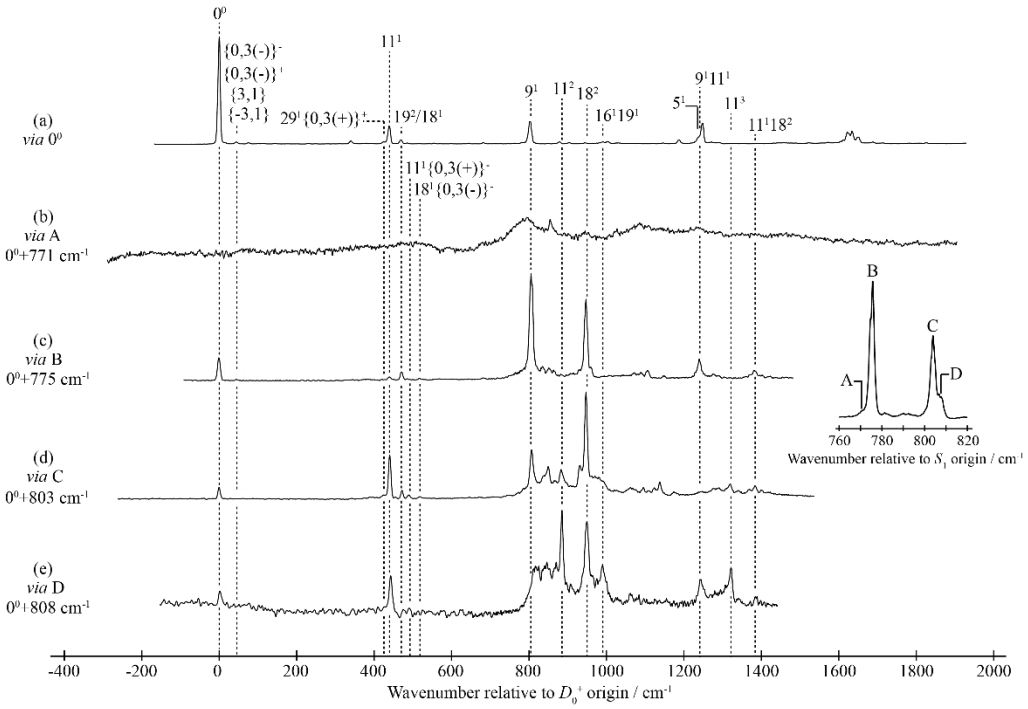


Figure 6.12 – Four ZEKE spectra recorded for pXyl at excitation wavenumbers across the range 760 to 820 cm^{-1}. The top trace (a) is the origin ZEKE spectrum, for comparison, and the trace on the right side of the figure shows the excitation positions on the REMPI spectrum.

This suggests that the S_1 levels D_9 and $2D_{18}$ are coupled, with the ZEKE spectra at first glance indicating a traditional, two level, Fermi resonance. Band B at 0^0+775 cm^{-1} arises from an eigenstate composed of both zero-order levels, but dominated by D_9, while the 0^0+803 cm^{-1} band C is an eigenstate dominated by $2D_{18}$ with a smaller D_9 contribution. Although these levels are coupled, based upon the activity in the other *para*-disubstituted benzene molecules discussed earlier, both 9_0^1 and 18_0^2 are thought to be intrinsically bright. These assignments are in general agreement with the previous studies[13–15,17] on *p*Xyl, which suggested that one of these REMPI bands corresponded to 9_0^1, and confirm the suggestion of Blease *et al.*[16] that the 0^0+803 cm^{-1} band is (dominantly) 18_0^2, with $2D_{18}$ and D_9 coupled. However, there are additional contributions in this region which will be discussed shortly.

In both of these ZEKE spectra, the more intense structure to higher wavenumber can be readily assigned as these $\Delta v\{m_1,m_2\} = 0$ transitions in combination with D_{11}, as expected. It is noted that $9^1 11^1$ is almost coincident with 5^1, which

would be an alternative possible assignment. However, ZEKE spectra recorded *via* the D_5 level (presented in Chapter 7) will show that the 5^1 transition lies to slightly lower wavenumber; in the origin ZEKE spectrum presented at the top of Figure 6.12, 5^1 is assigned to slightly lower wavenumber, as a shoulder on the $9^1 11^1$ band. Thus, this ZEKE band can be firmly assigned as $9^1 11^1$. It does have a slight broadening on its low wavenumber side, suggesting a possible observation of 5^1 with similar relative intensities to in the origin ZEKE spectrum, perhaps implying a coupling of D_5 and $D_9 D_{11}$ in the cation.

Moving on to position D at 0^0+808 cm^{-1}, which is a shoulder to band C, one sees an intense band at 885 cm^{-1}, and an intense 18^2 transition. Although this S_1 position could contain some of the "tail" of the 18_0^2 REMPI band profile, the relative intensity of the 18^2 band in the ZEKE spectrum suggests that perhaps the $2D_{18}$ level is coupled in the S_1 state to whatever is giving rise to the ZEKE band at 885 cm^{-1}. To lower wavenumber in the spectrum is a reasonably intense band at 442 cm^{-1} which is readily assigned as 11^1 based on its observation in the origin ZEKE spectrum, and so the $\Delta v\{m_1,m_2\} = 0$ transition at 885 cm^{-1} can thus be assigned as 11^2, which is expected at this excitation position in the S_1 state. The activity in this ZEKE spectrum suggests that $2D_{18}$ and $2D_{11}$ are coupled in the S_1 state (formally a Darling-Dennison resonance[21]), and one can see evidence of $2D_{11}$ in the ZEKE spectrum recorded *via* band C, supporting this coupling.

The low wavenumber ZEKE structure supports these assignments, with the ZEKE spectra *via* the D_9 and $2D_{18}$ dominated eigenstates showing what appears to be the 18^1 band at 472 cm^{-1}. However, this could also be 19^2, expected at roughly the same position in the cation from the ZEKE spectrum recorded *via* $2D_{19}$, shown in Chapter 5. In either case, this band is thought to confirm the $2D_{18}$ character of the initial levels at these excitation positions. The ZEKE spectra *via* the eigenstates proposed to contain contributions from $2D_{11}$ (bands C and D) show a transition to 11^1, which is very weak *via* the D_9 dominated eigenstate (band B).

To summarise, the dominant structure in this region of the REMPI spectrum has been assigned as 9_0^1, 18_0^2 and 11_0^2, with suggested coupling of D_9 with $2D_{18}$, and $2D_{18}$ with $2D_{11}$, but not between D_9 and $2D_{11}$. Indeed, the ZEKE spectrum recorded *via* the D_9 dominated eigenstate at 0^0+775 cm^{-1} shows effectively no activity for 11^2, with only weak activity for 11^1. Similarly, the ZEKE spectrum recorded *via* the $2D_{11}$ dominated eigenstate at 0^0+808 cm^{-1} shows seemingly only limited 9^1 activity, although this is difficult to judge owing to the broad structure in that spectrum. The amount of broad, unresolved, structure depends quite strongly on the position excited, with a relatively clean ZEKE spectrum recorded at 0^0+775 cm^{-1}, with more structure in the 0^0+803 cm^{-1} spectrum, and this broad structure becoming more dominant in the 0^0+808 cm^{-1} spectrum.

Finally, considering the ZEKE spectrum recorded at 0^0+771 cm^{-1}, one can see that it is effectively unstructured, with a single sharp transition at 855 cm^{-1}. If one assumes that this is a $\Delta v\{m_1,m_2\} = 0$ transition, the only assignment which fits in both states is $18^1 29^1$, which is of a_3' symmetry (a *c*-type $S_1 \leftarrow S_0$ transition) and so is expected to be weak at best in the REMPI spectrum. It should be noted that there may be other S_1 contributions, masked by the broadening in the spectrum. This will be elaborated upon slightly in the below.

6.D.2. Discussion

In ZEKE spectroscopy[e] the appearance of broad, unresolved, structure (such as in the ZEKE spectrum recorded *via* band D, shown in Figure 6.12) suggests that couplings between levels may be occurring to a significant degree. This is because the bright state is coupled (directly or indirectly) to many levels, and so intensity from the bright zero-order state is spread over many eigenstates; additionally, any individual eigenstate contains a significant number of zero-order state contributors. Owing to this, the projection then often leads to broad, unresolved structure arising from the many different zero-order states; in

[e] Or indeed any photoelectron spectroscopy or dispersed fluorescence technique where one is projecting the S_1 eigenstates onto a different electronic state.

other words, the ZEKE spectrum is a superposition of the many spectra arising from each zero-order state contribution.

Thus, the broadening of the ZEKE spectrum recorded *via* band D at 0^0+808 cm^{-1} could very well be indicative of widespread coupling, or what is also known as statistical IVR, compared to the restricted IVR suggested by the D_9 and $2D_{18}$ coupling. It appears that D_9 and $2D_{18}$ are coupled to one another, with $2D_{18}$ then coupled to $2D_{11}$, which is losing population to the bath of states by some mechanism. It could be that $2D_{11}$ is itself coupled to the bath of states, or it could be coupled to the bath of states by a currently unknown doorway state. If $2D_{11}$ itself were directly coupled to the bath of states, one might expect more loss of structure in the $2D_{18}$ dominated ZEKE spectrum, since $2D_{11}$ would then be acting as a doorway state to $2D_{18}$, and thus it is thought that there is another doorway state coupled to $2D_{11}$, allowing access to the bath.

This proposal goes some way to rationalising why the 0^0+775 cm^{-1} ZEKE spectrum is relatively clean, since D_9 is not directly coupled to $2D_{11}$, only indirectly *via* $2D_{18}$. Since $2D_{18}$ is directly coupled to $2D_{11}$, more of its intensity is spread among the bath states, and $2D_{11}$ has much more of its intensity spread among the bath states as it is coupled to the doorway state.

Although the nature of this doorway state is not known from the current work, some general remarks can be made. One option is that the doorway state is the REMPI shoulder observed at 0^0+771 cm^{-1}, with the broadness in this spectrum possibly attributable to it being a doorway state for $2D_{11}$. If this is the case, the doorway state assignment is not obvious owing to the broadness, and some care must be taken with the interpretation here since the ZEKE spectrum is very weak and this broadness could also arise from very subtle changes in UV intensity across the region scanned.

Recalling the lower wavenumber region discussed in Chapter 5, the 11_0^1 transition was observed weakly in the REMPI spectrum just below a complicated set of three features involving 19_0^2, $29_0^1 m_{\{0,0\}}^{\{0,3(+)\}^-}$, 14_0^2 and

$18_0^1 m_{\{0,0\}}^{\{0,3(-)\}^-}$, as well as perhaps $14_0^1 m_{\{0,0\}}^{\{0,6(-)\}^+}$. Coupling was suggested between $2D_{19}$ and $D_{29}\{0,3(+)\}^-$, with the possible involvement of D_{11} and $D_{14}\{0,6(-)\}^-$. Thus, in the region under discussion here, one could imagine these lower wavenumber transitions (particularly the $19_0^2/29_0^1 m_{\{0,0\}}^{\{0,3(+)\}^-}$ ones) in combination with D_{11} also being coupled in a similar way, but this time involving $2D_{11}$, and it is possible that one of those levels is the/a doorway state. Such assignments are given in red in Figure 6.13, which shows an overview of the REMPI assignments for this region.

Note that the REMPI position where the $11_0^1 19_0^2$ and $11_0^1 29_0^1 m_{\{0,0\}}^{\{0,3(+)\}^-}$ transitions would be expected also matches the expected position of $9_0^1 m_{\{0,0\}}^{\{0,3(+)\}^+}$, and a band to higher wavenumber matches $18_0^2 m_{\{0,0\}}^{\{0,3(+)\}^+}$. These represent totally symmetric vibrations with their "m = 3(+)" level, akin to the observation of "m = 3(+)" above the electronic origin band. These transitions are presumably observed here owing to the intensity of the 9_0^1 and 18_0^2 transitions. However, there is some broadening around the base of the $9_0^1 m_{\{0,0\}}^{\{0,3(+)\}^+}$ band, most obvious in the inverted, lower resolution, trace, which could be these expected "doorway state" levels. No ZEKE spectra were recorded *via* these levels, so no definitive conclusions can be made regarding this. It is suggested that future work, such as tr-PES or perhaps 2D-LIF, could shed more light on the possible couplings in this region and elucidate the nature of any doorway state or states.

Also included in Figure 6.13 are two bands to lower wavenumber, where again ZEKE spectra were not recorded. One of these matches $14_0^1 19_0^2 20_0^1$, i.e. 19_0^2 in combination with $14_0^1 20_0^1$, both of which are intrinsically bright and observed (or thought to be) to lower wavenumber. This would be of a_4'' symmetry, and so allowed by vibronic coupling in the same way as $14_0^1 20_0^1$. Additionally, a very weak band at 0^0+744 cm^{-1} can be assigned as 29_0^2.

Finally, there is also some weak structure between the 9_0^1 and 18_0^2 transitions. The band at ~0^0+781 cm^{-1} is currently unassigned, but the broad band at

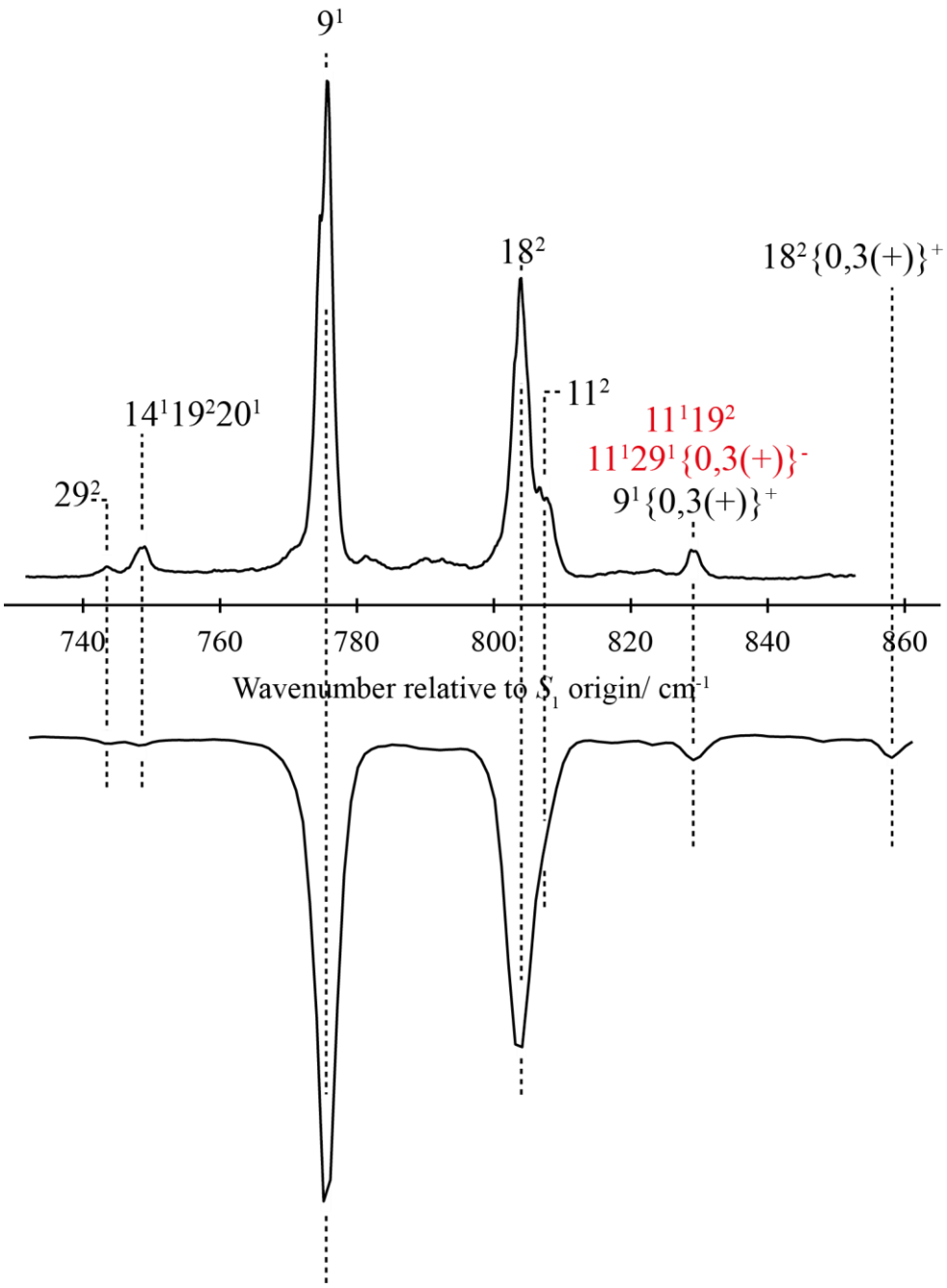


Figure 6.13 – REMPI spectrum of pXyl over the range 730 – 860 cm^{-1}. The top, upright, trace is recorded with a finer step size than the lower, inverted trace, allowing more of the band profiles to be resolved. The assignments given in red are possible doorway states based on proposed couplings in the lower wavenumber region discussed in Chapter 5.

~0^0+793 cm^{-1} could be a transition to the "D_9 m = 2" levels, on similar grounds to the observation of "D_9 m = 3(+)".

6.E. Comparison to *para*-difluorobenzene and *para*-chlorofluorobenzene

Having assigned the most intense REMPI structure up to 900 cm^{-1}, one can compare the activities between *p*DFB, *p*ClFB, *p*FT and *p*Xyl and draw some general conclusions. Figure 6.14 shows the assigned REMPI spectra up to 900 cm^{-1} including the key assignments discussed for *p*FT and *p*Xyl in this chapter.

One observes 10_0^1 for both *p*ClFB and *p*FT, where this vibration is totally symmetric, and it is not observed for *p*DFB or *p*Xyl, where it is non-totally symmetric. This makes sense based on the symmetries of the respective molecules, but one might note that it is also quite weak in the *p*ClFB and *p*FT spectra. This suggests that although it is totally symmetric, and thus symmetry-allowed, the vibrational motion itself is not particularly active in the $S_1 \leftarrow S_0$ transition. This also makes sense, since the vibration is non-totally symmetric in *p*DFB and *p*Xyl but the vibrational motion remains very similar in all four molecules. In the next chapter, it will be seen that D_6 is also only observed in *p*FT and *p*ClFB, again on symmetry grounds, but the 6_0^1 transition is observed with significant intensity. In that case, it is because the vibration takes on a local mode character in the asymmetric *p*FT and *p*ClFB molecules, whereas the D_{10} vibration is very similar between the symmetric and asymmetric molecules. The form of the vibrations is a point worth bearing in mind when comparing the activities of similar symmetrically and asymmetrically substituted benzene molecules.

In all four molecules, an intense 9_0^1 transition was observed, as well as 11_0^2 and 18_0^2, all thought to be intrinsically bright. One also observes the 29_0^2 transition in all four molecules, but the intensity of this appears heavily dependent on the proximity of $2D_{29}$ to D_9. For example, in *p*ClFB and *p*FT, D_9 and $2D_{29}$ are thought to be in Fermi resonance[2], and $2D_{29}$ is almost as intense as D_9. In *p*DFB, D_9 is now thought to be in Fermi resonance with $2D_{11}$, while $2D_{29}$ is further away energetically and significantly weaker in the REMPI spectrum.[3,4] Finally,

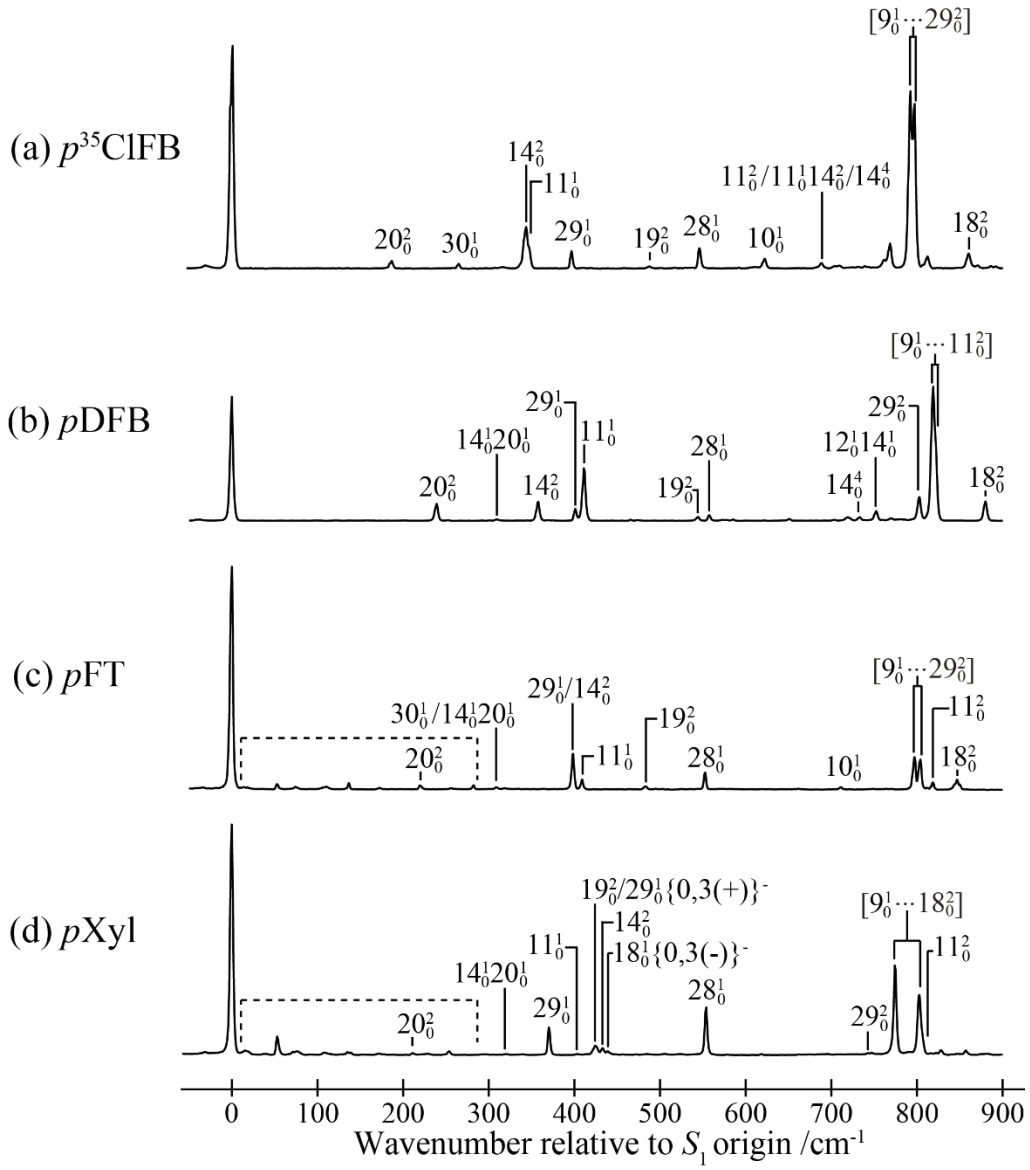


Figure 6.14 – The (a) p^{35}ClFB (b), pDFB (c) pFT and (d) pXyl $S_1 \leftarrow S_0$ REMPI spectra up to 900 cm^{-1} are shown. The assignments are those from Figure 6.1, with the addition of key assignments for pFT and pXyl ascertained in this chapter.

in *p*Xyl, where D_9 has been shown to be in Fermi resonance with $2D_{18}$, $2D_{29}$ is significantly lower in wavenumber, and it is very weak. This suggests that most of the intensity of 29_0^2 comes from coupling.

The observation of different levels coupling to D_9 in different molecules prompts a few thoughts. First, the levels involved in coupling are those which happen to be energetically close in each case. As an example, consider the case of D_9 and $2D_{18}$, both of which are thought to be intrinsically bright. In *p*Xyl, the two are coupled, and $2D_{18}$ is observed 28 cm^{-1} above D_9, while in *p*FT they do not appear

to be coupled and $2D_{18}$ is 49 cm^{-1} higher than D_9. Similarly, $2D_{29}$ is energetically further from D_9 in *p*Xyl than in *p*FT, and appears not to be coupled in *p*Xyl, illustrating the dependence of the coupling on the energetics of the levels.

Second, presumably the coupled vibrational (or vibtor) levels have some motional similarities with which to couple in a dynamical sense. Finally, it may seem unusual that it is always the D_9 vibration which is observed to couple to different levels. This is because these 1+1/1+1′ REMPI experiments (from a jet cooled sample) observe the 9_0^1 as a very bright transition on Franck-Condon grounds, in all four molecules, and thus its couplings can be unravelled. In a gedanken experiment where 29_0^2 is observed very strongly in each molecule rather than 9_0^1, one would expect to be able to unravel couplings involving that vibration. Thus, owing to the nature of "bright" and "dark" transitions, spectroscopic experiments are only ever going to probe a small selection of coupled levels, and thus conclusions on the general nature of IVR must be made cautiously.

6.F. References

[1] W.D. Tuttle, A.M. Gardner, and T.G. Wright, *Chem. Phys. Lett.*, **684**, 339 (2017).

[2] D.J. Kemp, L.E. Whalley, W.D. Tuttle, A.M. Gardner, B.T. Speake, and T.G. Wright, *Phys. Chem. Chem. Phys.*, **20**, 12503 (2018).

[3] A.E.W. Knight and S.H. Kable, *J. Chem. Phys.*, **89**, 7139 (1988).

[4] D.J. Kemp, A.M. Gardner, W.D. Tuttle, J. Midgley, K.L. Reid, and T.G. Wright, *J. Chem. Phys.*, (submitted).

[5] G. Reiser, D. Rieger, T.G. Wright, K. Müller-Dethlefs, and E.W. Schlag, *J. Phys. Chem.*, **97**, 4335 (1993).

[6] K. Okuyama, N. Mikami, and M. Ito, *J. Phys. Chem.*, **89**, 5617 (1985).

[7] E.B. Wilson Jr., *Phys. Rev.*, **45**, 706 (1934).

[8] G. Varsányi, *Assignments of the Vibrational Spectra of Seven Hundred Benzene Derivatives* (Wiley, New York, 1974).

[9] V.L. Ayles, C.J. Hammond, D.E. Bergeron, O.J. Richards, and T.G. Wright, *J. Chem. Phys.*, **126**, 244304 (2007).

[10] A. Andrejeva, A.M. Gardner, W.D. Tuttle, and T.G. Wright, *J. Mol. Spectrosc.*, **321**, 28 (2016).

[11] Z.-Q. Zhao and C.S. Parmenter, *Ber. Bunsenges. Phys. Chem.*, **99**, 536 (1995).

[12] J.A. Davies and K.L. Reid, *Phys. Rev. Lett.*, **109**, 193004 (2012).

[13] K. Walter, K. Scherm, and U. Boesl, *Chem. Phys. Lett.*, **161**, 473 (1989).

[14] B. Zhang, U. Aigner, H.L. Selzle, and E.W. Schlag, *Opt. Commun.*, **183**, 95 (2000).

[15] T. Ebata, Y. Suzuki, N. Mikami, T. Miyashi, and M. Ito, *Chem. Phys. Lett.*, **110**, 597 (1984).

[16] T.G. Blease, R.J. Donovan, P.R.R. Langridge-Smith, and T. Ridley, *Laser Chem.*, **9**, 241 (1988).

[17] F. Gunzer and J. Grotemeyer, *Int. J. Mass Spectrom.*, **228**, 921 (2003).

[18] A.M. Gardner, W.D. Tuttle, L.E. Whalley, and T.G. Wright, *Chem. Sci.*, **9**, 2270 (2018).

[19] W.D. Tuttle, A.M. Gardner, L.E. Whalley, D.J. Kemp, and T.G. Wright, *Phys. Chem. Chem. Phys.*, (In press).

[20] J.A. Davies and K.L. Reid, *J. Chem. Phys.*, **135**, 124305 (2011).

[21] B.T. Darling and D.M. Denison, *Phys. Rev.*, **57**, 128 (1940).

7. High wavenumber region of *para*-fluorotoluene and *para*-xylene (900 – 1400 cm^{-1})

This chapter focuses on what is termed the "high" wavenumber range, where the D_5 and D_6 vibrations are expected in the S_1 state (based on B3LYP/aug-cc-pVTZ calculations, given in Table B.1 in Appendix B). As with the previous two chapters, some consideration will be given to the bands observed in this region in the resonance-enhanced multiphoton ionisation (REMPI) spectra of *para*-difluorobenzene (*p*DFB) and *para*-chlorofluorobenzene (*p*ClFB), before turning to the zero-electron-kinetic-energy (ZEKE) photoelectron spectroscopy (PES) spectra presented for *para*-fluorotoluene (*p*FT) and *para*-xylene (*p*Xyl).

As throughout this thesis, the aim is to assign unambiguously the structure in the REMPI spectra, utilising the ZEKE technique to aid in assigning the bands and to probe any couplings between the levels. ZEKE spectra recorded *via* 5_0^1 and 6_0^1 for *p*FT have been presented by previous workers[1,2] (referred to as $7a_0^1$ and 13_0^1 respectively in the Wilson[3]/Varsányi[4] notation of those studies), and show signs of significant congestion in the 5_0^1 case, suggestive of intramolecular vibrational redistribution (IVR) owing to many couplings in the S_1 state.

In the current work, as well as re-recording those spectra, ZEKE spectra *via* the surrounding features will also be presented. Corresponding ZEKE spectra will be presented for the first time for *p*Xyl, and comparisons made between the two molecules. In both cases, based on the couplings observed in the ~800 cm^{-1} region discussed in the previous chapter, one would expect even more widespread coupling here, since these vibrations are at higher internal energies, and the ZEKE spectra will shed some light on this.

7.A. Expected vibrations in this wavenumber range

Figure 7.1 shows the REMPI spectra of *p*ClFB, *p*DFB, *p*FT and *p*Xyl up to 1400 cm^{-1}, with the assignments below 900 cm^{-1} having been discussed in the previous chapters. As in previous chapters, the assignments come from the

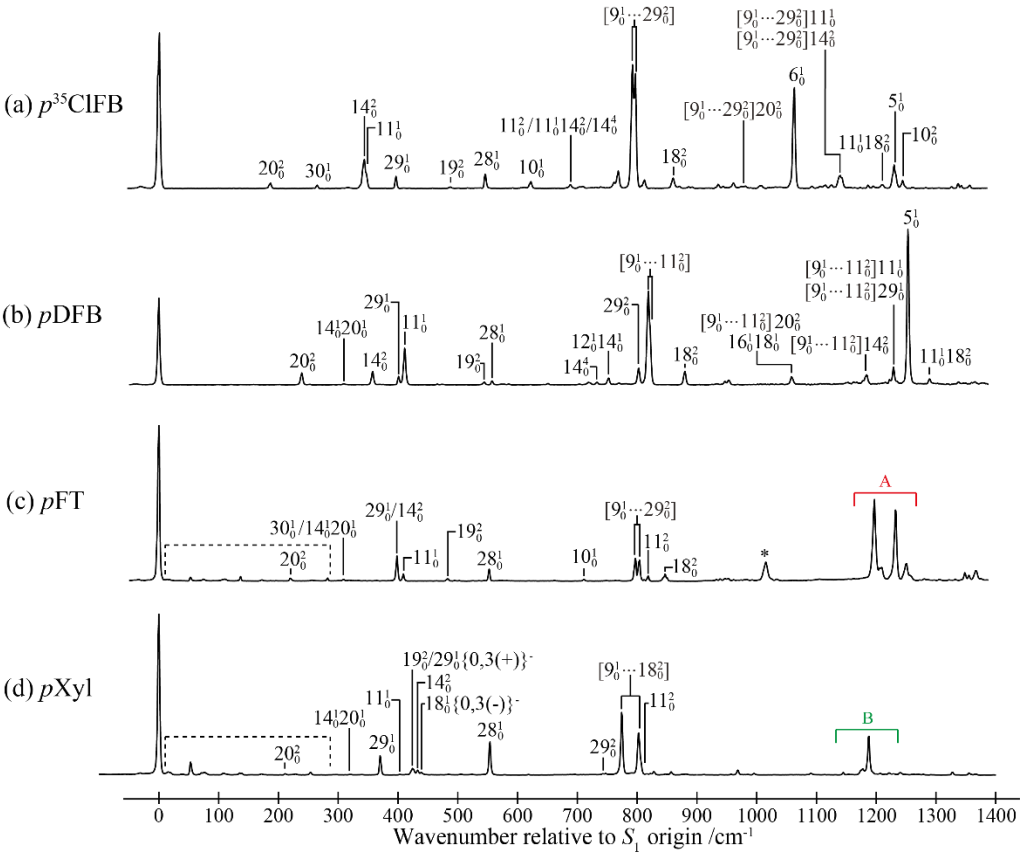


Figure 7.1 – The (a) p^{35}ClFB (b), pDFB (c) pFT and (d) pXyl $S_1 \leftarrow S_0$ REMPI spectra up to 1400 cm^{-1} are shown. Below 900 cm^{-1}, the assignments are those discussed in the previous chapters, with the most intense structure in the region from 900 – 1400 cm^{-1} considered in this chapter for pFT and pXyl. For p^{35}ClFB, the assignments are taken from the published REMPI and ZEKE studies of our group[5,6]*. For pDFB, the assignments are taken from Knight and Kable*[7]*, and have been converted to ${}^{p}D_i$ labels from the Mulliken assignments given therein, as well as recent pDFB ZEKE work by our group*[9]*.*

REMPI and ZEKE spectroscopy studies of our group[5,6] for *p*ClFB, and the laser-induced fluorescence (LIF) and dispersed fluorescence (DF) work of Knight and Kable[7] for *p*DFB. Reiser *et al.*[8] reported a ZEKE spectrum for *p*DFB *via* the S_1 D_5 level in their work, confirming the assignment of the most intense transition in this region as 5_0^1. This is in agreement with the LIF/DF results from Knight and Kable[7], and our recent *p*DFB study[9]. In *p*ClFB, intense 5_0^1 and 6_0^1 transitions are observed, with 6_0^1 completely absent in *p*DFB. This is because D_5 is totally symmetric in both the C_{2v} (a_1) and D_{2h} (a_g) point groups, whereas D_6 is only totally symmetric in the C_{2v} *p*ClFB molecule; in the D_{2h} *p*DFB molecule

it is of b_{1u} symmetry. As such, it is not symmetry-allowed in *p*DFB, in line with it not being observed. One other key aspect of this is that the D_5 and D_6 vibrations in a symmetrically substituted *para*-disubstituted benzene molecule are in-phase and out-of-phase carbon-substituent stretches respectively. However, in asymmetrically substituted molecules, these appear to evolve into local modes[10]; in particular, in *p*ClFB D_5 is a carbon-fluorine stretch while D_6 is a carbon-chlorine stretch. In this way it is easy to rationalise why both are observed with significant intensity in the *p*ClFB REMPI spectrum, and why the D_6 vibration lies to significantly lower wavenumber than D_5. In *p*FT, D_5 is also the carbon-fluorine stretch, while D_6 in that case is the carbon-methyl stretch. Obviously in the G_{72} symmetry *p*Xyl molecule (of D_{2h} point group symmetry, analogous to *p*DFB, if treating the methyl groups as point masses), these are again symmetric and asymmetric stretches, and one expects only to observe 5_0^1, as in *p*DFB.

For *p*DFB and *p*ClFB, other than these intense 5_0^1 (and 6_0^1 in the latter case) transitions, one can see transitions to the ~800 cm^{-1} D_9 Fermi resonance, in combination with other vibrations. For example, in *p*ClFB, one observes the [D_9…$2D_{29}$] Fermi resonance in combination with $2D_{14}$ and D_{11}, while in *p*DFB, it is the [D_9…$2D_{11}$] Fermi resonance in combination with $2D_{14}$, D_{29} and D_{11} that are thought to be observed. As such, analogous combinations are also expected for *p*FT and *p*Xyl, with their respective D_9 Fermi resonances.

With regard to previous work covering this wavenumber region, for *p*FT Okuyama *et al.*[11] assigned the intense band at 1195 cm^{-1} as a transition to D_6 (ν_{13} in the Wilson[3]/Varsányi[4] notation of that study) and the intense band at 1231 cm^{-1} as a transition to D_5 (ν_{7a} in that work). These assignments were also employed by Ayles *et al.*[1], with analogous assignments given in the picosecond time-resolved photoelectron spectroscopy (tr-PES) studies of Reid and co-workers[2,12–14]. Early time-resolved work by Parmenter and co-workers[15,16] assigned one of the 1195/1231 cm^{-1} bands as a transition to D_5 (vibration 3 in that work), but there is some confusion about which band they were actually referring to, as discussed later in this chapter.

For *p*Xyl, Zhang *et al.*[17,18] assigned the most intense REMPI band in this region as 5_0^1 ($7a_0^1$), and a band in their mass-analysed threshold ionisation (MATI) spectrum recorded *via* the S_1 origin as 5^1. Similarly, Ebata *et al.*[19], Blease *et al.*[20] and Walter *et al.*[21] assigned the same band in their REMPI spectra at 0^0+1186 cm^{-1} to 5_0^1 (again, $7a_0^1$ in those papers). As such, as far as the author is aware, before the work of this thesis, no ZEKE/MATI spectrum has been recorded *via* this band to probe any potential couplings at this internal energy/for this vibration in *p*Xyl.

7.B. *para*-fluorotoluene: 1180 – 1270 cm^{-1}

7.B.1. Overview of ZEKE spectra

Before continuing, it should be noted that the relatively intense band in the *p*FT REMPI spectrum at 0^0+1013 cm^{-1} will not be discussed in this thesis. Preliminary "2D-ZEKE" and 2D-LIF results have been obtained for this band by our group, and it shows particularly complicated behaviour with a number of contributing transitions, but its absence in this thesis does not affect any of the current assignments or conclusions.

The intense transitions previously assigned as 6_0^1 and 5_0^1 are both in the region labelled A in Figure 7.1, and Figure 7.2 illustrates a selection of ZEKE spectra recorded over this region, with a REMPI spectrum over this region presented as the top trace, showing the excitation positions. The origin ZEKE spectrum is also included in this figure, for comparison.

Starting with position a, recorded *via* the maximum of the 0^0+1196 cm^{-1} band, one observes a relatively clean ZEKE spectrum, with a $\Delta(v,m) = 0$ transition at 1235 cm^{-1}. This is in fair agreement with the B3LYP/aug-cc-pVTZ calculated value for D_6 in both states (see Tables B.1 and B.2 in Appendix B) and, based on the previous work and comparison to *p*ClFB, this assignment seems secure. One also observes the $\Delta(v,m) = 0$ transition in combination with the D_{11} and D_9 vibrations, but other than this there is no other intense structure in this ZEKE spectrum. There is some congestion to higher wavenumber but, compared to the

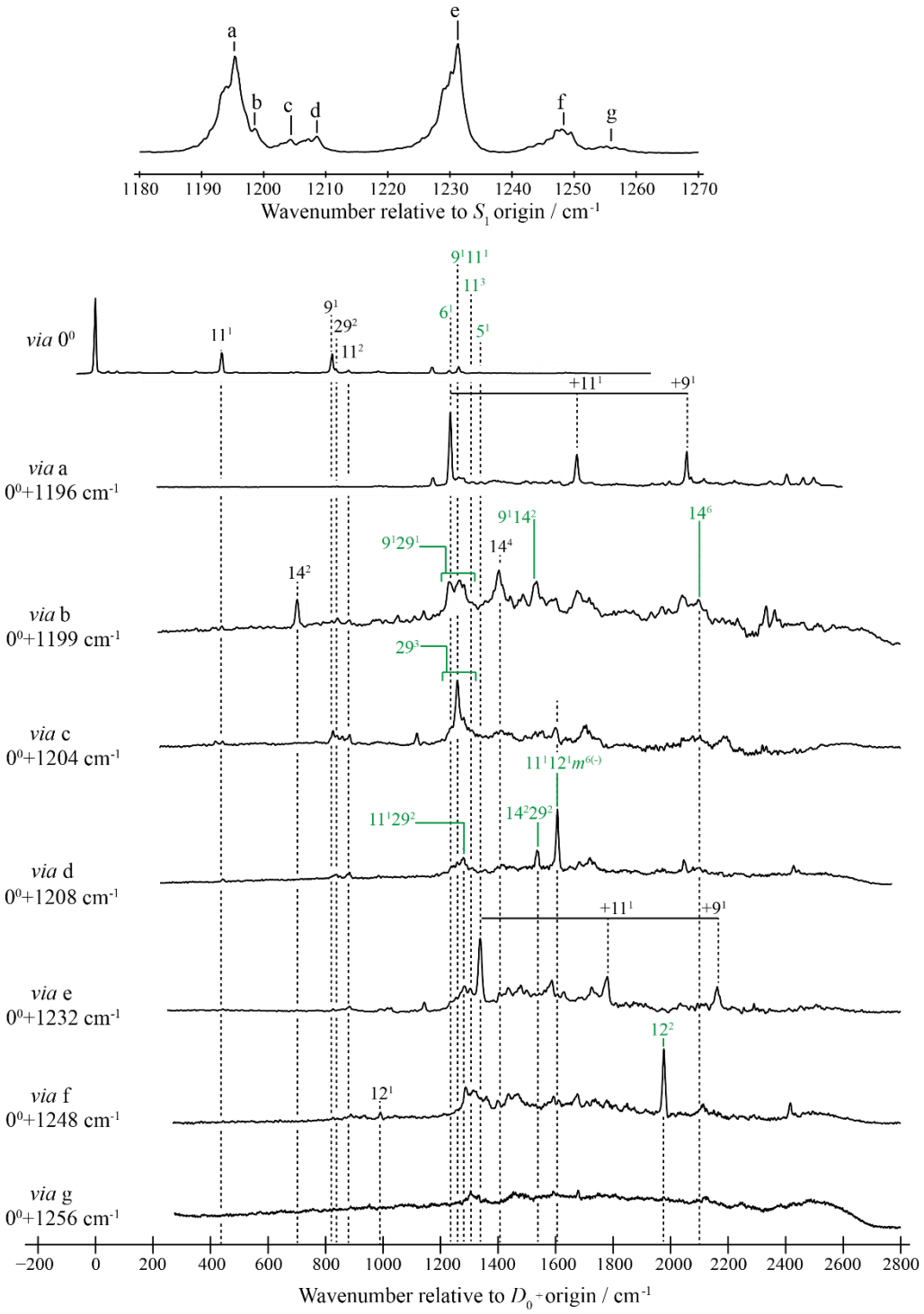


Figure 7.2 – ZEKE spectra recorded for pFT at positions a – g are presented, with the top trace illustrating a REMPI spectrum over the range 1180 – 1270 cm^{-1}, with the excitation positions labelled. The green transition labels indicate something which is a Δ(v,m) = 0 transition in at least one trace, and a green brace indicates that the transition lies within a broad, structureless, feature.

rest of the ZEKE spectra recorded over this region, this is quite weak. This implies that the D_6 level in the S_1 state is not coupled strongly to any surrounding

levels. One might recall that D_6 is the carbon-methyl stretch, and so this might seem unusual, owing to the potential for vibration-torsion coupling to open coupling pathways, and this point will be returned to later.

Considering next the ZEKE spectrum recorded at 0^0+1232 cm^{-1} (position e in Figure 7.2), one observes a $\Delta(v,m) = 0$ transition at 1338 cm^{-1}, in fair agreement with the B3LYP/aug-cc-pVTZ values for D_5 in both states (see Tables B.1 and B.2 in Appendix B). This, based on previous assignments and the *p*DFB and *p*ClFB assignments, suggest that the REMPI band can be assigned as 5_0^1. One can again assign the $\Delta(v,m) = 0$ transition in combination with D_{11} and D_9, but unlike the ZEKE spectrum recorded *via* D_6, there is significant broad underlying structure in this spectrum. This implies that D_5 in the S_1 state is coupled to many levels, either directly or *via* a doorway state, such that the projection of the S_1 eigenstate (composed of many zero-order levels) onto the D_0^+ state has intensity spread over transitions to many different levels. As such, this kind of broad, underlying, structure in ZEKE spectra is a useful fingerprint for widespread coupling. Glancing at the other ZEKE spectra presented in Figure 7.2 one can see similar underlying broadness in all of the spectra recorded over this region, other than for the 6^1 case discussed above. It is not possible to assign all of the broad structure, but some general comments regarding the expected activity in this region, and thus the potential couplings, can be made.

Considering the lower wavenumber portions of the *p*FT REMPI spectrum, discussed in Chapters 3, 5 and 6, the most intense features were at 400, 410, 797, 804, 819 and 846 cm^{-1}, with the 797 – 846 cm^{-1} features containing many different zero-order level contributors, as discussed in the previous chapter. One might note that this complicated 797 – 846 cm^{-1} region in combination with the 400 – 410 cm^{-1} features would fall within the range 1197 – 1256 cm^{-1} (assuming a simple sum of the band positions), i.e. the region under discussion. From low to high wavenumber over the 797 – 846 cm^{-1} range, the transitions $14_0^2 29_0^1$, $12_0^1 m_0^{6(-)}$, 9_0^1, 14_0^4, 29_0^2, $11_0^1 29_0^1$, $11_0^1 14_0^2$, 11_0^2, $12_0^1 14_0^1$ and 18_0^2 were assigned.[a]

[a] Note that other levels have been assigned in a recent 2D-LIF/ZEKE study by our group[22] associated with the 18^2 transition. These were referred to in Chapter 6, in a brief summary of that publication, and will be referred to later.

Combinations of each of these with $2D_{14}$, D_{29} and D_{11} are then to be expected in the wavenumber range currently under consideration. The full list of these possible transitions is as follows:

Transition	G_{12} Symmetry	Transition	G_{12} Symmetry
$12^1 14^2 m^{6(-)}$	a_1'	$11^1 14^2 29^1$	a_1''
14^6	a_1'	$11^1 29^2$	a_1'
$12^1 29^1 m^{6(-)}$	a_1''	$12^1 14^3$	a_1'
$9^1 14^2$	a_1'	$11^2 14^2$	a_1'
$14^4 29^1$	a_1''	$12^1 14^1 29^1$	a_1''
$9^1 29^1$	a_1''	$11^2 29^1$	a_1''
$14^2 29^2$	a_1'	$11^1 12^1 14^1$	a_1'
29^3	a_1''	11^3	a_1'
$11^1 12^1 m^{6(-)}$	a_1'	$14^2 18^2$	a_1'
$11^1 14^4$	a_1'	$18^2 29^1$	a_1''
$9^1 11^1$	a_1'	$11^1 18^2$	a_1'

For simplicity, here and going forward, the lower levels have been omitted since they are the zero-point vibrational levels of the ground electronic state.

Although all of these terminating levels will exist, they will not necessarily be intrinsically bright, or be involved in any couplings in the region currently under discussion. One might expect intrinsic intensity for a combination of two transitions which themselves had intrinsic intensity. Additionally, some of these transitions require vibronic coupling for their intensity (or for them to couple to a totally symmetric level). As such, to simplify the picture slightly, it will be assumed that only the key dominant component of each 790 – 850 cm^{-1} REMPI band (D_9, $2D_{29}$, $2D_{11}$ and $2D_{18}$) will be observed in combination with $2D_{14}$, D_{29} and D_{11}. This is illustrated in the upright trace in Figure 7.3, which takes the 400 – 410 cm^{-1} REMPI bands and offsets them to the expected positions of their combinations with D_9, $2D_{29}$, $2D_{11}$ and $2D_{18}$, shown as coloured traces.

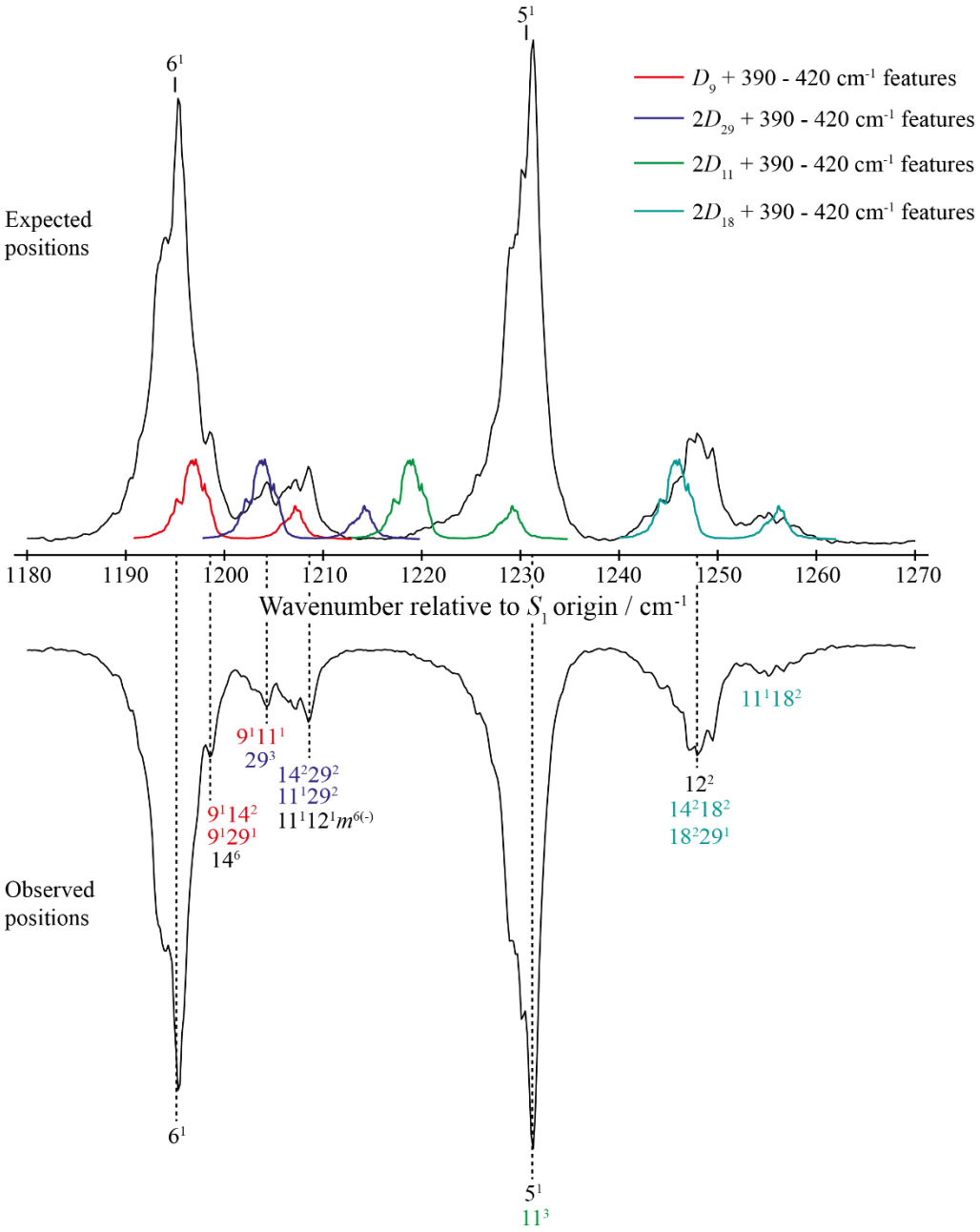


Figure 7.3 – Upright: The pFT REMPI spectrum from 1180 – 1270 cm^{-1} is presented as a black trace. The coloured traces are the 400 and 410 cm^{-1} REMPI bands offset to match the expected positions of the combinations of these with the intense 797, 804, 819 and 846 cm^{-1} REMPI transitions. This gives an indication of where, in the absence of coupling, these combination bands would be expected in the REMPI spectrum. Inverted: the same REMPI spectrum is shown, with the assigned transitions indicated.

The red trace shows the expected positions of the D_9 combination bands: $9^1 14^2$, $9^1 29^1$ and $9^1 11^1$. The $9^1 14^2$ and $9^1 29^1$ bands are expected close to 0^0+1199 cm^{-1}, a position at which a ZEKE spectrum was recorded, shown in

Figure 7.2, trace b. This ZEKE spectrum appears to show some 6^1 character, which is to be expected at this excitation position since it will still be coincident with some of the rotational profile of the 6^1 REMPI transition. There is additional structure compared to the ZEKE spectrum recorded *via* the peak of the 6^1 REMPI band, such as a relatively broad band at 1522 – 1540 cm^{-1}. The low wavenumber side of this can be readily assigned as the expected $9^1 14^2$ transition, with the higher wavenumber side matching $14^2 29^2$, perhaps owing to the coupling of D_9 and $2D_{29}$ in the cation. The $9^1 29^1$ ZEKE transition is expected at around 1238 cm^{-1}, and there is broad structure in the 1225 – 1285 cm^{-1} region in this spectrum. There appear to be contributions from 6^1 (1235 cm^{-1}) and seemingly from $9^1 11^1$ (1260 cm^{-1}, discussed below) to this broad structure, but it is certainly possible that $9^1 29^1$ also contributes to this region. It would not couple strongly to either 6^1 or $9^1 11^1$ in the cation even though they are energetically close, since it is of a different symmetry. It should be noted that the range from ~1220 – 1300 cm^{-1} is broad and structureless in most of these ZEKE spectra, and this is thought to be due to several overlapping transitions as discussed below.

The $9^1 11^1$ transition in the REMPI spectrum is expected at ~1207 cm^{-1}, and the ZEKE spectrum recorded at 0^0+1204 cm^{-1} shows a sharp, intense, $\Delta(v,m) = 0$ transition at 1260 cm^{-1}, which can be assigned to $9^1 11^1$. It is slightly lower than expected in the S_1 state, suggesting that it has been pushed down in wavenumber by coupling with some higher level.

The dark blue trace in Figure 7.3 shows the expected REMPI positions of the $14^2 29^2$, 29^3 and $11^1 29^2$ transitions. Note that $3D_{29}$ is of a_1'' symmetry while the other two are totally symmetric. $14^2 29^2$, 29^3 are expected close to the excitation position 0^0+1204 cm^{-1} used for the ZEKE spectrum shown in trace c of Figure 7.2. In the cation 29^3 is expected at around 1242 cm^{-1}. This would place 29^3 under the broadness at 1220 – 1300 cm^{-1}, and its assignment is possible. However, it if is present it seems to be present only weakly and, as mentioned above, its activity in the $S_1 \leftarrow S_0$ transition would necessitate vibronic

coupling, with no intense transition nearby that this would be expected to couple to strongly. Thus, this assignment is tentative.

Although there is a weak band in the correct place for $14^2 29^2$ in the 0^0+1204 cm^{-1} ZEKE spectrum, there is a more intense band at the same position (1535 cm^{-1}) when exciting at 0^0+1208 cm^{-1}, and this is thought to be the $\Delta(v,m) = 0$ transition, placing $14^2 29^2$ at around 1208 cm^{-1} in the S_1 state, slightly higher than expected, perhaps owing to coupling with some lower level. Note that no attempt is made here to explicitly find coupling "partners" for these levels, since the evidence from the ZEKE spectra is that a significant number of zero-order levels are being accessed, leading to the broad structure observed in these ZEKE spectra.

The $11^1 29^2$ band, as can be seen from Figure 7.3, would be expected in a region of the REMPI spectrum where there are no observed transitions, but it fits well the maximum of a ZEKE feature (at 1280 cm^{-1}) when exciting at 0^0+1208 cm^{-1}, and so it is assigned as this. It has already been discussed that this region of these ZEKE spectra contains many transitions, with seemingly a different dominating transition depending on the excitation position. The ZEKE assignments within this broad clump of transitions from 1220 – 1300 cm^{-1} are supported by the shifting maximum, illustrating the changing contributions, but it is not possible to be certain about exactly which contributions are present in which spectra.

Regarding the green trace in Figure 7.3, only the 11^3 transition lies under an observed feature – underneath the 5^1 band – but it is possible that the $11^2 14^2$ and $11^2 29^1$ might be perturbed and observed at a different excitation position. These could also be present at the red tail of the 5^1 band, close to their expected position, but no ZEKE spectrum was recorded at this position. In the cation, $11^2 29^1$ would be expected at 1221 cm^{-1}, placing it effectively within the broad clump of ZEKE transitions observed in all of these ZEKE spectra (apart from the one *via* D_6). Thus, no firm conclusion can be drawn regarding $11^2 29^1$. There is a ZEKE band at 1579 cm^{-1} when exciting at 0^0+1232 cm^{-1} (i.e. exciting the maximum of the 5^1 REMPI band), and this could be assigned as $11^2 14^2$, which would be expected at around 1578 cm^{-1}. Whether this is a $\Delta(v,m) = 0$ transition,

or suggestive of coupling, is unknown, and so no further comment can be made regarding this. Returning to the 11^3 transition, this would be expected at ~1320 cm^{-1} in the cation, placing it under the broad clump of features, just below 5^1, in the ZEKE spectrum recorded at 0^0+1232 cm^{-1}. If present at this position, this would be a $\Delta(v,m) = 0$ transition.

Finally, the turquoise trace in Figure 7.3 shows the expected positions of $14^2 18^2$, $18^2 29^1$ and $18^2 11^1$. These are expected to contribute to the bands above 5^1, with ZEKE spectra recorded at 0^0+1248 and 0^0+1256 cm^{-1} expected to contain these contributions if they are present in the S_1 state. Note that these REMPI bands, from 1240 – 1260 cm^{-1}, have profiles very similar to the ~846 cm^{-1} region of the REMPI spectrum, suggesting that the levels assigned there[22] – $2D_{18}$, as well as $2D_{14}D_{18}$ $m = 2$, $D_{29}D_{18}$ $m = 2$ and $D_{11}D_{18}$ $m = 2$ – also contribute here, in combination with the $2D_{14}$, D_{29} and/or D_{11} vibrations.

The $14^2 18^2$ and $18^2 29^1$ would be expected at 1687 and 1401 cm^{-1} respectively in the cation and, in the ZEKE spectrum recorded at 0^0+1248 cm^{-1}, there are bands in these positions, but these are on top of a broad, structureless, underlying signal. In the ZEKE spectrum recorded at 0^0+1256 cm^{-1}, there is no obvious band at 1427 cm^{-1}, where $11^1 18^2$ would be expected, but this spectrum is particularly unstructured. This is thought to be due to the intensity being spread among a huge bath of zero-order states[b], smearing out any obvious bright contributions. A similar argument applies to the broad underlying structure in all of these ZEKE spectra, but applies particularly to the 0^0+1248 cm^{-1} and 0^0+1256 cm^{-1} ZEKE spectra, a point which will be returned to in the discussion below. In summary, although difficult to ascertain from the ZEKE spectra, owing to the REMPI band profiles being very similar to those of the ~846 cm^{-1} bands, the $14^2 18^2$, $18^2 29^1$ and $11^1 18^2$ are thought to be present, and the $2D_{14}$, D_{29} and D_{11} combinations with $2D_{14}D_{18}$ $m = 2$, $D_{29}D_{18}$ $m = 2$ and $D_{11}D_{18}$ $m = 2$ are also expected to contribute.

[b] It is also likely that this spectrum is particularly sensitive to the changing UV intensity over the range scanned, something which is often the case in ZEKE spectra where bright state intensity is particularly spread out, i.e. in particularly weak ZEKE spectra.

The above assignments include only the expected contributions from combinations of the most intense lower wavenumber structure to this region of the REMPI spectrum. But there are other intense transitions in these ZEKE spectra yet to be assigned. For example, when exciting at 0^0+1248 cm^{-1}, a sharp, intense, transition is observed at 1977 cm^{-1}, suggesting a $\Delta(v,m) = 0$ transition. This is a very large S_1 to D_0^+ shift, and the only assignment which fits is 12^2. This would be expected at 1238 cm^{-1} in the S_1 state and 1972 cm^{-1} in the D_0^+ state, based on the D_{12} fundamental obtained from $D_{12}D_{14}$ in Chapter 6. Although slightly higher than anticipated in the S_1 state, it could be perturbed to this higher wavenumber by coupling to a lower wavenumber level, or the obtained D_{12} value in the previous chapter could come from a perturbed level. The assignment of 12^2 in the 0^0+1248 cm^{-1} ZEKE spectrum is supported by the observation of the 12^1 transition (a $\Delta v = -1$ transition) at 991 cm^{-1}. Additionally, the assignment of 12^2 in the REMPI spectrum is supported by the work of Knight and Kable[7], who assigned 12^2 in their LIF spectrum of *p*DFB, an assignment which was confirmed in a recent ZEKE study[9].

When exciting at 0^0+1208 cm^{-1}, there is an intense ZEKE band at 1607 cm^{-1}, thought to be a $\Delta(v,m) = 0$ transition. This band almost perfectly matches the expected S_1 and D_0^+ positions for $11^1 12^1 m^{6(-)}$, i.e. $12^1 m^{6(-)}$ (thought to be coupled to D_9 in Chapter 6) in combination with D_{11}. The fact that this yields such an intense ZEKE transition is unusual, especially since neither $29^1 12^1 m^{6(-)}$ or $14^2 12^1 m^{6(-)}$ seem to yield significant ZEKE bands. However, those are expected on the low wavenumber side of the 0^0+1196 cm^{-1} band in the S_1 state, and no ZEKE spectra were recorded over that region, so they may simply have not been observed. The appearance of the same 1607 cm^{-1} band, weakly, in the 0^0+1204 cm^{-1} ZEKE spectrum could suggest that $D_{11}D_{12}$ m = 6(-) is coupled to D_9D_{11} in the same way that D_{12} m = 6(-) is thought to be coupled to D_9.

Finally, in the ZEKE spectrum recorded at 0^0+1199 cm^{-1}, one observes a progression in the $2D_{14}$ coordinate; bands assignable to 14^2, 14^4 and 14^6 are observed. This would be the correct excitation position for $6D_{14}$, and its

appearance would be consistent with also observing 29^3 and 11^3, i.e. "second overtones" of the 400 – 410 cm^{-1} bands. As such, 14^6 is assigned as a $\Delta(v,m) = 0$ transition.

As a significant number of S_1 levels have been assigned from this handful of ZEKE spectra, the following will summarise the transitions discussed above, all of which could carry some intrinsic brightness. A pictorial form of the following summary is given in Figure 7.3, where the inverted trace shows these assignments at their respective band positions.

The band at 0^0+1196 cm^{-1} is dominated by 6^1, seemingly in isolation. The shoulder to this band at 0^0+1199 cm^{-1} has contributions from $9^1 14^2$ and $9^1 29^1$, as well as 14^6.

The 0^0+1204 cm^{-1} band has contributions from $9^1 11^1$ and 29^3, while the overlapping band 0^0+1208 cm^{-1} has contributions from $14^2 29^2$, $11^1 29^2$ and $11^1 12^1 m^{6(-)}$.

The band at 0^0+1232 cm^{-1} appears to be dominated by 5^1, with a possible contribution from 11^3, and a lot of broad underlying structure suggesting contributions from many other zero-order levels.

The band at 0^0+1248 cm^{-1} appears dominated by 12^2, with expected contributions from $14^2 18^2$ and $18^2 29^1$, while the band at 0^0+1256 cm^{-1} shows an almost unstructured spectrum, with $11^1 18^2$ expected at this position, with its activity seemingly smeared out among a myriad of other zero-order levels.

Finally, it was not possible to identify the S_1 positions of $14^2 11^2$ and $11^2 29^1$, but they are possibly under the 0^0+1232 cm^{-1} band or its low wavenumber edge.

7.B.2. Discussion

Although the above assignments consider the expected main contributions, they do not consider all of the possibilities, for example, the $2D_{14}$, D_{29} and D_{11}

combinations with $D_{12}D_{14}$, but there are also many other possible zero-order levels in this region. One can calculate the density of states (DOS), as discussed in detail later in this chapter, including up to four vibrational quanta and *m* levels up to $m = 7$. Over the range 1180 – 1215 cm^{-1}, i.e. a range of ±17.5 cm^{-1} roughly equally split either side of D_6, there are calculated to be a total of 409 vibrational and vibtor levels, of which 59 are of a_1' symmetry and 98 are of e'' symmetry, i.e. 157 levels which could couple to the $m = 0$ or $m = 1$ levels of the totally symmetric D_6 vibration. Over the range 1215 – 1250 cm^{-1}, i.e. a range of ±17.5 cm^{-1} roughly equally split either side of D_5, there are 525 levels, of which 60 are of a_1' symmetry and 133 are of e'' symmetry, i.e. 193 levels which could couple to the $m = 0$ or $m = 1$ levels of the totally symmetric D_5 vibration.

One can see a similarity in the number of a_1' levels, but an increase of around 35% in e'' levels in the window for D_5 compared to D_6. This is a possible explanation for the increased coupling for the D_5 vibration compared to D_6, but this is also quite a large energetic window, and one must take care when drawing conclusions from specific "windows" of the DOS. This is because of the prevalence of coupling in *p*FT (and *p*Xyl), since some extracted vibrational fundamentals may have been obtained from perturbed levels, and also because the required "window" to include all levels involved in coupling may be different for different cases. This point will be returned to later in this chapter, where a discussion of the overall trends in the DOS is provided, which is thought to be the more reliable approach, and a standardised set of ±5 cm^{-1} windows will be used to probe the local DOS (for a range of different S_1 levels) at various internal energies.

All of the ZEKE spectra recorded over this region, with the possible exception of the one recorded *via* the maximum of the 6^1 band, show broad underlying signal in the spectra. Sometimes this is structured, but particularly in the cases of the 0^0+1248 and 0^0+1256 cm^{-1} bands it is unstructured. This is taken to indicate significant coupling to the bath of states in the S_1 state, spreading bright state intensity among many zero-order states and leading to activity across the whole ZEKE spectrum. Owing to the almost complete loss of structure of the 0^0+1256 cm^{-1} ZEKE spectrum, followed closely by the 0^0+1248 cm^{-1} ZEKE

spectrum, it is thought that levels at these positions are more strongly coupled to the bath states – either directly or *via* a doorway state.

One must recall that these REMPI features from 1240 – 1270 cm^{-1} are thought to contain the ~846 cm^{-1} REMPI features in combination with $2D_{14}$, D_{11} and D_{29}. This is supported by the similarity of the band profiles here to those of the ~846 cm^{-1} REMPI features. Recent work by our group[22] showed that the $2D_{18}$ level which dominates the 846 cm^{-1} feature is coupled to the bath of states *via* three doorway states; $2D_{14}D_{18}$ $m = 2$, $D_{18}D_{29}$ $m = 2$ and $D_{11}D_{18}$ $m = 2$. Two of these are of e'' symmetry, while one is of e' symmetry, allowing access to different symmetry bath state levels (with the e' symmetry doorway state accessed from the bright $2D_{18}$ $m = 1$ level by vibronic coupling). It was shown that only $2D_{18}$ $m = 1$ was coupled to the bath, *via* these doorway states, and not $2D_{18}$ $m = 0$.

Since the region of the REMPI spectrum under discussion here includes these levels in combination with $2D_{14}$, D_{29} and D_{11}, it seems plausible that the resulting levels are also coupled to the bath of states here. Thus, the proximity of D_5 to these levels could explain why it shows evidence of widespread coupling in its ZEKE spectrum, while the ZEKE spectrum recorded *via* D_6 shows effectively none of this[c]. It is possible that, through couplings of the various zero-order level contributions across this region, even levels at 0^0+1199 cm^{-1} could end up coupled to the bath of states through a series of couplings terminating in the bath states. This would again mirror the lower wavenumber activity, since the activities from the 1196 – 1208 cm^{-1} REMPI bands are combinations of the coupled levels around D_9 and $2D_{29}$ with $2D_{14}$, D_{29} and D_{11}. Thus, it seems that the widespread coupling observed in this region of the REMPI spectrum derives from a myriad of coincidences: a set of lower wavenumber zero-order levels involved in restricted couplings (effectively Fermi resonance) in combination with $2D_{14}$, D_{29} and D_{11} lie in this region, and a set of lower wavenumber

[c] Note that if combinations of the ~846 cm^{-1} levels are acting as, effectively, doorway states here, one would only expect loss of population from D_5 $m = 1$ and not from D_5 $m = 0$, a point which will be returned to shortly.

zero-order levels involved in widespread coupling in combination with $2D_{14}$, D_{29} and D_{11} lie in this region.

One might then question why such widespread coupling was not so prevalent in the lower region, given the contributors were very similar. This could be due to several factors, such as the increased DOS at higher wavenumber, the influence of D_5 (which will be discussed more later in this chapter), or that the level energetics here are more favourable for these couplings; it is likely a combination of these factors.

With regard to the vibrational motions, it was mentioned earlier that D_5 is a carbon-fluorine stretch while D_6 is a carbon-methyl stretch. If it is the addition of the methyl groups that is key to the widespread coupling under discussion, owing to the increased build up in the DOS and the widespread nature of vibration-torsion coupling, then one might expect D_6 to be more strongly coupled to the bath of states than D_5, owing to the involvement of the methyl group in its motion. However, this is not the case based on the spectra discussed above. This seems to emphasise that proximity of levels and energetic coincidences are key in accessing the bath of states, such that the proximity of D_5 to some "doorway state(s)" (or particular bath level(s) to which it can couple directly) is more important than any methyl-based motion of the D_6 vibration.

It should be noted that there is ongoing work in our group recording 2D-LIF spectra over this region, which should help in understanding the coupling pathways. For the purposes of this thesis, i.e. comparing IVR in the single rotor *p*FT and double rotor *p*Xyl systems, it is sufficient to note the extent to which coupling (in the S_1 state) of D_5 to the bath of states leads to broadness in the ZEKE spectrum recorded *via* the D_5 dominated band. Below, it will be seen that the *p*Xyl ZEKE spectra show evidence of even more widespread coupling.

7.B.3. Comparison to time-resolved studies

Early time-resolved studies by Parmenter and co-workers used the method of chemical timing[23]. These studies involved recording DF spectra from S_1

intermediate levels with different pressures of the quenching gas, O_2. Higher pressures of O_2 lead to more collisions, effectively supressing fluorescence at long times. By recording DF spectra at different picosecond time delays (*via* the different O_2 pressures) after excitation, this effectively enables a temporal study and so extraction of IVR lifetimes. Early results[15,16] exciting the *p*FT vibration labelled 3^1 (in the *p*DFB Mulliken scheme[24] used to label the vibrations in that work, corresponding to 5^1 in this thesis) in a 300 K sample suggested an IVR lifetime of ~15 ps. However, there is some confusion over the initial level excited here; in Reference 15, it is suggested that this lifetime comes from excitation at 0^0+1195 cm^{-1} for *p*FT-h_3, while in reference 16 this is given as 0^0+1230 cm^{-1} for *p*FT-h_3, with 0^0+1195 cm^{-1} for *p*FT-d_3. Thus, it appears that this lifetime could be from exciting either the 6^1 (0^0+1195 cm^{-1}) or 5^1 (0^0+1230 cm^{-1}) transition, and it is not clear which level this lifetime corresponds to – something also remarked upon by Hammond *et al*.[25] Work by Baskin *et al*.[26], utilising time-resolved fluorescence decays to study jet-cooled *p*FT, showed a fluorescence decay when exciting at 0^0+1195 cm^{-1}, and this showed little evidence of IVR. These experiments were carried out with ~5cm^{-1} laser bandwidth, and suggested a much longer lifetime than that given by Parmenter and co-workers[15]. Thus, it will be assumed that the ~15 ps IVR lifetime derived by Parmenter and co-workers corresponds to excitation of the higher 5^1 level, and the longer lifetime suggested by Baskin *et al*. corresponds to excitation of the lower 6^1 level. These lifetimes are consistent with the ZEKE spectra discussed above, and those presented previously[1,2].

The above studies each used quite different conditions, in terms of temperature, laser bandwidth and pulse duration, all of which have been commented on by Hammond *et al*.[25] This makes it unreliable to compare the IVR lifetimes obtained for the two levels, D_5 and D_6. Reid and co-workers have carried out multiple studies[2,13,27,28] relevant to these levels, utilising picosecond tr-PES and using the same laser bandwidth (~13 cm^{-1}) and pulse duration (1 ps) to study both levels, so attention will now be turned to these studies.

King *et al*.[13] present tr-PES at 0, 8, 30 and 60 ps delays when exciting D_6 (the transition was labelled 8^1 in that work) and at 0, 20, 80 and 160 ps when exciting

D_5 (labelled 7^1 in that work). Although these are not the same delays, and thus not directly comparable, by inspection it appears that the D_6 spectra have lost their structure at shorter delays than the D_5 spectra, implying that 6^1 has a shorter IVR lifetime than 5^1. Additionally, King *et al*. assign one of the dark states that D_5 is thought to couple to as D_7; based on the B3LYP/aug-cc-pVTZ calculated value (Table B.1 in Appendix B) of this thesis, D_7 would be expected to be 100 cm^{-1} lower that D_5 in the S_1 state, and so this is thought to be unlikely. Additionally, there is no evidence of D_7 in the ZEKE spectra presented above recorded *via* the D_5 intermediate level.

A preliminary IVR lifetime of 26 ps was obtained by King *et al*.[13] for D_5, with Hammond *et al*[25]. citing a value of 16 ps for D_6 (from unpublished work), i.e. a shorter lifetime for D_6 than D_5, in contrast to the work of Parmenter and co-workers[15,16], Baskin *et al*.[26], and the ZEKE spectra presented here and previously. However, later work by Davies *et al*.[2,28] gives IVR lifetimes for D_5 and D_6 as 13 ps and 50 ps respectively, in contrast to the earlier preliminary findings. The cause of this difference is unknown, but the ZEKE spectra presented here agree with the most recent findings of Davies *et al*., and with the earlier work discussed above.

Davies *et al*.[2] comment that the IVR lifetime (50 ps) observed when exciting D_6 for *p*FT is longer than for the analogous toluene and toluene-d_3 vibrations, and this is proposed to be due to the role of doorway states in the toluene species but not for this level in *p*FT. They also comment that their earlier work when exciting at 845 cm^{-1} in *p*FT gave a shorter lifetime (17 ps) than exciting *via* this higher wavenumber, D_6, vibration, supporting the role of doorway states at that lower position. The current ZEKE work supports these comments, with no obvious strong couplings to D_6 (with only some weak congestion to higher wavenumber in the ZEKE spectrum).

Additionally, Davies *et al*.[2] comment that only half of the tr-PES ($\Delta(v,m) = 0$) intensity is lost over 500 ps when exciting D_6 in *p*FT, whereas almost all of it is lost for the analogous vibration in toluene. This suggests selective coupling of only one of the D_6 m levels, either D_6 $m = 0$ or D_6 $m = 1$. The ZEKE spectra

presented here do not allow any definitive conclusion to be made on which level is losing population, however on DOS grounds, there will be more nearby levels that D_6 $m = 1$ would be able to couple to than D_6 $m = 0$.

If one compares the tr-PES, $\Delta(v,m) = 0$, intensity decays for D_6 and D_5 for *p*FT, given in reference 28, one can see a much more significant loss of population for D_5 than for D_6, suggesting that the coupling is not $m = 0/m = 1$ selective for D_5. This is consistent with the ZEKE spectra presented here, which show more widespread coupling when exciting D_5 than D_6.

This being the case, the (tentatively proposed) doorway states discussed above, which could only couple to D_5 $m = 1$, would only be part of the picture, and other zero-order levels coupling to $m = 0$ will be important in the coupling pathway. It is notable that all of the ZEKE spectra recorded over the range 1200 – 1260 cm^{-1} show similar congestion to the D_5 ZEKE spectrum, and are thus expected to be involved in this (or similar) couplings.

In the recent work of Davies *et al*.[28], they showed that the D_5D_9 level undergoes faster IVR than the D_6D_9 level, following the same pattern as D_5 compared to D_6. They rationalised the faster IVR they observed for D_5D_9 compared to D_6D_9 as arising from a stronger van der Waals interaction between the methyl hydrogen atoms and the ring hydrogen atoms when undergoing a D_5 vibration compared to a D_6 vibration. Since this would couple the vibrational and torsional motions more strongly for D_5, it was suggested that levels involving D_5 were more susceptible to vibration-torsion coupling than those involving D_6. This is supported by the congestion in the ZEKE spectra recorded here *via* D_5 and D_6.

7.C. *para*-xylene: 1120 – 1260 cm^{-1}

Turning now to the *p*Xyl molecule, in Figure 7.1 one can observe an intense REMPI feature at 0^0+1187 cm^{-1}, previously assigned[17–20] as 5^1 in the absence of any ZEKE or DF studies. ZEKE spectra recorded *via* this feature and the surrounding bands are presented in Figure 7.4, with a REMPI spectrum shown in the inset to illustrate the excitation positions, and the origin ZEKE spectrum

(the lower wavenumber part of which is discussed in Chapter 4) included at the top for comparison purposes.

7.C.1. Overview of ZEKE spectra

The ZEKE spectra recorded at 0^0+1186 and 0^0+1187 cm^{-1}, *via* the two maxima of the intense REMPI feature, show almost identical activity. There is a sharp ZEKE transition at 1189 cm^{-1}, and a broader band with maxima at 1238 and 1246 cm^{-1}, all superimposed on a very significant, broad, underlying signal. This suggests coupling to a significant number of zero-order levels in the S_1 state, and the broadness of the ZEKE spectra renders assigning these in detail an impossible task. The most intense of the resolved transitions, at 1238 cm^{-1}, can be assigned as 5^1, with the 1246 cm^{-1} ZEKE band fitting the assignment of $9^1 11^1$. Both also appear in the origin ZEKE spectrum, and it is suggested that they could be coupled in the cation. Note that 5^1 is thought to be a $\Delta v\{m_1,m_2\} = 0$ transition, giving its S_1 position at 1187 cm^{-1}. The $9^1 11^1$ would be expected at 1179 cm^{-1} in the S_1 state, and so the $\Delta v\{m_1,m_2\} = 0$ transition would be expected in the spectrum recorded at 0^0+1177 cm^{-1} (trace j). No sharp features are observed here; in both traces recorded *via* this band (i and j), only broad, featureless, signal is observed. This suggests that $9^1 11^1$ is masked by the broad signal in these traces, or that it is perturbed to higher wavenumber in the S_1 state, and is observed as a $\Delta v\{m_1,m_2\} = 0$ transition at positions k and l, alongside 5^1. It could also be observed in traces k and l owing to coupling with D_5 in the cation, and the different couplings of D_5 and D_9D_{11} in the S_1 and D_0^+ states.

The sharp band at 1189 cm^{-1} in the ZEKE spectra recorded *via* the intense feature (traces k and l) can be assigned as 7^1, in reasonable agreement with its calculated value. This is also observed in the origin ZEKE spectrum, as well as in the *p*FT origin ZEKE spectrum. It is noted that King *et al*.[13] assigned D_7 as being coupled to D_5 in *p*FT, but in the ZEKE spectra presented here for *p*FT it was not present when exciting *via* the D_5 level, but seemingly was observed weakly when exciting D_6. This is thought to be on Franck-Condon grounds, owing to the observation of both D_7 and D_6 in the *p*FT origin ZEKE spectrum. Here, for *p*Xyl,

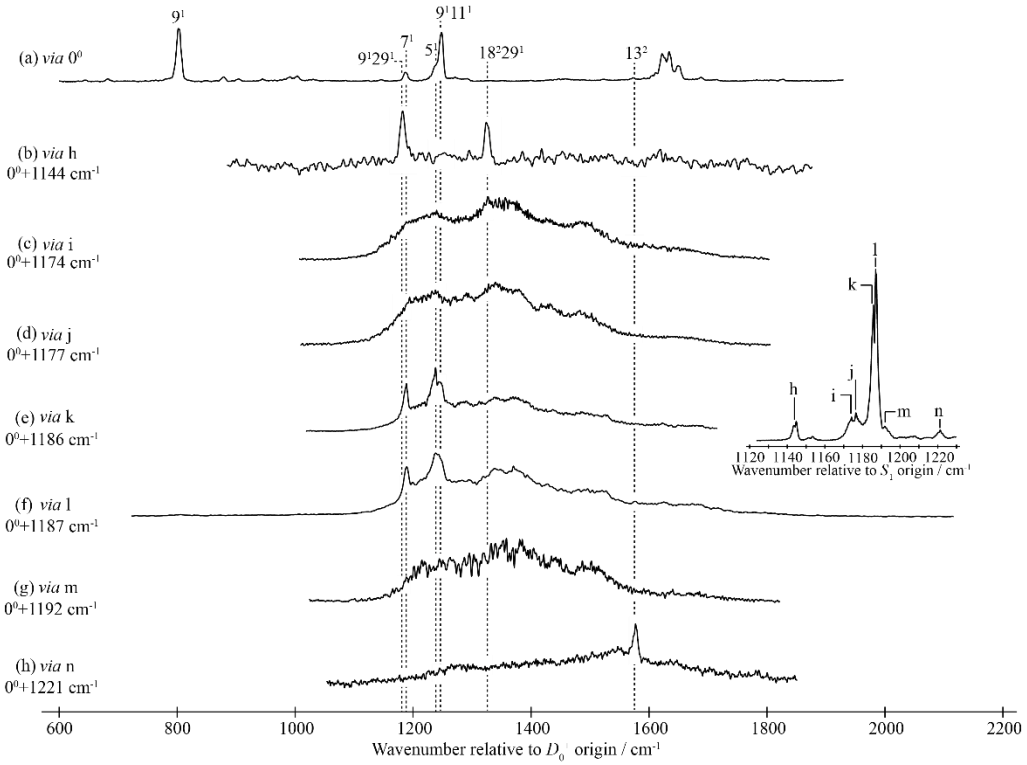


Figure 7.4 – ZEKE spectra recorded over the range 1120 – 1230 cm^{-1} for pXyl are presented (traces h – n). The top ZEKE trace is the origin ZEKE spectrum, for comparison, and the inset REMPI spectrum to the right illustrates the excitation positions.

the intensity of 7^1 suggests it is not just Franck-Condon behaviour, and it only appears in the ZEKE spectra in which 5^1 and $9^1 11^1$ are discernible. This suggests it could arise from a Duschinsky rotation between D_7 and D_5 from the S_1 to D_0^+ state. The 7^1 was observed in the S_1 state for *p*DFB[7,9], but it was not observed for *p*ClFB[5,6] or *p*FT. The ZEKE band is not thought to be a $\Delta v\{m_1,m_2\} = 0$ transition here, since it is expected to lower wavenumber than this excitation position in the S_1 state (based on the calculated B3LYP/aug-cc-pVTZ D_7 value given in Table B.1 in Appendix B).

If one assigns $9^1 11^1$ in the REMPI spectrum, one would also expect $11^1 18^2$ and 11^3, based on the combination of the 775 – 810 cm^{-1} features with D_{11}. These would be expected around 1205 – 1215 cm^{-1}, and although there is weak structure here in the REMPI spectrum, no ZEKE spectra have been obtained exciting at these positions. Based on the observed activity in *p*FT, however, i.e. combinations of lower wavenumber structure with D_{11} (and other vibrations)

being observed in the region of D_5, it is suggested that the $11^1 18^2$ and 11^3 transitions do indeed lie under the weak structure at ~1210 cm^{-1}.

One can see that all of the ZEKE spectra in traces i – m show broad, structureless, spectra, with sharp transitions on top of this in only two cases. Each of these excitation positions is within a set of REMPI features that contains signal across the whole range 1170 – 1200 cm^{-1}, and this supports the argument of coupling to many zero-order levels in the S_1 state. ZEKE spectra were also recorded *via* two bands, one to higher and one to lower wavenumber, to which attention will now be given.

Trace h was recorded *via* the band to lower wavenumber at 0^0+1144 cm^{-1} and shows a remarkably flat baseline with two sharp ZEKE transitions, one at 1183 cm^{-1} and the other at 1323 cm^{-1}. At first glance, this lower ZEKE band could be assigned to 7^1, perhaps as a $\Delta v\{m_1,m_2\} = 0$ transition. However, this makes it difficult to assign the 1323 cm^{-1} ZEKE band, which must be another $\Delta v\{m_1,m_2\} = 0$ transition owing to its intensity. If one looks for an alternative assignment, both ZEKE bands can be assigned, to $9^1 29^1$ and $18^2 29^1$ respectively. This excitation position is correct for $9^1 29^1$, and this is then a $\Delta v\{m_1,m_2\} = 0$ transition. The observation of $18^2 29^1$ in this ZEKE spectrum suggests that $D_9 D_{29}$ and $2D_{18} D_{29}$ are coupled to one another in the same way the D_9 and $2D_{18}$ were to lower wavenumber. The $18^2 29^1$ transition in the REMPI spectrum would then be expected at ~1173 cm^{-1}, but ZEKE spectra recorded around this position are effectively structureless. One might note that there appears to be a (weak) feature on top of the structureless background in the correct place for $18^2 29^1$ when exciting at 0^0+1174 cm^{-1}, supporting its presence at this S_1 position. If the broad, structureless, signal arises from zero-order states coupling to D_5 and $D_9 D_{11}$, i.e. totally symmetric levels, then the absence of that broad signal in the 0^0+1144 cm^{-1} ZEKE spectrum is likely because there, the $D_9 D_{29}$ level is non-totally symmetric. Thus, its coupling partner, $2D_{18} D_{29}$, is likely also not coupled to these bath states, but its $\Delta v\{m_1,m_2\} = 0$ transition when exciting at 0^0+1174 cm^{-1} is masked by other, totally symmetric, levels at this position. One would also expect to observe $11^2 29^1$ based on the observation of

$9^1 29^1$ and $18^2 29^1$. This would be expected at close to the same position as $18^2 29^1$, and is likely masked by the broad signal.

Finally, trace n was recorded *via* the band to higher wavenumber, at 0^0+1221 cm^{-1}, and shows a single sharp feature at 1577 cm^{-1}. Such a large shift for the $\Delta v\{m_1,m_2\} = 0$ transition suggests the involvement of out-of-plane vibrations, and this transition does not fit any combinations of the known (D_{14}, D_{20}, D_{19}, D_{18}) out-of-plane fundamentals. Based on the calculations, this is likely either 13^2 or 16^2. In the previous chapter, there was a possible assignment of a $\Delta v\{m_1,m_2\} = 0$ transition, $16^1 19^1$, to a ZEKE band at 990 cm^{-1} when exciting at 0^0+808 cm^{-1}, shown in Figure 6.12, which would give D_{16} a value of 595 cm^{-1} in the S_1 state and 754 cm^{-1} in the D_0^+ state. As such, the band under discussion here could not be due to 16^2. This then allows the band here to be assigned as the $\Delta v\{m_1,m_2\} = 0$ transition 13^2, yielding a value for D_{13} of 611 cm^{-1} in the S_1 state and 789 cm^{-1} in the D_0^+ state.

7.C.2. Discussion

Given the broad, structureless, ZEKE spectra obtained from most of the excitation positions in this region, it is difficult to comment on specific couplings. What is obvious is that there is significant, widespread, coupling between zero-order levels, leading to statistical IVR that is manifesting in the ZEKE spectra. The bright 5^1 transition appears to dominate the region but, as for *p*FT, combinations of the intense 9^1 transition and its Fermi resonance partner(s) with lower wavenumber vibrations are expected in this region of the spectrum. In the case of *p*Xyl, the 9^1, 18^2 and 11^2 lower wavenumber transitions are expected in this range, in combination with D_{29} and D_{11}, as discussed above. The combinations involving the triplet of features at 426, 434 and 440 cm^{-1} (assigned as 19^2, $29^1 m^{\{0,3(+)\}^-}$, 14^2 and $18^1 m^{\{0,3(-)\}^-}$) with D_9, $2D_{18}$ and $2D_{11}$ are expected from 1201 to 1250 cm^{-1}. Although no evidence of these 426 – 440 cm^{-1} combinations has been observed in the ZEKE spectra recorded, they could contribute to some of the broad structure observed through couplings. Additionally, there will be other zero-order levels in this region not

directly related to combinations of lower wavenumber structure, and if one explicitly includes the torsional levels for the above suggested vibrational combinations, this alone will increase the DOS significantly.

One can calculate the DOS, as for *p*FT (again, including up to four vibrational quanta and $\Delta\{m_1 + m_2\} = 6$), over the range 1170 – 1205 cm^{-1} (i.e. ~±17.5 cm^{-1} from D_5, as for *p*FT). This gives 2277 total levels, of which 71 are of a_1' symmetry, 297 are of g'' symmetry, 146 are of e_3' symmetry and 143 are of e_1' symmetry. This gives a total of 657 $a_1' + g'' + e_3' + e_1'$ levels which could couple to a totally symmetric vibration (since a totally symmetric vibration will have transitions to its {0,0}, {0,1}, {1,1} and {1,-1} levels, which take each of these symmetries respectively). This compares with the 193 levels which could couple to D_5 in *p*FT over the analogous range, an increase of 240%.

If one compares only the vibrational levels in each range, one finds 67 vibrations for *p*Xyl (1170 – 1205 cm^{-1}), of which 9 are totally symmetric (including D_5 itself), and for *p*FT (1215 – 1250 cm^{-1}) one finds 86 vibrational levels, of which 20 are totally symmetric[d] (again including D_5 itself), i.e. more vibrational levels which could couple in the *p*FT case than for *p*Xyl. As above, one must take care with such "localised" DOS arguments as energetic coincidences appear to be key, and the choice of "window" for the DOS calculation has a significant effect on the conclusions. Bearing this in mind, one can still note the number of vibrations is fairly similar between the two molecules, but with significantly more vibtor levels for *p*Xyl. This point will be returned to shortly, when the DOS is discussed for the whole S_1 spectral range covered by this thesis for *p*DFB, *p*ClFB, *p*FT and *p*Xyl.

The increased DOS for *p*Xyl compared to *p*FT is proposed as the reason for the seemingly increased coupling for D_5 in *p*Xyl compared to *p*FT. One must also bear in mind that in *p*FT, D_5 is a carbon-fluorine stretch while for *p*Xyl it is a symmetric stretch of the two methyl groups. One will recall that for *p*FT, the

[d] Although it may at first seem surprising that there are more totally symmetric vibrational levels for *p*FT, one must recall that it has a lower molecular symmetry and thus has almost twice as many totally symmetric fundamentals as *p*Xyl.

ZEKE spectra recorded *via* D_6 (the carbon-methyl stretch) showed significantly less evidence of widespread coupling than D_5 (the carbon-fluorine stretch). As such, one might not expect the involvement of the methyl groups in the vibrational motion to play an important role in the enhanced couplings for D_5 in *p*Xyl. However, if one looks at the D_5 motion for *p*Xyl, which is shown in Appendix A, it can be seen that when the carbon-methyl bonds contract, the adjacent ring hydrogens are bending towards the methyl groups, increasing interaction between the ring hydrogens and the methyl groups. This is, coincidentally, similar to what the ring hydrogens do in the D_5 (carbon-fluorine) stretch[e] in *p*FT, and Davies *et al*.[28] suggested that this increased vibration-torsion interaction was important in the observed IVR for D_5 compared to D_6 in that molecule. As such, a similar effect could be important here, but now with two methyl groups exacerbating the effect, and this will be combined with the greatly increased DOS for *p*Xyl in enhancing the IVR.

Finally, it is suggested that to unravel the nature of the couplings in this region further, 2D-LIF and picosecond tr-PES experiments would be useful; with a picosecond system akin to that employed by the Reid group, centring the pulse on the 5^1 transition should allow most of the contributions to the broad underlying REMPI structure to be excited in the wavepacket. This type of experiment would also be useful in deducing whether doorway states are involved, or whether D_5 is directly coupled to the bath of states.

7.D. Comparison to *para*-difluorobenzene and *para*-chlorofluorobenzene

Figure 7.5 shows the REMPI spectra of *p*ClFB, *p*DFB, *p*FT and *p*Xyl up to 1400 cm^{-1}, with the addition of the assignments from this chapter for *p*FT and *p*Xyl in addition to those given in Figure 7.1. One can see an intense 5^1 transition in all four molecules, with an intense 6^1 transition in the lower molecular symmetry *p*ClFB and *p*FT cases. Also observed is 13^2 in *p*Xyl, thought to be intrinsically bright, which preliminary, unpublished, work by our group suggests

[e] For the interested reader, this carbon-fluorine D_5 stretch is shown in Figure 7.8.

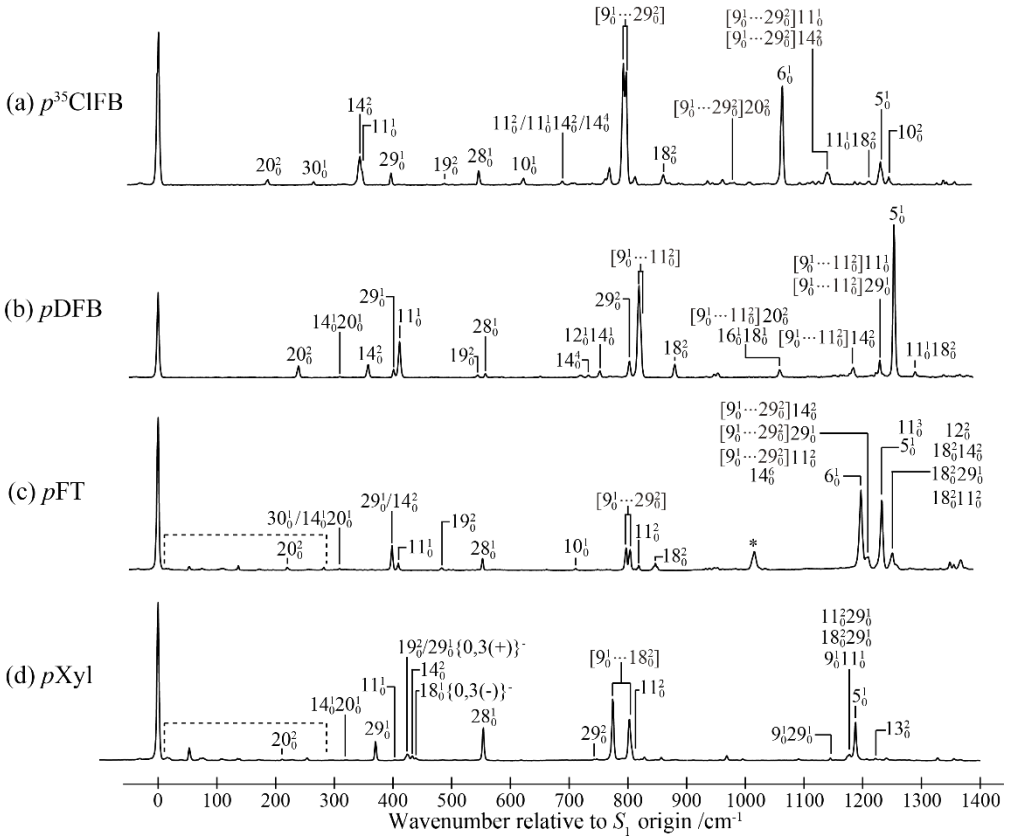


Figure 7.5 – The (a) p^{35}ClFB (b), pDFB (c)pFT and (d) pXyl $S_1 \leftarrow S_0$ REMPI spectra up to 1400 cm^{-1} are shown. The assignments are the same as those in Figure 7.1, with the addition of assignments for pFT and pXyl discussed in this chapter.

lies under the band with an asterisk in the *p*FT spectrum. For *p*FT, 12^2 was observed and this would be expected to higher wavenumber in *p*Xyl. However, based on the B3LYP/aug-cc-pVTZ value for *p*Xyl (given in Table B.1 in Appendix B), which for the other molecules is not in good agreement with experiment for D_{12}, this cannot be definitively assigned to any of the weak bands present to higher wavenumber. 12^2 was also assigned in *p*DFB by Knight and Kable[7] to a weak band at 1166 cm^{-1}, and this was confirmed in a recent REMPI/ZEKE study by our group.[9]

For all four molecules, combinations of intense lower wavenumber structure is observed, with the $[9^1 \ldots 29^2]$ Fermi resonance for *p*ClFB observed in combination with $2D_{14}$ and D_{11}, while for *p*DFB, the $[9^1 \ldots 11^2]$ Fermi resonance was observed in combination with $2D_{14}$, D_{29} and D_{11}. For *p*FT, the $[9^1 \ldots 29^2]$ Fermi resonance was also observed in combination $2D_{14}$, D_{29} and D_{11}, and the 11^2 and 18^2 bands were also observed (or proposed to be present) in

combination with $2D_{14}$, D_{29} and D_{11}. Finally, for *p*Xyl the $[9^1 \ldots 18^2]$ and 11^2 were observed (or proposed to be present) in combination with D_{29} and D_{11}. Although such combinations will always exist, exactly which are observed depends on their intrinsic brightness, the relative energetics of the levels, and the strength of any couplings.

Even though these combinations of lower wavenumber structure were observed in all four molecules, widespread couplings that appear to lead to statistical IVR have only been observed for *p*FT and *p*Xyl. In *p*DFB, D_5 was suggested to be effectively uncoupled by Knight and Kable[7], while for *p*ClFB, recent work by our group[6] has shown D_5 and $2D_{10}$ to be coupled, but this appears to be only restricted IVR, in the form of a traditional Fermi resonance.

For *p*FT, D_5 is suggested to be strongly coupled to the bath of states, with tr-PES suggesting that both $m = 0$ and $m = 1$ are coupled to the bath of states[28]. One possibility for the $m = 1$ coupling pathway, involving doorway states, was proposed in this chapter, involving the $2D_{18}$ $m = 1$, $2D_{14}D_{18}$ $m = 2$, $D_{18}D_{29}$ $m = 2$ and $D_{11}D_{18}$ $m = 2$ levels (which were coupled at lower internal energy) in combination with $2D_{14}$, D_{29} and D_{11}. Although these levels involve significant quanta changes from D_5, and so would only be expected to be weakly coupled, if D_5 can access them, either directly or *via* coupling with other levels, statistical IVR would be expected to be observed. Other doorway states are possible, or alternatively a direct coupling of D_5 to the bath of states is possible. Given the number of zero-order levels expected in this region from DOS calculations, the above discussion is only one proposal, and it is not possible in the current work to deduce the coupling pathway.

For *p*Xyl, ZEKE spectra recorded *via* D_5 show even more pronounced widespread coupling than for *p*FT. Combinations of lower wavenumber vibrations may again be responsible and acting as doorway states; $2D_{11}$ shows significant loss of structure in its ZEKE spectrum, and combinations of this level with D_{29} and D_{11} are expected in this region. However, owing to the almost structureless nature of the ZEKE spectra recorded *via* D_5, very little can be said

regarding possible doorway states, or whether D_5 is coupled directly to the bath of states.

Finally, for *p*Xyl, a ZEKE spectrum was recorded *via* a weak band just below 5^1 and this showed a flat baseline with sharp transitions, suggesting no widespread coupling (it was assigned as one component of a traditional Fermi resonance). This was proposed to be due to the non-totally symmetric nature of the contributing levels. A ZEKE spectrum was also recorded *via* a weak feature above 5^1, and here the baseline was not flat but the broad, structureless signal appeared to be reduced in intensity. This suggests that the couplings in this high wavenumber region are localised to the region closest to D_5. It appears that the increased DOS leads to energetic coincidences, giving rise to widespread coupling around the D_5 level, and this can be probed owing to the bright nature of the 5^1 transition.

One might conclude from the above that *p*Xyl shows the most widespread coupling involving the D_5 vibration, followed by *p*FT, with *p*ClFB showing restricted IVR[5,6] (a traditional Fermi resonance) and *p*DFB showing effectively no signs of IVR[7,9]. This general trend can be rationalised with DOS calculations, which are the focus of the next section.

7.E. Density of states calculations

This thesis has focused on comparing the activity in REMPI and ZEKE spectra of *p*FT and *p*Xyl, with further comparison to the *p*ClFB and *p*DFB molecules. The ZEKE spectra presented *via* many different intermediate levels up to ~1200 cm^{-1} have shown increasingly more widespread coupling at higher internal energies, as well as more widespread coupling for the methyl rotor-containing *p*FT and *p*Xyl than has been shown in previous literature[6,7,9] for *p*ClFB and *p*DFB. Earlier in this chapter, it was observed that the ZEKE spectrum recorded for D_5 in *p*Xyl showed signs of significantly more IVR than the analogous spectrum for *p*FT, emphasising the importance of the second methyl group in further enhancing couplings. Since there are two important factors at work in relation to the DOS and thus the nature of the couplings in

these molecules, these factors being the symmetry of the molecule and the number of methyl groups, it is important to try to separate these effects. As such, this section will investigate the calculated DOS for all four molecules, and with *p*FT and *p*ClFB belonging to the C_{2v} point group and *p*Xyl and *p*DFB belonging to the D_{2h} point group (treating the methyl groups as point masses), the effect of symmetry can be investigated independently from the addition of the methyl group(s).

7.E.1. Total density of states up to 1400 cm^{-1}

The REMPI and ZEKE spectra have allowed many S_1 vibrational fundamentals to be obtained for *p*FT and *p*Xyl (given in Table B.1 in Appendix B), with many of these known from previous work[5–7,9] for *p*ClFB and *p*DFB. As such, it is now possible to use these to calculate the vibrational and vibration-torsional S_1 DOS for these four molecules over the region of interest, 0 – 1400 cm^{-1}, using calculated values in cases where the experimental fundamentals are not known. It should be noted that the B3LYP/aug-cc-pVTZ calculated vibrational fundamentals in the S_1 state (Table B.1, Appendix B) will not be as reliable as the experimentally determined ones, but since the poorest calculated vibrations appear to be out-of-plane ones, and most of these are known experimentally, the calculated vibrational wavenumbers used are thought to be a reasonable approximation.

The DOS calculation for *p*DFB and *p*ClFB is a simple task, with the vibrational DOS simply given by all vibrational fundamentals, overtones and combinations in the given range. In this thesis, all overtones and combinations of up to four vibrational quanta are included in the DOS calculation, and although there will be other levels in this wavenumber range of higher quanta, this is thought to be representative of the total DOS, and especially the levels which are likely to be involved in significant couplings. Note that no attempt is made to account for the diagonal anharmonicity of overtones or combination levels; these effects are likely to be small and so can be safely neglected.

One can also calculate such a vibrational DOS for *p*FT and *p*Xyl. Here, although there are more than 30 vibrations – owing to the additional methyl-localised vibrations – only the thirty ring-localised vibrations are included in the DOS calculation. This is still representative of the total DOS, since almost all of the methyl-localised vibrations are to higher wavenumber than the region currently being considered.

For *p*FT and *p*Xyl, one also needs to include the pure torsional levels and the vibtor levels associated with each vibration to give a total DOS. To account for these levels, the internal rotational constant for methyl rotation, *F*, is assumed to take a value of 5.45 cm^{-1}, as it did in toluene and as discussed in Chapters 3 and 4 for *p*FT and *p*Xyl respectively. This allows a calculation of the free rotor level positions. Then, to account for the splitting in a hindered rotor, for m = 3(-) and m = 3(+) the observed band positions are used. For m = 6, these levels are assumed to be effectively unsplit by the V_6 torsional barrier, since they are expected to lie far above the estimated barrier. Thus, a set of torsional levels is generated and levels of m = 0 – 7 are included in the DOS calculation, both as pure torsions and for each vibrational level. In doing this, no account is taken of perturbations arising from vibration-torsion coupling.

For *p*Xyl, the situation is analogous, but this two-rotor system means dealing with levels described by two torsional quantum numbers, as $\{m_1,m_2\}$. Levels are included from {0,0} through to a total change in $\{m_1+m_2\}$ of six. This includes up to the "m = 7" levels (such as {0,7}), as well as "double excitations" of up to Δm = 3 on each rotor (such as $\{3,3\}^+$ or {4,4}). This is somewhat approximate, since there will be other levels (such as {7,7}), but mirrors the limit of Δm = 6 imposed in the *p*FT case. This Δm = 6 limit is similar to the limit for vibrational overtones and combinations of four vibrational quanta, since these are the levels thought to be most important to any couplings, owing to the generally expected reduction in coupling strength as the quanta difference between two levels increases.[29]

Thus, the DOS calculations are made with the following assumptions:

- Inclusion of only ring-localised vibrations
- Inclusion of up to four vibrational quanta
- Neglect of diagonal anharmonicity
- Inclusion of all m or $\{m_1,m_2\}$ levels which are a $\Delta m \leq 6$ or $\Delta\{m_1+m_2\} \leq 6$ from the "cold" torsional levels, and the analogous vibtor levels

One should also note that the DOS presented here for *p*FT and *p*Xyl do not offset the different torsional ladders, i.e. m = 0 and m = 1 are both assumed to be at "0 cm^{-1}" for *p*FT. In reality, m = 1 is F (~5.45 cm^{-1}) higher than m = 0, but since coupling can only occur within the same torsional ladder (i.e. m = 1, 2, 4, 5 and 7 cannot couple to m = 0, 3(-), 3(+), 6(-) and 6(+)), this does not affect any of the coupling arguments. This approach allows for easier comparison to the REMPI spectra than offsetting the different ladders.

The DOS from 0 – 1400 cm^{-1} generated in this way for *p*ClFB, *p*DFB, *p*FT and *p*Xyl are presented in Figure 7.6, with the number of levels summed over 10 cm^{-1} increments for the purposes of the diagram. One can immediately see the difference in magnitude for the number of levels at high internal energies (1400 cm^{-1}), with ~35 levels in the highest 10 cm^{-1} increment for *p*ClFB and *p*DFB, ~200 for *p*FT, and ~1000 for *p*Xyl.

Some general comments on these DOS plots can now be made, and information from them is also given in Table 7.1. First, the number of totally symmetric vibrational levels in this range is fairly similar for *p*ClFB and *p*FT, but there are (very approximately) 50% fewer of these for *p*DFB and *p*Xyl, owing to the higher symmetry of those molecules. Additionally, the total number of vibrational levels is fairly consistent between molecules, but this will obviously fluctuate as in some molecules certain vibrations will be in the chosen window and in other molecules they will not. For example, for *p*ClFB the heavier chlorine substituent shifts some vibrations to lower wavenumber, explaining why this molecule has the highest number of vibrational levels in the chosen window.

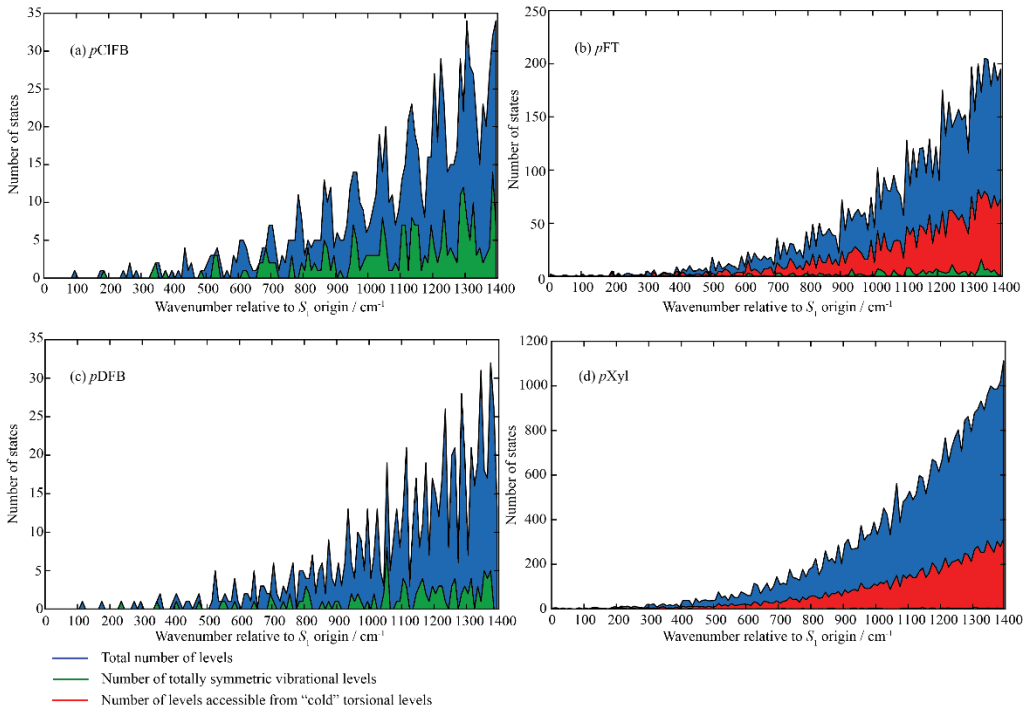


Figure 7.6 – The (a) p^{35}ClFB, (b) pFT, (c) pDFB and (d) pXyl calculated density of states are given from 0 – 1400 cm^{-1}. The blue traces indicate the total number of levels, and the green traces the number of totally symmetric vibrational levels (this trace is very small for pXyl). The red trace shows the number of accessible levels from the "cold" torsional levels, i.e. accessible from m = 0 and m = 1 for pFT, and from {0,0}, {0,1}, {1,1} and {1,-1} for pXyl; these levels can all couple to (the different m/{m_1,m_2} levels of) a totally symmetric vibration, and are thus (effectively) comparable to the green traces for pClFB and pDFB.

To some degree, all four molecules show significant oscillations in their DOS, which are particularly prominent for *p*ClFB and *p*DFB. This is due primarily to overtones and combinations of lower wavenumber structure, with levels in such progressions always (assuming negligible anharmonicity) falling a set number of wavenumbers apart. This means that for these molecules, the concept of local maxima or minima in the DOS is likely important in rationalising any widespread coupling, even at relatively high internal energies. For example, for *p*ClFB, from 1300 – 1400 cm^{-1} the local minimum has ~half the DOS of the local maximum.

For *p*DFB, one can see that the number of totally symmetric levels falls to zero in the highest 10 cm^{-1} increment (1390 – 1400 cm^{-1}), while for *p*ClFB (of lower symmetry) there are totally symmetric levels in all the 10 cm^{-1} ranges plotted

Table 7.1 – Total density of states information (0 – 1400 cm^{-1})

	*p*ClFB (C_{2v})	*p*FT (G_{12})	*p*DFB (D_{2h})	*p*Xyl (G_{72})
Total number of levels (all symmetries)	1030	6821	795	36181
Total number of vibrational levels (all symmetries)	1030	879	795	923
Number of vibrational levels (totally symmetric)	271	229	113	134
Number of vibtor levels (totally symmetric)	N/A	862	N/A	1182
Total accessible levels from "cold" vibrational/torsional levels	271	2574	113	10359

from ~1000 cm^{-1}. This suggests that for the two molecules without methyl rotors, the molecular symmetry is significant in determining the DOS structure, something commented on by others[30–32], and this would suggest that widespread coupling (or statistical IVR) would be prevalent at lower internal energies for *p*ClFB than for *p*DFB.

For *p*FT and *p*Xyl, although there is some periodicity, even at relatively low internal energies there is an almost continuous underlying increase in the number of levels accessible from "cold" torsional levels, owing to the significantly increased number of low wavenumber (torsion and vibtor) levels and thus more combinations to higher energy, as well as the torsional levels for each vibration.

Thus, it seems that the vibtor levels arising from the presence of the methyl group(s) are dominating the DOS[f], and this effect appears far more significant than the molecular symmetry for substituted molecules. Indeed, the G_{72} molecular symmetry *p*Xyl molecule has around four times the number of accessible levels from "cold" torsional levels from 1390 – 1400 cm^{-1} than the lower symmetry G_{12} *p*FT molecule, owing to the addition of a second methyl group. Additionally, the ZEKE spectrum recorded *via* D_5 for *p*Xyl (Figure 7.4) showed significantly more congestion than the analogous one for *p*FT (Figure

[f] Note the ~eightfold increase in the DOS for *p*FT (and ~thirty-ninefold increase for *p*Xyl) when moving from only vibrational levels to inclusion of the torsion and vibtor levels (from 0 – 1400 cm^{-1}) in Table 7.1.

7.2), suggesting more widespread coupling in the *p*Xyl case, supported by the DOS presented here. One might also note the large increase in the number of accessible levels from "cold" levels for the methyl-containing molecules compared to the non-methyl-containing ones, which again correlates with more widespread coupling being observed in the methyl-containing species.

It is important to take a moment to clarify what is meant by "number of levels accessible from "cold" vibrational/torsional levels" in Table 7.1. For *p*DFB and *p*ClFB, this is simply the vibrations which are symmetry-allowed, i.e. the totally symmetric vibrations, and represents all levels that can couple to a totally symmetric level. For *p*FT, if one observes a totally symmetric vibration, one is observing transitions to both the $m = 0$ and $m = 1$ levels. These can undergo different couplings and, since they correspond to different nuclear spin symmetries which cannot be changed during these experiments, levels in the $m = 0$ and $m = 1$ ladders cannot couple to one another. As such, the "number of levels accessible from "cold" torsional levels" implies all levels which can couple to either $m = 0$ or $m = 1$ for a totally symmetric vibration, i.e. those levels which are of the same symmetry as $m = 0$ and $m = 1$, making this effectively analogous to the number of totally symmetric levels in *p*ClFB and *p*DFB. It is important to bear in mind, as mentioned, that not all of these levels can couple to one another, as some will couple to $m = 0$ and some to $m = 1$. The situation is analogous in *p*Xyl, but now accessing {0,0}, {0,1}, {1,1} and {1,-1} for a totally symmetric vibration, with each coupling to different levels.

Additionally, one might note that "Number of vibtor levels (totally symmetric)" includes all totally symmetric levels in the range. For example, for a totally symmetric vibration this will include the $m = 0$ level, i.e. effectively the "pure" vibration.

The remainder of this chapter will look at different regions – low, intermediate and high wavenumber – where different IVR regimes appear to be prevalent in different molecules. These DOS calculations will be used to further rationalize the conclusions in the earlier parts of this thesis. In each section, bright transitions common to the four molecules will be chosen, and the DOS in their

vicinity compared between the species. DOS calculations for these transitions are over a 10 cm^{-1} range, ±5 cm^{-1} either side of a transition.

This is a relatively small window, and obviously the findings depend on the window chosen, so care must be taken. A small, rather than large, window was chosen owing to the importance of energetic proximity in the couplings, but it is likely that couplings outside of these windows are also relevant to IVR processes, especially when it comes to the involvement of the bath states. These calculations are simply to illustrate the role of the DOS in observed couplings, and in particular to illustrate the influence of the methyl groups.

7.E.2. The density of states at low wavenumber (0 – 600 cm^{-1})

From Figure 7.6 the vibrational DOS over this region may be seen to be quite sporadic for *p*ClFB and *p*DFB, owing to there being only a handful of vibrational fundamentals which fall in this range. As such, any couplings observed are going to be heavily dependent on energetic coincidences between levels. While this will still be true for *p*FT and *p*Xyl, one can see an almost continuous underlying build-up in the DOS by 600 cm^{-1} for *p*Xyl, illustrating that the low-lying torsional levels and vibtor levels are making the DOS less patchy than for the *p*ClFB and *p*DFB molecules. In this region, transitions to the totally symmetric levels D_{11}, $2D_{14}$ and $2D_{19}$ are observed for each of the four molecules, and so localised "windows" of the DOS within ±5 cm^{-1} of these levels are given in Table 7.2. One can see similar numbers of totally symmetric vibrations for each species within the given range, with only 1 or 2 in each case (including the bright level itself). A specific point of interest is in the *p*ClFB case, where D_{11} and $2D_{14}$ lie within this ±5 cm^{-1} window of one another, but recent REMPI and ZEKE work by our group[5,6] suggests that these levels are not coupled significantly, illustrating that the motion of the vibrations is important in the coupling of vibrational levels. For *p*FT and *p*Xyl, these levels are further apart and so not in this ±5 cm^{-1} window, and are still thought not to couple significantly.

The number of accessible levels for *p*FT and *p*Xyl is larger, owing the addition of the vibtor levels, with, for example D_{14} m = 6(-) now in the window for $2D_{14}$

Table 7.2 – Density of states for D_{11}, $2D_{14}$ and $2D_{19} \pm 5$ cm^{-1}

	*p*ClFB (C_{2v})	*p*DFB (D_{2h})	*p*FT (G_{12})	*p*Xyl (G_{72})
$D_{11} \pm 5$ cm^{-1}				
Total number of levels (all symmetries)	2	2	5	36
Number of vibrational levels (totally symmetric)	2	1	1	1
Total accessible levels from "cold" vibrational/torsional levels	2	1	3	13
$2D_{14} \pm 5$ cm^{-1}				
Total number of levels (all symmetries)	2	2	7	22
Number of vibrational levels (totally symmetric)	2	1	1	1
Total accessible levels from "cold" vibrational/torsional levels	2	1	3	8
$2D_{19} \pm 5$ cm^{-1}				
Total number of levels (all symmetries)	2	1	10	32
Number of vibrational levels (totally symmetric)	1	1	1	2
Total accessible levels from "cold" vibrational/torsional levels	1	1	6	12

for *p*FT, as well as both $2D_{14}$ $m = 0$ and $2D_{14}$ $m = 1$, with the D_{14} $m = 6(-)$ observed in ZEKE spectra recorded *via* $2D_{14}$, and potentially involved in coupling with $2D_{14}$ $m = 0$, as discussed in Chapter 5. For *p*Xyl, there are even more accessible levels, with, for example, D_{29} $m = 3(+)$ within ± 5 cm^{-1} of $2D_{19}$, and the ZEKE evidence suggests that these are coupled, as discussed in Chapter 5.

This leads to the general conclusion that, at lower internal energies, coupling pathways are dominated by coincidences in level energetics (with vibrational motions also important). As such, for *p*DFB and *p*ClFB, no significant couplings occur, while for *p*FT and *p*Xyl, some couplings are observed, owing to the higher DOS, as well as the reduced patchiness of it. Even when couplings are observed in this region, they are restricted in nature, akin to traditional Fermi resonances, and this is likely due to the DOS not being high enough to access a significant number of bath states; the highest DOS in the 10 cm^{-1} windows given here is 36

for *p*Xyl (around D_{11}), and although this seems high, compared to the DOS at higher internal energies, this is a very small number of levels.

One should also note that for the methyl-containing species, as discussed in Chapters 3 and 4 for *p*FT and *p*Xyl, vibration-torsion coupling pervades this low wavenumber region. This is not evident from these DOS windows, which aim to compare couplings involving vibrations at different internal energies rather than look at the widespread vibration-torsion coupling.

7.E.3. The density of states at intermediate wavenumber (600 – 900 cm^{-1})

Table 7.3 shows the DOS within ±5 cm^{-1} of D_9, $2D_{29}$, $2D_{11}$ and $2D_{18}$ for the four molecules under discussion. Treating *p*ClFB first, D_9 and $2D_{29}$ are thought to be in Fermi resonance in that molecule[5,6], and these are the two totally symmetric levels in the window for D_9 and $2D_{29}$. For $2D_{11}$, there are four totally symmetric levels, three of which are the "overtones" of the overlapped D_{11} and $2D_{14}$ levels (i.e. $2D_{11}$ itself, $4D_{14}$ and $D_{11}2D_{14}$). Since these were not thought to be interacting to lower wavenumber, similar expectations apply here. Finally, there are only two totally symmetric levels within the window for $2D_{18}$, one being $2D_{18}$ itself. Similar arguments apply for *p*DFB, where the number of totally symmetric levels in each window is similar to *p*ClFB. The primary difference for *p*DFB is that D_9 and $2D_{11}$ are thought to be coupled[7,9], and these two levels are within ±5 cm^{-1} of one another. Additionally, in *p*DFB, the D_{11} and $2D_{14}$ levels were not overlapping, so one does not find $4D_{14}$ or $D_{11}2D_{14}$ in the $2D_{11}$ window.

For *p*FT, there are an order of magnitude more accessible levels which could couple to a totally symmetric vibrational level. The ZEKE spectra presented in this thesis in Chapter 6 suggest D_9 and $2D_{29}$ are coupled, while recent work by our group[22] suggested $2D_{18}$ to be coupled to the bath of states *via* several doorway states. Based solely on the number of accessible levels within ±5 cm^{-1}, one would expect more coupling for $2D_{11}$ than for $2D_{18}$, and as the experiment shows the reverse of this, one can make some general remarks. One such remark, already discussed, is that local DOS pictures are not rigorous owing to the need

Table 7.3 – Density of states for D_9, $2D_{29}$, $2D_{11}$ and $2D_{18} \pm 5$ cm^{-1}

	*p*ClFB (C_{2v})	*p*DFB (D_{2h})	*p*FT (G_{12})	*p*Xyl (G_{72})
$D_9 \pm 5$ cm^{-1}				
Total number of levels (all symmetries)	9	8	33	183
Number of vibrational levels (totally symmetric)	2	2	3	2
Total accessible levels from "cold" vibrational/torsional levels	2	2	10	56
$2D_{29} \pm 5$ cm^{-1}				
Total number of levels (all symmetries)	9	5	25	153
Number of vibrational levels (totally symmetric)	3	3	2	2
Total accessible levels from "cold" vibrational/torsional levels	3	3	11	45
$2D_{11} \pm 5$ cm^{-1}				
Total number of levels (all symmetries)	6	9	49	197
Number of vibrational levels (totally symmetric)	4	2	2	1
Total accessible levels from "cold" vibrational/torsional levels	4	2	18	59
$2D_{18} \pm 5$ cm^{-1}				
Total number of levels (all symmetries)	12	10	38	212
Number of vibrational levels (totally symmetric)	2	1	2	2
Total accessible levels from "cold" vibrational/torsional levels	2	1	12	64

to choose a "window". Additionally, again it is noted that the nature of the coupled levels, i.e. the motions and/or quanta difference between the levels, is likely important in determining coupling strength, and thus pathways to accessing doorway states (or the bath states directly). One then concludes that it is the nature of the levels nearby $2D_{18}$ in *p*FT that allows them to act as doorway states, providing $2D_{18}$ with access to the bath states, something which is discussed in reference 22 based on 2D-LIF results.

Turning to *p*Xyl, here the ZEKE spectrum recorded *via* $2D_{11}$ (shown in Chapter 6) showed significantly more congestion – evidence of widespread coupling –

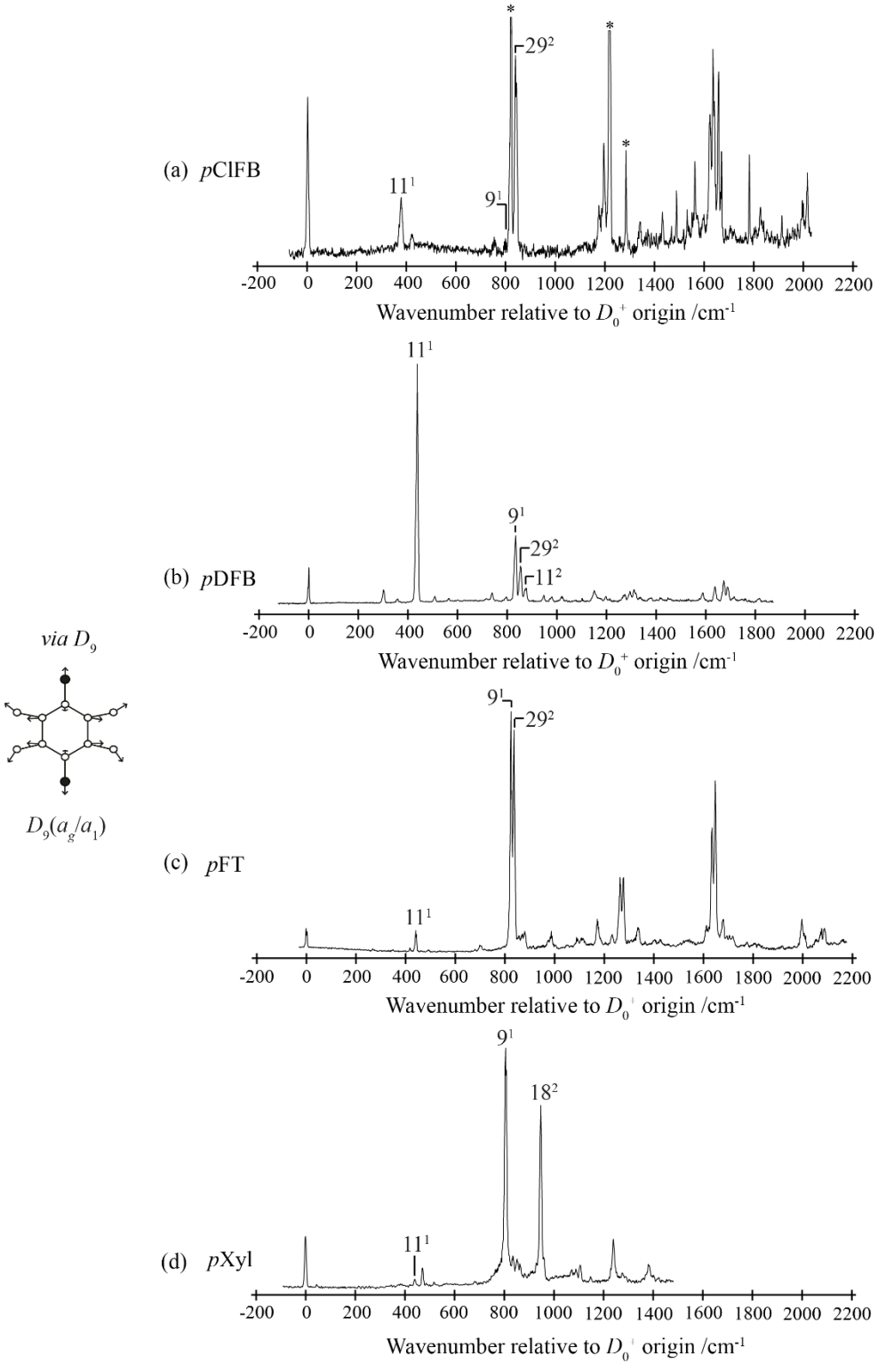


Figure 7.7 – The (a) p[35]ClFB, (b) pDFB, (c) pFT and (d) pXyl ZEKE spectra recorded via the D_9 level are shown. The pClFB one is taken from reference 6, and the pDFB one is from reference 33*. The pClFB one is of poorer signal-to-noise than the others, and the asterisks indicate "accidental resonances", which are not related to the ZEKE spectrum.*

than the ZEKE spectrum recorded *via* $2D_{18}$, which itself showed more congestion than the one recorded *via* D_9. However, $2D_{18}$ has more accessible (and more total) levels than $2D_{11}$ in the local DOS picture given here, again supporting the idea of the nature of nearby levels being key.

If it is indeed the motion of nearby levels, or quanta differences, which are key to coupling, then what is the role of the methyl groups? It is very clear that there are an order of magnitude more accessible (and more total) levels for the methyl rotor-substituted *p*FT than for *p*ClFB (or *p*DFB), and even more levels for the double rotor *p*Xyl molecule. Thus, simply by virtue of the number of levels, the likelihood that one (or some) of these levels can strongly couple to the bright level is increased for the methyl rotor-containing molecules. Additionally, considering the nearby bath of states for each molecule, it becomes apparent that the bath for *p*ClFB or *p*DFB is not particularly sizeable, while for *p*Xyl this is now potentially hundreds of nearby levels, and this assumes only a ±5 cm^{-1} window. A large bath of states is required for statistical IVR, accessing it either directly, by coupling to the bright level, or *via* a doorway state, and so for *p*DFB and *p*ClFB the likelihood of coupling to the (very small) bath of states is significantly lower than for *p*FT or *p*Xyl. Referring to Figure 7.6, at 800 cm^{-1} (roughly where the transitions to these levels are observed) the DOS in a 10 cm^{-1} window for *p*FT and *p*Xyl is higher than at 1400 cm^{-1} for *p*ClFB or *p*DFB, illustrating how the methyl group leads to a build-up of levels at much lower internal energies.

Figure 7.7 shows the ZEKE spectra recorded *via* D_9 for the four molecules of interest, with the *p*ClFB and *p*DFB ones reproduced from references 6 and 33. Note that the *p*ClFB one is of poorer signal-to-noise, and has additional transitions, referred to as "accidental resonances", which arise from the scanning ionisation laser becoming resonant with an $S_1 \leftarrow S_0$ transition.

All four of these spectra show effectively restricted IVR, with Fermi resonance type interactions between two levels dominating. However, the *p*FT and *p*Xyl

ZEKE spectra show slightly more congestion than the *p*ClFB or *p*DFB[g] ones, owing to the additional levels thought to be involved in the couplings in those two species. In Chapter 6, it was discussed that a number of zero-order levels are thought to be coupled in the case of *p*FT, while in *p*Xyl, further congestion was observed when exciting *via* $2D_{11}$ to slightly higher wavenumber. This contrasts with the, effectively, two level Fermi resonances observed in the non-methyl-containing molecules.

7.E.4. The density of states at high wavenumber (900 – 1400 cm^{-1})

Table 7.4 shows the DOS within ±5 cm^{-1} of D_5 and D_6 for the four molecules of interest, with D_6 only included for *p*ClFB and *p*FT, the two molecules where it was totally symmetric and a transition to it was observed. Figure 7.8 shows the ZEKE spectra recorded *via* the D_5 level for each molecule. One can see no evidence of widespread coupling for *p*DFB and *p*ClFB (barring the poorer signal-to-noise ratio and accidental resonances of the *p*ClFB spectrum). The *p*ClFB case illustrates a Fermi resonance between $2D_{10}$ and D_5, as discussed in reference 6, while there is no evidence of any strong coupling in the *p*DFB

Table 7.4 – Density of states for D_5 and D_6 ± 5 cm^{-1}

	*p*ClFB (C_{2v})	*p*DFB (D_{2h})	*p*FT (G_{12})	*p*Xyl (G_{72})
D_5 ± 5 cm^{-1}				
Total number of levels (all symmetries)	29	16	154	656
Number of vibrational levels (totally symmetric)	7	3	4	1
Total accessible levels from "cold" vibrational/torsional levels	7	3	53	190
D_6 ± 5 cm^{-1}				
Total number of levels (all symmetries)	15	N/A	126	N/A
Number of vibrational levels (totally symmetric)	2	N/A	7	N/A
Total accessible levels from "cold" vibrational/torsional levels	2	N/A	49	N/A

[g] Note the non-Δv = 0 behaviour shown in this spectrum, with 11^1 the most intense transition rather than 9^1. This could be suggestive of a Duschinsky rotation, and/or evidence of the $2D_{11}$ and D_9 coupling, with progressions formed in $2D_{11}$ and D_9 spreading the intensity out in a non-Δv = 0 manner in the cation, as discussed in reference 9.

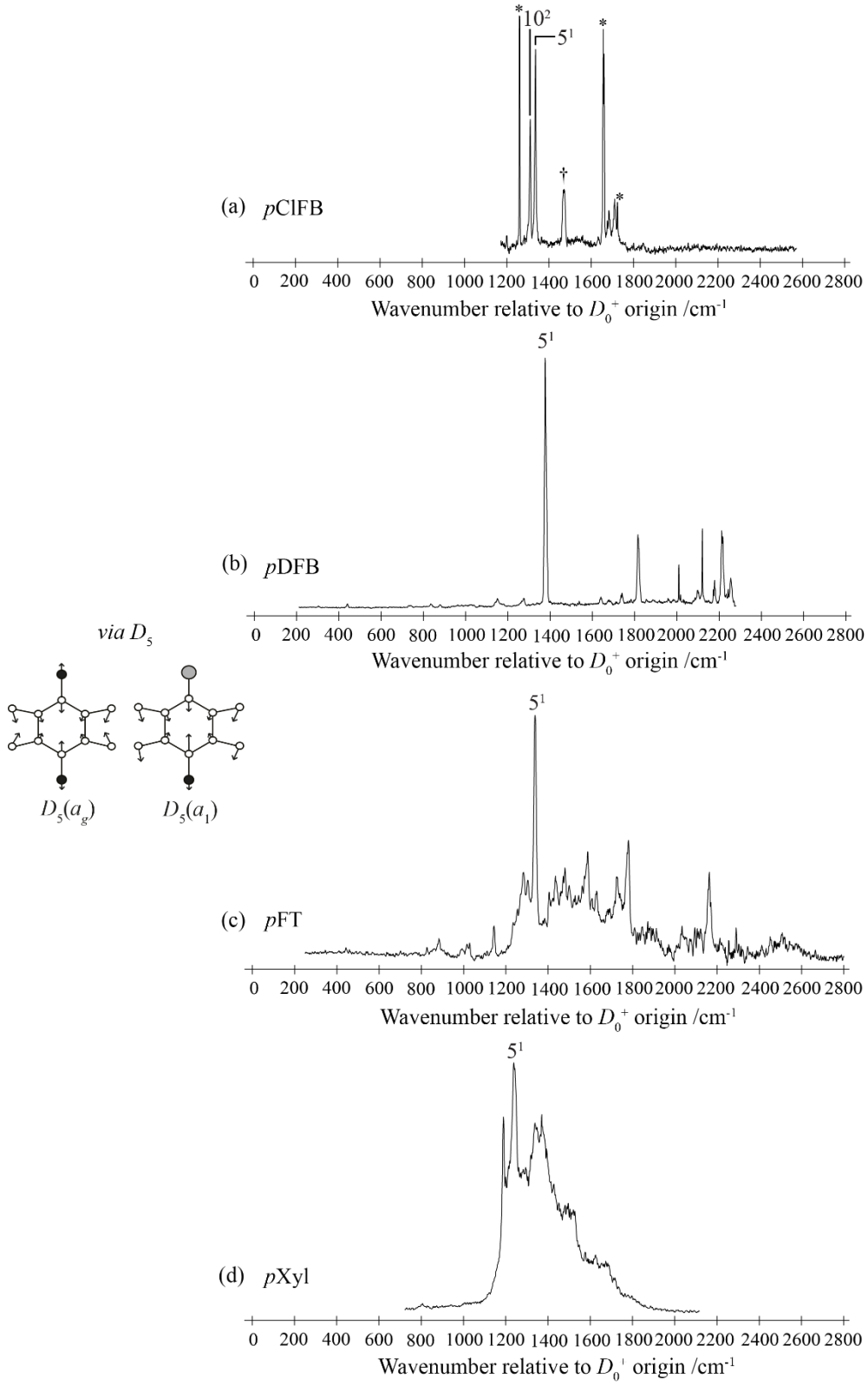


Figure 7.8 – The (a) p[35]ClFB, (b) pDFB, (c) pFT and (d) pXyl ZEKE spectra recorded via the D_5 level are shown. The pClFB one is taken from reference 6, and the pDFB one is from reference 33*. The pClFB one is of poorer signal-to-noise than the others, and the asterisks indicate "accidental resonances", which are not related to the ZEKE spectrum.*

case[9]. For *p*FT, there is significant underlying spectral congestion, which is enhanced further in the case of *p*Xyl. This follows the trend in the number of accessible levels that the bright level can couple to; for *p*DFB and *p*ClFB, there are 2 and 6 levels[h] which the bright level could couple to, while for *p*FT and *p*Xyl there are 52 and 189 levels respectively. This compares to 58 for the $2D_{11}$ level in *p*Xyl and 11 for the $2D_{18}$ level in *p*FT, which both showed signs of relatively widespread coupling in Chapter 6, further evidence that the nature of the nearby levels is important.

Regarding D_6, slightly less can be said regarding the comparison between molecules, owing to it only appearing in the REMPI spectra of two of the four species, and D_6 having different motions in those two cases. However, comparison can be made within species. For example, for *p*ClFB there are far fewer total (and totally symmetric) levels within ±5 cm^{-1} of D_6 compared to D_5, likely owing to D_6 being almost 200 cm^{-1} to lower wavenumber. For *p*FT, D_6 is still to lower wavenumber, but only by ~40 cm^{-1}, since it is now a carbon-methyl stretch rather than the carbon-chlorine stretch of *p*ClFB. However, it still has a lower number of total levels, but has nearly the same amount of accessible levels as D_5, with 52 within ±5 cm^{-1} for D_5 and 48 for D_6. Once again, this supports the idea that the nature of the bright levels and the nearby levels is key to the coupling pathways.

Note that the local minima and maxima on the DOS plots in Figure 7.6 do not appear to correlate consistently with the observation of widespread coupling for one level over another. This supports the ideas discussed in this chapter, that the almost continuous build-up of levels owing to the methyl group(s), in combination with factors that affect coupling strength (quanta changes between levels, vibrational and torsional motions), are the dominating factors in widespread coupling and statistical IVR in the methyl-containing *p*FT and *p*Xyl molecules.

[h] These values are the tabulated values minus one, to remove the bright levels.

7. F. References

[1] V.L. Ayles, C.J. Hammond, D.E. Bergeron, O.J. Richards, and T.G. Wright, *J. Chem. Phys.*, **126**, 244304 (2007).

[2] J.A. Davies, A.M. Green, A.M. Gardner, C.D. Withers, T.G. Wright, and K.L. Reid, *Phys. Chem. Chem. Phys.*, **16**, 430 (2014).

[3] E.B. Wilson Jr., *Phys. Rev.*, **45**, 706 (1934).

[4] G. Varsányi, *Assignments of the Vibrational Spectra of Seven Hundred Benzene Derivatives* (Wiley, New York, 1974).

[5] W.D. Tuttle, A.M. Gardner, and T.G. Wright, *Chem. Phys. Lett.*, **684**, 339 (2017).

[6] D.J. Kemp, L.E. Whalley, W.D. Tuttle, A.M. Gardner, B.T. Speake, and T.G. Wright, *Phys. Chem. Chem. Phys.*, **20**, 12503 (2018).

[7] A.E.W. Knight and S.H. Kable, *J. Chem. Phys.*, **89**, 7139 (1988).

[8] G. Reiser, D. Rieger, T.G. Wright, K. Müller-Dethlefs, and E.W. Schlag, *J. Phys. Chem.*, **97**, 4335 (1993).

[9] D.J. Kemp, A.M. Gardner, W.D. Tuttle, J. Midgley, K.L. Reid, and T.G. Wright, *J. Chem. Phys.*, (submitted).

[10] A. Andrejeva, A.M. Gardner, W.D. Tuttle, and T.G. Wright, *J. Mol. Spectrosc.*, **321**, 28 (2016).

[11] K. Okuyama, N. Mikami, and M. Ito, *J. Phys. Chem.*, **89**, 5617 (1985).

[12] J.A. Davies, K.L. Reid, M. Towrie, and P. Matousek, *J. Chem. Phys.*, **117**, 9099 (2002).

[13] A.K. King, S.M. Bellm, C.J. Hammond, K.L. Reid, M. Towrie, and P. Matousek, *Mol. Phys.*, **103**, 1821 (2005).

[14] J.A. Davies and K.L. Reid, *J. Chem. Phys.*, **135**, 124305 (2011).

[15] C.S. Parmenter and B.M. Stone, *J. Chem. Phys.*, **84**, 4710 (1986).

[16] D.B. Moss and C.S. Parmenter, *J. Chem. Phys.*, **98**, 6897 (1993).

[17] B. Zhang, U. Aigner, H.L. Selzle, and E.W. Schlag, *Opt. Commun.*, **183**, 95 (2000).

[18] B. Zhang, U. Aigner, H.L. Selzle, and E.W. Schlag, *Chem. Phys. Lett.*, **380**, 337 (2003).

[19] T. Ebata, Y. Suzuki, N. Mikami, T. Miyashi, and M. Ito, *Chem. Phys. Lett.*, **110**, 597 (1984).

[20] T.G. Blease, R.J. Donovan, P.R.R. Langridge-Smith, and T. Ridley, *Laser Chem.*, **9**, 241 (1988).

[21] K. Walter, K. Scherm, and U. Boesl, *Chem. Phys. Lett.*, **161**, 473 (1989).

[22] A.M. Gardner, W.D. Tuttle, L.E. Whalley, and T.G. Wright, *Chem. Sci.*, **9**, 2270 (2018).

[23] R.A. Coveleskie, D.A. Dolson, and C.S. Parmenter, *J. Phys. Chem.*, **89**, 645 (1985).

[24] R.S. Mulliken, *J. Chem. Phys.*, **23**, 1997 (1955).

[25] C.J. Hammond, V.L. Ayles, D.E. Bergeron, K.L. Reid, and T.G. Wright, *J. Chem. Phys.*, **125**, 124308 (2006).

[26] J.S. Baskin, T.S. Rose, and A.H. Zewail, *J. Chem. Phys.*, **88**, 1458 (1988).

[27] S.M. Bellm, P.T. Whiteside, and K.L. Reid, *J. Phys. Chem. A*, **107**, 7373 (2003).

[28] J.A. Davies, L.E. Whalley, and K.L. Reid, *Phys. Chem. Chem. Phys.*, **19**, 5051 (2017).

[29] D.J. Nesbitt and R.W. Field, *J. Phys. Chem.*, **100**, 12735 (1996).

[30] L.W. Peng, B.W. Keelan, D.H. Semmes, and A.H. Zewail, *J. Phys. Chem.*, **92**, 5540 (1988).

[31] M. Hippler, R. Pfab, and M. Quack, *J. Phys. Chem. A*, **107**, 10743 (2003).

[32] R.S. von Benten, L. Yaxing, and B. Abel, *J. Chem. Phys.*, **133**, 134306 (2010).

[33] W.D. Tuttle, A.M. Gardner, L.E. Whalley, D.J. Kemp, and T.G. Wright, *Phys.*

Chem. Chem. Phys., (In press).

8. Concluding remarks and further work

8.A. Concluding remarks

This thesis has presented resonance-enhanced multiphoton ionisation (REMPI) and zero-electron-kinetic-energy (ZEKE) photoelectron spectroscopy (PES) spectra for the single rotor *para*-fluorotoluene (*p*FT) and double rotor *para*-xylene (*p*Xyl) molecules, with the aim of assigning the structure in the REMPI spectra with the aid of the ZEKE spectra, and to gain insight into vibration-vibration and vibration-torsion couplings in the S_1 state of these two molecules. One can also obtain information about coupling in the cation from these experiments, and this has been commented on for a number of different levels throughout. Comparison has been made to the *para*-chlorofluorobenzene (*p*ClFB) and *para*-difluorobenzene (*p*DFB) molecules, where *p*ClFB and *p*FT both belong to the C_{2v} point group, and *p*DFB and *p*Xyl both belong to the D_{2h} point group (treating the methyl groups as point masses). This allows an effective separation of the effect of the molecule's symmetry on the density of states (and thus the couplings) from the effect of the presence of methyl group(s). Previous work has compared *p*FT to different molecules, primarily to *p*DFB[1,2], its *ortho*- and *meta*- analogues[3,4], and more recently to toluene[5], with similar comparison of *p*Xyl to its isomers and to toluene[6,7]. While useful, such comparisons still effectively convolute the influence of the methyl group and the symmetry[a], and the work presented in this thesis allows for a more systematic approach to separate the symmetry effects.

Chapters 3 and 4 discussed the lowest wavenumber regions of the REMPI and ZEKE spectra, with assignments of transitions terminating in torsional and vibration-torsion (vibtor) levels. These were seen to dominate the REMPI spectrum at low internal energies when compared to the non-methyl containing molecules *p*ClFB and *p*DFB, as was observed for toluene by Gascooke and Lawrance[11,12], with these torsional and vibtor levels underpinning the vastly

[a] While *ortho*-, *meta*-, *para*- comparisons might seem to avoid this, the vibrations of those three species are very different, as discussed in the set of papers on vibrational labelling schemes by our group.[8–10]

increased build-up of the density of states for the methyl-containing molecules. Additionally, many of the low-wavenumber levels of the same (molecular) symmetry are thought to be coupled to one another, with vibration-torsion coupling seemingly important across the whole region.

Chapters 5, 6 and 7 each discussed progressively higher wavenumber regions of the REMPI spectra. At ~0^0+800 cm^{-1}, the ZEKE spectra recorded for both *p*FT and *p*Xyl showed signs of coupling between several levels, with the *p*Xyl case showing signs of more widespread coupling, i.e. statistical intramolecular vibrational redistribution (IVR). At ~0^0+1200 cm^{-1}, ZEKE spectra recorded *via* the D_5 level showed widespread coupling for both molecules, and this appeared to be further enhanced in the *p*Xyl case, whereas for *p*DFB and *p*ClFB, previous work[13–15] has shown, at most, traditional Fermi resonance interactions, i.e. restricted IVR, for the D_5 vibration.

This increased coupling for *p*FT and *p*Xyl was shown to correlate with the increased density of states arising from the addition of the methyl group(s). Indeed, at similar internal energies, significantly more IVR was observed for *p*FT than for the analogous *p*ClFB molecule, both of which, as discussed above, belong to the C_{2v} point group. Similar arguments apply for *p*Xyl in comparison to *p*DFB, both belonging to the D_{2h} point group, clearly illustrating the importance of the methyl group(s) in enhancing coupling and, effectively, leading to statistical IVR at lower internal energies than for the non-methyl containing species.

Additionally, at similar internal energies, there were signs in the ZEKE spectra of more widespread coupling for *p*Xyl than for *p*FT, even though *p*Xyl is formally of a higher molecular symmetry (G_{72} for *p*Xyl versus G_{12} for *p*FT). This suggests that the influence of the additional methyl group on the coupling outweighs the influence of the higher molecular symmetry. This is supported by *p*Xyl ZEKE spectra showing more widespread coupling than *p*ClFB ZEKE spectra recorded *via* analogous levels[15], where *p*Xyl may be viewed as the higher symmetry case. Additionally, the density of states calculations in Chapter 7 showed that lowering the symmetry from D_{2h} to C_{2v} (*p*DFB to *p*ClFB) led to an

increase of ~140% in the number of totally symmetric levels below 1400 cm^{-1}, while moving from *p*ClFB to *p*FT (adding a methyl group) gave a ~850% increase in the number of accessible levels below 1400 cm^{-1} (accessible from the "cold" vibrational/torsional levels).

In this thesis, the increased coupling in the methyl-containing molecules was discussed to be due to a combination of the sheer number of torsional (and thus vibtor) levels added by the methyl rotor, vastly increasing the density of states for methyl-containing species, and additionally the nuclear spin symmetries associated with these levels. For example, the m = 1 level in *p*FT is of e'' G_{12} symmetry, which means that for both a_1' (a_1 in C_{2v}) and a_2' (a_2 in C_{2v}) vibrations, the corresponding m = 1 vibtor levels are of the same symmetry, and so can couple to one another, (although the m = 0 levels still cannot). Thus, more levels can couple to one another than in the *p*DFB and *p*ClFB cases, and analogous arguments apply to the more complex *p*Xyl molecule.

These conclusions are somewhat different to certain earlier work[16–18], which suggested point group symmetry played a significant role in IVR processes. These studies looked at breaking the symmetry of: anthracene with deuteration[16], benzene with a ^{13}C substituent[17], and benzene with deuteration[18], and all concluded that the reduction in symmetry led to increased IVR. Additionally, the current work is not in agreement with the conclusion of von Benten *et al.*[19] that an internal rotor has effectively no impact on the observed IVR. This disagreement is likely owing to the different conditions (high temperatures) and laser pulses (60 fs pulse widths, ~300 cm^{-1} bandwidth) of the experiments in reference 19, and additionally, it is notable that they were probing at very high internal energies, not the comparatively low internal energies studied in this thesis.

It is apparent from the previous work that, for molecules without a flexible substituent, point group symmetry is likely important, but this thesis has shown that the additional levels added by the substituent are key to understanding methyl-containing systems, and likely also systems with other flexible substituents.

A more general conclusion can also be taken from this work – one must be careful when drawing conclusions regarding IVR, as it is necessary to disentangle different effects such as symmetry and the influence of a polyatomic substituent, as well as different experimental conditions. For example, previous work has been carried out involving room temperature samples[1,3,16] (such as the influential chemical timing work of Parmenter and co-workers, exemplified in references 1 and 3), while jet-cooled samples were used by others[20,21]. Similarly, different workers have used different laser pulses; this includes both frequency and time domain studies, and within the latter, different bandwidths (and so different levels excited in the wavepacket) as well as temporal lengths. These factors were discussed previously by Hammond *et al.*[22], and they necessitate caution when comparing studies, and thus conclusions, regarding IVR rates and coupled levels. This thesis has presented only frequency domain work, with jet expansion conditions employed for all molecules, utilising nanosecond laser pulses, allowing an effective comparison to be made. Additionally, comparisons have been made to the time-resolved studies of the Reid group for *p*FT[5,20,21,23,24], both in this thesis and in publications by our research group[14,25,26], and it has been possible to deduce a consistent picture with the data from both experiments.

The work presented here has illustrated that levels that are close in wavenumber can show significantly different couplings, such as D_9 and $2D_{11}$ in *p*Xyl or D_6 and D_5 in *p*FT, where in each case the latter level showed more evidence of widespread coupling than the former. In these cases, such as D_6 and D_5 in *p*FT, the density of states within ±5 cm^{-1} of each level is similar, and so the observed behaviour does not appear to be rationalised by the density of states. As such, this suggests that the nature of the bright level, and the efficiency of coupling to any doorway levels and bath levels, are important in determining the overall coupling picture. Thus, for specific bright levels, one can observe widespread coupling/statistical IVR at lower internal energies than might be expected, as was the case for $2D_{18}$ in *p*FT, discussed in reference 25.

Finally, this thesis has demonstrated similar spectral activities in the observed transitions to torsional, vibtor and vibrational levels for *p*FT and *p*Xyl (consistent with the vibrational activities of *p*ClFB and *p*DFB), with the use of

a formal G_{72} framework for *p*Xyl for the first time. Understanding the expected bright transitions is important for unravelling coupling information, as it infers knowledge of both bright and dark levels. Additionally, observing analogous torsional and vibtor levels in *p*FT and *p*Xyl in this thesis, consistent with previous work on toluene[11,12], gives a firm understanding of what structure one expects to see in the excitation spectra of methyl-containing substituted benzene molecules, allowing future workers to more readily assign observed torsional and vibtor structure.

8.B. Further work

As mentioned elsewhere in this thesis, by its very nature, spectroscopy as a probe for IVR can only shine a light on levels which are coupled to an observed, bright level, and the "brightness" depends upon the experimental technique used and the populations of the initial levels, as well as other factors such as Franck-Condon factors. This is, to some degree, both a help and a hinderance, since it allows a comparison of the couplings of the same bright level between different molecules, as presented here, but also makes it difficult to probe particular, desired, levels, which one would like to do to investigate if widespread coupling is mode specific at particular internal energies. As such, a natural extension of the current work would be to use a different experimental technique to attempt to probe different bright levels, such as an IR+UV double resonance experiment.

Additionally, further work utilising other techniques to supplement the work presented here would be useful in unravelling the details of the observed couplings. Two-dimensional laser-induced fluorescence (2D-LIF) studies, such as those carried out by Gascooke and Lawrance for toluene[11,12,27], as well as recently by our group for *p*FT[25], would be particularly useful. These can give confirmation of assignments by projecting onto the S_0 state, for which the vibrational wavenumbers are often well established from IR and Raman studies, and the 2D images can yield information about the rotational contours of bands that the ZEKE spectra are not of sufficient resolution to provide. Time domain experiments would also be useful, to extract IVR lifetimes and confirm proposed

restricted couplings. A laser pulse with a full-width at half-maximum (FWHM) of ~13 cm^{-1}, such as the one used by the Reid group[5,20,21,24], would be useful for untangling the proposed couplings, especially in *p*Xyl where there is no significant body of previous work. A pulse FWHM such as this gives an effective compromise between time and frequency resolution. The ZEKE (and "2D-ZEKE") spectra presented here form a useful companion to such time-resolved photoelectron spectroscopy (tr-PES) studies; since the resolution in the ZEKE spectra is significantly higher, they allow one to assign what contributes to broader bands in the tr-PES spectra.

Moving on to other molecules would also be an obvious next step. For example, investigating the *ortho*- and *meta*-fluorotoluenes and/or xylenes would be a natural progression, particularly in the xylene case where the molecular symmetry is lowered and the molecule has two methyl groups; one would perhaps expect even more widespread coupling in that case. An alternative point of interest is the extension of the flexible side chain, for example from a methyl to an ethyl, or a methoxy, group. In the case of a methoxy group, the methyl group is somewhat isolated from the phenyl ring, owing to the oxygen atom, and so vibration-torsion coupling is likely to be less prevalent, as discussed by Moss and Parmenter[28]. Additionally, one could look at other "flexible" groups, such as a hydroxyl group.

One could also use the information gained from this work, and the previously-mentioned studies regarding IVR processes in these substituted benzene molecules, to study more complex molecules. This could be amino acids such as phenylalanine (for which toluene is a model for the side chain) or tyrosine (for which *para*-cresol is a model for the side chain).

Finally, a natural evolution of the concepts discussed here is investigating the solvation of these types of molecules, with examples of this in the literature such as the work Chakraborty and co-workers[29,30]. If this is done in a stepwise fashion, one can introduce the effect of a solvent slowly to probe its impact on the couplings. This could be a simple solvation, such as investigating *p*FT.Ar and *p*FT.Ar_2, with work previously carried out on substituted benzene argon

complexes by others[31–33], or a more complex solvent such as water or methanol could be used such as in references 29 and 30. A REMPI/ZEKE, or 2D-LIF, study of the molecules discussed in this thesis where solvent is added stepwise and different internal energies are probed for each species is suggested, and this would allow a clear comparison between the gas phase discussed here and, in the limiting case, solution phase. Since a system like, for example, solvated tyrosine, is very complex, this kind of stepwise approach is necessary in order to understand the couplings and the effect of the solvent.

A sensible end goal might be a combination of all of the above suggestions, with understanding of any couplings within a particular molecule (be it a biological molecule such as tyrosine or a model such as *para*-cresol) first, followed by a solvation study. It is hoped that the work presented in this thesis will form a stepping stone to the study of such systems, and that they can be studied with a combination of frequency domain techniques and time domain techniques to yield the most complete picture of any couplings.

8.C. References

[1] C.S. Parmenter and B.M. Stone, *J. Chem. Phys.*, **84**, 4710 (1986).

[2] J.S. Baskin, T.S. Rose, and A.H. Zewail, *J. Chem. Phys.*, **88**, 1458 (1988).

[3] P.J. Timbers, C.S. Parmenter, and D.B. Moss, *J. Chem. Phys.*, **100**, 1028 (1994).

[4] K. Okuyama, N. Mikami, and M. Ito, *J. Phys. Chem.*, **89**, 5617 (1985).

[5] J.A. Davies, A.M. Green, A.M. Gardner, C.D. Withers, T.G. Wright, and K.L. Reid, *Phys. Chem. Chem. Phys.*, **16**, 430 (2014).

[6] A. Held, H.L. Selzle, and E.W. Schlag, *J. Phys. Chem. A*, **102**, 9625 (1998).

[7] P.J. Breen, J.A. Warren, E.R. Bernstein, and J.I. Seeman, *J. Chem. Phys.*, **87**, 1917 (1987).

[8] W.D. Tuttle, A.M. Gardner, A. Andrejeva, D. Kemp, J.C.A. Wakefield, and T.G. Wright, *J. Mol. Spectrosc.*, **344**, 46 (2018).

[9] D.J. Kemp, W.D. Tuttle, F.M.S. Jones, A.M. Gardner, A. Andrejeva, J.C.A. Wakefield, and T.G. Wright, *J. Mol. Spectrosc.*, **346**, 46 (2018).

[10] A. Andrejeva, A.M. Gardner, W.D. Tuttle, and T.G. Wright, *J. Mol. Spectrosc.*, **321**, 28 (2016).

[11] J.R. Gascooke and W.D. Lawrance, *J. Chem. Phys.*, **138**, 134302 (2013).

[12] J.R. Gascooke, E.A. Virgo, and W.D. Lawrance, *J. Chem. Phys.*, **143**, 044313 (2015).

[13] A.E.W. Knight and S.H. Kable, *J. Chem. Phys.*, **89**, 7139 (1988).

[14] D.J. Kemp, A.M. Gardner, W.D. Tuttle, J. Midgley, K.L. Reid, and T.G. Wright, *J. Chem. Phys.*, (submitted).

[15] D.J. Kemp, L.E. Whalley, W.D. Tuttle, A.M. Gardner, B.T. Speake, and T.G. Wright, *Phys. Chem. Chem. Phys.*, **20**, 12503 (2018).

[16] L.W. Peng, B.W. Keelan, D.H. Semmes, and A.H. Zewail, *J. Phys. Chem.*, **92**, 5540 (1988).

[17] M. Hippler, R. Pfab, and M. Quack, *J. Phys. Chem. A*, **107**, 10743 (2003).

[18] R.S. von Benten, L. Yaxing, and B. Abel, *J. Chem. Phys.*, **133**, 134306 (2010).

[19] R.S. von Benten, Y. Liu, and B. Abel, *J. Phys. Chem. A*, **114**, 11522 (2010).

[20] J.A. Davies and K.L. Reid, *J. Chem. Phys.*, **135**, 124305 (2011).

[21] J.A. Davies and K.L. Reid, *Phys. Rev. Lett.*, **109**, 193004 (2012).

[22] C.J. Hammond, V.L. Ayles, D.E. Bergeron, K.L. Reid, and T.G. Wright, *J. Chem. Phys.*, **125**, 124308 (2006).

[23] J.A. Davies, K.L. Reid, M. Towrie, and P. Matousek, *J. Chem. Phys.*, **117**, 9099 (2002).

[24] J.A. Davies, L.E. Whalley, and K.L. Reid, *Phys. Chem. Chem. Phys.*, **19**, 5051 (2017).

[25] A.M. Gardner, W.D. Tuttle, L.E. Whalley, and T.G. Wright, *Chem. Sci.*, **9**, 2270 (2018).

[26] W.D. Tuttle, A.M. Gardner, L.E. Whalley, and T.G. Wright, *J. Chem. Phys.*, **146**, 244310 (2017).

[27] J.R. Gascooke, E.A. Virgo, and W.D. Lawrance, *J. Chem. Phys.*, **142**, 024315 (2015).

[28] D.B. Moss and C.S. Parmenter, *J. Chem. Phys.*, **98**, 6897 (1993).

[29] D.P. Mukhopadhyay, S. Biswas, and T. Chakraborty, *J. Phys. Chem. A*, **120**, 9159 (2016).

[30] D.P. Mukhopadhyay, S. Biswas, and T. Chakraborty, *Chem. Phys. Lett.*, **674**, 71 (2017).

[31] S. Georgiev, T. Chakraborty, and H.J. Neusser, *J. Phys. Chem. A*, **108**, 3304 (2004).

[32] Y. Hu, X. Wang, and S. Yang, *Chem. Phys.*, **290**, 233 (2003).

[33] J.R. Gascooke and W.D. Lawrance, *J. Chem. Phys.*, **138**, 084304 (2013).

Appendix A – Vibrational mode diagrams

This appendix contains the thirty ring-localised vibrational modes that comprise the D_i vibrational labelling scheme. These are reproduced from the published work of our research group, see reference 1 for details.

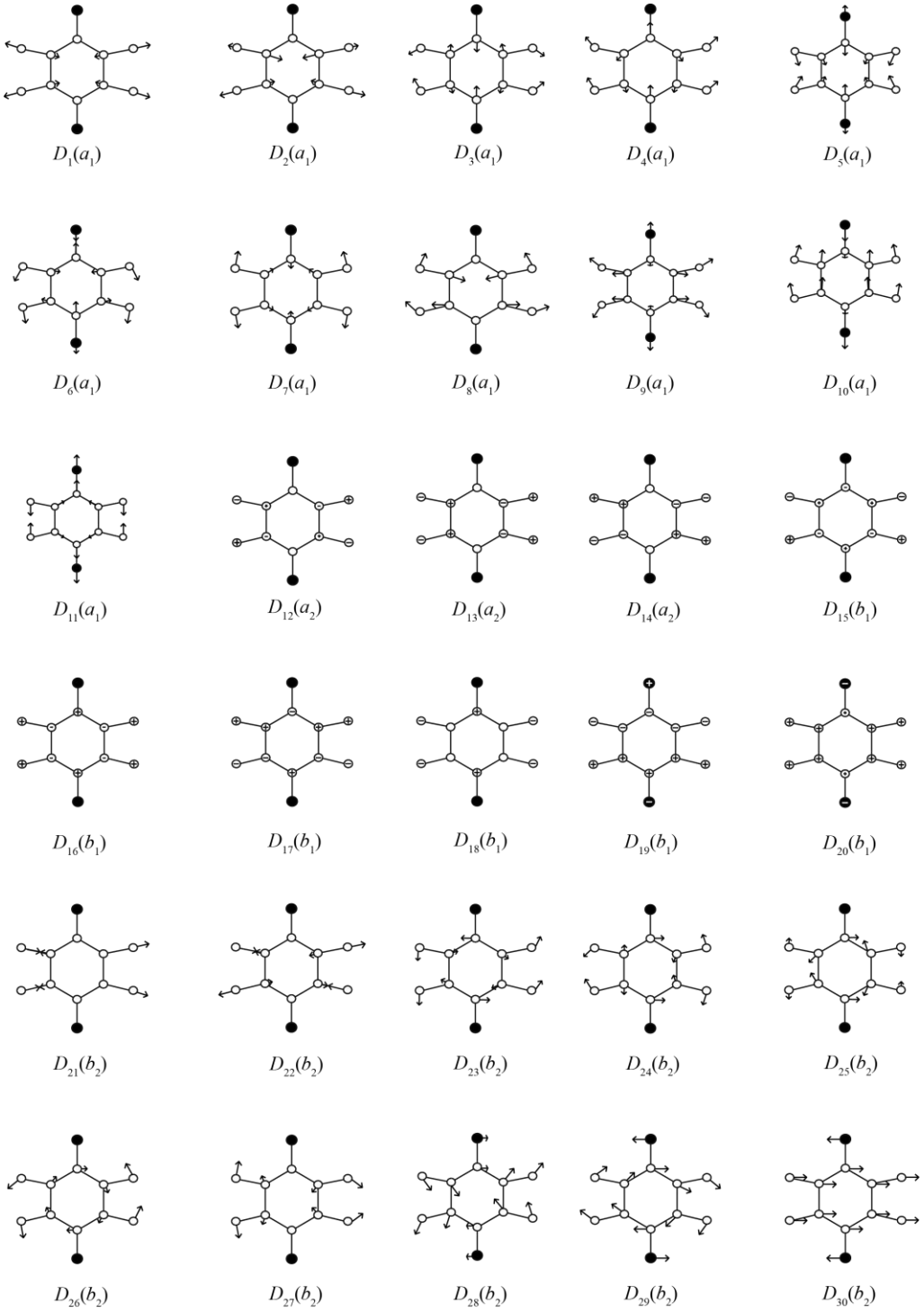


Figure A.1 – Vibrational motions of the thirty D_i modes for *para*-disubstituted benzene molecules.

References

[1] A. Andrejeva, A.M. Gardner, W.D. Tuttle, and T.G. Wright, *J. Mol. Spectrosc.*, **321**, 28 (2016).

Appendix B – Calculated and experimental vibrational wavenumbers

This appendix contains the calculated and experimental vibrational wavenumbers for the four molecules *para*-difluorobenzene (*p*DFB), *para*-chlorofluorobenzene (*p*ClFB), *para*-fluorotoluene (*p*FT) and *para*-xylene (*p*Xyl) in their S_1 and D_0^+ states. Both states for all four molecules were found to be planar at this level of theory with these basis sets, and the lowest energy conformers for *p*FT and *p*Xyl are discussed in Chapter 2.

The experimental values are the "best" values for each vibration, and so where possible they have been taken from the transitions/levels thought to be least perturbed. Some values are obtained from vibrational combinations and overtones, and no attempt was made to account for anharmonicity in obtaining these fundamentals.

Table B.1 – (TD)-B3LYP/aug-cc-pVTZ scaled calculated and experimental S_1 vibrational wavenumbers (cm^{-1})

D_i	Mulliken (D_{2h})	p^{35}ClFB		*p*DFB		*p*FT		*p*Xyl	
		Calc.[a]	Exp.[b]	Calc.[a]	Exp.[c]	Calc.[a]	Exp.[d]	Calc.[a]	Exp.[e]
					a_1				
D_1	1 (a_g)	3143		3143		3130		3105	
D_2	10 (b_{1u})	3130		3131		3105		3088	
D_3	2 (a_g)	1491	1489	1519		1528		1542	
D_4	11 (b_{1u})	1411		1422		1432		1437	
D_5	3 (a_g)	1211	1231	1235	1256	1213	1232	1176	1187
D_6	12 (b_{1u})	1037	1064	1198		1185	1195	1192	
D_7	4 (a_g)	1112		1099	1114	1120		1147	
D_8	13 (b_{1u})	963	962	951		954		959	
D_9	5 (a_g)	796	793	820	818	805	797	784	775
D_{10}	14 (b_{1u})	617	623	710		700	711	694	
D_{11}	6 (a_g)	348	347	414	411	410	410	402	404
					a_2				
D_{12}	7 (a_u)	532	(598)	501	585	588	619	653	
D_{13}	9 (b_{1g})	482	538	429	477	484	512	546	611
D_{14}	8 (a_u)	60	172	97	179	172	199	201	217
					b_1				
D_{15}	15 (b_{2g})	696	676	697	660	706	682	719	
D_{16}	28 (b_{3u})	653	611	667	626	651	624	640	595
D_{17}	16 (b_{2g})	558	519	567	529	538	509	502	
D_{18}	29 (b_{3u})	486	431	487	440	468	423	443	402
D_{19}	17 (b_{2g})	254	244	279	273	243	242	203	213
D_{20}	30 (b_{3u})	99	94	124	120	110	110	104	106
					b_2				
D_{21}	18 (b_{2u})	3138		3139		3126		3100	
D_{22}	23 (b_{3g})	3125		3126		3100		3084	
D_{23}	24 (b_{3g})	1366		1407		1427		1445	
D_{24}	19 (b_{2u})	1303		1397		1315		1322	
D_{25}	20 (b_{2u})	1408		1317		935		1390	
D_{26}	25 (b_{3g})	1225		1232		1255		1277	
D_{27}	21 (b_{2u})	1018		1022		1053		920	
D_{28}	26 (b_{3g})	542	546	553	558	546	549	545	554
D_{29}	27 (b_{3g})	394	397	396	401	395	401	367	370
D_{30}	22 (b_{2u})	263	265	347	355	307	311	283	

[a] TD-B3LYP/aug-cc-pVTZ scaled by 0.97.
[b] From the REMPI and ZEKE studies of references 1 and 2. The value in parenthesis is a tentative assignment.
[c] From the recent work of our group[3], which confirms and rejects some assignments from the LIF/DF study of Knight and Kable (reference 4), and the REMPI spectrum shown in this thesis.
[d] From the REMPI and ZEKE work of this thesis, published in references 5 and 6.
[e] From the REMPI and ZEKE work of this thesis, published in references 7 – 9.

Table B.2 – UB3LYP/aug-cc-pVTZ scaled calculated and experimental D_0^+ vibrational wavenumbers (cm^{-1})

D_i	Mulliken (D_{2h})	p^{35}ClFB		*p*DFB		*p*FT		*p*Xyl	
		Calc.[a]	Exp.[b]	Calc.[a]	Exp.[c]	Calc.[a]	Exp.[d]	Calc.[a]	Exp.[e]
					a_1				
D_1	1 (a_g)	3122		3118		3116		3106	
D_2	10 (b_{1u})	3110		3108		3101		3093	
D_3	2 (a_g)	1604	1624	1628	1642	1628	1631	1633	
D_4	11 (b_{1u})	1444		1457		1454		1450	
D_5	3 (a_g)	1305	1334	1350	1377	1311	1338	1229	1238
D_6	12 (b_{1u})	1085	1122	1274		1211	1235	1209	
D_7	4 (a_g)	1158	1176	1137	1152	1158	1172	1175	1189
D_8	13 (b_{1u})	965	986	956		969		965	
D_9	5 (a_g)	804	821	823	839	811	824	791	806
D_{10}	14 (b_{1u})	639	658	726		710	721	693	
D_{11}	6 (a_g)	370	373	435	441	437	440	440	439
					a_2				
D_{12}	7 (a_u)	976	984	972	980	987	986	994	
D_{13}	9 (b_{1g})	773	782	760	765	770	778	782	789
D_{14}	8 (a_u)	359	358	360	361	356	349	349	342
					b_1				
D_{15}	15 (b_{2g})	981	987	978	955	998	1007	1005	
D_{16}	28 (b_{3u})	855	863	864	845	832	841	784	754
D_{17}	16 (b_{2g})	702	718	710	730	671	685	641	
D_{18}	29 (b_{3u})	497	504	506	512	488	494	470	474
D_{19}	17 (b_{2g})	270	277	289	305	266	271	232	236
D_{20}	30 (b_{3u})	99	102	123	127	109	111	100	102
					b_2				
D_{21}	18 (b_{2u})	3121		3117		3115		3104	
D_{22}	23 (b_{3g})	3111		3109		3101		3092	
D_{23}	24 (b_{3g})	1400		1472		1383		1399	
D_{24}	19 (b_{2u})	1458		1388		1470		1470	
D_{25}	20 (b_{2u})	1295		1311		1301		1300	
D_{26}	25 (b_{3g})	1245		1238		1250		1250	
D_{27}	21 (b_{2u})	1100		1096		1115		1133	
D_{28}	26 (b_{3g})	573	582	572	584	564	570	553	556
D_{29}	27 (b_{3g})	412	421	424	429	412	414	376	378
D_{30}	22 (b_{2u})	268	280	357	369	313	321	289	

[a] UB3LYP/aug-cc-pVTZ scaled by 0.97.

[b] From the ZEKE study of reference 2.

[c] From the recent REMPI/ZEKE study of our group[3], which itself discussed the previous ZEKE and one-photon MATI studies of references 10 and 11.

[d] From the REMPI and ZEKE work of this thesis, published in references 5, 6 and 12.

[e] From the REMPI and ZEKE work of this thesis, published in references 7 – 9.

References

[1] W.D. Tuttle, A.M. Gardner, and T.G. Wright, *Chem. Phys. Lett.*, **684**, 339 (2017).

[2] D.J. Kemp, L.E. Whalley, W.D. Tuttle, A.M. Gardner, B.T. Speake, and T.G. Wright, *Phys. Chem. Chem. Phys.*, **20**, 12503 (2018).

[3] D.J. Kemp, A.M. Gardner, W.D. Tuttle, J. Midgley, K.L. Reid, and T.G. Wright, *J. Chem. Phys.*, (submitted).

[4] A.E.W. Knight and S.H. Kable, *J. Chem. Phys.*, **89**, 7139 (1988).

[5] A.M. Gardner, W.D. Tuttle, L. Whalley, A. Claydon, J.H. Carter, and T.G. Wright, *J. Chem. Phys.*, **145**, 124307 (2016).

[6] W.D. Tuttle, A.M. Gardner, L.E. Whalley, and T.G. Wright, *J. Chem. Phys.*, **146**, 244310 (2017).

[7] A.M. Gardner, W.D. Tuttle, P. Groner, and T.G. Wright, *J. Chem. Phys.*, **146**, 124308 (2017).

[8] W.D. Tuttle, A.M. Gardner, K.B. O'regan, W. Malewicz, and T.G. Wright, *J. Chem. Phys.*, **146**, 124309 (2017).

[9] W.D. Tuttle, A.M. Gardner, L.E. Whalley, D.J. Kemp, and T.G. Wright, *Phys. Chem. Chem. Phys.*, (In press).

[10] G. Reiser, D. Rieger, T.G. Wright, K. Müller-Dethlefs, and E.W. Schlag, *J. Phys. Chem.*, **97**, 4335 (1993).

[11] C.H. Kwon, H.L. Kim, and M.S. Kim, *J. Chem. Phys.*, **118**, 6327 (2003).

[12] A.M. Gardner, W.D. Tuttle, L.E. Whalley, and T.G. Wright, *Chem. Sci.*, **9**, 2270 (2018).

Appendix C – *para*-xylene torsion and vibration-torsion symmetries

This appendix contains the G_{72} molecular symmetry group (MSG) symmetries of the low wavenumber *para*-xylene torsion and vibration-torsion levels, discussed in Chapter 4.

Table C.1. – G_{72} symmetries of *para*-xylene torsion and vibration-torsion levels

$\{m_1,m_2\}$	Pure	$D_{20}(a_2'')$	$D_{19}(a_3'')$	$D_{14}(a_3')$
{0,0}	a_1'	a_2''	a_3''	a_3'
{0,1}	g''	g'	g'	g''
{1,1}	e_3'	e_4''	e_3''	e_3'
{1,-1}	e_1'	e_1''	e_2''	e_2'
{0,2}	g'	g''	g''	g'
$\{1,2\}^+$	e_1''	e_1'	e_2'	e_2''
$\{1,2\}^-$	e_2''	e_2'	e_1'	e_1''
$\{1,-2\}^+$	e_3''	e_4'	e_3'	e_3''
$\{1,-2\}^-$	e_4''	e_3'	e_4'	e_4''
$\{0,3(+)\}^+$	a_1''	a_2'	a_3'	a_3''
$\{0,3(+)\}^-$	a_4''	a_3'	a_2'	a_2''
$\{0,3(-)\}^+$	a_3''	a_4'	a_1'	a_1''
$\{0,3(-)\}^-$	a_2''	a_1'	a_4'	a_4''
{3,1}	g'	g''	g''	g'
{-3,1}	g'	g''	g''	g'
{0,4}	g'	g''	g''	g'
$\{1,4\}^+$	e_3''	e_4'	e_3'	e_3''
$\{1,4\}^-$	e_4''	e_3'	e_4'	e_4''
$\{1,-4\}^+$	e_1''	e_1'	e_2'	e_2''
$\{1,-4\}^-$	e_2''	e_2'	e_1'	e_1''
{0,5}	g''	g'	g'	g''
$\{1,5\}^+$	e_1'	e_1''	e_2''	e_2'
$\{1,5\}^-$	e_2'	e_2''	e_1''	e_1'
$\{1,-5\}^+$	e_3'	e_4''	e_3''	e_3'
$\{1,-5\}^-$	e_4'	e_3''	e_4''	e_4'
$\{0,6(+)\}^+$	a_1'	a_2''	a_3''	a_3'
$\{0,6(+)\}^-$	a_4'	a_3''	a_2''	a_2'
$\{0,6(-)\}^+$	a_3'	a_4''	a_1''	a_1'
$\{0,6(-)\}^-$	a_2'	a_1''	a_4''	a_4'
{6,1}	g''	g'	g'	g''
{-6,1}	g''	g'	g'	g''
{0,7}	g''	g'	g'	g''
$\{1,7\}^+$	e_3'	e_4''	e_3''	e_3'
$\{1,7\}^-$	e_4'	e_3''	e_4''	e_4'
$\{1,-7\}^+$	e_1'	e_1''	e_2''	e_2'
$\{1,-7\}^-$	e_2'	e_2''	e_1''	e_1'